# Conjugated Donor-Acceptor Molecules, Flexible Molecular Receptors and Bis(dithiolato)Ni(III) Complexes: Synthesis, Crystal Structure, Computation and Molecular Sensing

Thesis Submitted for the Degree of
**DOCTOR OF PHILOSOPHY**

*By*

**Indravath Krishna Naik**


School of Chemistry
University of Hyderabad
Hyderabad 500 046
INDIA

**June 2017**

*Dedicated to*

*My Parents and Teachers.....*

# CONTENTS

# Statement

I hereby declare that the matter embodied in the thesis is the result of investigation carried out by me in the School of Chemistry, University of Hyderabad, Hyderabad, India, under the supervision of **Prof. Samar K. Das**.

In keeping with the general practice of reporting scientific observations, due acknowledgements have been made wherever the work described is based on the findings of other investigators. Any omission, which might have occurred by oversight or error, is regretted.

**Indravath Krishna Naik**

**University of Hyderabad**

**June, 2017**

## CERTIFICATE

This is to certify that the thesis entitled "**Conjugated Donor-Acceptor Molecules, Flexible Molecular Receptors and Bis(dithiolato)Ni(III) Complexes: Synthesis, Crystal Structure, Computation and Molecular Sensing**" submitted by **Indravath Krishna Naik** bearing registration number **11CHPH11** in partial fulfillment of the requirements for award of Doctor of Philosophy in the School of Chemistry is a bonafide work carried out by him under my supervision and guidance.

This thesis is free from plagiarism and has not been submitted previously in part or in full to this or any other University or Institution for award of any degree or diploma.

**Parts of this thesis have been:**

**A. Published in the following publications:**

1. **Indavath K. Naik**, Sarkar. R and Samar K. Das *Eur. J. Inorg. Chem.* **2015,** *33*, 5523-5533. (**Chapter 2**)
2. **Indavath K. Naik**, Ramakrishna.B, Sarkar. R, Mondal. N and Samar K. Das (*Manuscript to be submitted*). (**Chapter 3)**
3. **Indravath K. Naik**, Sarkar. R and Samar K. Das (*Manuscript under preparation*). (**Chapter 4)**
4. **Indravath K. Naik**, Sarkar. R, Madhu. V, Bolligarla. R, Kishore. R and Samar K. Das J. Phys. Chem A **2017**, 121, 3274-3286. (**Chapter 5)**
5. Madhu. V, Bolligarla. R, **Indravath K. Naik**, Raju. M and Samar K. Das *Eur. J. Inorg. Chem.* **2016**, *26*, 4257-4264.
6. Madhu. V, Supriya. S, Kishore. R , **Indravath K. Naik** and Samar K. Das *CrystEngComm* **2015**, *17*, 3219-3223.

&

**B. Presented in the following Conferences:**

1. Chemfest-2015, 12th Annual In-House Symposium, Feb-2015, UoH.
2. Modern Trends in Inorganic Chemistry (MTIC-XVI), Dec-2015, Jadavpur University, India (International).

Further the student has passed the following courses towards fulfillment of course work requirement for Ph. D:

| Course code | Name of the course | Credits | Pass/Fail |
|---|---|---|---|
| CY-801 | Research proposal | 3 | Pass |
| CY-806 | Instrumental Methods B | 3 | Pass |
| CY-820 | Main Group & Inner Transition Elements | 3 | Pass |
| CY-886 | Supramolecular Chemistry | 2 | Pass |
| CY-893 | Advanced Magnetic Resonance | 2 | Pass |

**Prof. Samar K. Das**
**(Thesis Supervisor)**

**Dean**
**School of Chemistry**

# Acknowledgements

*I take the opportunity of placing on record, my deep appreciation for all who have been instrumental in shaping up my research efforts*

*To begin with I express my deepest sense of gratitude and profound thanks from the core of my heart to my supervisor* ***Prof. Samar K. Das*** *for his valuable guidance, patience, encouragement, and for the freedom he gave me in carrying out research. His constant encouragement and meticulous workaholism inspired me to tackle problems whenever I got stuck during research activities and primed me to complete my work successfully. Throughout my Ph.D tenure, he is always approachable, helpful, friendly and extremely tolerant. I consider my association with him as a cherishable memory in my life.*

*I take this opportunity to thank Prof. T. P. Radhakrishnan, Dean, School of Chemistry for providing us the facilities needed for our research. I extend my sincere thanks to former Dean Prof. M. Durga Prasad, and all the faculty members, School of Chemistry for their co-operation on various aspects.*

*I would like to thank Prof. S. Mahapatra (School of chemistry, Hyderabad) and his research group especially, Mr. Rudraditya Sarkar, for his tireless efforts in computational studies. I thank Prof. A. Samanta. (School of chemistry, Hyderabad) and his student Mr. N. Mondal for helping me in analyzing the fluorescence data.*

*It is great pleasure to thank my lab seniors Dr. V. Shivaiah, Dr. S. Supriya, Dr. V. Madhu, Dr. P. Raghavaiah, Dr. Arumuganathan, and Dr. Tanmay , Dr. A Srinivasa rao anna, Dr. B. Ramababu anna, , Dr. Monima sarma ,, Dr. Sridevi madam, Dr. Paulami Manna madam for their help, and cooperation during my Ph.D. tenure. I am grateful to my beloved seniors Dr. R. Kishore anna and Dr. Bharat Kumar Tripuramallu anna for initiating and guiding my work, and Dr.G.D.P anna for his generous love towards me. I wish to thank my batchmates Praveen Reddy, Mr. Veeranna and my juniors Mrs. Tulasi, Mr. Ramakrishna Bodapati(RK), Mr. Suresh, Miss. Olivia, Mr. Sathish, Mr. Subhabrata Mukhopadhay Miss.Chandani singh, Mr.Tanmay Kumar and Miss. Joycy N Haokip and postdoc fellows Dr. K.Pratap(Chitti), Dr. N.Veera reddy, Dr. Girijesh Kumar, Dr. Joyashish Debugupta, Dr. Suranjana Bose and UGC students Rita, Savita, Ramu, Asha kumar for creating cheerful work atmosphere.*

*I also thank all the non-teaching staff of the School of Chemistry for their assistance on various occasions. I thank DST funded National Single Crystal X-ray Diffraction Facility, UGC / UPE for providing the basic requirements and CSIR for the financial support.*

*I would like to acknowledge Prof. S. Sarkar, Prof. R. N. Mukherjee and Prof. M. K .Ghorai, and all my teachers during my Post graduation at Indian Institute of Technology, Kanpur. I take this opportunity to thank my teacher from my childhood Nagaraju sir at my school level and Brahma Chary sir at my graduation level for shaping me in the right direction.*

*'If one wants an accounting of one's worth, count his/her friends' I am indeed fortunate to have friends like Laxmaiah Iietheraju (babai), Dr. Ravi Kiran (mama), Dr. Hari krishna (school of life sciences), Dr. P.N Venkata Anudeep Sharma ( IIT Kharagpur), and Srinu (Prof. KMD lab) who have been good friends over the years, and make my moments with them as a bunch of joyful memories throughout my life. I also thank*

*my M.Sc friends especially Sudheer Jhoshi , and Narayan Rakshit for their warmth of friendship towards me.*

*A Special note of thank to my friends Ravi, Vara Prasad, Shravan Kumar, Swapna and divya who have been with me for a long period to cherish the valuable and blissful occasions of my teenage.*

*I am lucky enough to have the support of many School of Chemistry friends, seniors and colleagues, Dr. Satish (S.Pal Lab) anna, Dr. DK anna, Dr. M. Ramu, Vikram, Dr. Anjaneyalu, Dr. Balu, Dr. Narayana, Dr.Chandrsekhar, Dr.Ajay, Dr.Sunny,Dr. Nagarjuna(VB lab), Dr. Srinivas (Allu),Dr. Gupta, Dr.Hari, (LGP lab), Dr. Karunakar, Dr. Ramu Yadav, Mallesh, Bhanu, Dr. Shesu, Dr.Rama Krishna, Madhu, , Dr. Sekhar Reddy, Dr. Ganesh, Dr. Vigensh,Dr. Praveen, , Dr. Malakappa, Dr. K.S.N Raju,Dr. Swami, Dr.Nagaraju, Dr. Krishna Chary, Dr.Geetha, Dr. Rajesh, Dr. Ashok, Dr.Chandu, Dr. Babu Ramavath. anna, Dr. Ramesh, Dr.Gangadhar, Dr.Nagarjuna reddy, Dr.Vijji, Dr.Ramaraju, Dr.Ramesh, Dr.RamKumar, Dr. Mallikarjun, Dr. Guru Braham, ,Dr. Rajgopal, , Vikaranth anna, Obaiah, Satish (PKP), Dr. Kesav, Dr. Basik, Pramithi, Krishna Dasari(RC Lab), Ramudu, Dr. Suman, Dr. Leela, Ranjani, Sakthivel, Dr. Aannadhasan, Radhika, Amala Rasamshetty, Sruthi K.S exceptionally generous in helping me at various occasions.*

*Undoubtedly great pleasure of thanks to my mother for her indeed confidence on me. The greatest debt I owe is to my father, sisters, brother-in-law, Raju and Linga naik for lending me an emotional boost for this arduous task. I feel fortunate to have an imperative support from my brother Mr.Bheemla and Basha. It is indeed a pleasure to thank my wife Mrs. Padma for giving me moral support to my educational career.*

*In all reverence, I dedicate this work to my loving Mother. A strict disciplinarian with a tender heart, an intelligent teacher and a careful worker ---- That's how I can best describe her. Her blessings have always directed me onto the right track following which here I am.*

Indravath Krishna Naik

**University of Hyderabad**

**June, 2017**

# SYNOPSIS

This thesis work entitled with "**Conjugated Donor-Acceptor Molecules, Flexible Molecular Receptors and Bis(dithiolato)Ni(III) Complexes: Synthesis, Crystal Structure, Computation and Molecular Sensing**" consists of five chapters: (**1**) Introduction, (**2**) Bis(quinoxaline-dithiolato)Nickel(III)-Complexes: Synthesis, Crystal Structures, Spectroscopy, Electrochemistry and DFT Calculations, (**3**) A Functional Molecular System of Bis(pyrazolyl)pyridine Derivatives: Photo physics, Spectroscopy and Computation, (**4**) Chromophore 4, a Unique $Cu^{2+}$ Sensor: Emergence of a New Fe(II) Complex with Conjugated Bis(pyrazolyl)pyridine Derivative and (**5**) A Flexible Molecular Receptor Isolated in an Unusual Intermediate Conformation: Computation, Crystallography, Hirshfeld Surface Analysis and Synthesis of $\{Cu(mnt)_2\}_2$ Ion pair Complex and Future Scope. The work described in this thesis is in the direction towards the synthesis and characterization of metal (Ni and Cu) bis(dithiolene) complexes and π-conjugated 2,6-Bis(pyrazolyl)pyridine derivatives and their electronic and electrochemical properties with well explained theoretical calculations. Apart from the first chapter (introduction), all the chapters are sub-divided into Introduction, Experimental Section, Results and Discussion and Conclusions followed by References. The last section of the thesis is described by "Conclusions and Future Scope".

## Chapter 1

## Introduction

This chapter deals with two different systems *viz*. metal 1,2–dithiolene complexes and metal complexes of 2,6-bis(pyrazolyl)pyridine derivatives. Both the systems are well-known in different areas of the chemical research. Metal 1,2-dithiolene complexes are solids with chemical formula ($M(S_2C_2R_2)_n$) and the 2,6-bis(pyrazolyl)pyridine are nitrogen-containing heterocyclic based compounds. Metal 1,2-dithiolene complexes are known in the field of catalysis, electrochemistry, magnetic material chemistry etc., and the transition metal complexes of the 2,6-bis(pyrazolyl)pyridine are also good candidates in optoelectronic, photovoltaics, nonlinear optics, spin crossover phenomenon,ligand-driven, light- induced spin-crossover effects and sensors. This chapter gives a general overview of these two systems and is divided into four

sections *viz*., dithiolene, 2,6-bis(pyrazolyl)pyridine, the motivation of the work and references. An account on these two systems includes structural features and synthesis followed by their applications in the area of materials chemistry, each in brief.

## Chapter 2

## Bis(quinoxaline-dithiolato)nickel(III) Complexes $[Bu_4N][Ni^{III}(6,7\text{-qdt})_2]$ and $[Ph_4P][Ni^{III}(Ph_2 6,7\text{-qdt})_2]\cdot CHCl_3$(6,7-qdt=Quinoxaline-6,7-dithiolate; $Ph_2$6,7-qdt=Diphenylquinoxaline-6,7-dithiolate):Synthesis,Spectroscopy, Electrochemistry, DFT Calculations, Crystal Structures and Hirshfeld Surface Analysis

This chapter describes the synthesis and structural characterization of two square planar nickel(III)-bis(quinoxalene-6,7-dithiolate) compounds with formulas $[Bu_4N][Ni^{III}(6,7\text{-qdt})_2]$ (**1**) and $[Ph_4P][Ni^{III}(Ph_2 6,7\text{-qdt})_2].CHCl_3$ (**2**), that have been synthesized by $I_2$ oxidation of corresponding $[Bu_4N]_2[Ni^{II}(6,7\text{-qdt})_2]$ and $[Ph_4P]_2[Ni^{II}(Ph_2 6,7\text{-qdt})_2]$ respectively. To investigate the supramolecular structure, we looked at the C–H···S and C-H···N hydrogen bonding interactions in the crystal structure of compound **1**. We found that a supramolecular chain-like arrangement is formed from anion-anion C–H···N interactions. On the other hand, inter-anion C–H···S hydrogen-bonding interactions are responsible for the formation of a two-dimensional layer-like supramolecular arrangement. The crystal structure of compound **2** is also characterized by C–H···N and C–H···S supramolecular hydrogen-bonding interactions. The inter-anion C–H···N weak interactions lead to the formation of one-dimensional chain-like structure. On the other hand, the C–H···S hydrogen–bonding interaction between the complex anions and tetraphenylphosphonium cations lead to the construction of sandwich-type extended arrangement. The solution state electronic absorption bands for compounds **1** and **2**, are observed in the near-infrared region (for compound **1**: $\lambda_{max}$ = 850 nm and for compound **2**: $\lambda_{max}$ = 880 nm), All transitions are well explained by density functional theory calculations. The ESR spectra of solid samples of compounds **1** and **2** were recorded at 123 K, as presented in Figure 1. Compound **1** exhibits a rhombic type signal: $g_x$ = 2.246, $g_y$ = 2.156 and $g_z$ = 2.06. However, compound **2** shows an axial signal with $g_{\perp} > g_{\parallel}$ : $g_{\perp}$ = 2.133 and $g_{\parallel}$ = 2.049. We performed the

cyclic voltammetric studies of compounds **1** and **2**, that undergo reversible one electron redox processes as shown in Figure 2.

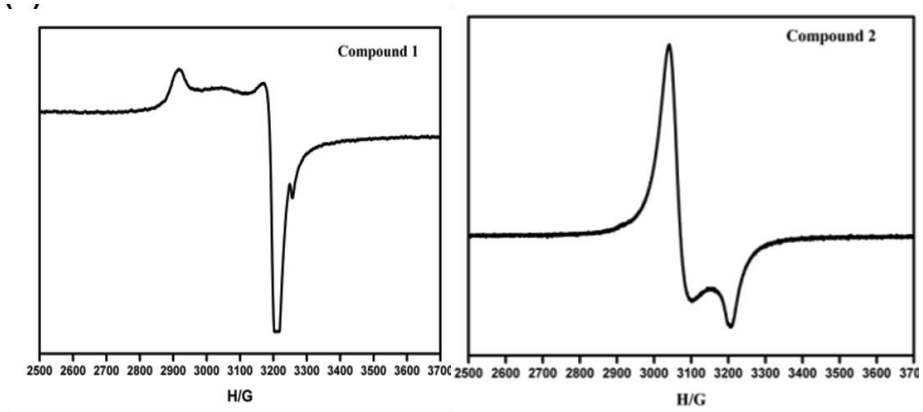


**Figure 1.** Solid state ESR spectra of **Complex 1** (left) and **Complex 2** (right) (at 123K).

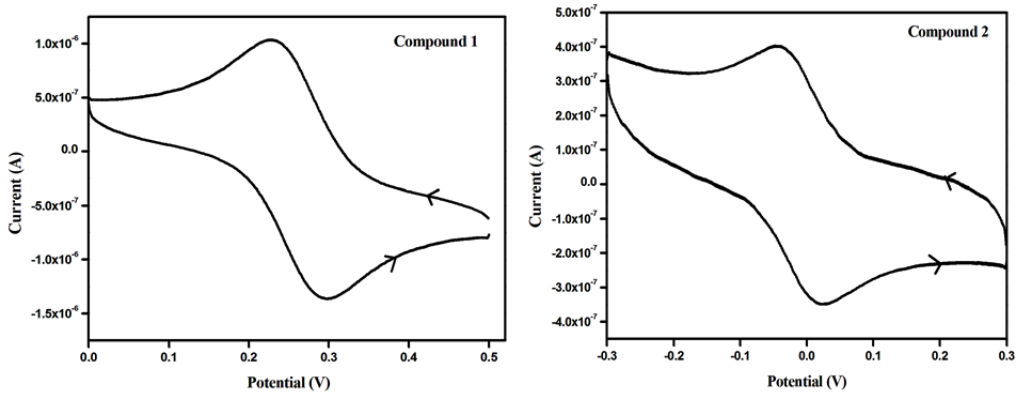


**Figure 2.** Cyclic voltammetric studies of complex (**1)** (left) complex (**2) (**right) in DMF solution at scan rate 100 $mVs^{-1}$, V *vs* Ag/AgCl.

## Chapter 3

## A Functional Molecular System of Bis(pyrazolyl)pyridine Derivatives: Photo physics, Spectroscopy and Computation

This chapter describes a new series of conjugated donor-π-acceptor type of 2,6-bis(pyrazolyl)pyridine compounds (**3-9**), that have been synthesized *via* Horner-Wadsworth-Emmons (HWE) reaction [scheme 1], starting from a common phosphonate precursor (compound **2**) having 2,6-bis(pyrazolyl)pyridine moiety and diverse donor aromatic aldehydes and characterized by routine spectral analysis including elemental analysis. Compound **2**, one of

the starting precursors and molecule **3**, the first member of the donor-π-acceptor series, are additionally characterized by single crystal X-ray structure determination. Compounds **2** and **3** crystallize in *P-1* (triclinic) and $P2_1/c$ (monoclinic) space groups respectively. Interestingly in the crystal structure of compound **3**, the molecules undergo C−H···N intermolecular hydrogen bonding interactions leading to a supramolecular dimer structure.

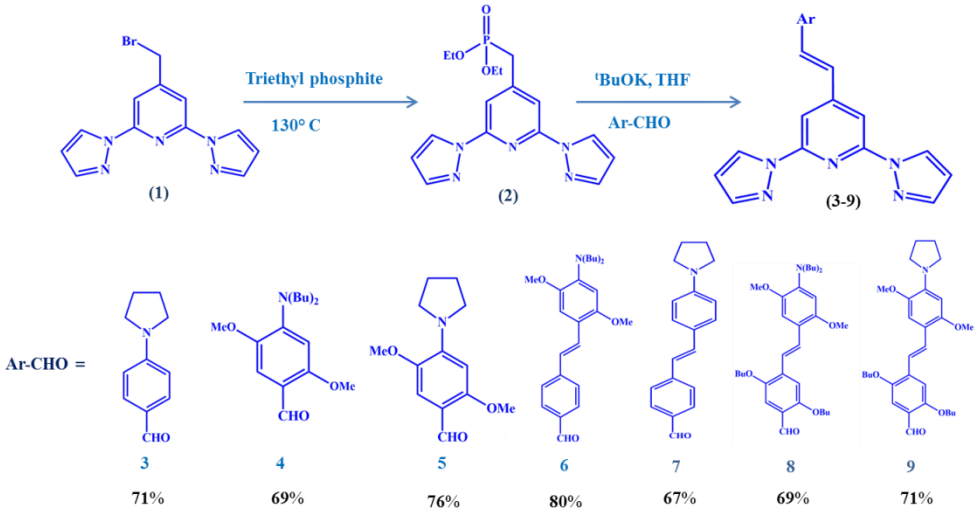


**Scheme 1.** Molecules synthesized and studied in the present work

The absorption maxima in the electronic spectra of the title compounds shift mainly due to intra-molecular charge transfer (ICT) between different donor (dibutyl and cyclic pyrrolidine) groups and the acceptor moiety [2,6-bis(pyrazolyl) pyridine]. Solution state emission spectral studies of all these compounds show large solvent sensitive behavior with significant amounts of stroke shifts. The large solvent dependence of the emission indicates that the excited state is stabilized in more polar solvents due to the intramolecular charge transfer. The role of the position and nature of the donor functionalities in the conjugated backbone of overall donor moiety of compounds **3-9**,on the electronic absorption properties of title chromophores has been demonstrated, which has further been corroborated by DFT and TD–DFT computation studies. The emission spectral results of compounds **3**, **5** and **7** have also been supported by DFT and TD–DFT calculations. Fluorescence lifetime studies of all the chromophore (**3-9**) have also been studied. From DFT calculations, it is found that the nature of the HOMO of the each compound belongs to a π-bonding type, whereas the same for the LUMO is the π-antibonding type. The maximum charge density (electron density) of the HOMO is situated at the donor moieties

(pyrrolidine or dibutyl amino) and in the case of LUMO, the maximum charge density is situated at the 2,6-bis(pyrazolyl)pyridine acceptor moiety. So the overall $\pi \rightarrow \pi^*$ type of electronic transitions in the synthesized compounds occur from pyrrolidine or dibutyl amino donor moiety to the 2,6-bis(pyrazolyl)pyridine acceptor moiety in the same compound. As a result, this $\pi \rightarrow \pi^*$ electronic transition can be called as intramolecular charge transfer (ICT).

## Chapter 4

## Chromophore 4, a Unique $Cu^{2+}$ Sensor: Emergence of a New Fe(II) Complex with Conjugated Bis(pyrazolyl)pyridine Derivative

The preceding chapter demonstrated syntheses and photo-physical properties of a series of conjugated bis(pyrazolyl)pyridine derivatives (**3-9**, Scheme 1). Chapter 4 deals with one of these chromophores, namely chromophore **4**, which has been explored further as a selective $Cu^{2+}$ ion sensor. An extensive screening studies of chromophore **4** (see Scheme 2) with diverse metal acetates prompted us to explore the syntheses of diverse metal coordination complexes with chromophore **4** as a ligand. However, we could succeed to synthesize only Fe(II) coordination complex with a particular chromophore **3** as a ligand $\mathbf{L_1}$ (see Scheme 2). Figure 3 shows fluorescence quenching with various metal acetates and it has been found that copper acetate quenches the fluorescence completely with chromophore **4** in MeOH solution. The resulting synthesized Fe(II) coordination complex (complex **1**, Scheme 2) has unambiguously been characterized by single crystal X-ray crystallography.

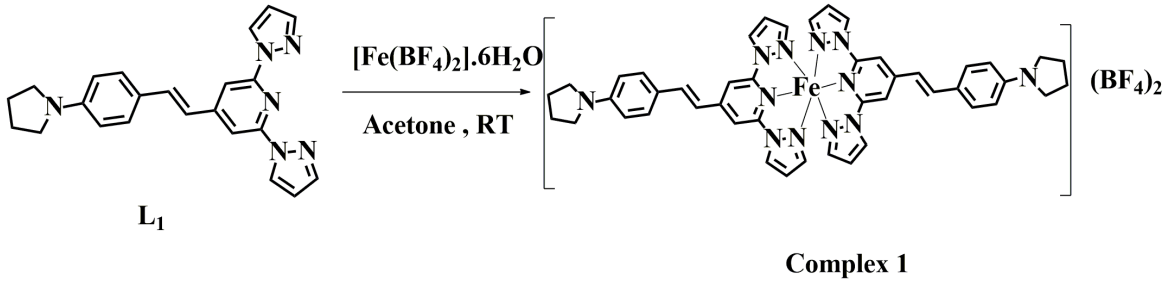


**Scheme 2.** Synthesis of complex **1** presented in the study.

Complex **1** crystallizes in monoclinic space group $P2_1/n$. Fe−N bond distances and concerned bite angles around the coordination sphere are good indicators of the spin state of a $Fe^{II}$ complex. Relevant literature shows that 2,6-bis(pyrazolyl)pyridine ligand complexes yield a range of Fe−N bond distances of 1.93−1.97 Å occurs in low spin Fe(II) complexes and a range of Fe−N bond distances of 2.14−2.20 Å happens in high spin Fe(II) complexes. Also, the Σ parameter (deg), which is the summation of the deviation from 90° of the twelve bite angles around the central $Fe^{II}$ ion, can range from 85° to 96° in low-spin complexes and from 145° to 197° in high-spin complexes. In the present study, the average Fe−N bond distance and Σ parameter were found 2.03 Å and 116.81° respectively. This indicates that, the complex **1** is associated with low spin state of Fe(II). We performed DFT and TDDFT calculations in solution state to corroborate the low spin state Fe(II). The concerned electronic transitions [ligand to metal charge transfer (LMCT) and ligand to ligand charge transfer (LLCT)] are well explained by density functional theory (DFT) calculations.

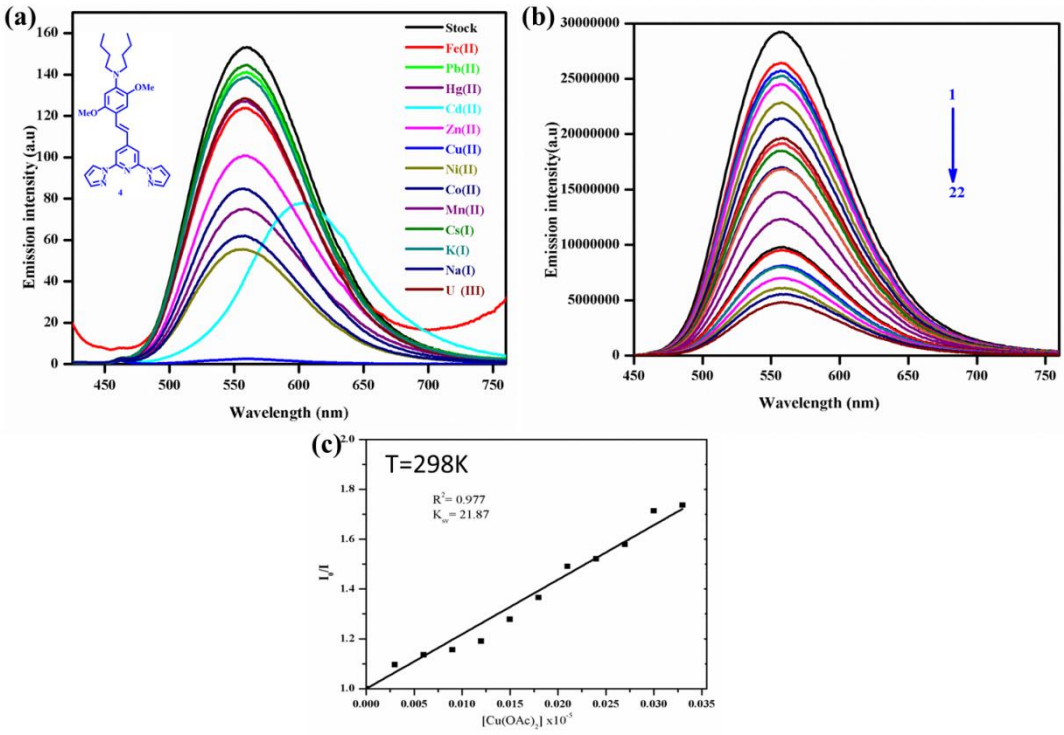


**Figure 3.** (a) Fluorescence spectra of chromophore **4** upon addition of different cations (Mn+) in methanol ($\lambda_{ex}$ = 408 nm). (b) Fluorescence titration of **4** in methanol with increasing $Cu^{2+}$ concentration (addition 1mm solution of 10 μL $Cu^{2+}$ ions per time); $\lambda_{ex}$ = 408 nm). (c) Stern–Volmer plot for the chromophore 4 with $Cu^{2+}$.

## Chapter 5

## A Flexible Molecular Receptor Isolated in an Unusual Intermediate Conformation: Computation, Crystallography, Hirshfeld Surface Analysis and Synthesis of $\{Cu(mnt)_2\}_2$ Ion pair Complex

1,1"-1,4-Phenylene-bis(methylene)bis-4,4'-bipyridinium cation $[C_{28}H_{24}N_4]^{2+}$ (**c**), an organic receptor that generally crystallizes in its *anti*-conformation, has recently been shown to be isolated in its *syn*-conformation in an ion paired compound $[C_{28}H_{24}N_4][Zn(dmit)_2] \cdot 2DMF$ ($dmit^{2-}$ = 1,3-dithiole-2-thione-4,5-dithiolate). In this chapter, we have demonstrated that the same receptor $[C_{28}H_{24}N_4]^{2+}$ (**c**) can also be stabilized in an unusual intermediate conformation (neither *syn* nor *anti*) with $PF_6^-$ anion in compound $[C_{28}H_{24}N_4](PF_6)_2 \cdot$(1,4-dioxane) [**1·(1,4-dioxane)**].

Compound **1·(1,4-doxane)** crystallizes in triclinic system with space group *P-1*. Interestingly, the cation **c**, observed in the crystal structure of **1·(1,4-dioxane)** adopts an intermediate conformation which is in-between *syn*- and *anti*- conformation. We believe that inter-cation-anion hydrogen bonding interactions (mostly C–H···F hydrogen bonds) between the cation receptor **c** and anion $PF_6^-$ are responsible for this unusual intermediate conformation of **c** in the crystal structureof compound **1·(1,4-dioxane)** as shown in Figure 4a showing the C–H···F hydrogen bonding environment around the $PF_6^-$ anion. The stability of intermediate conformation (between *syn* and *anti*) of the organic receptor $[C_{28}H_{24}N_4]^{2+}$ (**c**) in compound $[C_{28}H_{24}N_4](PF_6)_2 \cdot$(1,4-dioxane) [**1·(1,4-dioxane)**] can be rationalized by its strong hydrogen bonding interactions with surrounding $PF_6^-$ anions resulting in a three-dimensional supramolecular network that have well-defined void spaces, occupied by the solvent 1,4-dioxane molecules. The X-ray analysis of a single crystal of compound **2·2H$_2$O** reveals that the dication $[C_{28}H_{24}N_4]^{2+}$ (**c**) adopts an usual *anti*-conformation with respect to the two bipyridine units of the para-xylene ring. In the crystal structure of compound **2·2H$_2$O**, there are balanced/equivalent C–H···O hydrogen bonding interactions around **c** with respect to the central phenylene ring as represented in Figure 4b. Both side arms of **c** are hydrogen bonded with its surrounding $NO_3^-$ anions in such a way that hydrogen bonding force of one arm would cancel that of other arm. Thus there is an equivalent force along all the sides of cationic receptor $[C_{28}H_{24}N_4]^{2+}$ (**c**), which

implies that there is no more distortion from its usual *anti*-conformation. This justifies the *anti*-conformation of **c** in compound **2·2H$_2$O**.

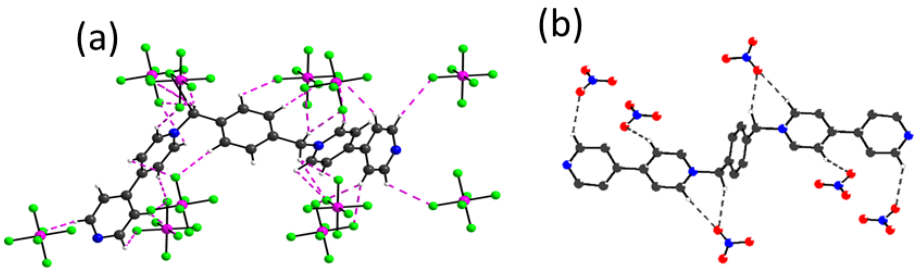


**Figure 4.** (a) Unbalanced/unsymmetrical C–H···F (b) Balanced /symmetrical C–H···O hydrogen bonding interactions around the cationic receptor $[C_{28}H_{24}N_4]^{2+}$.

The density functional theory calculations are performed to understand the internal mechanism of the stability of various conformers of cationic receptor **c** and compound **1**. In conjunction with the electronic stability of the conformers, the natural bond orbital analysis and conformational equilibrium constants at different temperatures are also calculated to find out the sources of the different stability of the various conformers of experimentally synthesized compounds.The ion pair complex **1** (Figure 5) of the same cation receptor was synthesized under acidic condition and obtained as needle shaped crystals in DMF solution. The single crystals are crystallized in the monoclinic space group *P2$_1$/c*. A thermal ellipsoidal plot of complex **1** with non-hydrogen atom labeling is presented in Figure 5. This shows the abundance of $[4,4'–H_2bpy]^{2+}$ as a cation and $[Cu(mnt)_2]^{2-}$ as an anion resulting the formation of 1:1 ion-pair complex **1**.

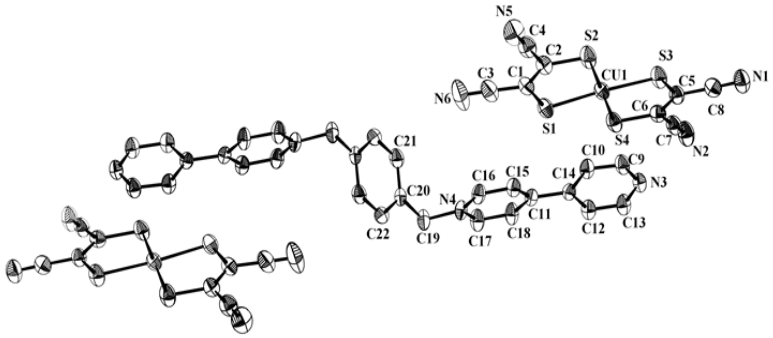


**Figure 5**.Thermal ellipsoid plot of complex **1**

## Summary: Future Scope

This part will demonstrate the future scope of this thesis work. In the second chapter of this thesis, we have described the new square-planar nickel (III)-bis(quinoxaline-6,7-dithiolate) complexes demonstrating their electronic spectral properties. Ion-pair compounds of cationic organic molecule with anionic metal dithiolene complexes will be taken up further to demonstrate their device properties such as magnetic, conducting, NLO, liquid crystals, *etc*. properties. This work is under progress in our laboratory. Work demonstrated in the chapters 3 and 4, includes spectroscopy as the main characterization tool. A series of donor-acceptor π-conjugated 2,6-bis(pyrazolyl)pyridine derivatives has been synthesized following standard and well-known organic synthetic methodologies and characterized through spectroscopy. 2,6-bis(pyrazolyl)pyridine derivatives are excellent tridentate chelating ligands for metal ion coordination. Metal complexes of 2,6-bis(pyrazolyl)pyridines are more useful as photosensitizers and they act as electron reservoirs due to their π-conjugated aromatic systems and they have the ability to photo stabilize the complexes. So we wish to extend this interesting system and a large amount of work has already been obtained in this direction. In the chapter 5 of this thesis, we have discussed about unusual intermediate conformation of 1,1''-1,4-phenylene-bis(methylene)bis-4,4'-bipyridinium cation $[C_{28}H_{24}N_4]^{2+}$ (**c**) receptor, which can interconvert between its *syn*- and *anti*- conformations, which were explaind by theoritical calculation.This work has opened a new area, that explores the possibility of interactions between $[M(dithiolene)_2]^{2-}$ anions and variety of mechanically interlocked cationic systems such as cyclophane, rotaxane and catenane. It would be very interesting to assemble interlocked components (such as cyclophane, rotaxane, and catenane as cations) and the classical metal dithiolene complex anion in a single supramolecular system. The syntheses of such systems are in progress in our laboratory.

**********End of Synopsis**********

# Introduction and Importance of 1,2–Dithiolene and 2, 6–Bis(pyrazolyl)pyridine Metal Complexes and Their Applications: Motivation of Present Thesis Work

1

**Abstract:** This chapter deals with two different systems *viz*. metal 1,2–dithiolene complexes and metal complexes of 2,6-bis(pyrazolyl)pyridine derivatives. It gives a general overview of these two systems and it is divided into four sections *viz*., dithiolene, 2,6-bis(pyrazolyl)pyridine, the motivation of the work and references.

## 1.1. Introduction

Dithiolene ligands are called non–innocent ligands. Dithiolene ligands are often thought to exist in two oxidation states separated by two electrons. These are dianionicene-1,2-dithiolate and the neutral 1,2-dithioketone, which possess different electronic characteristics as shown in scheme 1.1. Hence, the electronic structures of 1,2-dithiolene ligands are generally observed as dianionic form or neutral form. The dianionic form has six π–electrons and at the same time neutral form has four π–electrons as shown in Scheme 1.1. This indicates that two-electron oxidation of the dianionic form, ene–1,2–dithiolate resulting in the formation of the 1,2–diketone. Moreover, these resonance forms decide the oxidation state of the concerned metal coordinating 1,2-dithiolene ligands. The syntheses, characterization and properties of different types 1,2-dithiolene complexes were reported by McCleverty, Eisenberg, Müller–Westerhoff, and Vance.[1, 2]

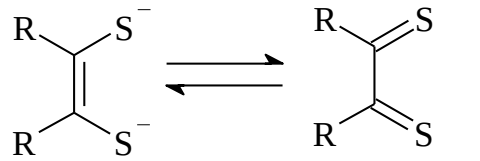


dianionic form $6\pi e^-$ neutral form $4\pi e^-$

**Scheme 1.1.** The resonance forms of 1,2–dithiolate anion.

### 1.2. Nomenclature

The general formula of 1,2-dithiolate dianion is $R_2C_2S_2^{2-}$. This 1,2-dithiolate can also be described by different nomenclatures such as 1,2-alkenedithiol or 1,2-dithiete or 1,2-dithione depending on the oxidation states. This concept can be expressed by the Scheme 1.2.

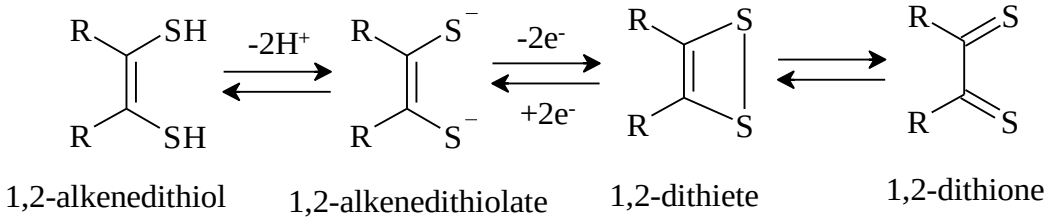


1,2-alkenedithiol 1,2-alkenedithiolate 1,2-dithiete 1,2-dithione

**Scheme 1.2.** Nomenclature for common 1,2–dithiolene precursors.

### 1.3. Classifications of Dithiolenes

The unsaturated dithiolato ligands have been divided into two different groups like odd and even depending on the presence of the numbers of π–orbitals.

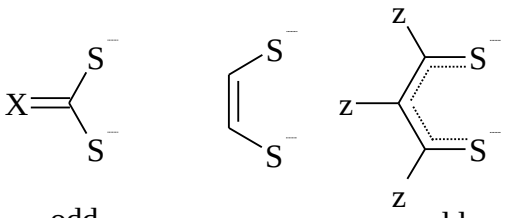


odd even odd

This classification results in the recognition of three unique classes: 1,2–dithiolates (even), 1,1'–dithiolate (odd) and 1,3–dithiolates (odd) as represented below.

**<u>The examples of 1,1'–dithiolates:</u>**

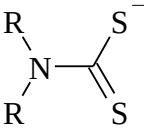


R = alkyl dithiocarbamate

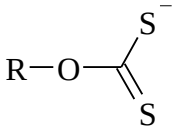


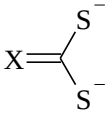


R = alkyl xanthate

X = $CR_2$ = dithiocarbamate

X = NR = dithiocarbamate

X = S = dithiocarbamate

**The example of 1,3–dithiolates**

1,8–Napthalenedithiolate

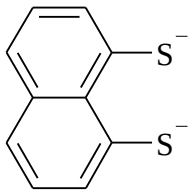

**The examples of 1,2-dithiolates:**

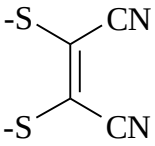

mnt

1,2-Maleonitrile-1,2-dithiolate

1,2-Dicyanoethene-1,2-dithiolate

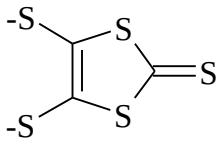

dmit

1,3-Dithiole-2-thione-4,5-dithiolate

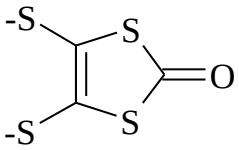

dmio

1,3-Dithiole-2-one-4,5-dithiolate

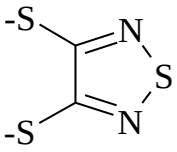

tdas

1,2,5-thiadiazole-3,4-dithiolate

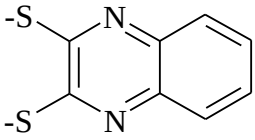

qdt

2,3-quinoxalinedithiolate

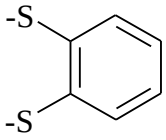

bdt

1,2-benzenedithiolate

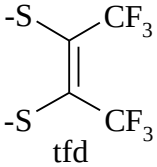

tfd

1,2-bis(trifluoromethyl)ethylenedithiolate

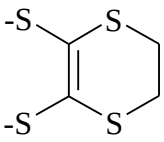

dddt

5,6-dihydro-1,4-dithiine-2,3-dithiolate

### 1.4. Metal bis(1,2–dithiolene) Complexes

Metal bis(1,2-dithiolene) complexes are known to exhibit a non-innocent character originating from the quasi-aromaticity and strong π–electron donor ability due to the involvement of sulfur atoms. Dithiol and dithiolate ligands were used for analytic purpose in the early of 1930s. In 1960s, three research groups started working in the field of dithiolene research, namely, Schrauzer and co–workers[3, 4] Eisenberg et al.[5] and Davison-Holm and co–workers.[6] First they established the square–planar nature, redox activity, and broad scope of the highly colored bis(dithiolene) complexes of late transition metals, such as Fe, Co, Rh, Ir, Ni, Pd, Pt, Cu, Au and Zn. In the last three decades, tremendous progress in research in this area arose because of their enormous contributions in materials science, enzymology, analytical science and reactivity. These areas of research extended the impact and importance of dithiolene chemistry. Metal dithiolene complexes are often exist in various oxidation states, because the more delocalized nature of dithiolene ligands. The reduced dithiolene complexes have relatively more in ene-1,2-dithiolate character. In oxidized dithiolene complexes, the ligand assumed to be more of 1,2-dithioketone character. These descriptions are evaluated by examination of differences in C–C and C–S bond distances. The Scheme 1.3 represents various bonding descriptions of a representative complex, in which the formal oxidation states of the metal and ligand vary. Such electronic versatility may make it difficult to establish bonding description of a dithiolene complex. However, bond distances such as S−C lengths have been used as good indicators to understand the electronic configuration of a dithiolene complex.[7] The short S−C distances of ~1.64 Å are characteristic of ligand bonding with metal in dithione form whereas the long S−C distances of as high as ~1.77 Å, are more characteristic of ligand in the ene-1,2-dthiolate.

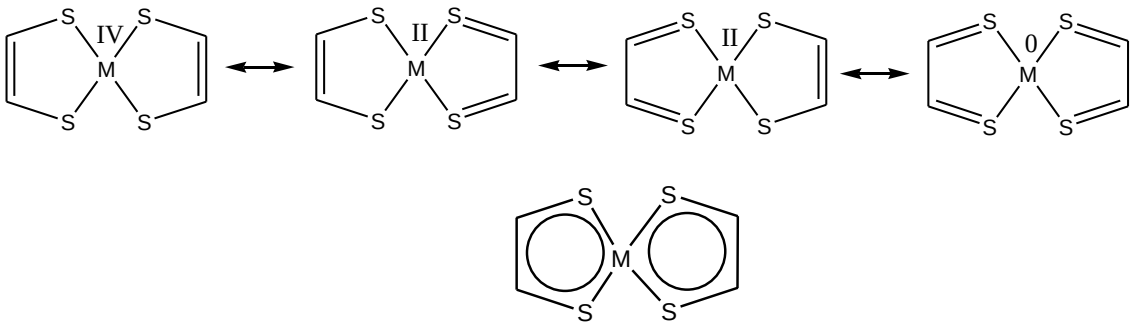


**Scheme 1.3.** Various bonding description of M(dithiolene)$_2$ complexes.

### 1.4.1. Properties and Applications of Metal 1, 2–Dithiolene complexes:

Metal bis(1,2-dithiolene) complexes have been extensively studied since last five decades due to novel properties and applications in different areas of chemistry, such as, near infrared materials, catalysts, magnetic materials, materials for bioinorganic chemistry and non-linear optics. These properties and applications arise due to the combination of functional properties like diversity of molecular geometries, rich redox behavior, magnetic moments and specific intermolecular interactions. A brief explanation of the properties (solid-state properties, electrochemical properties) and applications (near Infra-red dyes) of metal dithiolene complexes are discussed in the following sections.

#### 1.4.1.1. Solid-State Properties

Since last two decades metal-dithiolene coordination compounds are known to demonstrate interesting magnetic,[8-10] electrical and optical properties.[11, 12] In metal (dithiolene) complexes, metal can exhibit various oxidation states and overall charge of the complex may vary from anionic to cationic. Different spin states like S = 0, 1, 1/2, or 3/2, can be easily attained by changing the type of transition metal (M) and its oxidation state which makes these complexes suitable for solid magnetic materials. For example, in 2002 an ion-pair complex [RbzPy][Ni(mnt)$_2$] (R= Br, Cl and $NO_2$) was reported by Meng and his coworkers,[13] in which the [Ni(mnt)$_2$]$^{1-}$ anion favors one-dimensional columnar molecular arrangements and this ion-pair complex exhibits spin-Peierls-like transition (magneto-elastic transition that occurs in quasi one-dimensional antiferromagnetic materials) in solid state as shown in Figure 1.

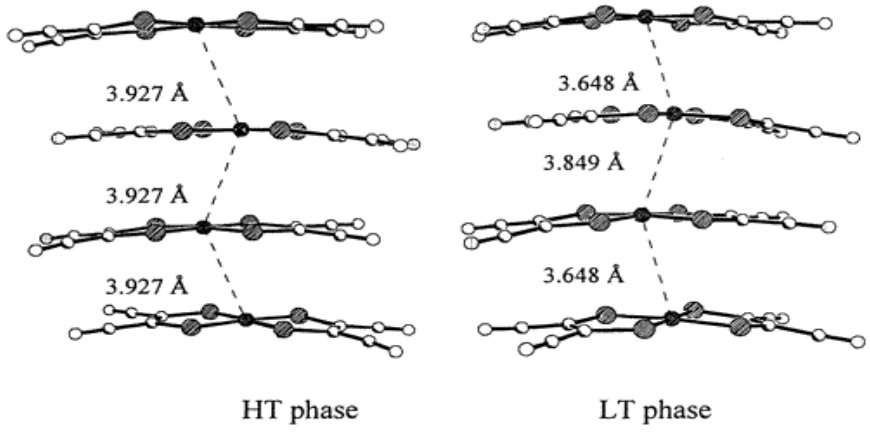


**Figure 1.** Side view of 1-D anion chain for [BrBzPy][Ni(mnt)$_2$] in the high-temperature (HT) and low-temperature phases.

### 1.4.1.2. Electrochemical Properties

The electrochemical properties of the metal-dithiolene complexes are very interesting because of their unique redox properties and non-innocent behavior of the ligand. The extensive π-electron delocalization in metal bis-dithiolene complexes makes it possible for the existence of variable charge levels and also difficult to assign oxidation state of the metal and ligands. Interestingly, square planar bis(dithiolene) complexes undergo one-, two-, and even three- electron reversible redox processes. Because of rich redox chemistry of metal-bis(dithiolene) chemistry and the redox active nature of the dithiolene ligands, these complexes display much reactivity related to the redox properties and is often centered on the dithiolene ligands**.** A large number of bis(dithiolene) complexes has been reported for the metals, such as, Ni, Pd, Pt, Cu, Au. The ease of oxidation of $[M(S_2C_2R_2)]^{z-}$ for a particular metal decreases in the order R = H > alkyl > aryl > $CF_3$> CN. This series parallels to the electron donating or withdrawing ability of the substituent on group R. For the transition metals, oxidative stability increases in the order Fe < Co < Ni < Cu for dianionic species (Z = 2).

$$[M(dithiolene)_2]^{+} \underset{-e^-}{\overset{+e^-}{\rightleftharpoons}} [M(dithiolene)_2]^{0} \underset{-e^-}{\overset{+e^-}{\rightleftharpoons}} [M(dithiolene)_2]^{-} \underset{-e^-}{\overset{+e^-}{\rightleftharpoons}} [M(dithiolene)_2]^{2-}$$

### 1.4.1.3. Near–infrared (NIR) dyes

Metal bis(dithiolene) complexes have been used as good candidates for Near-IR dyes, especially, Ni-dithiolene complexes shows an intense electronic absorption in NIR region. Many research groups are involved in synthesis of nickel containing metal-dithiolene complexes for near-IR absorption due to the ease of electron density delocalization within the complexes compared to the corresponding Pd and Pt analogues. Mulller-Westerhoff et al.[14] reviewed several NIR absorption compounds and described a number of Ni-based dithiolene complexes which show absorption at wavelengths > 700 nm. The long-wavelength absorption bands are observed in the case of Ni-dithiolene complexes, due to co-planarity of ligandπ-system, presence of an extended π-system and electron donating substituents. Some of the square planar neutral metal-dithiolene complexes exhibiting such strong absorption are shown in Scheme 1.4.

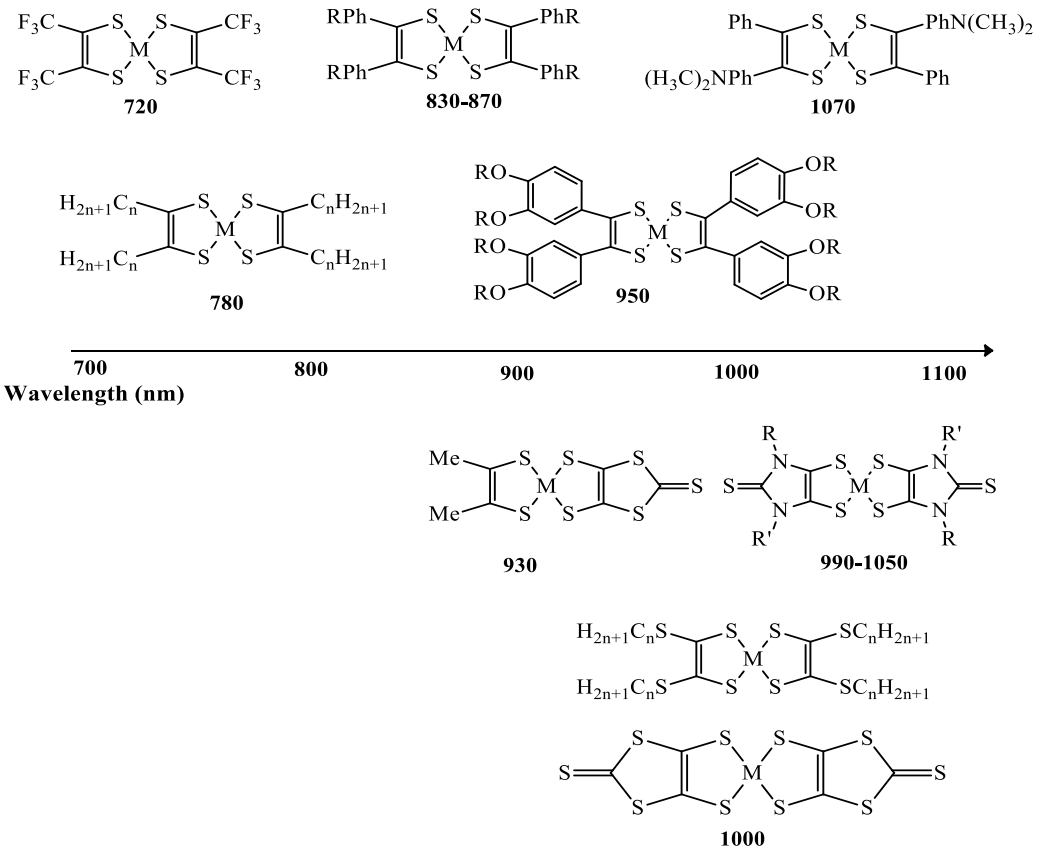


**Scheme 1.4.** Absorption area of various metal neutral bis-dithiolenes.

### 1.5. 2, 6–Bis(pyrazolyl)pyridine

Tridentate pyridine centered hetero aromatic ligands play an important role to prepare coordination frameworks that are used in different fields of research, such as, in supramolecular chemistry, coordination chemistry, magnetic materials, optoelectronics and photochemical application. Various tridentate coordinating motifs have been reported in the literature (Scheme 1.5).[15] Based on the position of C-N bond between pyridine and pyrazolyl ring, these heterocyclic molecules can be known as 2,6-bis(tetrazol-4-yl)pyridine (pytz), bis(1,2,4-triazolyl)pyridines (btp), 2,6-bis(oxazoline)-pyridine (pybox), 2,2;6'2''-terpyridine (terpy), 2,6-bis(pyrazol-1-yl)pyridine (bpp) and 2,6-di(pyrazol-3-yl)pyridine (3-bpp). These molecules readily coordinate to the transition metal ions and the resulting coordination complexes, that are formed, are highly stable, mostly with the formation of octahedron complexes. Herein, 2,6-bis(pyrazolyl)pyridine units are employed to create a new group of donor–acceptor molecules for various fluorescence applications and in synthesis of its Fe(II) coordination complexes.

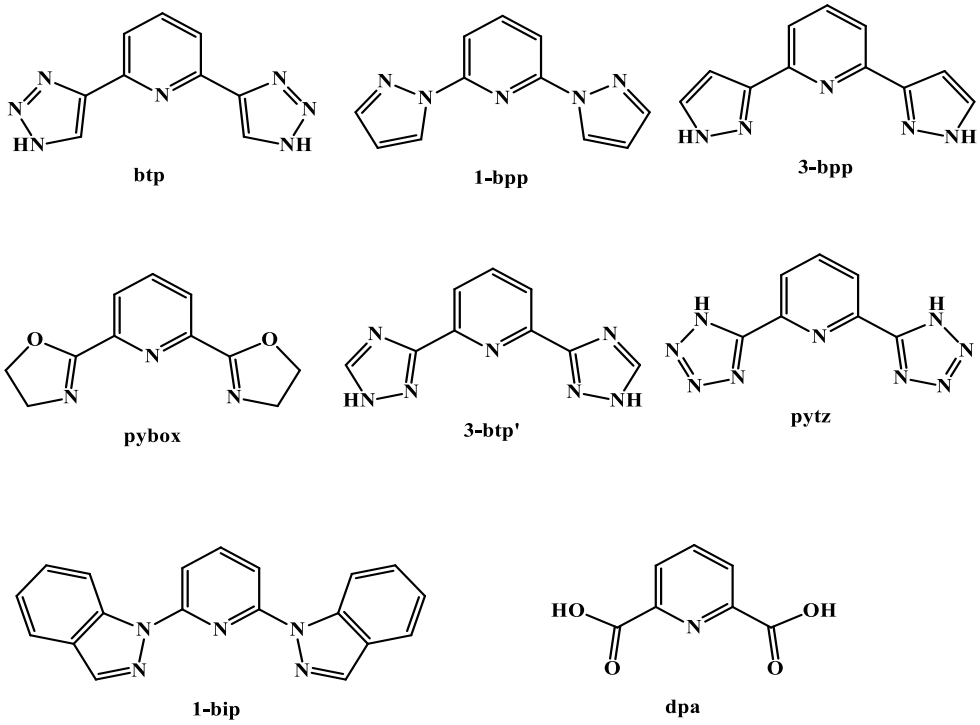


**Scheme 1.5.** Nitrogen containing tridentate ligands

### 1.5.1. Synthesis

2,6-bis(pyrazolyl)pyridines are different from terpyridine ligands in several essential ways.[16-18] For the synthesis of 2,6–bis(pyrazolyl)pyridine core moiety, used in different methodologies, is generated *in situ* reaction of 2,6–dihalopyridine (2,6-dibromo and 2,6-dichloropyridine) with sodium hydride (NaH) or potassium(K) metal.[19] In 1990, Goldsby and his co-workers,[20] for the first time, reported the synthesis of 2,6-bis(pyrazolyl)pyridine based ligands. Later on, this area is well-known for the synthesis of 2,6-bis(pyrazolyl)pyridine ligand containing metal complexes due to their structural similarity to the established tridentate ligands like bis(1,2,4-triazolyl)pyridine.

## 1.6. Metal 2,6–bis(pyrazolyl)pyridine complexes and application

In 2001, for the first time Halcrow and his co-workers[21] reported the metal complexes of nickel, cobalt, and copper with 2,6–bis(pyrazolyl)pyridine ligand. That time onwards, this area has further been explored in terms of synthesis and structural characterization and application in

various fields. Brunet and his coworkers[22,23] were studied water soluble pentetic acid substituted 2,6-bis(pyrazolyl)pyridine derivatives and corresponding metal (Eu(III) and Tb(III)) complexes which show high luminescence spectral properties. Interestingly, in their report, they also proposed the energy transfer from 2,6–bis(pyrazolyl)pyridine to lanthanide metal center. In 2006, Ruben and his coworkers[24] synthesized stable 1-D supramolecular Fe(II) metal complex with ligand center of various 2,6-bis(pyrazolyl)pyridine using head-to-tail supramolecular hydrogen bonding. In 2007, Halcrow and his co-workers[25] synthesized 2,6-bis(pyrazolyl)pyridines, substituted with different nucleobase substituents using $CH_2$-$CH_2$ spacer resulting in back-to-back coupled 2,6–bis(pyrazolyl)pyridine ligands.[26] Oshio *et al.*[27] established Fe(II) complexes of 2,6–bis(pyrazolyl)pyridines that support doublet state nitronyl nitroxide radicals. Finally, development of rare earth metal (Eu(III), Tb(III) and Yb(III)) complexes with 2,6-bis(pyrazolyl)pyridine ligands offer many applications in various fields of research, such as, near-infrared (NIR) emission, two-photon absorption spectroscopy and the development of radiant gels.

**1.7. Motivation of the present work**

The above description tells us that literature on complexes of 1,2–dithioleneis is vast. During the last few years, the field of ion-pair dithiolene complexes contain special class of compounds in metal–dithiolene chemistry. Interests have been grown in the synthesis of dithiolene complex anions with supramolecular chemistry with various cations. In this context, we have seen that the magnetism and conductivity properties are explored greatly. The application of dithiolene complexes as NIR dyes has also been demonstrated in details. The supramolecular interactions and related theoretical (DFT) studies based metal-dithiolene complexes, especially dithiolene complexes with oxidation state of nickel(III), have not been explored in that greater extent. This concept has motivated us to investigate/analyze the supramolecular interactions in the crystal structure of ion-pair dithiolene complexes of Ni(III). The relevant results have been reported in Chapter-2.

In 2010, Oshio and his co-workers[28] synthesized and studied the multiple bistability and tristability with dual spin conversions in the multicomponent mixed ion-pair systems of Fe(II)-bis(pyrazolyl)pyridine (as cation) and Ni(III)-maleonitriledithiolate metal complex as anion and it shows various bistability and tristability magnetism. Bistable magnetic materials are considered to be good candidates for molecular devices, such as sensors, switches, and

memories.[29] Not only magnetic materials but also development of several spectroscopic tools, interesting optical properties of the 2,6–bis(pyrazolyl)pyridine and applications of these compounds in optoelectronic devices have promoted us to synthesize of π–conjugated 2,6–bis(pyrazolyl)pyridines and to examine their optical behavior. We were also inspired to synthesize corresponding metal complex and relevant sensing studies. The relevant results have been reported in the Chapter–3 and Chapter–4.

Kom-Bei Shiu and coworkers[30] reported a series of crystals of 1,1"-1,4-phenylene-bis(methylene)bis-4,4'-bipyridinium $[C_{28}H_{24}N_4]^{2+}$ as cation receptor with counter anions ($Br^-$ and $PF_6^-$). They explained only the structural analysis and the supramolecular interactions between 1,1"-1,4-phenylene-bis(methylene)bis-4,4'-bipyridinium cation and hexafluorophosphate anions. In our study, we isolated an unusual intermediate conformation of 1,1"-1,4-phenylene-bis(methylene)bis-4,4'-bipyridinium$[C_{28}H_{24}N_4]^{2+}$ cation with different $PF_6^-$ anions as well as other regular conformers with $NO_3^-$ and $[Cu(mnt)_2]^{2-}$as anions. The stabilization of intermediate conformer supported by supramolecular hydrogen bond interactions is well explained by density functional theory calculations. The relevant results have been reported in the Chapter–5.

**1.8. References**

(1). McCleverty, J. A. Metal 1,2-Dithiolene and Related Complexes. *Progr. Inorg. Chem*, John Wiley & Sons, Inc.: **1968**; 49-221.

(2). Eisenberg, R. Structural Systematics of 1,1- and 1,2-Dithiolato Chelates. *Prog. Inorg. Chem*, John Wiley & Sons, Inc.: 1970; 295-369.

(3). Schrauzer, G. N.; Mayweg, V., Reaction of Diphenylacetylene with Nickel Sulfides. *J. Am. Chem. Soc.***1962**, *84*, 3221-3221.

(4). Smith, A. E.; Schrauzer, G. N.; Mayweg, V. P.; Heinrich, W., The Crystal and Molecular Structure of $MoS_6C_6H_6$. *J. Am. Chem. Soc.***1965**, *87*, 5798-5799.

(5). Eisenberg, R.; Ibers, J. A., Structure of Di(tetramethylammonium)bis(maleonitriledithiolate) nickelate(II). *Inorg. Chem.***1965**,*4*, 605-608.

(6). Davison, A.; Edelstein, N.; Holm, R. H.; Maki, A. H., E.s.r. Studies of Four-Coördinate Complexes of Nickel, Palladium and Platinum Related by Electron Transfer Reactions. *J. Am. Chem. Soc.***1963**,*85*, 2029-2030.

(7). Cowie, M.; Bennett, M. J., Trigonal-prismatic vs. octahedral coordination in a series of tris(benzene-1,2-dithiolato) complexes. Crystal and molecular structure of bis(tetramethylammonium) tris(benzene-1,2-dithiolato)zirconate(IV), $[CH_3)_4N]_2[Zr(S_2C_6H_4)_3]$. *Inorg. Chem.***1976**,*15*, 1595-1603.

(8). Coomber, A. T.; Beljonne, D.; Friend, R. H.; Bredas, J. L.; Charlton, A.; Robertson, N.; Underbill, A. E.; Kurmoo, M.; Day, P., Intermolecular interactions in the molecular ferromagnetic $NH_4Ni(mnt)_2$[middot] $H_2O$. *Nature* **1996**,*380*, 144-146.

(9). Ren, X. M.; Nishihara, S.; Akutagawa, T.; Noro, S.; Nakamura, T., Design of a Magnetic Bistability Molecular System Constructed by H-Bonding and π···π-Stacking Interactions. *Inorg. Chem.***2006**,*45*, 2229-2234.

(10). Robertson, N.; Cronin, L., Metal bis-1,2-dithiolene complexes in conducting or magnetic crystalline assemblies. *Coord. Chem. Rev.***2002**,*227*, 93-127.

(11). Chen, C.-T.; Liao, S.-Y.; Lin, K.-J.; Lai, L.-L.. Syntheses, Charge Distribution, and Molecular Second-Order Nonlinear Optical Properties of Push–Pull Bisdithiolene Nickel Complexes. *Adv. Mater.***1998**,*10*, 334-338.

(12). Kato, R., Conducting Metal Dithiolene Complexes: Structural and Electronic Properties. *Chem. Rev.***2004**, *104*, 5319-5346.

(13). Ren, X.; Meng, Q.; Song, Y.; Lu, C.; Hu, C.; Chen, X., Unusual Magnetic Properties of One-Dimensional Molecule-Based Magnets Associated with a Structural Phase Transition. Inorganic Chemistry 2002, 41 (22), 5686-5692.

(14).Mueller-Westerhoff, U. T.; Vance, B.; Ihl Yoon, D., The Synthesis of Dithiolene Dyes with Strong near-IR Absorption. *Tetrahedron* **1991**,*47*, 909-932.

(15).J. P. Byrne, J. A. Kitchenb, Gunnlaugsson, T. The btp [2,6-bis(1,2,3-triazol-4-yl)pyridine] Binding Motif: a new Versatile Terdentate Ligand for Supramolecular and Coordination Chemistry. Chem. Soc. Rev. **2014**, 43, 5302-5325.

(16). Halcrow, M. A., The synthesis and coordination chemistry of 2,6-bis(pyrazolyl)pyridines and related ligands — Versatile terpyridine analogues. *Coord. Chem. Rev.***2005**,*249*, 2880-2908.

(17). Halcrow, M. A., Iron(II) complexes of 2,6-di(pyrazol-1-yl)pyridines—A versatile system for spin-crossover research. *Coord. Chem. Rev.***2009**,*253*, 2493-2514.

(18). Olguín, J.; Brooker, S., Spin crossover active iron(II) complexes of selected pyrazole-pyridine/pyrazine ligands. *Coord. Chem. Rev.***2011**,*255*, 203-240.

(19). Vermonden, T.; Branowska, D.; Marcelis, A. T. M.; Sudhölter, E. J. R., Synthesis of 4-functionalized terdendate pyridine-based ligands. *Tetrahedron* **2003**, *59*, 5039-5045.

(20). Jameson, D. L.; Goldsby, K. A., 2,6-bis(N-pyrazolyl)pyridines: the convenient synthesis of a family of planar tridentate $N_3$ ligands that are terpyridine analogs. *J. Org. Chem.***1990**,*55*, 4992-4994.

(21). Solanki, N. K.; Leech, M. A.; McInnes, E. J. L.; Zhao, J. P.; Mabbs, F. E.; Feeder, N.; Howard, J. A. K.; Davies, J. E.; Rawson, J. M.; Halcrow, M. A., The effects of distal ligand substitution on the copper(II)/bis-(2,6-dipyrazol-1-ylpyridine) centre. *J. Chem. Soc. Dalt. Trans.***2001**,14, 2083-2088.

(22). Brunet, E.; Juanes, O.; Sedano, R.; Rodríguez-Ubis, J.-C., Synthesis of Novel Macrocyclic Lanthanide Chelates Derived from Bis-pyrazolylpyridine. *Org. Lett.***2002**,*4*, 213-216.

(23). Chryssou, K.; Stergiopoulos, T.; Falaras, P., Synthesis and spectroscopic properties of a new bipyridine-bipyrazoyl(pyridine)-thiocyanato-ruthenium(II) complex. *Polyhedron* **2002**,*21*, 2773-2781.

(24). Rajadurai, C.; Schramm, F.; Brink, S.; Fuhr, O.; Ghafari, M.; Kruk, R.; Ruben, M., Spin Transition in a Chainlike Supramolecular Iron(II) Complex. *Inorg. Chem.***2006**,*45*, 10019-10021.

(25). Elhaïk, J.; Pask, C. M.; Kilner, C. A.; Halcrow, M. A., Synthesis of 2,6-di(pyrazol-1-yl)-4-bromomethylpyridine, and its conversion to other 2,6-di(pyrazol-1-yl)pyridines substituted at the pyridine ring. *Tetrahedron* **2007**,*63*, 291-298.

(26). Rajadurai, C.; Qu, Z.; Fuhr, O.; Gopalan, B.; Kruk, R.; Ghafari, M.; Ruben, M., Lattice-solvent controlled spin transitions in iron(ii) complexes. *Dalt. Trans.***2007**, 32, 3531-3537.

(27). Nihei, M.; Han, L.; Oshio, H., Magnetic Bistability and Single-Crystal-to-Single-Crystal Transformation Induced by Guest Desorption. *J. Am. Chem. Soc.***2007**,*129*, 5312-5313.

(28). Nihei, M.; Tahira, H.; Takahashi, N.; Otake, Y.; Yamamura, Y.; Saito, K.; Oshio, H., Multiple Bistability and Tristability with Dual Spin-State Conversions in $[Fe(dpp)_2][Ni(mnt)_2]_2 \cdot MeNO_2$. *J. Am. Chem. Soc.***2010**,*132*, 3553-3560.

(29). Sato, O.; Tao, J.; Zhang, Y. Z., Control of magnetic properties through external stimuli. *Ang. Chem. Int Ed Engl* **2007**,*46*, 2152-87.

(30). Liu, S.-A.; Kuo, T.-S.; Lee, G.-H.; Shiu, K.-B., Sensitivity in Supramolecular Architectures of Polyaromatic Salts Containing Two Singly-Pimerized Bipyridines. *J. Chin. Chem. Soc.***2007**, *54* , 607-611.

# 2

# Bis(quinoxaline-dithiolato)nickel(III) Complexes $[Bu_4N][Ni^{III}(6,7\text{-qdt})_2]$ and $[Ph_4P][Ni^{III}(Ph_2 6,7\text{-qdt})_2]\cdot CHCl_3$ (6,7-qdt = Quinoxaline-6,7-dithiolate; $Ph_2$6,7-qdt =Diphenylquinoxaline-6,7-dithiolate): Synthesis, Spectroscopy, Electrochemistry, DFT Calculations, Crystal Structures and Hirshfeld Surface Analysis

**Abstract:–** The synthesis and crystal structure analyses of two square planar nickel(III)-bis(quinoxalene-6,7-dithiolate) compounds with formulae $[Bu_4N][Ni(6,7\text{-qdt})_2]$ (**1**) and $[Ph_4P][Ni(Ph_2 6,7\text{-qdt})_2].CHCl_3$ (**2**) have been described. The solution state electronic absorption bands for compounds **1** and **2**, observed in the near-infrared region for compounds **1** and **2** can be explained by density functional theory calculations. Compounds **1** and **2** undergo reversible one electron redox processes at $E_{1/2}$ = +0.084V and $E_{1/2}$= +0.01V vs Ag/AgCl respectively in dimethylformamide solutions. Compounds **1** and **2** undergo reversible one electron redox processes at $E_{1/2}$ = +0.084V and $E_{1/2}$= +0.01 V vs Ag/AgCl respectively in dimethylformamide solutions. The crystal structures of the title compounds exhibit weak C–H···S and C–H···N hydrogen bonding interactions and anion-anion interactions. Solid state and low temperature ESR spectrum of compound **1** and **2** show the g-values, that are consistent for a S = 1/2 system (when Ni (III) is in a low spin state).

## 2.1. Introduction

Metal-dithiolene complexes have been offering considerable interests to synthetic inorganic chemists for more than four decades. In recent time, the design and synthesis of metal bis(dithiolene) complexes have drawn great attention because of their potential applications as conducting- and magnetic,[1-3] nonlinear optical- materials[4-5] and near-infrared (NIR) dyes**.**[6-11] Square planar bis(dithiolene) metal coordination complexes are generally characterized by high degree of delocalization within the chelate ring involving the metal ion that considerably contributes to the low energy electronic transition between the HOMO and the LUMO.[12] This large delocalization is responsible for metal dithiolene complexes to show an absorption band in the near–infrared (NIR) region. Last several years, we and others have been working on transition metal-dithiolene coordination complexes in the perspective of supramolecular chemistry[13-18] as well as bioinorganic chemistry.[19-23] Recently we have reported the influence of substituents of coordinated dithiolate ligands on the electronic- and electrochemical properties of a new square-planar nickel(II)-bis(quinoxaline-6,7-dithiolate) system.[24] These ligands, because of their non-innocent behaviour, can stabilize a coordination complex in several oxidation states of the pertinent metal. Generally, the anionic state ($M^{II}$ oxidation state) is the most stable state for bis(dithiolene) complexes, but in some cases, they can be isolated as monoanionic ($M^{III}$ oxidation state) or even as neutral complexes ($M^{IV}$ oxidation state). Ni(III)-dithiolene complexes are of special interests because of their importance in the context of bioinorganic chemistry[25] and catalysis[26] The bioinorganic aspect of nickel(III)-dithiolene complexes can be described by modelling the active sites of [NiFe]$H_2$ase, for which the EXAFS/EPR studies indicate that the formal oxidation state of the Ni center in the resting state of the active site is paramagnetic Ni(III).[25] The catalytic importance of Ni(III) coordination complexes can be recognized by the fact that recently nickel(III) complexes have been employed as catalysts in C−C and C−heteroatom bond formation reactions[26]. This prompted us to explore Ni(III) coordination complexes. The present work deals with two nickel(III)-dithiolene complexes $[Bu_4N][Ni(6,7–qdt)_2]$ (**1**) and $[Ph_4P][Ni(Ph_26,7–qdt)_2]\cdot CHCl_3$ (**2**). Scheme 2.1 shows the molecular structures of the ligands and resulting coordination complexes in compounds **1** and **2**. We have described here synthesis, crystal

structures, spectroscopy and electrochemistry of compounds **1** and **2** including their DFT calculations and Hirshfeld surface analyses of the complex anions.

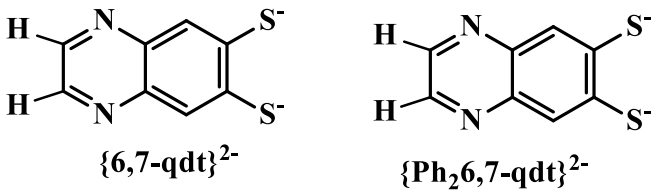


**(a)**

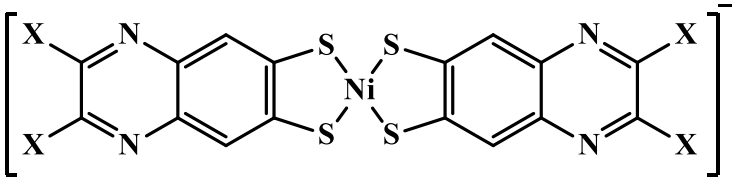


**X= H and Ph**

**(b)**

**Scheme 2.1.** (a) Structural representations of quinoxaline dithiolate ligands; (b) general molecular structural representation of synthesized nickel(III)-bis(quinoxaline-6,7-dithiolato) system**.**

## 2.2. Experimental

### 2.2.1. Material and Methods

All the chemicals for the synthesis were commercially available and used as received. 1,2-Diaminobenzene-bis(thiocyanate) (**A**),[27] quinoxaline-6,7-dithiol($H_2$6,7-qdt)(**$L_1$**), [$Bu_4N$]$_2$[Ni(6,7-qdt)$_2$] (**1a**), diphenyl-6,7-dithiol (**$L_2$**)[24], and [$Ph_4P$]$_2$[Ni($Ph_2$6,7–qdt)$_2$] [24] were prepared according to literature procedures. Syntheses of metal complexes were performed under $N_2$ using standard inert atmosphere techniques. Solvents were dried by standard procedures. Microanalytical (C, H, N) data were obtained with a FLASH EA 1112 Series CHNS Analyzer. Infrared (IR) spectra were recorded on KBr pellets with a JASCO FT/IR-5300 spectrometer in the region of 400-4000cm$^{-1}$. $^1$H NMR spectra of compounds were recorded on Bruker DRX- 400 spectrometer using Si($CH_3$)$_4$ (TMS) as an internal standard. Electronic absorption spectra of solutions and diffuse reflectance spectra of solid compounds were recorded on a UV-3600 Shimadzu UV-Vis-NIR spectrophotometer. A Cypress model CS-1090/CS-1087 electroanalytical system was used for cyclic voltammetric experiments. The electrochemical experiments were measured in

DMF containing $[Bu_4N][ClO_4]$ as a supporting electrolyte, using a conventional cell consisting of two platinum wires as working and counter electrodes, and an Ag/AgCl electrode as the reference. The potentials reported here are uncorrected for junction contributions.

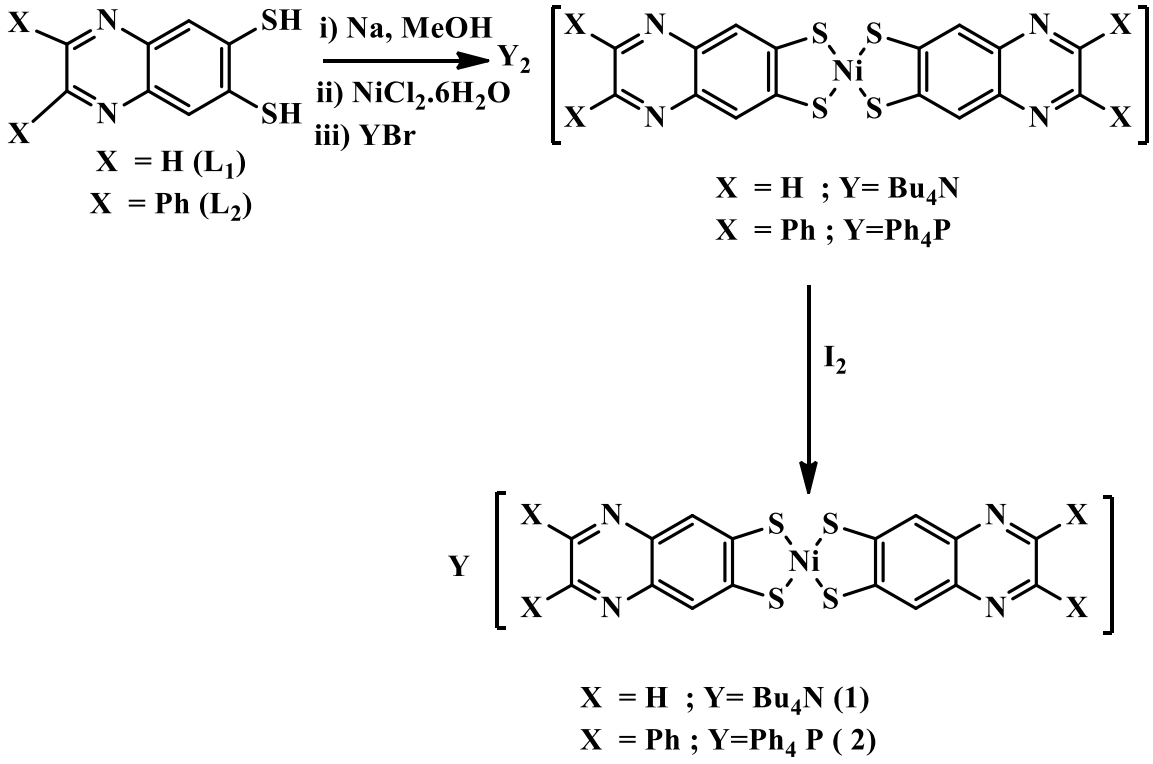


**Scheme 2.2.** Synthesis of Ni(III)-bis(6,7–quinoxaline-dithiolato) compounds **1** and **2.**

### 2.2.2. Synthesis

**Synthesis of compound $[Bu_4N][Ni(6,7\text{-qdt})_2]$ (1) :**

The monoanionic compound **1** was obtained as a brown powder by $I_2$ oxidation of the corresponding $[Bu_4N]_2[Ni^{II}(6,7\text{-qdt})_2]$ complex. To a filtered solution of $[Bu_4N]_2[Ni^{II}(6,7\text{-qdt})_2]$ (0.185g, 0.2 mmol) in 20 mL $CH_3CN$, a solution of $I_2$ (0.025g, 0.1 mmol) in 10 mL $CH_3CN$ was added dropwise and then allowed to stir for 2 hours at room temperature. The resulting brown precipitate was filtered and washed with a little amount of methanol and hexane. Single crystals, suitable for X-ray diffraction, were grown by slow diffusion of diethyl ether into a $CH_3CN$ solution of the obtained solid. Yield 72% (0.135g). IR(KBr, $cm^{-1}$): 3435, 1616, 1446, 1353, 1178, 1019, 980, 876, 613.

**Synthesis of compound $[Ph_4P][Ni(Ph_2$6,7-qdt$)_2]$ (2):**

The monoanionic compound **2** was obtained as a dark brown powder by $I_2$ oxidation of the corresponding $[Ph_4P]_2[Ni^{II}(Ph_2$6,7-qdt$)_2]$ complex. To a filtered solution of $[Ph_4P]_2[Ni(Ph_2$6,7-qdt$)_2]$ (0.284g 0.2mmol) in 20 mL $CH_3CN$, a solution of $I_2$ (0.025 g, 0.1 mmol) in 10mL of $CH_3CN$ was added dropwise, and allowed to stir for 2h at room temperature. The resulting dark brown powder precipitate was filtered and washed with a little amount of MeOH and hexane. Single crystals, suitable for X-ray diffraction, were grown by slow diffusion of diethyl ether into a $CHCl_3$ solution of the obtained dark brown powder. Yield 75% (0.213 mg). IR (KBr,$cm^{-1}$): 3441, 1578, 1453, 1336, 1249, 1200, 1112, 1079,1046,1024, 865, 827, 723, 690.

### 2.2.3. Single Crystal X-ray determination of the compounds 1 and 2

**X-ray crystallography**

Single crystals, suitable for facile structural determination for the compounds **1** and **2** were measured on a three circle Bruker SMART APEX CCD area detector system under Mo–Kα ($\lambda$ = 0.71073 Å) graphite monochromatic X–ray beam. The frames were recorded with an ω scan width of 0.3º, each for 10s, with crystal-detector distance of 60 mm, collimator 0.5 mm. Data reduction was performed by using SAINTPLUS.[28] Empirical absorption corrections were made using equivalent reflections performing SADABS program. The Structures were solved by direct methods and least-square refinement on $F^2$ for both compounds were made by using SHELXS-97.[28] All non-hydrogen atoms were refined anisotropically. The hydrogen atoms were included in the structure factor calculation by using a riding model. The crystallographic parameters, data collection and structure refinement of the compounds **1** and **2**are summarized in Table 2.1. Selected bond lengths and angles for the compounds **1** and **2** are listed in Table 2.2.

## 2.3. Results and discussion

### 2.3.1. Synthesis

The synthetic route for the synthesis of two dithiolate-ligands, used in this study (**$L_1$** and **$L_2$**) is been shown in Scheme 2.2. The synthesis of corresponding Ni(II)-(bis)dithiolato complexes $[Bu_4N]_2[Ni^{II}$(6,7–qdt$)_2]$ and $[Ph_4P]_2[Ni^{II}(Ph_2$6,7–qdt$)_2]$ has been performed by a procedure, reported earlier as shown in Scheme 2.3.[24] The electrochemical studies of these two Ni(II) compounds demonstrate that they can be oxidized at a lower potential to

the corresponding one-electron oxidized compounds $[Bu_4N][Ni^{III}(6,7–qdt)_2]$ (**1**) and $[Ph_4P][Ni^{III}(Ph_26,7–qdt)_2]\cdot CHCl_3$ (**2**). Accordingly, we have synthesized compounds **1** and **2** by chemical oxidation of $[Bu_4N]_2[Ni^{II}(6,7–qdt)_2]$and $[Ph_4P]_2[Ni^{II}(Ph_26,7–qdt)_2]$ respectively by iodine as shown in Scheme 2.2.

### 2.3.2. Description of Crystal Structures

**$[Bu_4N][Ni\ (6,7\text{-}qdt)_2]$ (1):**

The crystals of compound **1**, suitable for single crystal X-ray structure determination, were obtained from acetonitrile solution by the vapor diffusion of diethyl ether. Crystallographic analysis reveals that compound **1** crystallizes in monoclinic system with space group $P2_1/c$. The relevant asymmetric unit contains two crystallographically independent halves of $[Ni(6,7\text{-}qdt)_2]^{2-}$ molecule and one molecule of tetrabutylammonium cation. Thermal ellipsoid diagram of the asymmetric unit in the crystal structure of compound **1** is shown in Figure 2.1a. The relevant molecular packing diagram is shown in Figure 2.1b. The basic crystallographic data (compound **1**) are presented in Table 2.1 and selected bond angles and interatomic distances are described in Table 2.2. The geometry around nickel ion in both crystallographically independent complexes is roughly square planar, contributed by four sulfur donor atoms from two 6,7-$qdt^{2–}$dithiolato ligands.

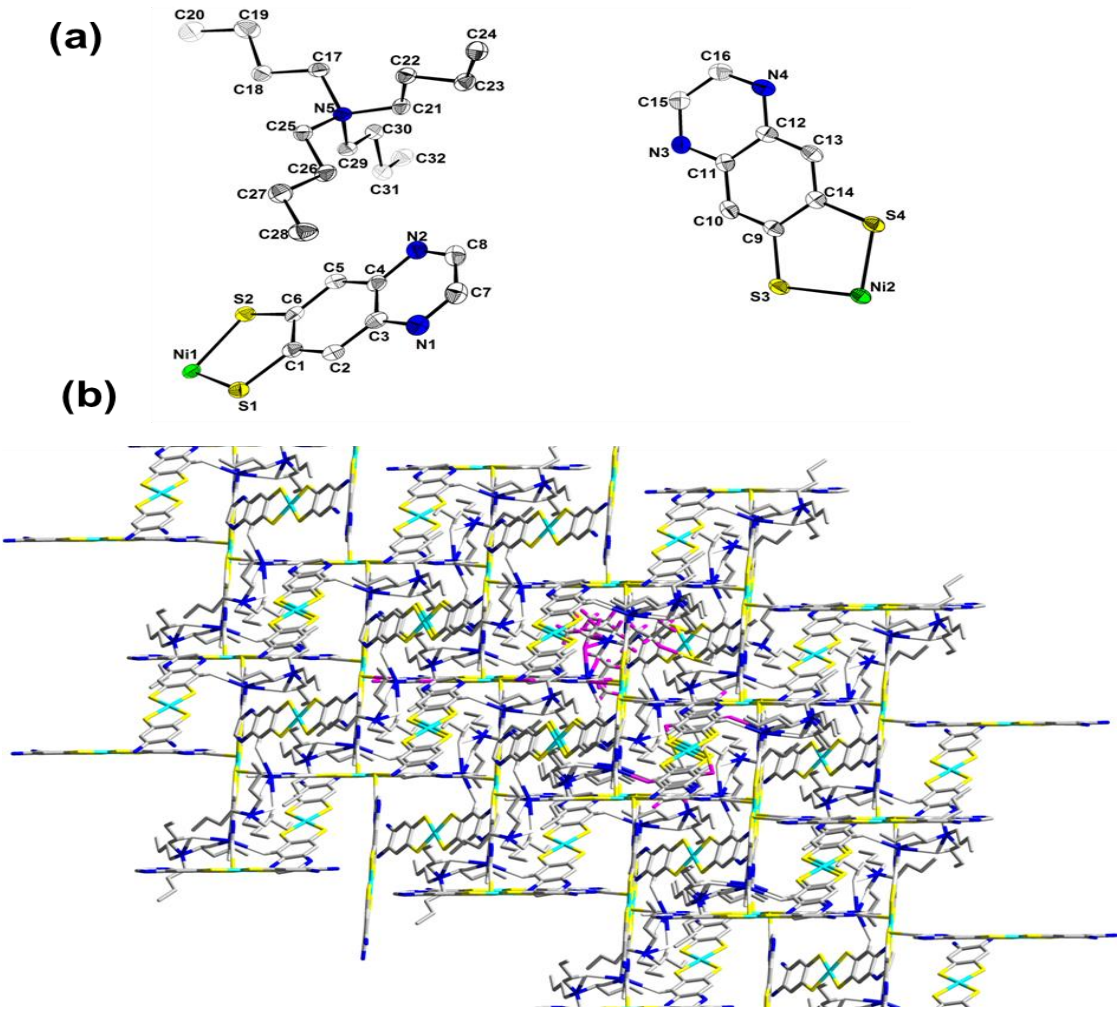


**Figure 2.1.** (a) Thermal ellipsoidal plot (50% probability) of the asymmetric unit in the crystal structure of compound **1** (hydrogen atoms are omitted for clarity). (b) Molecular packing diagram in the crystal structure of compound **1**.

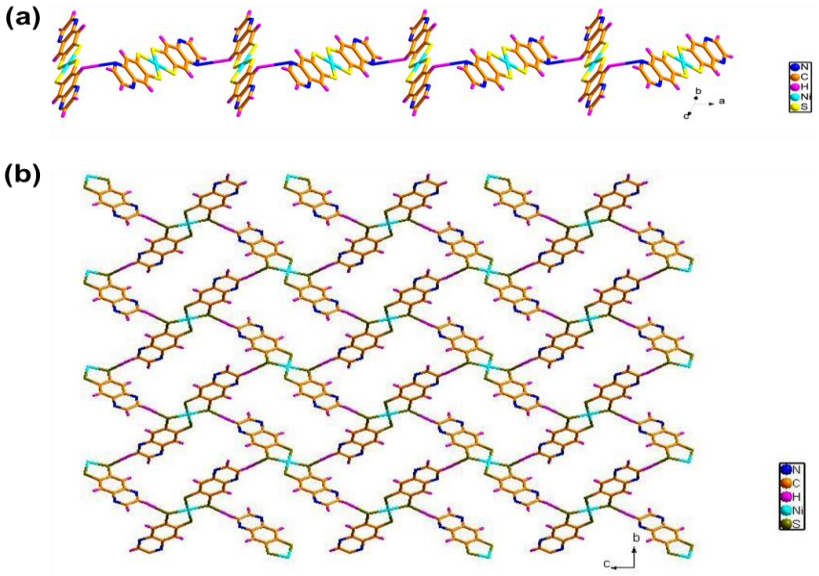


**Figure 2.2.** (a) Inter-molecular one-dimensional supramolecular chain of $[Ni(6,7\text{-qdt})_2]^{1-}$ formed by C–H···N weak interactions. (b) Two- dimensional supramolecular layer-like structure, formed by inter-anion C–H···S weak interaction in compound **1** (viewed along crystallographic a-axis).

The relevant coordination angles are in the range of $87.77(3)^0$ – $92.23(3)^0$ (see Table 2.2). In the five-membered chelate rings involving the nickel ion, the Ni-S, C-S, and C=C bond lengths are in the range of 2.1431(7) – 2.1555(7)Å, 1.737(3) –1.746(3) Å and 1.423(4)-1.426(4)Å respectively. The total charge of Ni(III) complex anion $[Ni(6,7\text{-qdt})_2]^{1-}$ in compound $[Bu_4N][Ni(6,7\text{-qdt})_2]$ (**1**) is unsurprisingly -1, and this anionic charge is compensated by a $[Bu_4N]^+$ cation as observed in the crystal structure (Figure 2.1a). In order to investigate the supramolecular structure, we looked into C–H---S and C–H---N interactions in the crystal structure of compound **1**. We found that a supramolecular chain-like arrangement (Figure 2.2a) is formed from anion-anion C–H---N interactions. On the other hand, inter anion C–H---S hydrogen bonding interactions are responsible for the formation of a two-dimensional layer-like supramolecular arrangement (Figure 2.2b). Hydrogen bonding parameters in the crystal structure of compound **1** are shown in Table 2.2.

**$[PPh_4][Ni(Ph_26,7\text{-}qdt)_2]\cdot CHCl_3$ (2):**

The crystals of compound $[Ph_4P][Ni(Ph_26,7\text{-}qdt)_2]\cdot CHCl_3$ (**2**), suitable for single crystal X-ray structure determination, were obtained from $CHCl_3$ solution by vapor diffusion of diethyl ether. Compound **2** crystallizes in triclinic space group P-1. The concerned asymmetric unit consists of two crystallographically independent halves of $[Ni(Ph_26,7\text{-}qdt)_2]^{2-}$complex anion and one molecule of tetraphenyl phosphonium cation along with a solvent molecule as shown Figure 2.3a. The geometry around the $Ni^{3+}$ ion, which is coordinated by four sulfur atoms from two $Ph_26,7\text{-}qdt^{2-}$ ligands, shows square planar geometry with S1N2S2 and S3Ni1S4 coordination angles of 92.17(11)$^o$ and 92.03(12) respectively from two different crystallographically independent molecules. In the five-membered coordinated chelate rings including both crystallographically independent molecules, the Ni-S, C-S, and C=C bond lengths are in the range of 2.1431(7) – 2.1555(7) Å, 1.711(3) –1.740(3) Å and 1.407(4) –1.419(4) Å respectively.

The crystal structure of the compound **2** is also characterized by C–H···N and C–H···S supramolecular hydrogen bonding interactions. The inter-anion C–H···N weak interactions lead to the formation of the one-dimensional chain like structure as shown in Figure 2.3b. On the other hand, the C–H···S hydrogen bonding interactions between the complex anions and tetraphenyl phosphonium cations lead to the construction of sandwich-type extended arrangement as shown in Figure 2.3c.

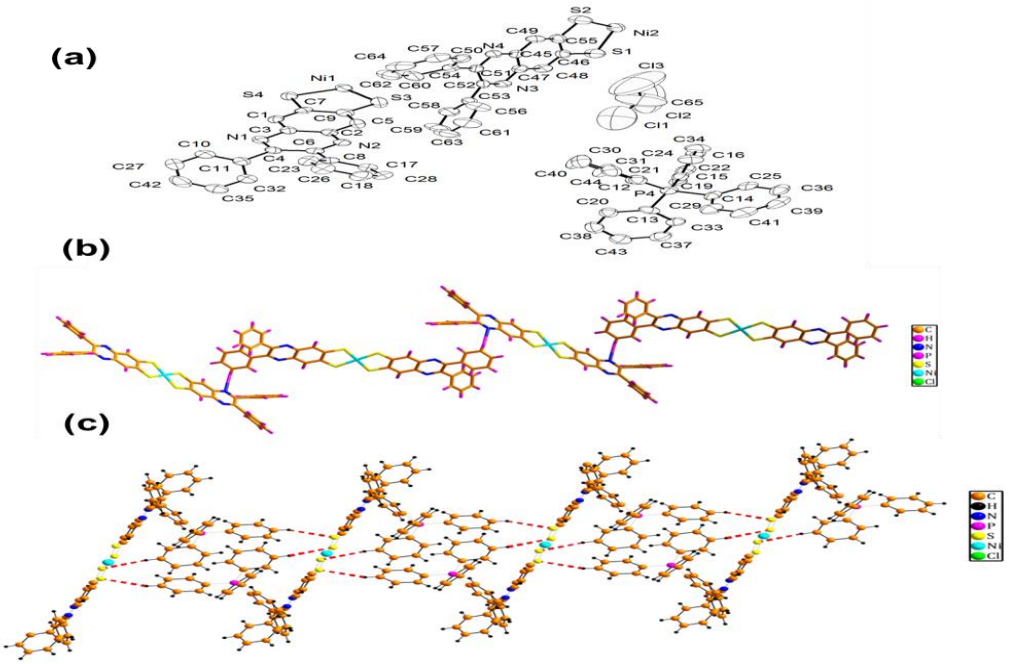

**Figure 2.3.** (a) Thermal ellipsoidal diagram of compound **2** (50% probability), H atoms have been omitted for clarity. (b) One-dimensional supramolecular chainlike arrangement formed inter anion interactions in the crystal structure of compound **2**, (c) Supramolecular chainlike structure, formed by C–H...S weak interactions in compound **2**.

### 2.3.3. Hirshfeld Surface Analysis

The hydrogen bonding supramolecular interactions around the complex anions $[Ni^{III}(6,7–qdt)_2]^{1-}$ and $[Ni^{III}(Ph_26,7–qdt)_2]^{1-}$ are further analysed by the Hirshfeld surfaces (HSs) and 2D finger print plots (FPs), which are generated by using Crystal explorer 3.1,[29-32] based on the CIF file. The 3D Hirshfeld surfaces offer additional insight into the long and short range interactions experienced by the complex anions, and 2D fingerprint plot, derived from the HSs, furnishes the nature, type and relative contribution of the intermolecular interactions.Generally, the directions and strengths of intermolecular interactions within the crystal are mapped onto the HSs defining a descriptor '$d_{norm}$', which is a ratio of the distance of any surface point to the nearest interior ($d_i$) and theexterior ($d_e$) atom to the van-der-Waals radii (vdW) of the concerned atoms. This, when $d_{norm}$is negative, the sum of $d_i$ and $d_e$, *i.e.*the contact distance, is shorter than the sum of the relevant van-der Waals radii, which is considered to be the closest contact and is visualized as red spots on the HSs as shown in Figure 2.4a. The white and blue color indicate the contacts at vdW separation ($d_{norm}$= 0) and at longer than thevdW sum (when $d_{norm}$is positive). The intermolecular contacts contained in Tables 2.2 is effectively summarized in spots of Hirshfeld surfaces; the large circular depressions (deep red), which are visible on the $d_{norm}$ surfaces, are an indicator of hydrogen bonding contacts. The small extent of area and light color on the surfaces indicate weaker and longer contacts other than hydrogen bonds. A plot of *d*i versus *d*e is a 2D fingerprint plot (Figure 2.4b) which identifies the occurrence of different kinds of intermolecular interactions. Complementary regions are visible in the fingerprint plots, where one molecule acts as a donor ($d_e > d_i$) and the other as an acceptor ($d_e < d_i$). The N···H closed contacts vary from 13.9% in compound **1** to 5.5% in compound **2**. The C···H contacts are varied from 20.5% in compound **1** to 15.6% in compound **2**. The S···H weak contacts vary from 21.8% in compound **1** to 8.4% in compound **2** (*vide infra*).

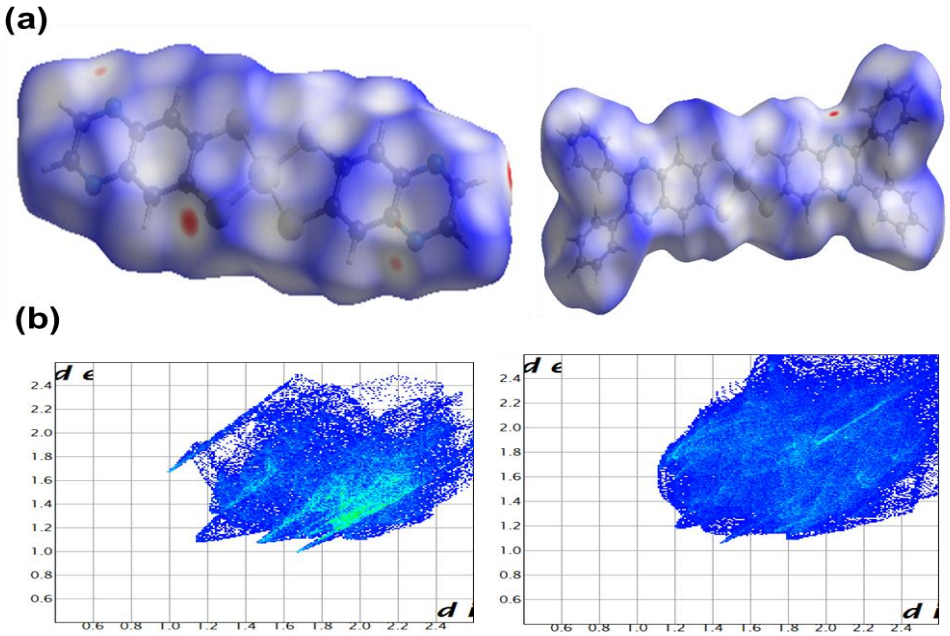


**Figure 2.4.** (a) Hirshfeld surfaces of the complex anions in compound **1** (top-left) and in compound **2 (**top-right**)**. (b) 2D Finger plots derived from HSs: compound **1** (bottom-left) and compound **2** (bottom-right).

### 2.3.4. UV–Vis–NIR Spectra

The UV–Vis–NIR spectra of compound **1** and its parent compound $[Bu_4N]_2[Ni^{II}(6,7–qdt)_2]$ are shown in Figure 2.5(a). The electronic spectra of compound **2** and its corresponding parent compound $[Ph_4P]_2[Ni^{II}(Ph_26,7–qdt)_2]$ in DMF solutions are shown in Figure 2.5(b). In our earlier report, we assigned the absorption bands at 619 nm and 662 nm in DMF solutions for parent Ni(II)-compounds $[Bu_4N]_2[Ni^{II}(6,7–qdt)_2]$ and $[Ph_4P]_2[Ni^{II}(Ph_26,7–qdt)_2]$ respectively to mixed-metal ligand-to-ligand charge transfer transitions based on DFT calculations because relevant HOMOs include metal-mixed ligand-based orbitals and LUMOs were defined as ligand-based π-MOs.[24] Careful observations of these spectra include the appearance of weak features beyond 800 nm, which was explained by the presence of oxidized impurities (corresponding Ni(III) complexes), formed by aerial oxidation of $[Bu_4N]_2[Ni^{II}(6,7–qdt)_2]$ and $[Ph_4P]_2[Ni^{II}(Ph_26,7–qdt)_2]$ having very low oxidation potentials. Thus when we oxidize these two Ni(II) complexes $[Bu_4N]_2[Ni^{II}(6,7–qdt)_2]$ and $[Ph_4P]_2[Ni^{II}(Ph_26,7–qdt)_2]$ chemically by iodine and isolate compounds $[Bu_4N][Ni(6,7\text{-}qdt)_2]$ (**1**) and $[Ph_4P][Ni(Ph_26,7\text{-}qdt)_2]\cdot CHCl_3$ (**2**), we observe that the absorption bands at 619 and 662 nm for compounds $[Bu_4N]_2[Ni^{II}(6,7–qdt)_2]$ and $[Ph_4P]_2[Ni^{II}(Ph_26,7–qdt)_2]$ respectively

disappear. At the same time, the broad bands at ~853 nm (ε = 16320 L $mol^{-1}cm^{-1}$) and ~530 nm (ε = 14280 L $mol^{-1}cm^{-1}$) appear for compound **1** as shown in Figure 2.5(a). Similarly for compound **2**, the absorption bands appear at ~880 nm (ε = 8160 L $mol^{-1}cm^{-1}$) and ~554 nm (ε = 12440 L $mol^{-1}cm^{-1}$) as shown in Figure 2.5(b). Compounds exhibit well-defined electronic absorption bands that are corroborated with theoretical (DFT) calculations. This is one of the rare reports, where theoretical calculations have been performed on a Ni(III)-bis(dithiolato) system.

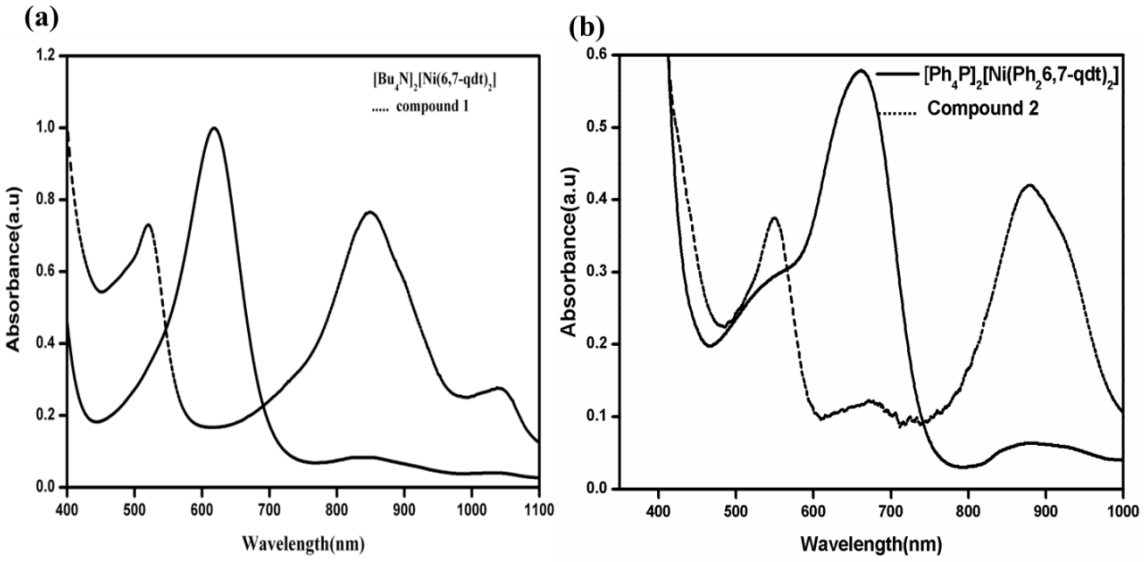


**Figure 2.5.** (a) UV-vis-NIR spectra of compound **1** ($3.42\times10^{-5}$ M) and corresponding parent compound $[Bu_4N]_2[Ni(6,7–qdt)_2]$(normalized) in DMF solutions. (b) UV-vis-NIR spectra of compound **2** ($5.4\times10^{-5}$ M) and corresponding parent compound $[Ph_4P]_2[Ni(Ph_26,7–qdt)_2]$ ($7.1\times10^{-5}$ M) in DMF solutions.

### 2.3.5. DFT calculations

**Computation**

Computational details for the groundstate, as well as the excited state electronic structure calculations of the complex anions of compounds **1** and **2**, have been performed with the help of well-known Density Functional Theory (DFT) by using GAUSSIAN-09 suite programming package.[33] It is well known that the DFT can evaluate the ground state electronic structure of a moiety (especially for bigger molecule e.g., a coordination complex anion) exactly depending upon the functional used in the procedure. Theoretical performance throughout the study has been done with one of the best hybrid functionals, B3LYP, where Hartree-Fock (HF) exchange, as well as DFT exchange correlations, are included. Non-local correlation part is taken care by Lee, Yang and Parr (LYP) functional. The LanL2DZ basis set was usedfor Ni; whereas for other atoms, 6-311G** basis set is used. Relativistic and other effects of the core electrons of the Ni atom have been taken care by inbuilt effective corepotential (ECP) LanL2 of LanL2DZ basis set. It should be mentioned that polarization effect on C, S and N has been taken care by incorporating five *d-type* Gaussian polarization functions into the basis set, whereas for H atom three *p-type* polarization functions are included. The ground state electronic structure calculation of the complex anions are performed by Self-consistent reaction field (SCRF) procedure of GAUSSIAN-09 programming package,[33] where solute complex ions are placed in the cavity of solvent (DMF). The ground state anionic complexes are obtained by full geometry optimization followed by frequency calculations. No imaginary frequencies are obtained, which ensures that the optimized structure is not situated at any saddle point of the ground state potential energy surface. Vertical excitations of the optimized structures are performed by TD-B3LYP method[34] using the same basis sets and same environment mentioned above.

We performed the ground state electronic structure calculations for mono anions of compound **1** and compound **2** using density functional theory (DFT) (see computational details in the experimental section), as implemented in Gaussian-09 program module. [33] Due to the odd number of total electrons ($Ni^{III}$ ion, $d^7$ system), we found singly occupied α-spin HOMO for both complex anions; at the same time, the comparable β-spin MO is vacant. Experimentally we found an observed absorption band for compound $[Bu_4N][Ni(6,7–qdt)_2]$ (**1**) at 1060 nm. From the theoretical vertical excitation by TD-DFT method, this low energy absorption has originated from the β-spin HOMO to β-spin LUMO transition, (Figure 2.6a (A)); the theoretical value of this band is approximately

1272 nm as shown in Figure 2.6a(A). The low intensity of this band (Figure 2.5a, dotted line) is explained by its low oscillator strength (*f* value) of 0.0172. The second high-intensity observed absorption band of compound **1** appeared at 853 nm (Figure 2.5a, dotted line), which can theoretically be attributed to the β-spin HOMO-2 to β-spin LUMO transition as shown in Figure 2.6a(B). The theoretical value of this band is approximately 985 nm with high oscillator strength of 0.2841. This transition at 853 nm (compound **1**) is also contributed by the transition from α-spin HOMO-6 to α-spin LUMO (Figure 2.6a(C). The former transition (β-spin HOMO-2 to β-spin LUMO) has maximum 88% impact on the total absorption and later transition (α-spin HOMO-6 to α-spin LUMO, Figure 2.6a(C) has 12% contribution to the total absorption at 853 nm (theoretical value 985 nm). The third experimental absorption band of compound **1**, which appears at 530 nm (Figure 2.5a, dotted line), cannot be explained properly by DFT calculation, because the corresponding theoretical value (553 nm) is characterized by a poor oscillator strength (0.0001), even though the observed absorption (at 530 nm) is an intense band. The nickel ion does not have any significant role in the low-energy absorption at 1060 nm (Figure 2.5a, dotted line) of compound **1** (theoretical value 1272 nm) as shown in Figure 2.6a(A). On the other hand, for the highly intense observed band at 853 nm (theoretical value 985 nm), central metal (nickel) ion plays a crucial role (see Figure 2.6a(B) and 2.6a(C). As shown in Figure 2.6(a)B, β-spin HOMO-2 is of π type character and β-spin LUMO is of π* type character. We also find a contribution of the central metal (nickel) in the HOMOs (both HOMO-2 and HOMO-6) and high electron density in the π* orbitals of dithiolate ligands in the LUMOs. Since both the HOMOs (Figure 2.6(a)B and 2.6(a)C) include metal-mixed ligand-based orbitals, we can say that the major transition (853 nm) is a "mixed-metal ligand-to-ligand" (MMLL) charge transfer transition.[24]

Next we concentrate our focus on compound $[Ph_4P][Ni(Ph_2$6,7–qdt$)_2]$ (**2**). A noticeable red shift of major intense peak is observed in the case of compound **2** compared to that of compound $[Bu_4N][Ni(6,7\text{-qdt})_2]$ (**1**). Experimentally the most intense absorption band is observed at 880 nm for compound **2**, which is 30 nm far away from the most intense peak of compound **1**. The theoretical value of this observed band at 880 nm is 1071 nm with *f value* of 0.4736. This theoretical peak is attributed mainly to the transition from β-spin HOMO-3 to β-spin LUMO (Figure 2.6b), which has 80% contribution to the total observed absorption band at 880 nm. The rest contributions arise from β-spin HOMO-5 to β-spin LUMO (11%, Figure 2.6b (B) and from α-spin HOMO-7 to α-spin LUMO (9%,

Figure 2.6b(C) transitions. The other major absorption of compound **2**, for which the observed (554 nm), as well as theoretical (553) valuses, are almost identical, is attributed to the transition from β-spin HOMO-5 to β-spin LUMO having 54% contribution to the total absorption at 554 nm (Figure 2.6b(B), which also takes part in previous absorption (880 nm) as mentioned earlier. As shown in Figure 2.6b, it is clearly evident that maximum electron density cloud is situated around the central metal ion nickel, which indicates that central metal ion has aconsiderable contribution to the electronic absorption at 880 nm (compound **2**). Lateral overlap in HOMO-3 (see Figure 2.3A) indicates that it is π bonding nature (metal mixed ligand π orbitals) whereas the corresponding LUMO is ligand π* in nature.

Therefore in the case of compound **2** also, the major absorption at 880 nm can be assigned to "mixed-metal ligand-to-ligand" (MMLL) charge transfer transition.[24]It has already been mentioned that the most intense absorption band is observed at 880 nm for compound $[Ph_4P][Ni(Ph_2$6,7–qdt$)_2]\cdot CHCl_3$ (**2**), which is around 30 nm red-shifted from the most intense peak (853 nm) of compound $[Bu_4N][Ni(6,7\text{-qdt})_2]$ (**1**). As we go from compound **1** to compound **2**, two phenyl groups are added as substituents per ligand replacing two protons (see Scheme 2.2). A particular substituent on an aromatic system can usually be understood in terms of mesomeric as well as inductive effects. The mesomeric effect arises from the delocalization of the

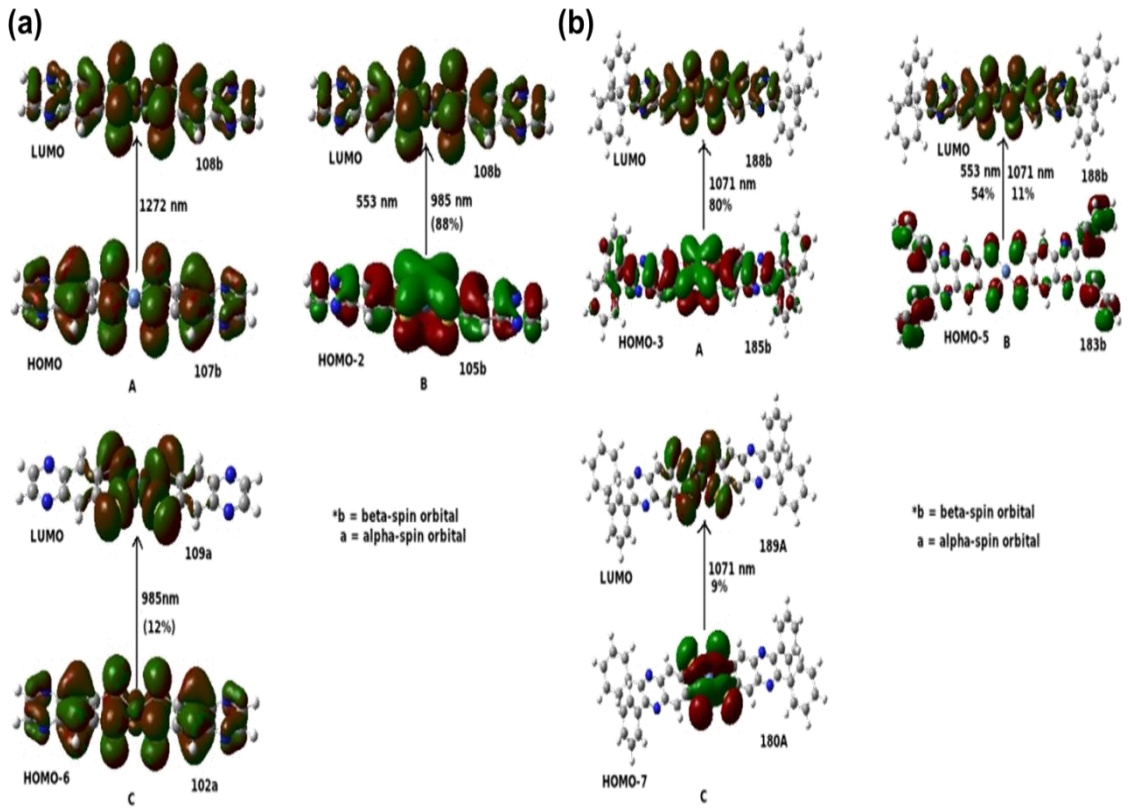


**Figure 2.6.** HOMO and LUMO diagrams originated from molecular orbital calculations for the mono anion of (a) compound **1** and (b) compound **2**.

π-electrons between the substituent and aromatic core. On the other hand, the inductive effect is fully associated with the σ-electron system of the aromatic ring. In the case of compound $[Ph_4P][Ni(Ph_2 6,7–qdt)_2] \cdot CHCl_3$ (**2**), both mesomeric and inductive effects are to be considered. This is because the substituted phenyl group (compound **2**) can be involved in both these effects. The inductive effect can be initiated by an electron withdrawing substituent or by an electron donating substituent. In the present study (compound **2**), the phenyl substituent acts as an electron withdrawing group, which can be established from the following discussion. An electron withdrawing group pulls the σ-electron density from the ligand by the inductive effect, thereby reducing the repulsive Coulombic interactions between the electrons occupying the ligand-localized π-MOs and the electrons of the σ-system. Thus an electron withdrawing substituent in the present system causes lowering the energy of LUMOs (because these are purely π-MOs of dithiolate ligand, Figures 2.6a and 2.6b) without lowering the energy of HOMOs

considerably (because there are mixture of nickel d-orbital character and dithiolate π-type), thereby should cause red-shift in the relevant electron absorption spectra (the energy gap between HOMO and LUMO would essentially be decreased). Conversely, an electron releasing substituent in the present system would cause a blue shift in the electronic absorption spectra because the energy gap between HOMO and LUMO would essentially be increased (an electron donating group increases the electron density toward dithiolate ligand and thereby increases the repulsive Columbic interactions between the ligand-centered π-MOs and σ-electrons). Therefore, in the case of compound **2**, the substituent phenyl group acts as an electron withdrawing group and causes redshift of 30 nm in the pertinent electron absorption spectra when we go from compound **1** (no substituent) to compound **2** (phenyl group as a substituent). In the case of mesomeric effect, the substituent phenyl group (compound **2**) can share its π-electrons with the aromatic core, associated with dithiolate ligand, by resonance. The prevalence of mesomeric effect in the present system is supported by DFT calculations. When we compare Figures 2.6a (A,C) with Figures 2.6b (B,C), we find more electron density at the central metal ion in compound **2** (where the phenyl substituent exerts mesomeric effect by resonance) in comparison to that at the central metal ion in compound **1** (there is no substituent in place of hydrogen). The higher electron density at the central metal ion makes the electronic transition easier in the case of compound **2**, which probably causes a red shift of the more intense band compared to compound **1**. Thus both inductive effect and mesomeric effect are responsible for this red-shift and consistent with DFT calculations.

As shown in Figures 2.5a and 2.5b, the major electron absorption bands for Ni(III) complexes (compounds 1 and 2, present study) appear in red-shifted regions compared to their parent Ni(II) analogues $[Bu_4N]_2[Ni^{II}(6,7–qdt)_2]$ and $[Ph_4P]_2[Ni^{II}(Ph_26,7–qdt)_2]$. Compounds 1 and 2 are one-electron oxidized products of their Ni(II) parent compounds $[Bu_4N]_2[Ni^{II}(6,7–qdt)_2]$ and $[Ph_4P]_2[Ni^{II}(Ph_26,7–qdt)_2]$. When compound $[Bu_4N]_2[Ni^{II}(6,7–qdt)_2]$ is oxidized by iodine to its Ni(III) analog (compound 1), the electronic absorption band at 619 nm (parent Ni(II) compound) shifts to 853 nm (compound 1). Similarly, when compound $[Ph_4P]_2[Ni^{II}(Ph_26,7–qdt)_2]$ is oxidized by iodine to its Ni(III) form (compound 2), the major electronic absorption band at 662 nm (parent Ni(II) compound) moves to 880 nm (compound 2). This large red shift (234 nm for compound 1 and 218 nm for compound 2) of major electronic absorption bands in going from Ni(II) to Ni(III) complexes can be attributed to the central metal ion $Ni^{3+}$ which, in

its +3 oxidation state, pulls the σ-electron density from the coordinated dithiolate ligand and reduces the repulsion type Coulombic interactions between the electrons in the σ-system and electrons occupying the ligand-localized π-MOs. This causes the lowering the energy of LUMOs (purely π-MOs of dithiolate ligand, Figures 2.6a and 2.6b) without lowering the energy of HOMOs (metal mixed ligand π orbitals, Figures 2.6a and 2.b), resulting in the decrease of theenergy gap between HOMO and LUMO. This explains the large red-shift in the electronic absorption maxima when Ni(II) complex is oxidized to its Ni(III) analog. Theoretically simulated absorption spectra for the Ni(III) complex anions of 1 and 2 have been displayed in the Figure 2.7.

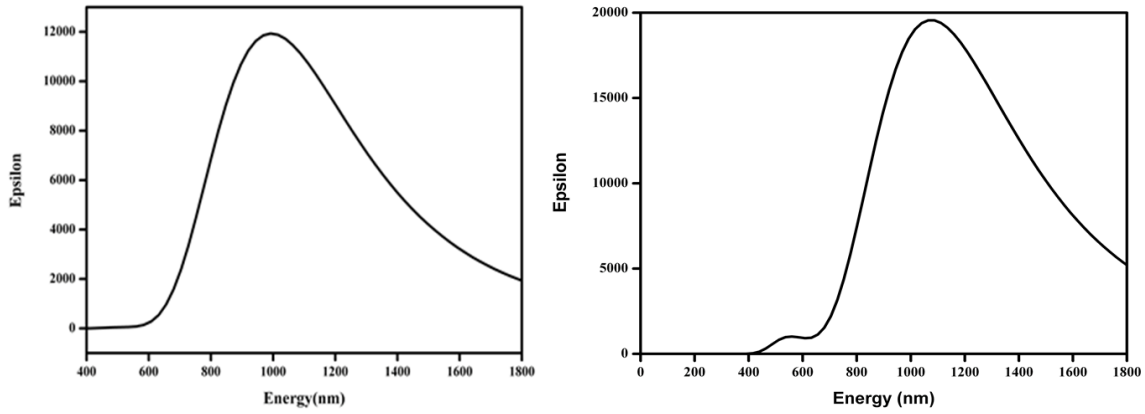


**Figure 2.7.** Theoretically Simulated UV–vis–NIR Spectra of $[Ni(6,7–qdt)_2]^{1-}$(left) and $[Ni(Ph_2 6,7–qdt)_2]^{1-}$(right).

### 2.3.6. Electron spin resonance spectra

The ESR spectra of solid samples for compounds $[Bu_4N][Ni^{III}(6,7\text{-}qdt)_2]$ (**1**) and $[Ph_4P][Ni^{III}(Ph_2 6,7\text{-}qdt)_2]\cdot CHCl_3$ (**2**) were recorded at room temperature and 123K. The ESR spectra, recorded at 123K, are presented in Figure 2.8. Compound **1** exhibits rhombic-type signal: $g_x$=2.246, $g_y$=2.156, and $g_z$=2.065. But compound **2** shows an axial signal with $g_\perp > g_\parallel$: $g_\perp$ = 2.133 and $g_\parallel$ = 2.049. This is consistent with low spin Ni(III) ($d^7$, S = 1/2) in a tetragonal geometry ($g_\perp > g_\parallel$) with one unpaired electron in $d_z^2$ orbital.[35] The anisotropy in the ESR spectra implies some contribution of the d orbital of nickel in the total spin density, which is consistent with DFT calculations (*vide supra*). The ESR data also suggest that the unpaired electrons in compounds **1** and **2** are not localized to the ligands because the resulting organic radical usually shows a sharp signal near g = 2.003. The present ESR data and their comparison with those of already known mononuclear

Ni(III) square-planar complexes[35] confirm that compounds **1** and **2** are formally Ni(III) complexes.

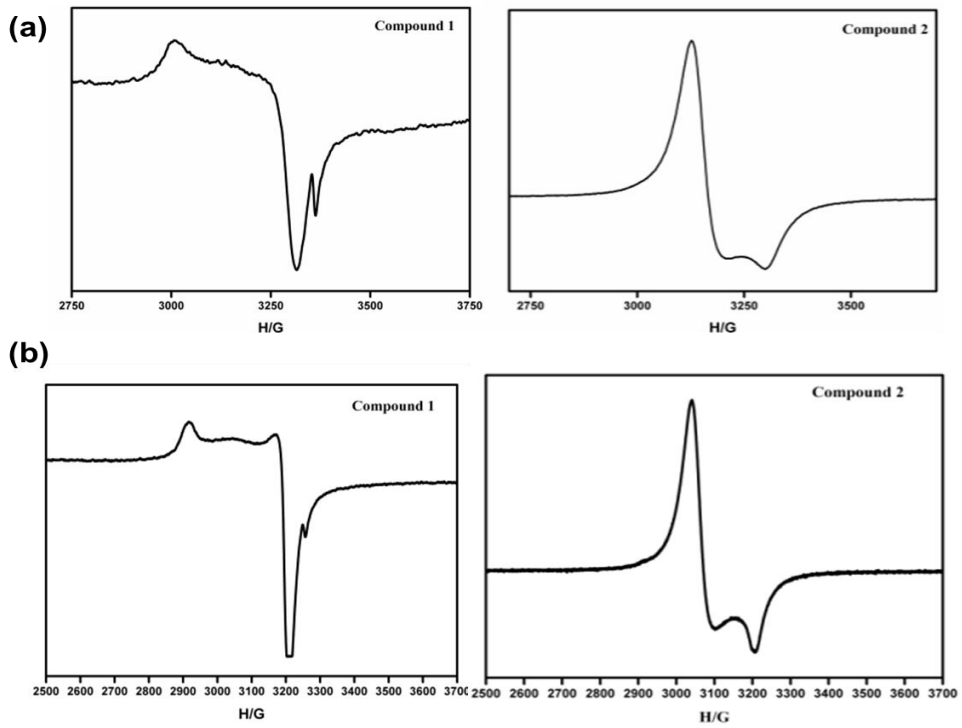


**Figure 2.8.** Electron spin resonance spectra of The compound **1** and **2 (**a) powder form at room temperature (top) ; (b) powder form at 123K (bottom).

### 2.3.7. Electrochemistry

We mentioned in our earlier report[24] that the parent compounds $[Bu_4N]_2[Ni^{II}(6,7–qdt)_2]$ and $[Ph_4P]_2[Ni^{II}(Ph_26,7–qdt)_2]$ of corresponding present Ni(III) compounds $[Bu_4N][Ni^{III}(6,7\text{-}qdt)_2]$ (**1**) and $[Ph_4P][Ni^{III}(Ph_26,7\text{-}qdt)_2]\cdot CHCl_3$ (**2**) undergo reversible oxidation at very low oxidation potentials in MeOH solutions: $[Bu_4N]_2[Ni^{II}(6,7–qdt)_2]$ undergoes oxidation at $E_{1/2}$ = + 0.12 V *vs* Ag/AgCl ($\Delta E$ = 74 mV) corresponding to $[Ni^{III}(6,7\text{-}qdt)_2]^{1–}/[Ni^{II}(6,7\text{-}qdt)_2]^{2–}$ redox couple and $[Ph_4P]_2[Ni^{II}(Ph_26,7–qdt)_2]$ undergoes oxidation at $E_{1/2}$ = +0.033 V *vs* Ag/AgCl ($\Delta E$ = 65 mV) corresponding to $[Ni^{III}(Ph_26,7–qdt)_2]^{1–}$ /$[Ni^{II}(Ph_26,7–qdt)_2]^{2–}$ couple. In the present study, we could not perform electrochemical studies in MeOH solvent due to solubility problem. Compounds **1** and **2** are not freely soluble in MeOH. We thus performed the cyclic voltammetry studies of compounds **1** and **2** in DMF solutions, each containing 0.10 M $[Bu_4N]ClO_4$ as supporting electrolyte. As shown in Figure 2.9, cyclic voltammograms of compounds **1** and **2** exhibit quasi-reversible reductive responses at $E_{1/2}$ = + 0.225 V *vs* Ag/AgCl ($\Delta E$ = 87 mV) and

$E_{1/2}$ = + 0.044 V *vs* Ag/AgCl ($\Delta E$ = 82 mV). Based on the $E_{1/2}$ values of oxidative responses of the Ni(II) analogues $[Bu_4N]_2[Ni^{II}(6,7–qdt)_2]$ and $[Ph_4P]_2[Ni^{II}(Ph_2 6,7–qdt)_2]$ in MeOH[24] as well as in DMF, we can assign these reductive responses of compounds **1** and **2** to $[Ni^{III}(6,7\text{-}qdt)_2]^{1–}$ / $[Ni^{II}(6,7\text{-}qdt)_2]^{2–}$ and $[Ni^{III}(Ph_2 6,7–qdt)_2]^{1–}$ / $[Ni^{II}(Ph_2 6,7–qdt)_2]^{2–}$ couples respectively. Thus electrochemical Experiments clearly point out that the oxidation state of nickel in the isolated compounds **1** and **2** is +3.

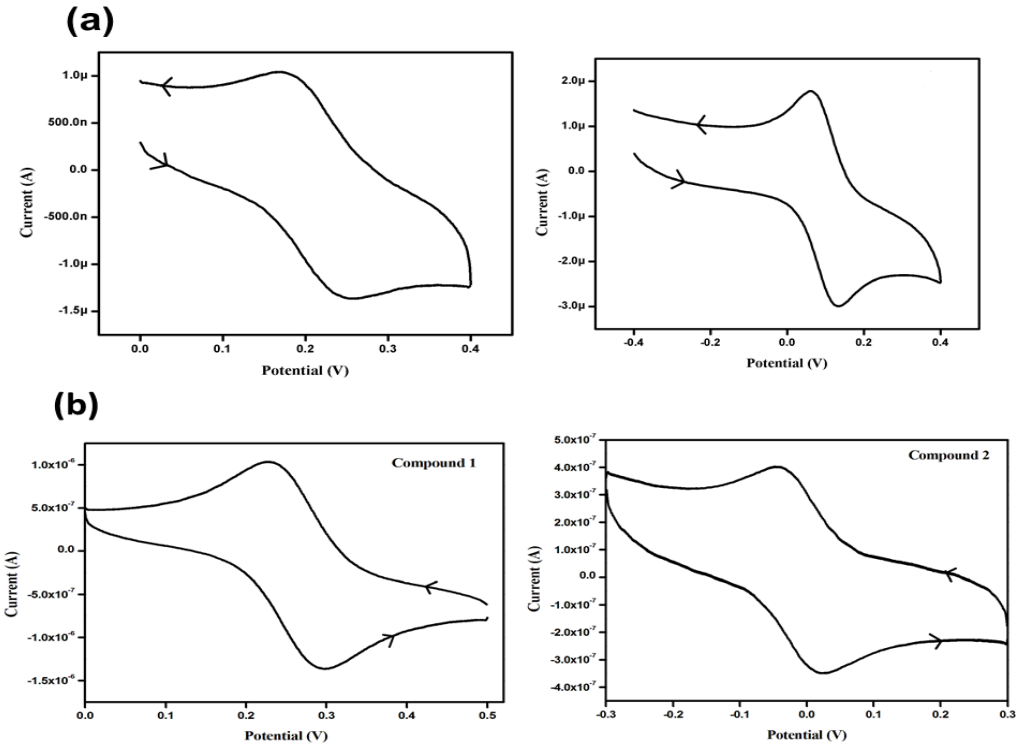


**Figure 2.9.** Cyclic voltammetric studies of (a) $[Bu_4N]_2[Ni^{II}(6,7–qdt)_2]$ (top-left) and $[Ph_4P]_2[Ni^{II}(Ph_2 6,7–qdt)_2]$ (top-right) (b) compounds **1** (bottom-left) and **2** (bottom-right) in DMF solution at scan rate 100 $mVs^{-1}$, V *vs* Ag/AgCl.

## 2.4. Summary

We have described synthesis and characterization of two Ni(III)-bis(dithiolato) complexes $[Bu_4N][Ni^{III}(6,7–qdt)_2]$ (**1**) and $[PPh_4][Ni^{III}(Ph_2 6,7–qdt)_2]$ (**2**), that are based on unique dithiolene ligands. Compounds **1** and **2** are additionally characterized by electrochemical and ESR studies, besides their unambiguous characterization by single crystal X-ray structure determination. The described compounds are unique in the sense that they get reduced reversibly at very low potentials. This demonstrates that their respective reduced analogues $[Bu_4N]_2[Ni^{II}(6,7–qdt)_2]$ and $[Ph_4P]_2[Ni^{II}(Ph_2 6,7–qdt)_2]$ can act as oxidation

catalysts. Title compounds exhibit well-defined electronic absorption bands that are corroborated with theoretical (DFT) collations. This is one of rare reports, where theoretical calculations have been performed on a Ni(III)-bis(dithiolato) system.The crystal structures of compounds **1** and **2** show interesting supramolecular hydrogen bonding networks, formed by C–H···S and C–H···N weak contacts. Hirshfeld surfaces (HSs) and 2D finger print plots (FPs) corroborate these supramolecular interactions.

**Table 2.1.** Crystal data and structural refinement parameters for compounds **1** and **2**

| | **1** | **2** |
|---|---|---|
| Empirical formula | $C_{32}H_{44}N_5NiS_4$ | $C_{65}H_{45}C_{13}N_4NiPS_4$ |
| Formula weight | 685.67 | 1206.32 |
| T(K) / λ(Å) | 100(2) | 100(2) |
| Crystal system | monoclinic | triclinic |
| Space group | $P2_1/c$ | P-1 |
| a (Å) | 13.8384(9) | 13.294(10) |
| b (Å) | 11.6926(8) | 15.018(12) |
| c (Å) | 22.4558(12) | 15.677(12) |
| α (°) | 90 | 70.818(12) |
| β (°) | 113.333 | 80.368(12) |
| γ (°) | 90 | 84.916(13) |
| Volume ($Å^3$) | 3336.3(4) | 2913 |
| Z, $\rho_{calcd}$ ($g\ cm^{-3}$) | 4, 1.365 | 2,1.375 |
| *F*(000) | 1452 | 1242 |
| goodness-of-fit on $F^2$ | 1.131 | 1.252 |
| R1/ wR2 [I > 2σ (I)] | 0.0488/0.1029 | 0.1335/0.3135 |
| R1/ wR2 (all data) | 0.0576/0.1069 | 0.1719/0.3319 |
| Largest diff peak/ hole (e $Å^{-3}$) | 0.548 and -0.281 | 1.275 and -0.944 |

**Table 2.2.** Selected bond lengths [Å] and angles [º] for the compounds **1** and **2**

| | | | |
|---|---|---|---|
| **Compound 1[a]** | | | |
| Ni(1)-S(1)#1 | 2.1431(7) | Ni(1)-S(2)#1 | 2.1442(7) |
| Ni(2)-S(3)#2 | 2.1555(7) | Ni(2)-S(4)#2 | 2.1473(7) |
| S(1)#1-Ni(1)-S(1) | 180.00(4) | S(1)-Ni(1)-S(2) | 92.23(3) |
| S(1)#1-Ni(1)-S(2) | 87.77(3) | S(4)-Ni(2)-S(3) | 92.16(3) |
| S(4)-Ni(2)-S(3)#2 | 87.85(3) | S(3)-Ni(2)-S(3)#2 | 180.00(4) |
| C(1)-S(1)-Ni(1) | 105.26(10) | C(6)-S(2)-Ni(1) | 105.33(10) |
| C(9)-S(3)-Ni(2) | 104.95(10) | C(14)-S(4)-Ni(2) | 104.92(10) |
| **Compound 2[b]** | | | |
| Ni(1)-S(3) | 2.126(3) | Ni(1)-S(4) | 2.129(3) |
| Ni(2)-S(1) | 2.136(3) | Ni(2)-S(2) | 2.134(3) |
| S(3)-Ni(1)-S(4) | 92.03(12) | S(3)-Ni(1)-S(4)#1 | 87.97(12) |
| S(2)-Ni(2)-S(1) | 92.17(11) | S(2)#2-Ni(2)-S(1) | 87.83 (11) |
| S(2)-Ni(2)-S(2)#2 | 180 | S(1)#2-Ni(2)-S(1) | 180.00(16) |
| S(3)-Ni(1)-S(3)#1 | 179.9(1) | S(4)-Ni(1)-S(4)#1 | 180.00(12) |

Symmetry transformation used to generate equivalent atoms:
a#1 -x+2,-y+2,-z+1 #2 -x+1,-y+1,-z+2; b #1 -x+1,-y,-z+1 #2 -x+2,-y+1,-z+1

## 2.5. References

(1). Kato, R. Conducting Metal Dithiolene Complexes: Structural and Electronic Properties. *Chem. Rev.* **2004**, *104*, 5319-46.

(2). Ren, X. M.; Nishihara, S.; Akutagawa, T.; Noro, S.; Nakamura, T. Design of a Magnetic Bistability Molecular System Constructed by H-Bonding and π···π-Stacking Interactions. *Inorg. Chem.* **2006**, *45*, 2229-2234.

(3). Mercuri, M. L.; Deplano, P.; Pilia, L.; Serpe, A.; Artizzu, F. Interactions Modes and Physical Properties in Transition Metal Chalcogenolene-based Molecular Materials. *Coord. Chem. Rev.* **2010**, *254*, 1419-1433.

(4). Serrano-Andres, L.; Avramopoulos, A.; Li, J.; Labeguerie, P.; Begue, D.; Kello, V.; Papadopoulos, M. G. Linear and Nonlinear Optical Properties of a Series of Ni-dithiolene Derivatives. *J. Chem. Phys.* **2009**, *131*, 134312.

(5). Chen, C.-T.; Liao, S.-Y.; Lin, K.-J.; Lai, L.-L. Syntheses, Charge Distribution, and Molecular Second-Order Nonlinear Optical Properties of Push–Pull Bisdithiolene Nickel Complexes. *Adv. Mater.* **1998**, *10*, 334-338.

(6). Mueller-Westerhoff, U. T.; Vance, B.; Ihl Yoon, D. The Synthesis of Dithiolene Dyes with Strong Near-IR absorption. *Tetrahedron* **1991**, *47*, 909-932.

(7). Bai, J.-F.; Zuo, J.-L.; Tan, W.-L.; Ji, W.; Shen, Z.; Fun, H.-K.; Chinnakali, K.; Abdul Razak, I.; You, X.-Z.; Che, C.-M. Synthesis, Structure and Optical Limiting Effect of two New Nickel Complexes Containing Strongly Bound Geometrically Fixed Multi-sulfur 1,2-dithiolene Ligands Showing Remarkable Near-IR Absorption. *J. Mater. Chem.* **1999**, *9*, 2419-2423.

(8). Deplano, P.; Mercuri, M. L.; Pintus, G.; Trogu, E. F. New Symmetrical and Unsymmetrical Nickel-Dithiolene Complexes Useful as Near-IR Dyes and Precursors of Sulfur-Rich Donors. *Comments Inorg. Chem.* **2001**, *22*, 353-374.

(9). Aragoni, M. C.; Arca, M.; Cassano, T.; Denotti, C.; Devillanova, Francesco A.; Frau, R.; Isaia, F.; Lelj, F.; Lippolis, V.; Nitti, L.; Romaniello, P.; Tommasi, R.; Verani, G. NIR Dyes Based on [M(R,R′timdt)$_2$] Metal-Dithiolenes: Additivity of M, R, and R′ Contributions To Tune the NIR Absorption (M = Ni, Pd, Pt; R,R′timdt = Monoreduced Form of Disubstituted Imidazolidine-2,4,5-trithione). *Eur. J. Inorg. Chem.* **2003**, 10, 1939-1947.

(10). Dias, S. I. G.; Rabaça, S.; Santos, I. C.; Pereira, L. C. J.; Henriques, R. T.; Almeida, M. Bisdithiolene Complexes Based on an Extended Ligand with TTF and Pyridine Moieties. *Inorg. Chem. Comm.* **2012**, *15*, 102-105.

(11). Basu, P.; Nigam, A.; Mogesa, B.; Denti, S.; Nemykin, V. N. Synthesis, Characterization, Spectroscopy, Electronic and Redox Properties of a New Nickel Dithiolene System. *Inorg. Chim. Acta*. **2010**, *363*, 2857-2864.

(12). K. D. Karlin, E. I. Stiefel, *Prog. Inorg. Chem. Vol -52; Dithiolene Chemistry: Synthesis Properties, and Applications, John Wiley, New York*, **2004**.

(13). Madhu, V.; Das, S. K. Diverse Supramolecular Architectures Having Well-Defined Void Spaces Formed from a Pseudorotaxane Cation: Influential Role of Metal Dithiolate Coordination Complex Anions. *Cryst. Growth & Design.* **2014**, *14*, 2343-2356.

(14). Madhu, V.; Das, S. K. Near-IR Absorption Due to Supramolecular Electronic Interaction in an Extended 3D Hydrogen-bonding Network Material: Synthesis, Crystal Structure and Properties of [4,4′-$H_2$bpy][Cu(mnt)$_2$]. *Polyhedron* **2004**, *23*, 1235-1242.

(15). Madhu, V.; Das, S. K. Neutral Coordination Polymers Based on a Metal-Mono(dithiolene) Complex: Synthesis, Crystal Structure and Supramolecular Chemistry of [Zn(dmit)(4,4′-bpy)]$_n$, [Zn(dmit)(4,4′-bpe)]$_n$ and [Zn(dmit)(bix)]n (4,4′-bpy = 4,4′-bipyridine, 4,4′-bpe = trans-1,2-bis(4-pyridyl)ethene, bix = 1,4-bis(imidazole-1-ylmethyl)-benzene. *Dalton. Trans.* **2011**, *40*, 12901-12908.

(16). Madhu, V.; Das, S. K. New Series of Asymmetrically Substituted Bis(1,2-dithiolato)-Nickel(III) Complexes Exhibiting Near IR Absorption and Structural Diversity. *Inorg. Chem.* **2008**, *47*, 5055-5070.

(17). Madhu, V.; Das, S. K. One-pot Synthesis of an Mn(III)-Cu(II)-Mn(III) Trinuclear Heterometallic Compound Formed by Mn…S-Cu-S…Mn Supramolecular Interactions: Crystal Structure of [$Mn^{III}$(salph)($H_2O$)$_2$$Cu^{II}$(mnt)$_2$].4DMF. *J. Chem. Sci.* **2006**, *118*, 611-617.

(18). Bolligarla, R.; Durgaprasad, G.; Das, S. K. Synthesis, Molecular Structure and Supramolecular Chemistry of a New Nickel-quinoxaline Dithiolate System [$Bu_4N$]$_2$[Ni(6,7-qdt)$_2$] (6,7-qdt = quinoxaline-6,7-dithiolate) and Comparison of its Electronic and Electrochemical Properties with those of [$Bu_4N$]$_2$[Ni(qdt)$_2$] (qdt = quinoxaline-2,3-dithiolate). *Inorg. Chem. Comm.* **2011**, *14*, 809-813.

(19). Durgaprasad, G.; Das, S. K. Modeling the Active Site of [FeFe]-hydrogenase: Electro-Catalytic Hydrogen Evolution from Acetic acid Catalysed by [$Fe_2$ (μ-L)(CO) $_6$ ]

and [$Fe_2$ (μ-L)$(CO)_5$ ($PPh_3$ )] (L=pyrazine-2,3-dithiolate, quinoxaline-2,3-dithiolate and pyrido[2,3-b]pyrazine-2,3-dithiolate). *J. Chem. Sci.* **2015**, *127*, 295-305.

(20). Durgaprasad, G.; Bolligarla, R.; Das, S. K. Synthesis, Crystal Structure and Electrocatalysis of 1,2-ene Dithiolate Bridged Diiron Carbonyl Complexes in Relevance to the Active Site of [FeFe]-hydrogenases. *J. Orgnomet. Chem.* **2012**, *706–707*, 37-45.

(21). Durgaprasad, G.; Bolligarla, R.; Das, S. K. Synthesis, Structural Characterization and Electrochemical Studies of [$Fe_2$(μ-L)$(CO)_6$] and [$Fe_2$(μ-L)$(CO)_5(PPh_3)$] (L = pyrazine-2,3-dithiolate, quinoxaline-2,3-dithiolate and pyrido[2,3-b]pyrazine-2,3-dithiolate): Towards Modeling the active site of [FeFe]–Hydrogenase. *J. Organomet. Chem.* **2011**, *696*, 3097-3105.

(22). Cerqueira, N. M. F. S. A.; Pakhira, B.; Sarkar, S. Theoretical studies on mechanisms of Some Mo enzymes. *J. Biol. Inorg. Chem.* **2015**, *20*, 323-335.

(23). Maiti, B. K.; Maia, L. B.; Pal, K.; Pakhira, B.; Avilés, T.; Moura, I.; Pauleta, S. R.; Nuñez, J. L.; Rizzi, A. C.; Brondino, C. D.; Sarkar, S.; Moura, J. J. G. One Electron Reduced Square Planar Bis(benzene-1,2-dithiolato) Copper Dianionic Complex and Redox Switch by $O_2/HO^-$. *Inorg. Chem.* **2014**, *53*, 12799-12808.

(24). Bolligarla, R.; Reddy, S. N.; Durgaprasad, G.; Sreenivasulu, V.; Das, S. K. Influence of the Substituents on the Electronic and Electrochemical Properties of a New Square-Planar Nickel-Bis(quinoxaline-6,7-dithiolate) System: Synthesis, Spectroscopy, Electrochemistry, Crystallography, and Theoretical Investigation. *Inorg. Chem.* **2013**, *52*, 66-76.

(25). Lee, C.-M.; Chuang, Y.-L.; Chiang, C.-Y.; Lee, G.-H.; Liaw, W.-F. Mononuclear Ni(III) Complexes $[Ni^{III}(L)(P(C_6H_3\text{-}3\text{-}SiMe_3\text{-}2\text{-}S)_3)]^{0/1-}$ (L = Thiolate, Selenolate, $CH_2CN$, Cl, $PPh_3$): Relevance to the Nickel Site of [NiFe] Hydrogenases. *Inorg. Chem.* **2006**, *45*, 10895-10904.

(26). Zheng, B.; Tang, F.; Luo, J.; Schultz, J. W.; Rath, N. P.; Mirica, L. M. Organometallic Nickel(III) Complexes Relevant to Cross-Coupling and Carbon–Heteroatom Bond Formation Reactions. *J. Am. Chem. Soc.* **2014**, *136*, 6499-6504.

(27). Brusso, J. L.; Clements, O. P.; Haddon, R. C.; Itkis, M. E.; Leitch, A. A.; Oakley, R. T.; Reed, R. W.; Richardson, J. F. Bistabilities in 1,3,2-Dithiazolyl Radicals. *J. Am. Chem. Soc.* **2004**, *126*, 8256-8265.

(28). Bruker. *SADABS*, *SMART*, *SAINT* and *SHELXTL*, **2000** (Bruker AXS Inc., Madison, Wisconsin, USA).

(29). S. K. Wolff, D. J. Grimwood, J. J. McKinnon, M. J. Turner, D. Jayatilaka, M. A. Spackmann, CrystalExplorer 3.1 (2013), University of Western Australia, Crawley, Western Australia, **2005– 2013**, http://hirshfeldsurface.net

(30). Hirshfeld, F. L. Bonded-atom Fragments for Describing Molecular Charge Densities. *Theor. Chim. Acta.* **1977,** *44*, 129-138.

(31). Spackman, M. A.; Jayatilaka, D. Hirshfeld surface analysis. CrystEngComm **2009**, 11, 19-32.

(32). McKinnon, J. J.; Jayatilaka, D.; Spackman, M. A. Towards Quantitative Analysis of Intermolecular Interactions with Hirshfeld Surfaces. *Chem. Comm.* **2007**, *37*, 3814-3816.

(33). Frisch, M. J.; Trucks, G. W.; Schlegel, H. B.; Scuseria, G. E.; Robb, M. A.; Cheeseman, J. R.; Scalmani, G.; Barone, V.; Mennucci, B.; Petersson, G. A.; Nakatsuji, H.; Caricato, M.; Li, X.; Hratchian, H. P.; Izmaylov, A. F.; Bloino, J.; Zheng, G.; Sonnenberg, J. L.; Hada, M.; Ehara, M.; Toyota, K.; Fukuda, R.; Hasegawa, J.; Ishida, M.; Nakajima, T.; Honda, Y.; Kitao, O.; Nakai, H.; Vreven, T.; Montgomery Jr., J. A.; Peralta, J. E.; Ogliaro, F.; Bearpark, M.; Heyd, J. J.; Brothers, E.; Kudin, K. N.; Staroverov, V. N.; Kobayashi, R.; Normand, J.; Raghavachari, K.; Rendell, A.; Burant, J. C.; Iyengar, S. S.; Tomasi, J.; Cossi, M.; Rega, N.; Millam, J. M.; Klene, M.; Knox, J. E.; Cross, J. B.; Bakken, V.; Adamo, C.; Jaramillo, J.; Gomperts, R.; Stratmann, R. E.; Yazyev, O.; Austin, A. J.; Cammi, R.; Pomelli, C.; Ochterski, J. W.; Martin, R. L.; Morokuma, K.; Zakrzewski, V. G.; Voth, G. A.; Salvador, P.; Dannenberg, J. J.; Dapprich, S.; Daniels, A. D.; Farkas, Ö.; Foresman, J. B.; Ortiz, J. V.; Cioslowski, J.; Fox, D. J. *Gaussian 09*, revision C.01, Gaussian, Inc., Wallingford CT, **2010**.

(34). Salzner, U. Quantitatively Correct UV-vis Spectrum of Ferrocene with TD-B3LYP. *J. Chem. Theory. Comput.* **2013**, *9*, 4064-4073..

(35). Madhu, V.; Das, S. K. New Series of Asymmetrically Substituted Bis(1,2-dithiolato)-Nickel(III) Complexes Exhibiting Near IR Absorption and Structural Diversity. *Inorg. Chem.* **2008**, *47*, 5055-5070.

.

# A Functional System of Bis(pyrazolyl)pyridine Derivatives: Photo-physics, Spectroscopy and Computation

# 3

**Abstract:** A new series of conjugated donor-π-acceptor type of 2,6-bis(pyrazolyl)pyridine derivatives (compounds **3-9**, see chart 3.1) has been synthesized *via* Horner-Wadsworth-Emmons (HWE) reaction, starting from a common phosphonate precursor (compound **2**, see chart 3.1) having 2,6-bis(pyrazolyl)pyridine moiety and diverse donor aromatic aldehydes (chart 1) and characterized by routine spectral analysis including elemental analysis. Compound **2**, one of the starting precursors and molecule **3**, the first member of the donor-π-acceptor series, are additionally characterized by single crystal X-ray structure determination. Compounds **2** and **3** are crystallized in *P-1*(triclinic) and $P2_1/c$ (monoclinic) space groups respectively. The absorption maxima in the electronic spectra of the title compounds shift mainly due to intra-molecular charge transfer (ICT) between different donor (dibutyl and cyclic pyrrolidine) groups and the acceptor moiety [2,6-bis(pyrazolyl) pyridine]. Solution state emission spectral studies of all these compounds show large solvent sensitive behavior with significant amounts of stroke shifts. The large solvent dependence of the emission indicates that the excited state is stabilized in more polar solvents due to the intramolecular charge transfer. We have also described quantum yields of all the compounds, recorded in different solvent media. All chromophores exhibit solid state fluorescence behavior except compound **7**. The role of the position and nature of the donor functionalities in the conjugated backbone of overall donor moiety of compounds **3-9**, on the electronic absorption properties of title chromophores has been demonstrated, which has further been corroborated by DFT and TDDFT computational studies. The emission spectral results of compounds **3**, **5** and **7** have also been supported by DFT and TDDFT calculations. A fluorescence lifetime study on this series shows that the excited states are stabilized in more polar solvents.

## 3.1 Introduction

Fluorescence[1] has turned out to be an essential analytical technique in various branches of science, most importantly, in the fields of analytical, biological, and medicinal sciences. Among the various classes of emissive organic π-systems, materials that absorb electromagnetic radiation by virtue of an intramolecular charge transfer and emit from corresponding photoexcited state, are the most interesting ones because of their prominent applications in the fields of molecular electronics, integrated photonic devices, nonlinear optics (NLO), *etc*.[2] The well-designed electron donor and acceptor (DA) or 'push-pull' architecture can be fabricated *via* the electronic association between the donor and acceptor mesomeric units in a chromophore system, which in turn, is linked with diverse functionalities for spontaneous charge redistribution. Particularly, π-conjugated chromophores with a donor and acceptor moieties are of considerably interest in terms of tuning their optical properties wisely, over a wide range simply by varying donor or acceptor moieties. During last three decades, dynamics of intramolecular charge transfer in the excited states of various aromatic molecules of the type D–Ar–A (where Ar is an aromatic system linking D and A through π conjugation) have been the subject of extensive theoretical and experimental investigations.[3–8] The most fundamental types of interaction in such D-A systems generally occur by virtue of intramolecular charge transfer between donor (D) and the acceptor (A), thereby tuning the HOMO-LUMO energy gap. Large stroke shifts of the fluorescence emission in more polar solvents by stabilization of the excited singlet state *via* solvent reorganization, called dipolar salvation, are well known in literature.[9-13] Numerous π-conjugated systems, that can be described as functional materials, are particularly important to the development of organic light emitting diodes (OLED),[14] electrogenerated chemiluminescence (ECL),[15] dye-sensitized solar cells (DSSCs),[16] and fluorescent sensors.[17] Some years ago, we have established a series of 4,4′-π-conjugated-2,2′-bipyridine chromophores and investigated their photo-physical and thermal properties.[18] We have also reported a series of asymmetrically substituted and π-conjugated 2,2′-bipyridine derivatives including their photophysics and computational studies.[19] In this work, we have chosen a π-conjugated tris-heterocyclic molecular system, namely, 2,6-bis(pyrazolyl)pyridine derivatives, because such tris-heterocyclic ligands are important in recent years not only due to their synthetic flexibility, strong metal binding tendency, and spin crossover properties of their iron complexes but also their potential to act as fluorescent sensor for a metal ion because of their strong

luminescence behavior. 2,6-bis(pyrazolyl)pyridine derivatives have recently been exploited in diverse areas including catalysis, solar cell photosensitization, magnetism etc.[20-25] We wish to report, in this chapter, the synthesis and characterization of π-conjugated donor-acceptor molecules (compounds **3-9**, chart 3.1) containing 2,6-bis(pyrazolyl)pyridine core as a common acceptor moiety and diverse donor moieties (second row, chart 3.1). The chromophores, **3-9** (Chart 3.1) were found to display bright fluorescence in solution and compounds (3-6, 8 and 9) exhibit solid state fluorescence at room temperature. We also have performed density functional theory (DFT) calculations to corroborate the UV-visible and emission spectral results of the title donor-π-acceptor chromophores.

## 3.2. Experimental section

### 3.2.1. Materials and Methods

All reagents and solvents were commercially available and used without purification. All reactions were carried out under inert atmosphere unless otherwise stated. Column chromatography was performed on silica gel (100-200 mesh). Thin-layer chromatography (TLC) plates were visualized with UV light in an iodine chamber. Unless stated otherwise, all reagents were purchased from commercial sources and used without additional purification. THF was freshly distilled over Na-benzophenone ketyl. $^{1}H$ NMR and $^{13}C$ NMR spectra were recorded on a Bruker 400 MHz machine in $CDCl_3$ as a solvent with TMS as a reference unless otherwise indicated. Micro-analytical (C, H, N) data were obtained with a FLASH EA 1112 Series CHNS analyzer. Infrared (IR) spectra were recorded as KBr pellets on a JASCO- 5300 FT-IR spectrophotometer at 298 K. High resolution mass spectroscopy (HRMS) (ESI-TOF) equipment was used to record mass spectra for isolated compounds where appropriate. Absorbance spectra were recorded on a Shimadzu model UV-3600 spectrophotometer and fluorescence emission spectra have been recorded on a Jobin Yvon Horiba model Fluoromax-4 spectrofluorometer. Time-resolved fluorescence decay measurements were performed using time-correlated single photon counting set-up (Horiba Jobin Yvon IBH). 375 nm diode laser and an MCP photomultiplier (Hamamatsu R3809U-50) were used as an excitation source and the detector, respectively. The lamp profile, which determines the instrumental resolution (~65 ps), was recorded using a Ludox scatterer. Fluorescence decay curves were analyzed using IBH DAS6 (version 2.2) decay analysis software.

### 3.2.2. Synthesis

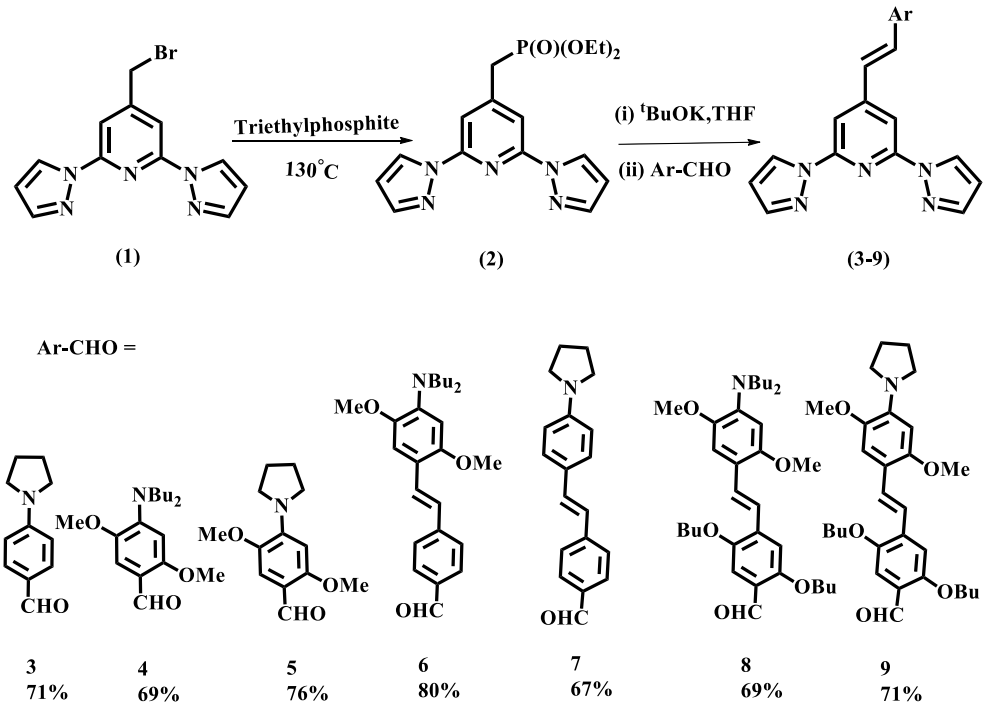


**Chart 3.1.** Molecules synthesized and studied in the present work

**A. Synthetic route of the alkylamino aldehydes**

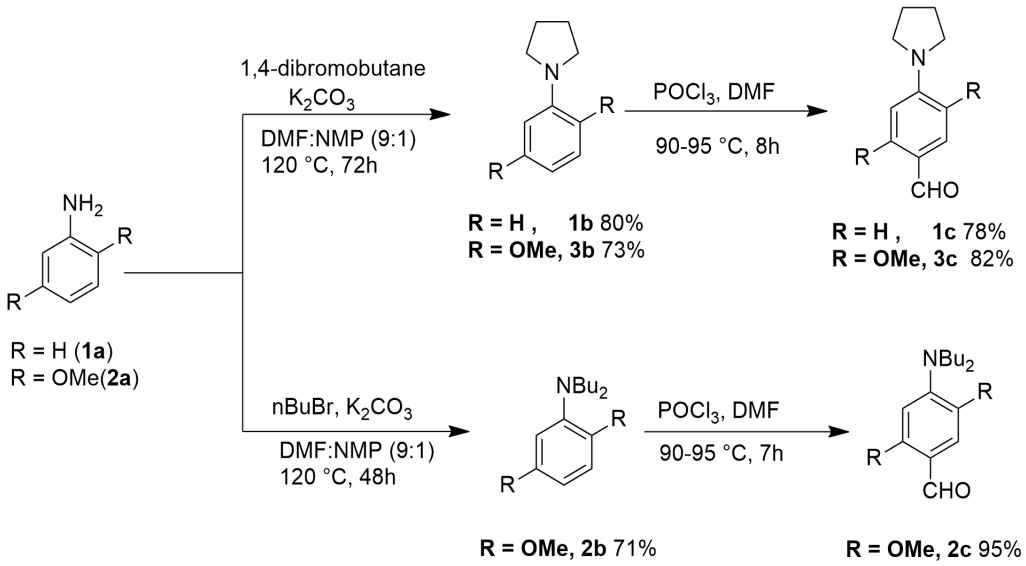

**B. Synthetic route of 4-Styrylbenzaldehydes**

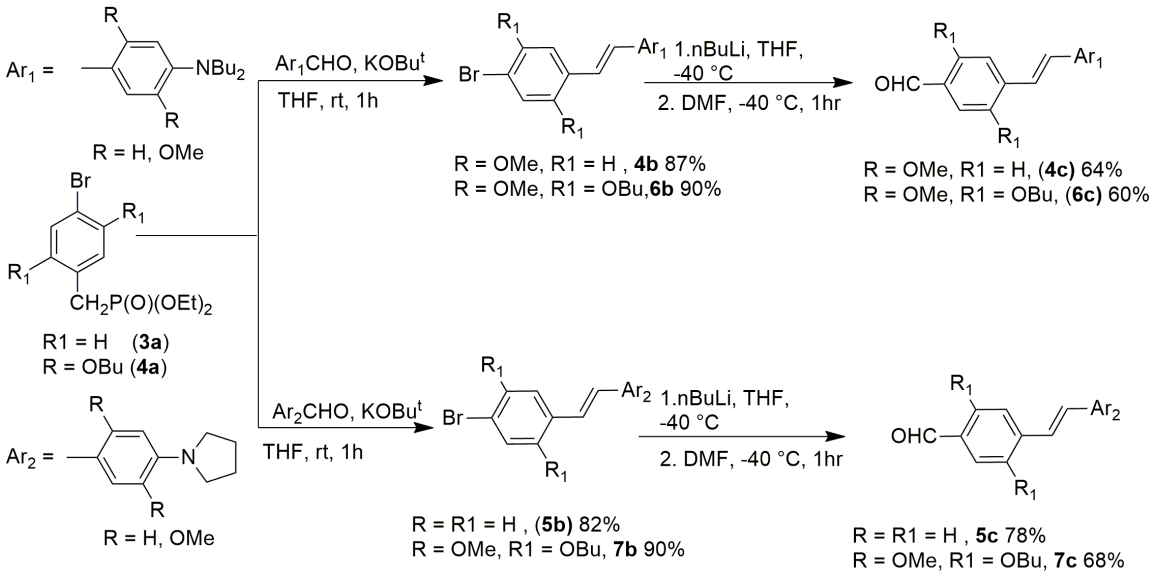


**Chart 3.2** Synthetic route of donor molecules and their staring materials (**1c-7c**)

**Synthesis of compound 2**

In the presence of nitrogen atmosphere, 304 mg (1 mmol) of compound **1** was dissolved in 5 mL of dry triethyl phosphate. It was then refluxed for 24 hours at 140°C. The reaction mixture was cooled to room temperature, whereby, the white solid was separated from the solution mixture. The precipitate was washed with petroleum ether and dried in vacuum. This crude product was recrystallized by vapor diffusion of petroleum ether into a dichloromethane solution of the crude product. After one week, colorless needle-shaped crystals of compound **2** were deposited in the bottom of a glass vial, which was inside the conical flask. Compound **1** crystallizes in the P-1 space group belonging to the triclinic crystal system (see Figure 3.1a and Table 3.1). Yield: 0.190 g (52%). Anal. calcd. for $C_{16}H_{20}N_5O_3P$: C, 53.18; H, 5.58; N, 19.38. Found: C, 53.25; H, 5.62; N, 19.28. IR(KBr pellet) ($\upsilon$/cm$^{-1}$) for **2**: 3159m, 3122s, 2986w, 2947s, 2918m, 1787m,1724w, 1269m (>P=O); 1153m, 1020w, 867m (>P-O-C); 758m. $^1$H NMR (400 MHz, CDCl3): δ 8.56(d, *J*=2 Hz, 2H), 7.83 (d, *J* = 2 Hz, 2H), 7.73(d, *J* = 1 Hz, 2H), 6.50 (d, *J* = 2 Hz, 2H), 4.16-4.10 (m, 4H), 3.29 (d, *J* = 23 Hz, 2H), 1.32 (t, *J* = 7 Hz, 6H). $^{13}$C NMR (100 MHz, CDCl3): δ 150.2, 147.4, 147.3, 142.4 (2C), 127.1 (2C), 110.6, 110.5, 108.0 (2C), 62.6,

62.5, 34.6-33.5, 16.4, 16.4; HRMS: m/z calcd.for $C_{16}H_{20}N_5O_3P$: 361.1304 ($M^+$), found: 362.1381 $(M + H)^+$.

**Synthesis of compound 3**

Solid potassium *tert*-butoxide (0.168 g, 1.5 mmol) was added to a THF solution (40 mL) of the dpp-phosphonate (**2**, 0.361 g, 1 mmol) and 4-(pyrrolidin-1-yl)benzaldehyde (**1c**, 0.175 g, 1mmol; for structural representation of **1c**) under nitrogen atmosphere at room temperature. The resulting heterogeneous reaction mixture was stirred for 2 h. The reaction mixture was subsequently quenched with water (15 mL) and the product was extracted with dichloromethane. The resulting mixture was washed several times with water and then with sodium chloride solution (brine). It was then purified on a silica gel (100-200 mesh) column using ethyl acetate/hexane 5:95 v/v as the eluent to obtain the compound **3** as a yellow colored solid. This crude product was crystallized by vapor diffusion of diethyl ether into a dichloromethane solution of the crude product. After one week, needle-shaped crystals were isolated as yellow crystals, which crystallize in $P2_1/c$ space group (*vide infra*). Yield: 0.272 g (71%). Anal. calcd. for $C_{23}H_{22}N_6$: C, 72.23; H, 5.80; N, 21.97. Found: C, 72.35; H, 5.72; N, 21.82. IR (KBr pellet) ($\upsilon$/$cm^{-1}$) for **3**: 2957s, 1598w, 1386m, 1200s, 1030w, 921s. $^1$H NMR (400 MHz, CDCl3): δ 8.61 (d, *J* = 2 Hz, 2H), 7.93 (s, 2H), 7.80 (s, 2H), 7.52-7.47 (m, 3H), 6.94 (d, *J* = 16 Hz, 1H), 6.59 (d, *J* = 8 Hz, 2H), 6.52 (d, *J* = 2 Hz, 2H), 3.37 (t, *J* = 6 Hz, 4H), 2.05 (t, *J* = 6 Hz, 4H). $^{13}$C NMR (100 MHz, CDCl3): δ 151.8, 150.4, 148.5, 142.1, 135.4,128.8, 127.2, 123.1, 111.8, 107.7, 105.9, 47.6, 25.5. HRMS: m/z calcd. for $C_{23}H_{22}N_6$: 382.1906 ($M^+$), found: 383.1986 $(M + H)^+$.

**Synthesis of compound 4**

The dpp-phosphonate (**2**, 0.361g, 1mmol) and aldehyde **2c** (0.29 g, 1 mmol) were dissolved in 15 mL of dry THF. Then, potassium *tert*-butoxide (0.168, 1.5 mmol) was added to the reaction mixture at 0°C (ice bath) under nitrogen atmosphere; the ice bath was then removed and the reaction mixture was allowed to stir at room temperature for 1h. Then resulting dark color solution was quenched with 10 mL of water and the product was extracted with dichloromethane. The organic layer was washed several times with water and brine, dried over $Na_2SO_4$, and the crude product was purified by column chromatography using silica gel (100-200 mesh) using ethyl acetate/hexane 5: 95 v/v as the eluent to obtain compound **4**, which is orange color solid. Yield: 0.11 g (69%). Anal.

calcd. for $C_{29}H_{36}N_6O_2$: C, 69.57; H, 7.25; N, 16.79. Found: C, 69.45; H, 7.15; N, 16.86. IR (KBr pellet) ($\upsilon$/$cm^{-1}$) for **4**: 2952s, 2855w, 1591w, 1280s, 1102m, 1044s. $^1$H NMR (400 MHz, CDCl3): δ 8.58 (m, 3H), 7.94 (s, 2H), 7.79 (d, *J* = 14 Hz, 2H), 7.07 (d, *J* = 18 Hz, 2H), 6.49 (m, 2H), 6.47(s, 1H), 3.87 (s, 3H), 3.86 (s, 3H), 3.19 (t, *J* = 7 Hz, 4H), 1.54-1.47 (m, 4H), 1.30 (sextet, 4H), 0.91 (t, *J* = 7 Hz, 6H). $^{13}$C NMR (100 MHz, CDCl3): δ 152.9, 151.9, 150.5 (2C), 146.8, 142.7, 142.1 (2C), 129.9, 127.2 (2C), 122.9, 116.7, 111.3, 107.7 (2C), 106.2 (2C), 104.1, 56.3, 56.1, 52.2 (2C), 29.5 (2C), 20.5 (2C), 14.0 (2C).HRMS: m/z calcd.for $C_{29}H_{36}N_6O_2$: 500.2900 ($M^+$), found: 501.2979 $(M + H)^+$.

**Synthesis of compound 5**

The compound was synthesized using the same pathway as described for compound **4**. Aldehyde **3c** (0.235 g, 1 mmol) was used instead **1c**. That resulting grey colored solid was subjected to chromatographic purification over silica gel (100-200 mesh) using ethyl acetate/hexane 5:95 v/v as the eluent to obtain the compound **5** as a brown colored solid. Yield: 0.335 g (76%). Anal. calcd. for $C_{25}H_{26}N_6O_2$: C, 67.85; H, 5.92; N, 18.99. Found: C, 67.73; H, 5.98; N, 18.82. IR (KBr pellet) ($\upsilon$/$cm^{-1}$) for **5**: 2958w, 1598w, 1396m, 1200s, 1107w, 957s. $^1$H NMR (400 MHz, CDCl3): δ 8.59 (s, 2H), 7.93 (s, 2H), 7.79 (d, *J* = 14 Hz, 3H), 7.06 (s, 1H), 7.01 (d, *J*=17 Hz, 1 H), 6.50 (d, *J*= 1 Hz, 2H), 6.24 (s, 1 H), 3.88 (s, 3H), 3.82 (s, 3H), 3.44 (br, 4H), 1.95 (br, 4H). $^{13}$C NMR (100 MHz, CDCl3): δ. 153.7, 152.2, 150.4 (2C), 143.6, 142.0 (2C), 130.1, 127.2 (2C), 127.0, 121.4, 111.9, 109.2, 107.6 (2C), 106.0 (2C), 98.8, 56.9, 56.0, 50.4 (2C), 25.2 (2C). HRMS: m/z calcd.for $C_{25}H_{26}N_6O_2$: 442.2117 ($M^+$), found: 443.2198 $(M + H)^+$.

**Synthesis of compound 6**

Synthesis of this compound follows the same procedure as described for compound **4**. Aldehyde **4c** (0.602 g, 1 mmol)as used instead of aldehyde **2c.** The crude product was purified through column chromatography using silica gel (100-200 mesh) and ethyl acetate/hexane 5:95 v/v as mobile phase to obtain compound **6** as a dark red color solid. Yield: 0.480 g (80%); IR (KBr pellet): $\nu_{max}$: 2956w, 2915s, 1727w, 1582s, 1510m, 1453s, 1386m, 1205s, 1102m, 952w. $^1$H NMR (400 MHz, CDCl3): δ 8.56 (s, 2H), 7.94 (s, 2H), 7.78 (s, 2H), 7.55-7.46 (m, 6H), 7.12-7.02 (m, 2H), 6.98 (d, *J* = 16 Hz, 1H), 6.51(s, 1H), 6.50 (br, 2H), 3.87 (s, 3H), 3.85 (s, 3H), 3.16 (t, *J* = 8 Hz, 2H), 1.54-1.46 (m, 4H), 1.31 (sextet, 4H), 0.91 (t, *J* = 7 Hz, 6H). $^{13}$C NMR (100 MHz, CDCl3): δ 151.9, 150.7, 150.5

(2C), 147.4, 142.2 (2C), 141.4, 139.4, 134.4, 134.3, 127.5 (2C), 127.2 (2C), 126.6 (2C), 125.5, 124.5, 124.2, 118.6, 110.3, 107.87, 106.4 (2C), 105.1, 56.4, 56.3, 52.3 (2C), 29.3 (2C), 20.5 (2C), 14.0 (2C). HRMS: m/z calcd. for $C_{37}H_{42}N_6O_2$: 602.3369 ($M^+$), found: 603.3448 $(M + H)^+$. Anal. Calcd for $C_{37}H_{42}N_6O_2$: C, 73.73; H, 7.02; N, 13.94. Found: C, 73.65; H, 7.14; N, 14.04.

**Synthesis of compound 7**

Synthesis of this compound follows the same procedure as described for **3**. Aldehyde **5c** (0.277 g, 1 mmol )The crude product was further purified over silica gel (100-200 mesh) column using ethyl acetate/hexane 5:95 v/v as the eluent to obtain the compound **7**, which was isolated as grey microcrystalline solid. Yield: 0.324 g (67 %). IR (KBr pellet): $\nu_{max}$: 2920w, 2853s, 1732s, 1608m, 1551w, 1458s, 1396m, 1210w, 1045s, 957m, 864s.; $^1$H NMR (400 MHz, $CDCl_3$): δ 8.61 (d, *J* = 2Hz, 2H), 7.98 (s, 2H), 7.81(d, *J* = 1Hz, 2H), 7.55 (s, 1H), 7.53 (d, *J* = 3Hz, 3H), 7.51 (s, 1H), 7.44 (d, *J* = 8Hz, 2H), 7.14 (d, *J* = 16 Hz, 1H), 7.13 (d, *J* = 16Hz, 1H), 6.91 (d, *J* = 16Hz, 1H), 6.59 (s, 1H), 6.57 (s, 1H), 6.54-6.53 (br, 2H), 3.35 ( t, *J* = 6Hz, 4H), 2.04 (t, *J* = 6Hz, 4H). $^{13}$C NMR (100 MHz, CDCl3): δ. 150.8, 150.5 (2C), 147.7, 142.3 (2C), 139.4, 134.6, 133.9, 130.9, 127.9 (2C), 127.6 (2C), 127.2 (2C), 126.3 (2C), 124.5, 124.3, 122.8, 111.8 (2C), 107.9 (2C), 106.4 (2C), 47.6 (2C), 25.5 (2C).; HRMS: m/z calcd. for $C_{31}H_{28}N_6$ 484.2375 ($M^+$), found: 485.2456 $(M + H)^+$. Anal. calcd for $C_{31}H_{28}N_6$: C, 76.83; H, 5.82; N, 17.34. Found: C, 76.93; H, 5.75; N, 17.25.

**Synthesis of compound 8**

This compound was synthesized using same procedure as described for **4**. Aldehyde **6c** (0.53 g, 1 mmol; was used instead of aldehyde **2c** of procedure for molecule **4**. The dark brown crude was purified over silica gel (100-200 mesh) column using ethyl acetate/hexane 10:90 v/v as the eluent to obtain the compound **8** as dark brown solid. Yield: 0.514g (69 %). IR (KBr pellet): $\nu_{max}$: 2956w, 2930s, 2863s, 1726w, 1582m, 1515s, 1468w, 1344s, 1199s, 1106m, 1034s, 957m, 853m.; $^1$H NMR (400 MHz, $CDCl_3$); 8.61 (d, *J* = 2 Hz, 2H), 7.99 (s, 2H), 7.80 (d, *J* = 1 Hz, 3H), 8.08 (d, *J* = 16 Hz, 1H), 7.37 (d, *J* =16 Hz, 1H), 7.27 (d, *J* = 16 Hz, 1H) 7.18 (s, 1H), 7.15 (s, 1H), 7.11 (s, 1H), 6.53–6.52 (br, 3H), 4.13 ( t, *J* = 7 Hz, 2H), 4.07 (t, *J* = 6 Hz, 2H), 3.88 (d, *J* = 5 Hz, 6H), 3.17 (t, *J* = 7 Hz, 4H), 1.92–1.86 (m, 4H), 1.66–1.60 (m, 4H), 1.52 (t, *J* =7 Hz, 4H), 1.35–1.30 (m,

4H), 1.09–1.04 (m, 6H), 0.93 ( t, *J* = 7 Hz, 6H). 13C NMR (100 MHz, $CDCl_3$): δ 152.0 (2C) , 151.9, 151.6, 150.8, 150.6 (2C), 147.6, 142.2 (2C), 141.2, 130.3, 129.8, 127.2 (2C), 125.5, 124.3, 121.0, 119.6, 112.0, 110.6, 110.5, 107.8 (2C), 106.5 (2C), 105.5, 69.3 (2C), 56.6, 56.3, 52.4 (2C), 31.6, 31.5, 29.4(2C), 20.5, 19.5 (2C).; HRMS: m/z calcd. for $C_{45}H_{58}N_6O_4$ 746.4520 ($M^+$), found: 747.4599 $(M + H)^+$. Anal. calcd for $C_{45}H_{58}N_6O_4$: C, 72.36; H, 7.83; N, 11.25. Found: C, 72.45; H, 7.76; N, 11.36.

**Synthesis of compound 9**

This compound was synthesized by same procedure as described for **5.** Aldehyde **7c** (0.48 g, 1.0 mmol) was used instead of aldehyde **3c**. The resultant dark red colored crude product was purified by a silica gel column (100-200 mesh) eluting with methanol/dichloromethane in 5:95 v/v as mobile phase. Compound **9** was isolated as a dark red gum. Yield: 0.48 g (71%). IR (Neat): $\nu_{max}$: 2954.6, 2923.5, 2853.9, 1734.4, 1588.6, 1504.7, 1463.2, 1376.7, 1202.4, 1042.1, 968.1, 853.3; $^1$H NMR (400 MHz, $CDCl_3$); 8.61(d, *J* = 1 Hz, 1H), 8.61(d, *J* =1 Hz, 1H), 7.99 (s, 2H), 7.81 (d, *J* =16 Hz, 1H), 7.80 (d, *J* =1 Hz, 2H) 7.50 (d, *J* =16 Hz, 1H), 7.31 (d, *J* =16 Hz, 1H), 7.26 (d, *J* =16 Hz, 1H), 7.17 (d, *J* =16 Hz, 2H), 7.10 (s, 1H), 6.52 (dd, $J_1$ =3 Hz, $J_2$ =2 Hz, 2H), 6.32 (s, 1H), 4.14 (t, *J* =7 Hz, 2H), 4.07 (t, *J* =6 Hz, 2H), 3.89 (s, 3H), 3.86 (s, 3H), 3.43(br, 4H), 1.98 (t, *J* =7 Hz, 4H), 1.96-1.87 (m, 4H), 1.66-1.60(m, 4H), 1.08 (t, *J* =7 Hz, 3H), 1.05 (t, *J* =7 Hz, 3H), $^{13}$C NMR (100 MHz, $CDCl_3$): δ 152.5,152.1, 151.6, 150.54, 150.5 (2C), 144.2, 142.2 (2C), 140.9, 130.4, 130.0, 127.2 (2C), 125.3, 124.4, 123.9, 119.4, 116.4, 120.0, 110.8, 110.0, 107.8 (2C), 106.5 (2C), 99.7, 69.2, 69.2, 56.8, 56.5, 50.5 (2C), 31.6, 31.5, 25.1 (2C), 19.5 (2C), 14.03, 14.01;; HRMS: m/z calcd. for $C_{41}H_{48}N_6O_4$ 688.3737 ($M^+$), found: 688.3795 ($M^+$). Anal. calcd for $C_{41}H_{48}N_6O_4$: C, 71.49; H, 7.02; N, 12.02. Found: C, 71.32; H, 7.08; N, 12.36.

### 3.2.3. Single crystal X-ray structure determination of the compounds 2-3

Single crystals, suitable for facile structural determination for the Compounds **2** and **3** were measured on a Bruker D8 quest PHOTON 100 CMOS system under Mo-Kα (λ = 0.71073 Å) graphite monochromatic X-Ray beam. Data processing was accomplished by using SAINT PLUS and structures were solved by using SHELXS-97 and refined using SHELXL-14/7 program.[26] All non-hydrogen atoms were refined anisotropically by full matrix least square cycles on $F^2$. Hydrogen atoms were introduced on calculated positions

and included in the refinement riding on their respective parent atoms. Detailed information about crystal data and structure for compounds **2** and **3** are summarized in Table 1.

### 3.3. Results and discussion

#### 3.3.1. Synthesis

The 2,6-bis(pyrazolyl)-4-bromomethyl pyridine precursor **1** (see chart 1 for the structural representation of **1**)[27] and required appropriate N, N-dialkylated- and pyrrolidine-substituted aldehydes **1c-7c**[18,19](Chart 3.2) along with their precursors were synthesized according to literature procedures in good yields. Compound **2** (phosphate derivative, see chart 3.1) was synthesized by Arbuzov reaction of compound **1** with triethyl phosphite. The target molecules (compounds **3-9**) have been synthesized using an efficient Horner-Wadsworth-Emmons (HWE) reaction path (Chart 3.1). The advantages of the HWE reaction pathway over the conventional Wittig reaction are of many folds: (i) the former one has a good response with the stabilized yields, (ii) it mainly gives E-stereo selectivity of the olefin bond and (iii) it generates a water soluble phosphate which can easily be removed from the reaction mixture through the aqueous process. The difficulty over the separation of Wittig by-product triphenylphosphine oxide is thus largely ruled out in the HWE reaction. After purification by column chromatography was done, the molecular structures of all the chromophores **3-9** were determined by IR-, NMR ($^{1}$H and $^{13}$C)-, and mass-spectral studies including CHNS analyses.

#### 3.3.2. Description of crystal structures

Compound **2** crystallizes in the triclinic system with space group *P-1*. The thermal ellipsoidal plot of the crystal structure of compound **2** is displayed in Figure 3.1(a). In the crystal structure, the concerned molecule undergoes C–H···O intramolecular hydrogen bonding interactions leading to a chainlike supramolecular arrangement (Figure 3.1b). Compound **3** crystallizes in monoclinic system with space group $P2_1/c$. The X-ray analysis of a single crystal of compound **3** reveals that the concerned asymmetric unit consists of the full molecule and the thermal ellipsoidal plot of the same is presented in Figure 3.2a. The crystal data and structure refinement parameters of compounds **2** and **3** have been given in Table 3.1. Interestingly, in the crystal structure of compound **3**, the molecules undergo C−H···N intermolecular hydrogen bonding interactions leading to a supramolecular dimer structure (Figure 3.2b). In the case of compound **3**, both

intermolecular hydrogen bonding and π–π stacking interactions play a vital role in the supramolecular ordering, that leads to the formation a pseudo sheet like structure as shown in Figure 2b. The sheet-like structure, formed from multilayered supramolecular aggregates *via* intramolecular π-π stacking interactions ($d$ = 4.474 Å) of the associated pyridine rings (*J*-aggregation), justifies the bathochromic shift in the absorption maxima in going from solution to solid state (*vide infra*).

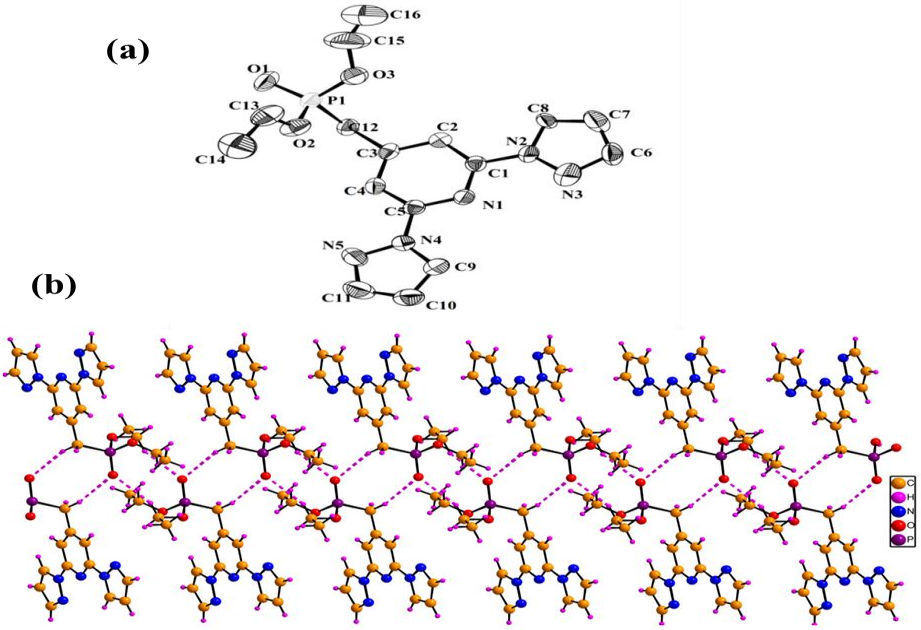


**Figure 3.1.** Thermal ellipsoidal plots of (a) compound **2** (50% probability) (top) hydrogens are omitted for clarity (b) Molecular packing diagram of compound **2** characterized by C–H···O weak interactions (bottom).

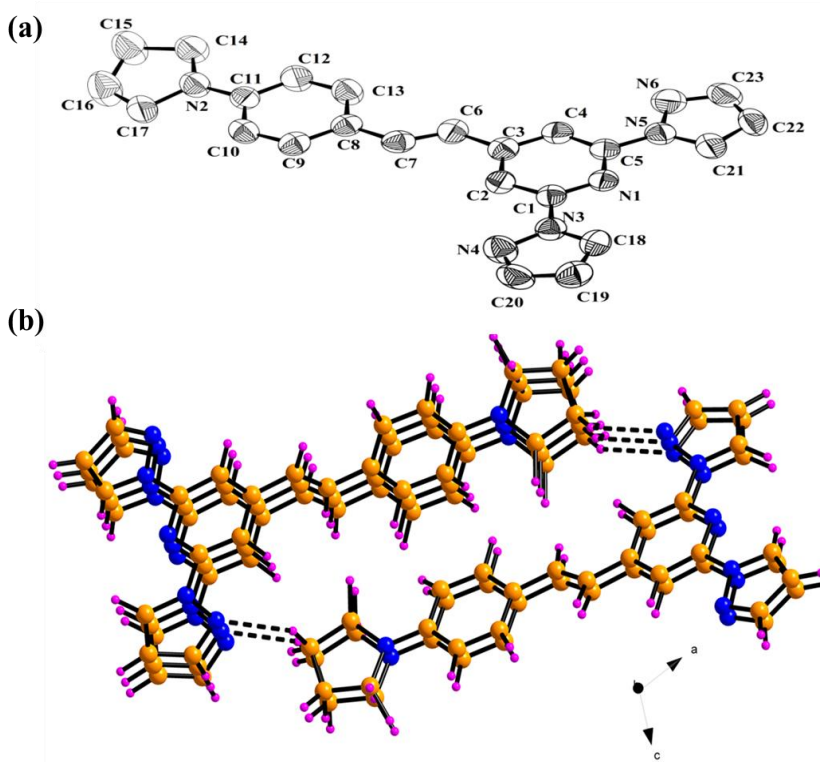


**Figure 3.2.** Thermal ellipsoidal plots of (a) compound **3 (**30% probability) (Top), hydrogens are omitted for clarity (b) The molecular packing diagram of compound **3** characterized by C–H···N weak interaction (bottom); color code: C, yellow; N, blue; H, pink.

### 3.3.3. Photophysical studies

The absorption and emission spectra of the title compounds were recorded in different solvents at room temperature (298±2 K). Figure 3.3a displays normalized UV–vis absorption and photo-luminescence (PL) spectra of compounds **3-9** in DCM solvent. The absorption spectra of all the title compounds exhibit a broad absorption band in visible region ($\lambda_{max}$ = 400-495 nm). These absorption bands are assigned to the intra-ligand charge transfer (ILCT) bands which are originated due to charge delocalization from the donor dialkyl (compounds **4**, **6** and **8**) or pyrrolidine (compounds **3**, **5**,**7** and **9**) amino group to (2,6-bis(pyrazolyl)pyridine) acceptor subunits through the π-transmitters in the 'push-pull' molecules. In all the cases, the single band is well resolved in this region, which has been confirmed due to its sensitivity to solvent polarity. Figure 3.3b depicts spectra, recorded in four different solvents, *viz*., toluene, dichloromethane (DCM), acetonitrile (MeCN) and dimethylformamide (DMF) at room temperature and the

corresponding optical data are summarized in Table 3.2. From the absorption spectra, it is quite evident that the compounds with pyrrolidine donors (**3**, **5**, **7** and **9**) exhibit bathochromic shift by ≈ 10 nm compared to the compounds with dibutyl amino group substituted donors (**4**, **6** and **8**). Photoluminescence has been observed for all the title chromophores **3-9** at room temperature (298±2 K). All the solutions have been excited at their respective lowest energy absorption maxima, and in all the cases, they exhibit excellent fluorescence behavior in various solvents (Figures 3.3a and 3.3b). The obtained photophysical data in various solvents and fluorescense (FL) lifetime studies suggest that the excited states of all the title compounds **3-9** are more polar than their respective ground states. On varying the solvent polarity from lower (toluene solvent) to higher (DMF solvent), the shifts in emission bands were found to be more profound than those in the corresponding absorption bands. Generally, the dipole character is increased in the excited state $S_1$, when the electrons are excited from the highest occupied molecular orbital (HOMO) to the lowest unoccupied molecular orbital (LUMO). As a result, the solvents with high polarity tend to stabilize such polarized excited state by reorienting the solvent molecules so as to lower the energy of the system thereby leading to a red shift in the emission spectra. This is well explained from DFT calculations and their molecular orbital (MO) diagrams (vide infra) and FL lifetime studies (see Figure 3.3c). The entire series of compounds (**3-9**) exhibits strong emission in solution as well as in solid state (except compound **7**) at room temperature. Thus the emission spectra of compounds **3-9** are strongly dependent on the polarity of the solvent (see Table 3.2 and Table 3.5). The emission light of the compound **3** varies from green to red with increasing polarity of the solvent, for example, in the solution of moderate polar solvent, such as toluene, it shows blue emission and emission maxima is centered at 460 nm as shown in Figure 3.3b. On the other hand, in the solution of more polar solvent, such as DMF, this shows green emission and the pertinent emission maxima centers at 562 nm as shown in Figure 3.3b. Hence the solvent dependence of the emission shows that the excited state is stabilized in more polar solvents, which is due to an intramolecular charge transfer (ICT). It has also been observed that on increasing the conjugation length in this series of compounds, the absorption and emission maxima are bathochromically shifted as shown in Figure 3.3(a). For example, when we compared the absorption and emission of compounds **3** *vs* **7** or **4** *vs* **6** in DCM, it has been observed that the $\lambda_{abs}$ and $\lambda_{em}$ increases with increasing the conjugation length (Table 3.2). Comparison between the chromophores, based on nature

and position of the donor functionalities, gives us some insight into the photophysical properties. In cyclic donor systems (compounds **3**, **5**, **7** and **9**), the absorption and emission bands in the chromophores are blue shifted with good quantum yields compared to their acyclic donor systems (compounds **4**, **6** and **8**).

**Solid-State emission of the compounds**

Except chromophore **7**, all other chromophores, the **3-6**, **8** and **9** showed solid state emissions, in addition to emission in solution. These compounds absorb in the range 400-500 nm and it is observed that there is a bathochromic shift in the absorption maxima in going from solution state to solid state, which signifies the presence of intermolecular interactions between the molecules (might be due to J aggregation) in the solid state. When these chromophores **3-6**, **8** and **9** are exited in their respective absorption maxima (422, 412, 438, 470, 445 and 453 nm), they exhibit emission maxima at 583, 575, 569, 665, 663 and 634 nm respectively.

### 3.3.4. Fluorescence lifetime studies

Fluorescence lifetime of the entire series of the compounds **3-9** (see Figure 3.3c) was measured through time-correlated single photon technique by monitoring their respective emission maximum using a picosecond laser diode of 375 nm as an excitation source. Fluorescence decay traces of all title compounds are best fitted using a bi-exponential decay function $I(t) = a1*\exp(-t/\tau_1) + a2*\exp(-t/\tau_2)$, where $\tau_1$ and $\tau_2$ are the lifetime components and a1, a2 are their respective amplitudes. Among all these derivatives, compound **3** in acetonitrile (MeCN) shows a shorter lifetime with a shortest component (<65 ps, IRF) having a minor amplitude and a major component of 0.4 ns, whereas chromophores **8** and **9** show longest lifetime (1.83 ns) as shown in Table 3. The fastest component can be attributed to the emission originating from the ICT state and the long component can be due to the solvent stabilized ICT state. With increase in π-electron conjugation length and electron donating ability of the donor counterpart (from **3** to **9**), we could see a progressive increase in fluorescence lifetime. On the other hand, the same π-conjugation length but different donating ability for compounds **6** and **7** or **8** and **9**, do not exhibit any difference in lifetime. This indicates that the extent of excited-state stabilization for these derivatives is very similar. To understand the effect of solvatochromism and origin of these decay components, we have recorded the decay

traces of compound **3** in different solvents, DCM, MeCN and DMF as shown in Figure 3.3d. In highly nonpolar solvent, like dichloromethane (DCM), we could not able to fit the decay trace, hence it is expected to be a life time of the order of <65 ps. However, with increase in medium polarity from MeCN to DMF, we have observed an increase in FL lifetime (0.49 to 0.63 ns) along with the decrease in non-radiative rate constant for compound **3**, indicating a stabilization of the excited state in more polar medium.

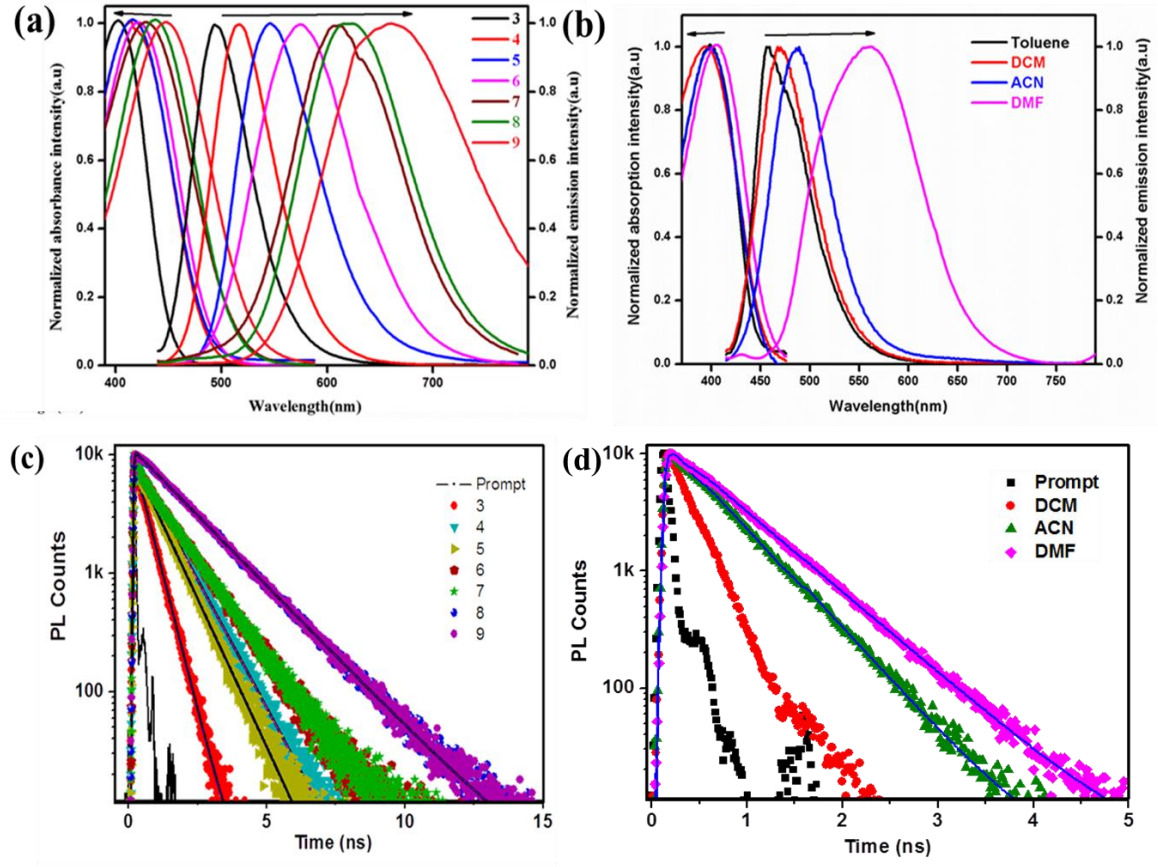


**Figure 3.3.** (a) Normalized UV–vis absorption and photo-luminescence (PL) spectra of compounds (**3-9**) in DCM solvent. (b) Normalized UV–vis absorption and PL spectra of compound **3** showing the solvatochromic effect. (c) Fluorescence decay traces of compounds **3-7** were measured in MeCN medium and that of compounds **8** and **9** were measured in toluene medium.(d) Fluorescence decay profiles of compound **3** in DCM (red) , MeCN (green) and DMF (pink). In DCM solvent, the decay profile cannot be fitted properly as it is very closed to the instrument response function.

### 3.3.5. Theoretical calculations

**Computation methods**

Energy minimization calculations of the ground electronic state ($S_o$) of the different chromophores (**3-9**) were performed with density functional theory (DFT) employing CAM-B3LYP hybrid functional and 6-31G(d, p) basis set of Pople, using Gaussian09 program modules.[28] The energy minima of the compounds were confirmed by subsequent frequency analysis with the same level of theory. The solvent effect of the title chromophores (compounds **3-9**) has been accounted by placing the compounds in the solvent cavity by following the self-consistent reaction field (SCRF) approach as implemented in Gaussian09 program modules.[28] The polarizable continun model approach was implemented to create the solvent cavity.[29] The selected solvents are toluene, dichloromethane (DCM), acetonitrile (MeCN) and dimethylformamide (DMF). The verticle excitation energy of the excited states of the chromophores was calculated with the time-dependent density functional theory (TDDFT) using same functional and basis set by a Gaussian09 program modules.[29] The verticle $S_o \rightarrow S_1$ transition energies were computed taking ground energy minimized structure as a reference. The geometry of the $S_1$ state of the compounds was calculated by analytic TDDFT gradients implemented in Gaussion09 suite program.[30,31] The frequency analysis of the $S_1$ state of the compounds was subsequently determined by numerical variation of the TDDFT gradients. This allows us to confirm the absence of imaginary frequencies and to compute the different thermodynamic data.

The vertical excitation energies from $S_o \rightarrow S_1$ transition for each compound was computed considering the solvent reaction field in both by the linear response (LR)[32] and state-specific (SS) model.[33] The polarization of the solvent cavity in the presence of solute (compounds **3-9**) is considered in the SS model. Therefore the accuracy of the SS model is greater than LR approach at the price of significant increase of computational cost. The properties of the excited states (mainly fluorescence transition) were calculated within the limits of both equilibrium (eq) and non-equilibrium (neq) schemes of solvation under modified PCM model. In eq scheme, the solvent molecules reorient themselves according to the polarization of the electronic distribution of the solute. However, in the neq scheme, solvent molecules find no time to reorient themselves according to the electronic distribution of the excited states of solute. Thus eq scheme needs higher computational

cost than neq scheme. Geometry optimization in the ground and excited states follows the eq scheme, whereas the vertical transitions (absorption or emission) follow the neq scheme. Overall, the emission spectra are calculated following the principle, discussed in literature[34-36] and references therein. The emission spectra of the compounds **3**, **5** and **7** were calculated by visualizing the following representation (Scheme 3.1).

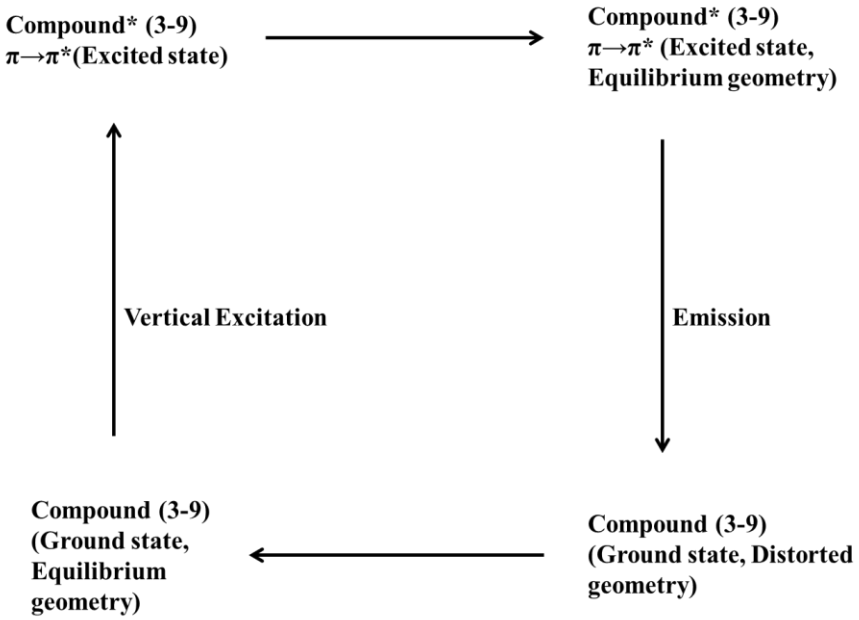


**Scheme 3.1**

The calculation of the fluorescence band structure of the compounds was obtained by convoluting the stick lines (*vide infra*) with the following Lorentzian line shape function with Γ full-width half maxima (fwhm) to reproduce the experimental resolution.

$$L(E) = \frac{1}{\pi} \frac{\frac{\Gamma}{2}}{E^2 + \left(\frac{\Gamma}{2}\right)^2}$$

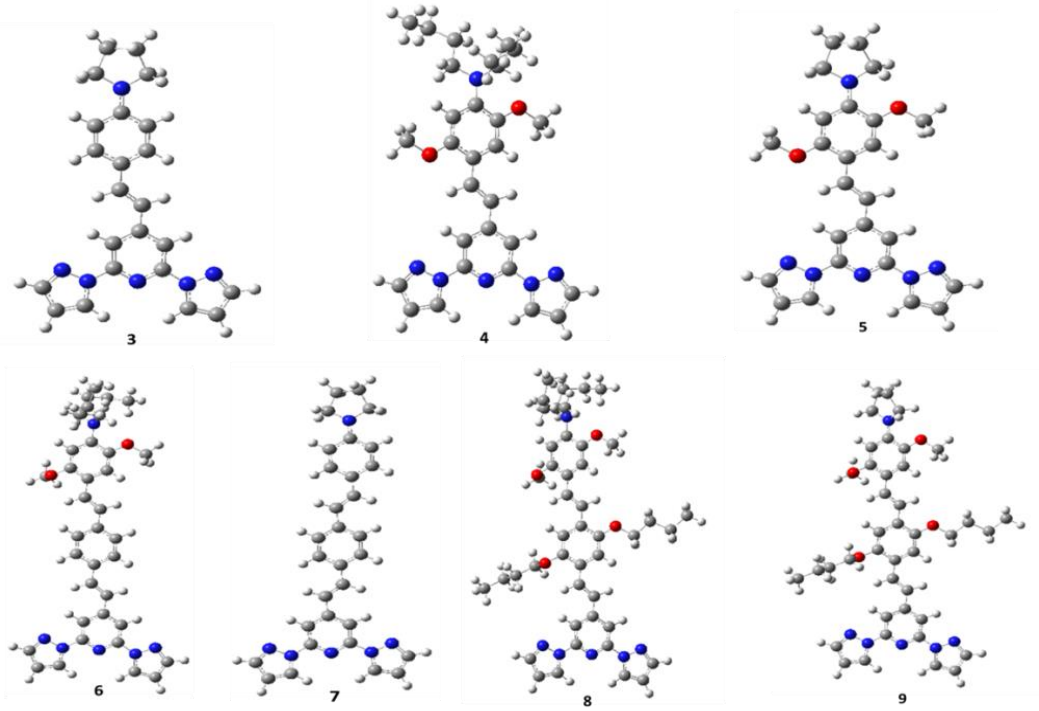


**Chart 3.3.** The energy minimized structure of the newly synthesized chromophores (**3-9**). The theoretical calculations are performed with CAM-B3LYP/6-31G (d,p) level of the theory in DCM solvent medium.

Energy minimizations of the newly synthesized π-conjugated chromophores **3-9** are performed in their ground electronic states in the gas phase and also in solvent media (toluene, DCM, MeCN and DMF). The energy minimized structures of all the title compounds in dichloromethane (DCM) solvent are shown in Chart 3.3. The optimized structures of the title compounds are treated as the reference points for the TDDFT calculations. The vertical excitation energy ($\lambda_{max}$ value for absorption) is calculated in the gas phase and solvent medium; the relevant data are given in Table 3.4. A uniform increment of $\lambda_{max}$ value is observed along the series from compounds **3** to **9** in gas phase calculation. This is attributed due to larger conjugation length between a pair of compounds (**3**, **7)** and (**4, 6).** The bathochromic shift between these pairs of compounds is larger in the case of cyclic pyrrolidine substitution ( ~47 nm) than the open chain dibutyl amino substitution (~15 nm). This indicates that the electron donation capability of the cyclic pyrrolidine rings is greater than that of the open chain dibutyl amino donor. The same statement is also applicable during the comparison between compounds **8** and **9**, where both the compounds have same vertical chain length and similar substitution (–

OMe and –OBu). A shift of the $\lambda_{max}$ values for the compounds are observed in the presence of solvents (toluene, DCM, MeCN, and DMF). This is attributed due to the change of energy gap between the highest occupied molecular orbital (HOMO) and lowest unoccupied molecular orbital (LUMO) of the compounds in the different solvent environment. The energy values of HOMO, LUMO, and LUMO-HOMO energy gap, ΔHOMO (GAS –DCM) and ΔLUMO (GAS-DCM) of the compounds, both in the gas phase (GAS) and solvent medium (in DCM) are given in Table 3.4. It is found from the calculations that the LUMO-HOMO energy gap for title compounds is reduced in the solvent medium compared to that in the gas phase. Both the HOMO and LUMO of compounds are stabilized in a solvent medium and the stabilization of LUMO [ΔLUMO (GAS-DCM] in solvent medium is greater than that of HOMO [ΔHOMO (GAS-DCM)]. As a result, excitation from HOMO to LUMO in each compound becomes easier in a solvent medium. Thus a bathochromic shift of the absorption spectra is observed from all the compounds in solvent medium (toluene, DCM, MeCN, and DMF). The molecular orbital (MO) diagram of HOMO and LUMO of the energy-minimized structure of the compounds are shown in Figure3.4. It is found that the nature of the HOMO of the each compound belongs to a π-bonding type, whereas the same for the LUMO is the π-antibonding type. The maximum charge density (electron density) of the HOMO is situated at the donor moieties (pyrrolidine or dibutyl amino) and in the case of LUMO, the maximum charge density is situated at the 2,6-bis(pyrazolyl)pyridine acceptor moiety. So the overall π→π* type of electronic transitions in the synthesized compounds occur from pyrrolidine or dibutyl amino donor moiety to the 2,6-bis(pyrazolyl)pyridine acceptor moiety (charge transfer in the same compound). As a result, this π→π* electronic transition can be called as intramolecular charge transfer (ICT). Results, given in Table 3.5, indicate that the calculated $\lambda_{max}$ values using the LR model are comparable with the experimental absorption values. An improved set of data of the calculated $\lambda_{max}$ values are obtained by using the SS model of solvation. The normalized theoretical UV-Vis absorption spectra (indicated by solid lines) of the compounds are shown in Figure 3.5. The solvatochromic shift of the absorption maxima ($\lambda_{max}$ ) of compounds was not found prominent, when the absorption was taken place in different solvents: toluene, DCM, MeCN and DMF by both LR and SS model approaches. For example, the calculated $\lambda_{max}$ values of compound **3** are 368 nm, 376 nm, 376 nm, and 380 nm in toluene, DCM, MeCN and DMF (SS model), respectively. This shows a slight change of absorption maxima for

compound **3** with the increasing polarity of the solvents. The same results are found for the other compounds also, when the calculations are performed in different solvents with increasing polarity. This indicates that the polarity of the solvents has less effect on the absorption spectra of the synthesized compounds. The overall bathochromic shifts of experimental absorption peaks in compounds **3**, **5**, **7** and **9**, with different conjugation length and different substitution, are well explained by the TDDFT calculation in different solvent medium (toluene, DCM, MeCN and DMF). The same scenario was observed in the case of compounds **4**, **6** and **8**. Another observation of bathochromic shift of absorption peaks is found among the title compounds with same substitution but different donor moieties (pyrrolidine *versus* dibutyl amino, see chart 3.1) in a solvent medium. An average bathochromic shift of ~16/18 nm and ~18/28 nm (*via* LR /SS model) is observed for the pair of compounds (**4**, **5**) and (**8**, **9**) respectively. The results are justified by the LUMO-HOMO energy gap of the compounds (see Table 3.4). For example, compound **9** has less LUMO-HOMO energy gap (~ 4.97 eV) than the compound **8** (~ 5.21 eV). This indicates that the electronic transition from HOMO ($\pi$) to LUMO ($\pi^*$) is easier in compound **9** compared to that in compound **8**. This observation also concludes that the electron donating capability of pyrrolidine donor is greater than that of dibutyl amino moiety.

The computed fluorescence spectra of the compounds **3**, **5** and **7** in DCM medium are shown in Figure 3.5, indicated by the dashed lines. As mentioned in the methodology section, the band structure of the fluorescence spectra is generated by convoluting the stick vibronic lines obtained, from theoretical calculations with Lorentzian type of function using 0.29 eV fwhm. The intensity of the spectra is normalized to match with experimental observation. This practice ensures a good comparison between the theoretical and experimental fluorescence spectra. It is noted that theoretically, we calculated only the fluorescence spectra for compounds **3**, **5** and **7** in DCM medium. It is well known that the evaluation of theoretical fluorescence spectra is computationally very costly and its cost increased with the size of the molecule. Another difficulty of this calculation is to find out the proper Franck-Condon geometry at the excited state ($S_1$). For the other compounds, we found this difficulty during calculations. We can be able to perform the fluorescence spectral calculation only for compounds **3**, **4**, **5** and **7** in DCM solvent within the limit of our computational facility. In the case of compound **4**, we found discrepancies in Franck-Condon geometry in the excited state. Thus we can only able to

get its $\lambda_{max}$ value, not its band structure. Theoretically obtained values for $\lambda_{max}$ in DCM medium of compounds **3**, **4**, **5** and **7** are 433 nm, 460 nm, 464 nm and 553 nm respectively. It is found from Figure 3.5, that a bathochromic shift of the emission maxima (energy gap between $\lambda_{max}$) between the pairs of compounds (**3**, **5** ) and (**5**, **7**) are 31 nm and 89 nm, respectively. The corresponding values for experimental findings are 51 nm and 63 nm respectively. This indicates that theoretical data underestimate the change of bathochromic shift in the first pair (**3**, **5**) of compounds and overestimate the change of bathochromic shift in a latter pair (**5**, **7**) of compounds. However, the same comparison between the pair of compounds **3** and **7** indicates that the theoretical data (120 nm) nicely reproduce the experimental observation (114 nm). So it can be concluded from above discussion that the change of emission property with the length of conjugation chain is well reproduced by theoretical calculations. The overall bathochromic shift of emission maxima from compounds **3** to **7** is properly explained by this TDDFT based calculations. It is also noted that the bathochromic shift of emission maxima is more prominent than the same for the absorption maxima when going from compounds **3** to **9**.

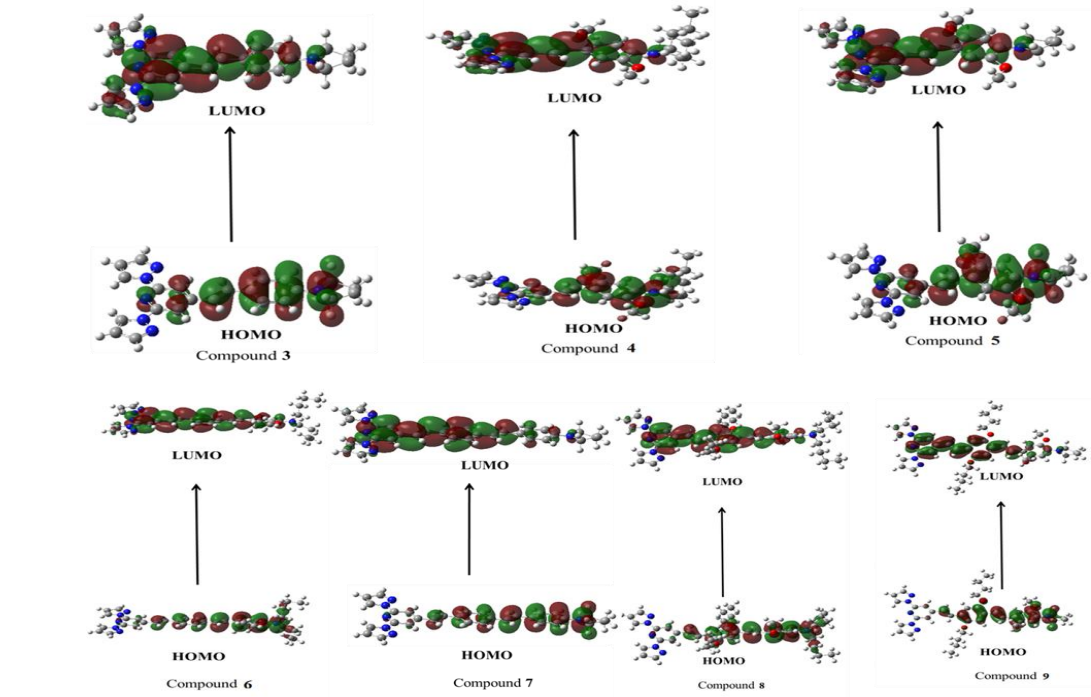


**Figure 3.4.** Molecular orbital (MO) diagrams of the energy-minimized structure of the newly synthesized compounds **3-9**.

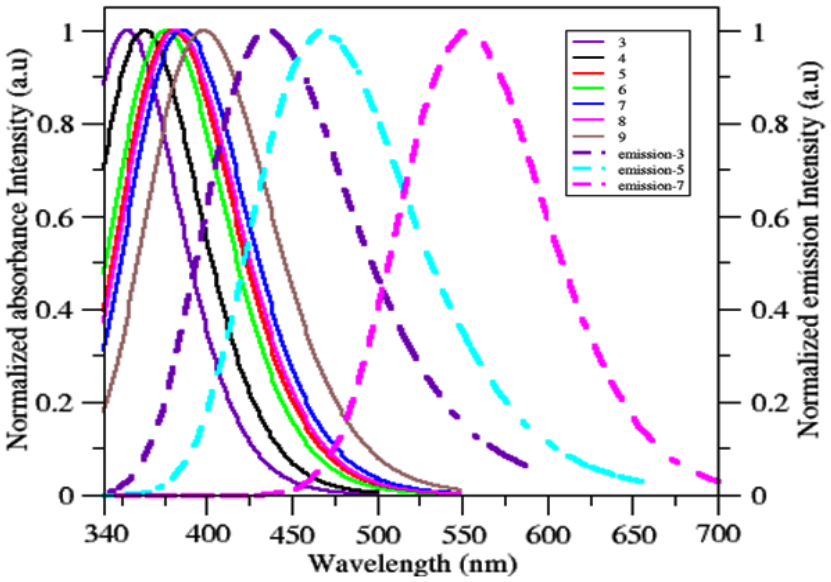


**Figure 3.5**. Normalized theoretical absorption spectra (thick line) of compounds (**3-9**) and normalized theoretical emission spectra (dotted line) of compounds **3**, **5** and **7** in dichloromethane (DCM) solvent.

### 3.4. Summary

We have described the synthesis and characterization of new conjugated family of 2,6-bis(pyrazolyl)pyridine derivatives with phenyl substituted donor-π-acceptor molecules (Chart 3.1). Precursor compound **2** and first member of the series (compound **3**) are additionally characterized by single crystal X-ray structure determination. The title compounds **3-9** represent a unique family in the sense that this series contains a common 2,6-bis(pyrazolyl)pyridine unit acting as an acceptor moiety, common to each member of the family and diverse donor functionalities. Chromophores **3-9** are characterized by an intramolecular charge transfer from the donors to the acceptor moiety. We have demonstrated that described compounds show large solvent sensitive emissive behavior and their photophysical properties are highly dependent on the number, nature and position of the donor functionalities, which have also been corroborated computationally by TDDFT calculations. We have demonstrated that fluorescence spectra of chromophores **3**, **5** and **7** can be explained by density functional calculations. We also have performed fluorescence lifetime studies, which indicate the stabilization of the excited state is more in polar medium.

**Table 3.1.** Crystallographic data and structure refinement for compounds **2** and **3**

| | **2** | **3** |
|---|---|---|
| Empirical formula | $C_{16}H_{20}N_5O_3P$ | $C_{23}H_{22}N_6$ |
| Formula weight | 361.34 | 382.47 |
| T(K) / λ(Å) | 298(2) K | 273(2) K |
| Crystal system | triclinic | monoclinic |
| Space group | P-1 | $P2_1/c$ |
| a (Å) | 7.4514(7) | 24.483(2) |
| b (Å) | 10.2478(9) | 4.4738(4) |
| c (Å) | 12.0251(10) | 19.705(2) |
| α (°) | 74.076(2) | 90 |
| β (°) | 89.7640(2) | 113.73 |
| γ (°) | 85.604(2) | 90 |
| Volume ($Å^3$) | 880.27(13) | 1975.9(3) |
| Z, $\rho_{calcd}$ ($g\ cm^{-3}$) | 2, 1.363 | 2, 1.286 |
| *F*(000) | 380 | 808 |
| goodness-of-fit on $F^2$ | 1.063 | 0.983 |
| R1/ wR2 [$I > 2\sigma(I)$] | 0.0781/ 0.1977 | 0.0810/0.1670 |
| R1/ wR2 (all data) | 0.1018 / 0.2177 | 0.2161/0.2150 |
| Largest diff. peak and hole $e.Å^{-3}$ | 0.840 and -0.875 | 0.114 and -0.122 |

**Table 3.2.** Photophysical data of all the *D-π-A* compounds **3-9**

| Compound | Solvent | $\lambda_{max}$(nm) | $\varepsilon^a$ ($M^{-1}cm^{-1}$) | $\lambda_{em}$(nm) | $\Phi^b_{em}$ % | $\Delta\bar{\nu}^c$ ($cm^{-1}$) |
|---|---|---|---|---|---|---|
| **3** | Toluene | 398 | 39473 | 460 | 21.5 | 3836 |
| | DCM | 391 | 28947 | 493 | 30.73 | 5292 |
| | MeCN | 399 | 34210 | 507 | 58.96 | 5339 |
| | DMF | 405 | 44736 | 562 | 81.66 | 6898 |
| **4** | Toluene | 402 | 26000 | 490 | 78.34 | 4467 |
| | DCM | 403 | 14000 | 521 | 74.14 | 5620 |
| | MeCN | 404 | 26000 | 537 | 38.37 | 6131 |
| | DMF | 412 | 16000 | 559 | 54.72 | 6382 |

| | | | | | | |
|---|---|---|---|---|---|---|
| **5** | Toluene | 417 | 11363 | 492 | 31.08 | 3655 |
| | DCM | 419 | 20361 | 527 | 27.96 | 4891 |
| | MeCN | 413 | 25000 | 548 | 50.33 | 5965 |
| | DMF | 426 | 27272 | 590 | 53.18 | 6525 |
| **6** | Toluene | 415 | 20000 | 635 | 32.52 | 8348 |
| | DCM | 422 | 8333 | 627 | 46.83 | 7748 |
| | MeCN | 413 | 20000 | 650 | 62.64 | 8829 |
| | DMF | 421 | 26666 | 722 | 85.92 | 9902 |
| **7** | Toluene | 424 | 20833 | 621 | 26.69 | 7481 |
| | DCM | 424 | 27083 | 618 | 38.42 | 7403 |
| | MeCN | 413 | | 674 | 45.16 | 9377 |
| | DMF | 419 | 25000 | 714 | 56.48 | 9861 |
| **8** | Toluene | 437 | 10723 | 635 | 34.82 | 7135 |
| | DCM | 436 | 17426 | 659 | 45.25 | 7761 |
| | MeCN | 433 | | 702 | 16.36 | 8849 |
| | DMF | 442 | 14745 | 723 | 67.78 | 8843 |
| **9** | Toluene | 449 | 10294 | 635 | 34.81 | 6523 |
| | DCM | 446 | 11764 | 676 | 46.16 | 7624 |
| | MeCN | 442 | | 712 | 18.92 | 8580 |
| | DMF | 451 | 8823 | 723 | 76.78 | 8341 |

[a]**ε** were measured in Toluene, DCM, MeCN, and DMF solution, but in the case where no data is reported, that is due to low solubility. [b]Fluorescence relative quantum yield of the compounds **3-9** was measured by using Fluorescein (in 0.1 N NaOH in EtOH) as the reference ($\Phi_{em}$ = 0.79).[c]Stokes shift $\Delta\bar{\nu} = \bar{\nu}_{abs} - \bar{\nu}_{em}$.

**Table 3.3.** Radiative ($k_r$) and Nonradiative ($k_{nr}$) Rate constant[a] for the compound **3-9**.

| **Sample** | **$\tau_1(a_1)$ [ps]** | **$\tau_2(a_2)$ [ns]** | **$K_r$ ($10^7$ $S^{-1}$)** | **$k_{nr}$ ($10^9$ $S^{-1}$)** |
|---|---|---|---|---|
| **3** | 65 (0.16) | 0.47 (0.84) | 1.25 | 0.87 |
| **4** | 19 (0.07) | 1.01 (0.93) | 0.38 | 0.62 |
| **5** | 13 (0.08) | 0.87 (0.92) | 0.57 | 0.57 |
| **6** | 116 (0.05) | 1.29 (0.95) | 0.48 | 0.29 |
| **7** | 122 (0.05) | 1.30 (0.95) | 0.35 | 0.42 |

| | | | | |
|---|---|---|---|---|
| **8** | --- | 1.83 (1.0) | 0.19 | 0.35 |
| **9** | --- | 1.82 (1.0) | 0.19 | 0.35 |

[a]The rate constants were estimated using the following equations $k_r = \phi_f/\tau_f$ and $k_{nr} = (1- \phi_f)/\tau_f$, where $\phi_f$ is the measured quantum yield and $\tau_f$ is the fluorescence lifetime.

**Table 3.4.** Comparison of energy values of HOMO (H), LUMO (L), HOMO-LUMO (H-L) gap, [ΔHOMO (GAS-DCM) = ΔH] and [ΔLUMO (GAS-DCM) = ΔL] of the newly synthesized chromophores (**3-9**)

| | Gas Phase | | | Solvent Medium (DCM) | | | ΔH | ΔL |
|---|---|---|---|---|---|---|---|---|
| Compound | H (a.u) | L (a.u) | H-L (a.u) (eV) | H (a.u) | L (a.u) | H-L a.u (eV) | a.u (eV) | a.u (eV) |
| **3** | -0.2276 | -0.0134 | 0.2142 (5.83) | -0.2287 | -0.0214 | 0.2073 (5.64) | 0.0011 (0.029) | 0.0079 (0.22) |
| **4** | -0.2254 | -0.0154 | 0.2101 (5.72) | -0.2299 | -0.0240 | 0.2059 (5.60) | 0.0045 (0.12) | 0.0087 (0.23) |
| **5** | -0.2162 | -0.0112 | 0.2049 (5.58) | -0.2198 | -0.0213 | 0.1985 (5.40) | 0.0036 (0.099) | 0.0100 (0.27) |
| **6** | -0.2270 | -0.0318 | 0.1952 (5.31) | -0.2289 | -0.0365 | 0.1924 (5.23) | 0.0019 (0.051) | 0.0048 (0.13) |
| **7** | -0.2184 | -0.0279 | 0.1905 (5.18) | -0.2205 | -0.0345 | 0.1860 (5.06) | 0.0021 (0.057) | 0.0066 (0.18) |
| **8** | -0.2226 | -0.0293 | 0.1933 (5.26) | -0.2276 | -0.0360 | 0.1917 (5.21) | 0.0051 (0.137) | 0.0067 (0.18) |
| **9** | -0.2114 | -0.0267 | 0.1847 (5.02) | -0.2180 | -0.0353 | 0.1826 (4.97) | 0.0066 (0.18) | 0.0086 (0.23) |

**Table 5**: Theoretical values of $\lambda_{max}$, computed in gas phase and solvent medium (toluene, DCM, MeCN and DMF) and compared with experimental values of compound (**3-9**).

| **Compound** | **$\lambda_{max}$ (Gas) nm** | **Solvent** | **$\lambda_{max}$ Experimental (nm)** | **$\lambda_{max}$ Linear Response (LR)** | **$\lambda_{max}$ State specific (SS)** |
|---|---|---|---|---|---|
| **3** | 330 | | 398 | 350 | 368 |
| **4** | 346 | | 402 | 362 | 378 |
| **5** | 355 | Toluene | 419 | 376 | 392 |
| **6** | 361 | | 415 | 375 | 387 |
| **7** | 367 | | 424 | 385 | 414 |
| **8** | 369 | | 437 | 381 | 388 |
| **9** | 382 | | 449 | 398 | 420 |
| **3** | | | 391 | 354 | 376 |
| **4** | | | 403 | 364 | 382 |
| **5** | | DCM | 419 | 380 | 401 |
| **6** | | | 422 | 376 | 387 |
| **7** | | | 424 | 386 | 417 |
| **8** | | | 436 | 382 | 387 |
| **9** | | | 446 | 398 | 418 |
| **3** | | | 399 | 354 | 376 |
| **4** | | | 404 | 363 | 381 |
| **5** | | MeCN | 413 | 380 | 401 |
| **6** | | | 413 | 376 | 385 |
| **7** | | | 413 | 385 | 411 |
| **8** | | | 433 | 386 | 390 |
| **9** | | | 442 | 397 | 413 |

| | | | | |
|---|---|---|---|---|
| **3** | | 405 | 355 | 380 |
| **4** | | 412 | 365 | 385 |
| **5** | DMF | 426 | 382 | 405 |
| **6** | | 421 | 378 | 390 |
| **7** | | 419 | 387 | 419 |
| **8** | | 442 | 388 | 393 |
| **9** | | 451 | 399 | 420 |

## Spectrum 3.1. $^{1}H$, $^{13}C$ NMR of compound 2

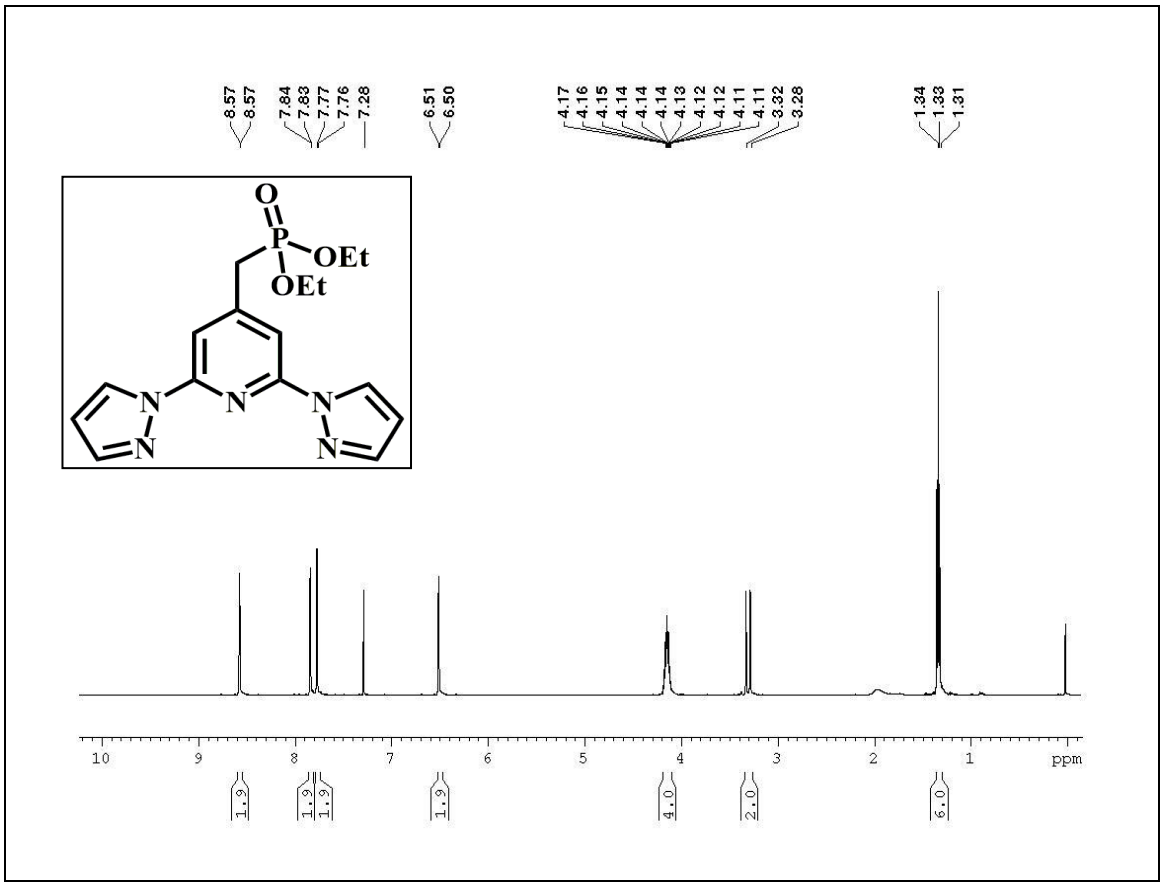


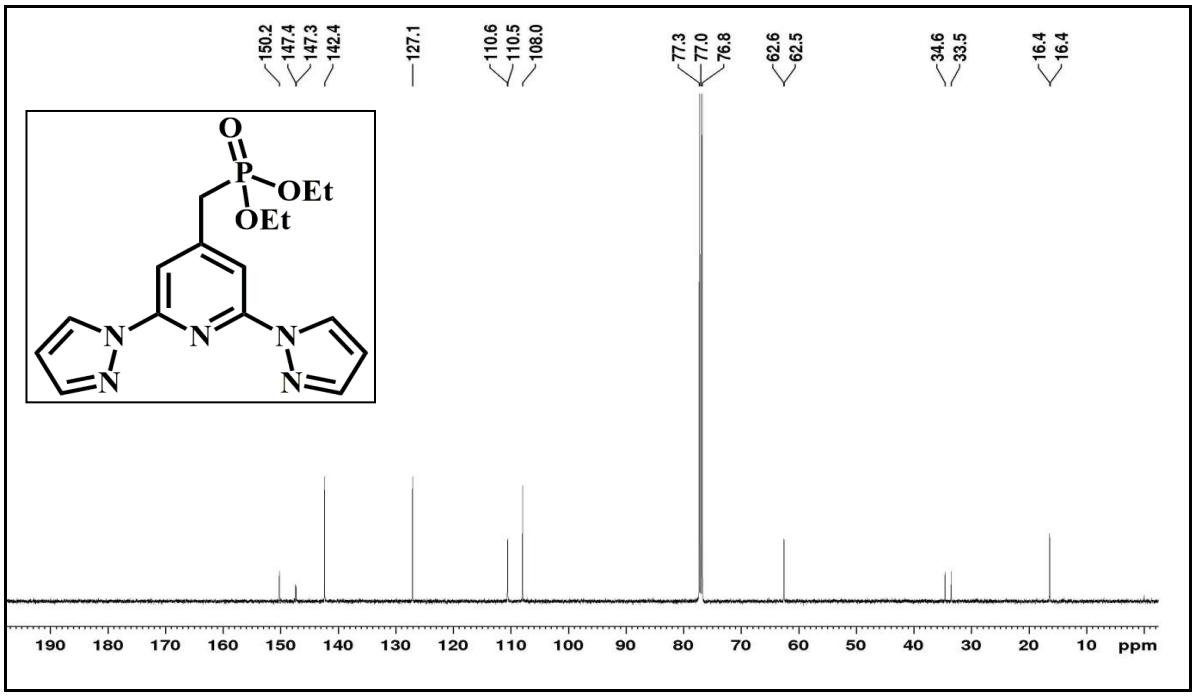

## Spectrum 3.2. $^{1}H$, $^{13}C$ NMR of compound 3

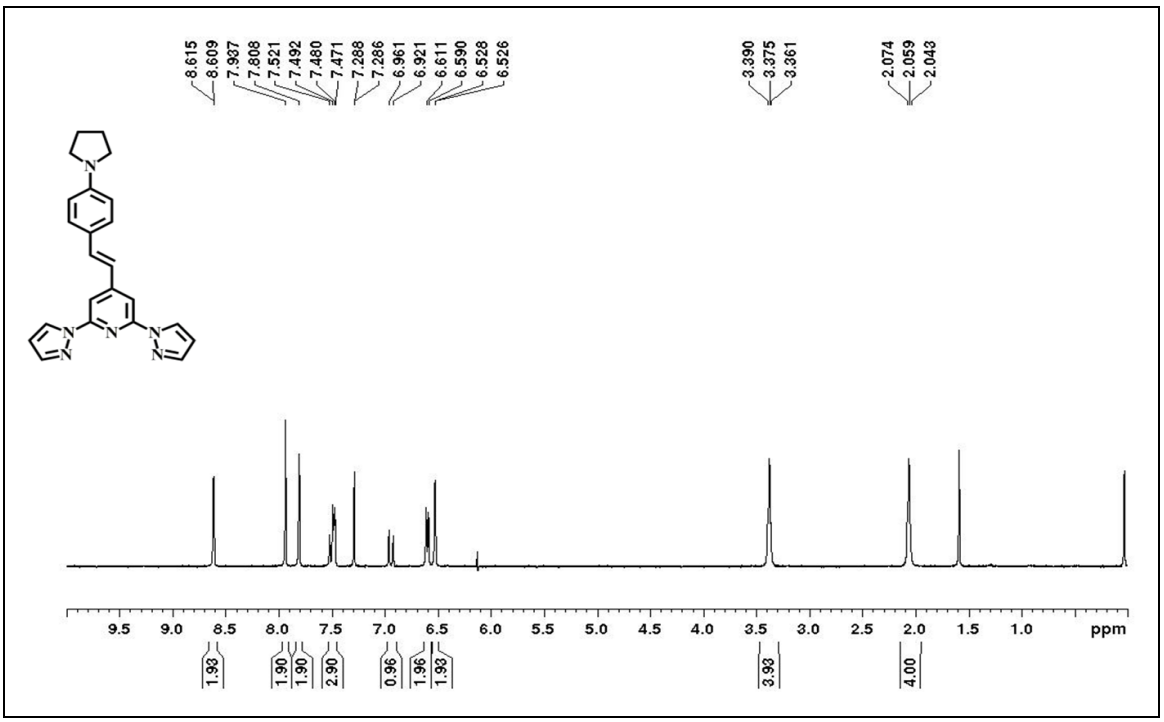


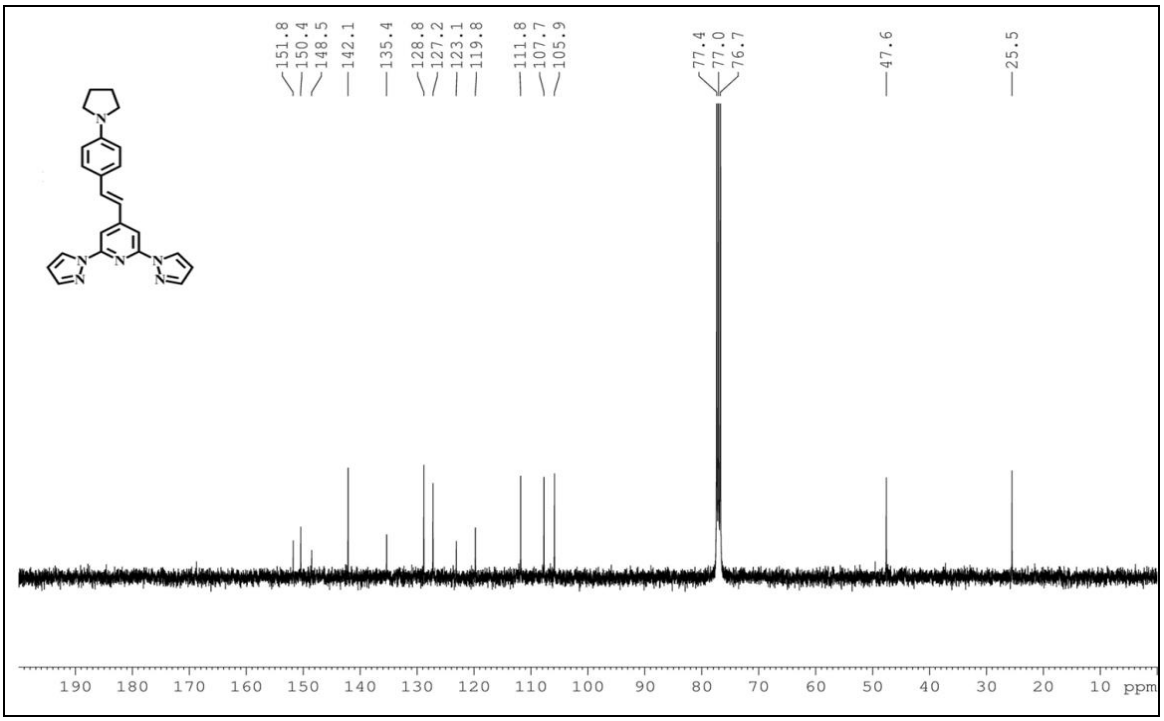

## Spectrum 3.3. $^{1}H$, $^{13}C$ NMR of compound 4

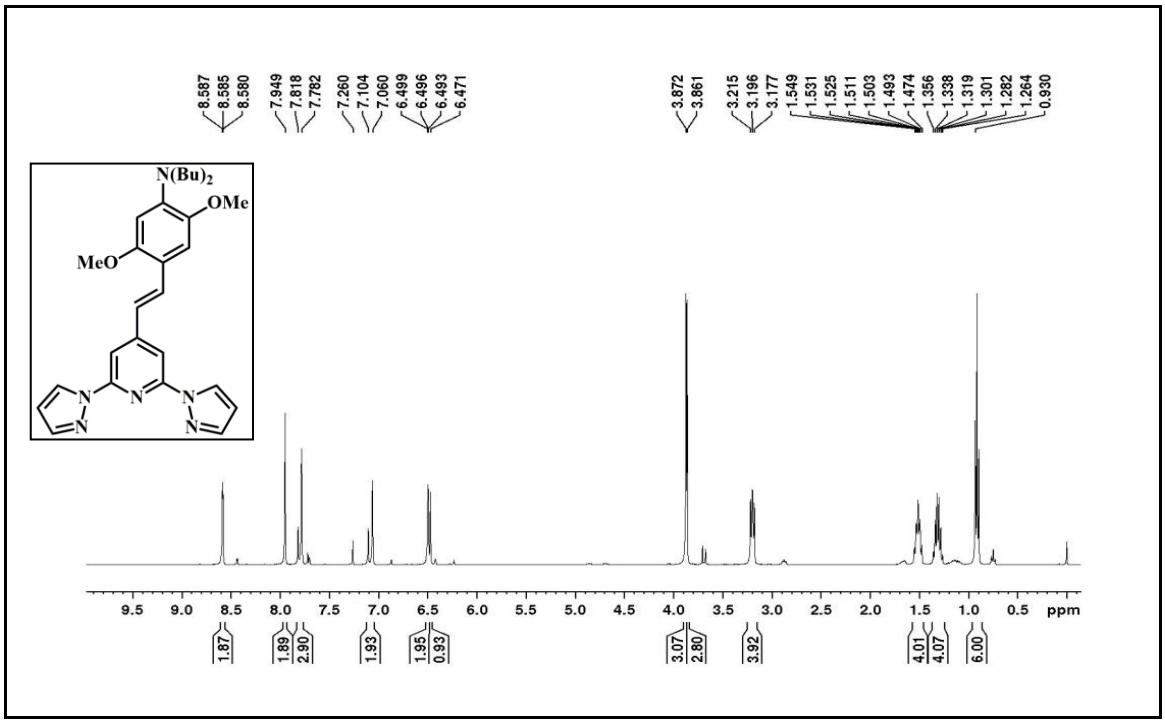


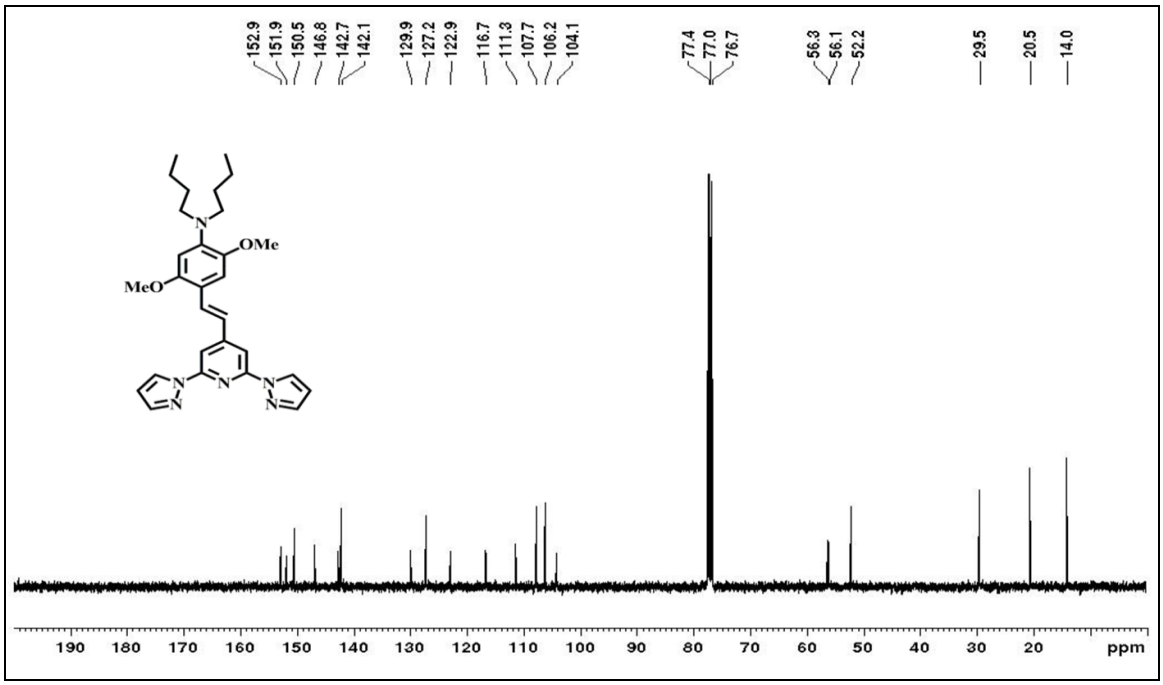

## Spectrum 3.4. $^{1}H$, $^{13}C$ NMR of compound 5

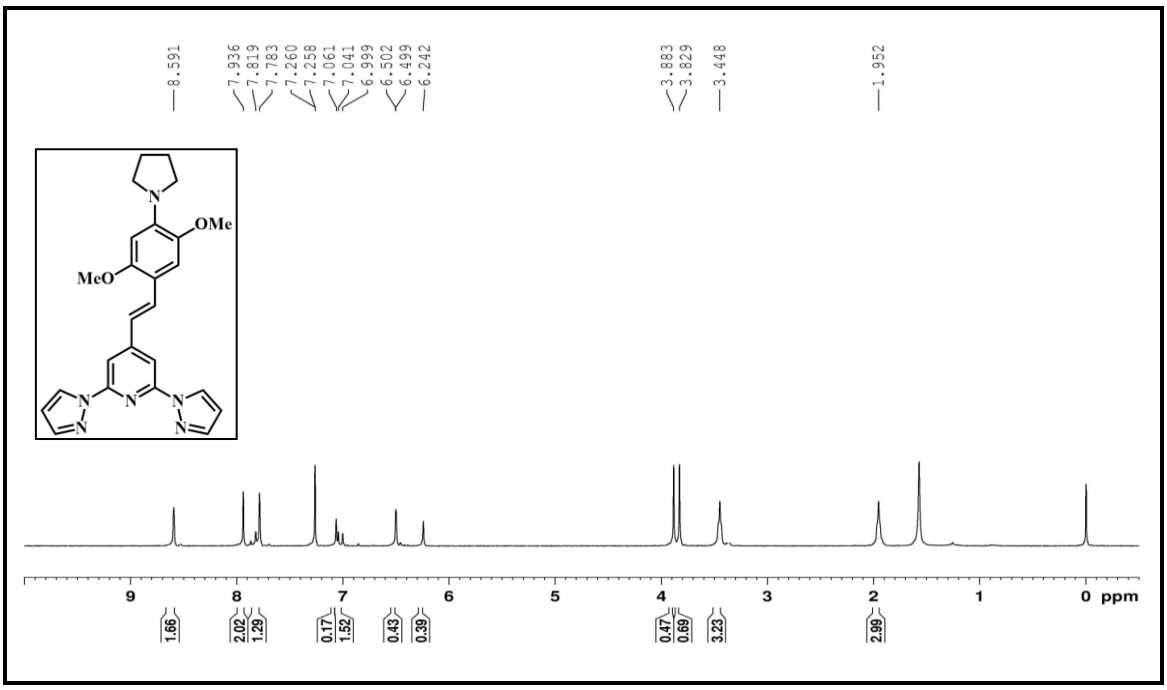


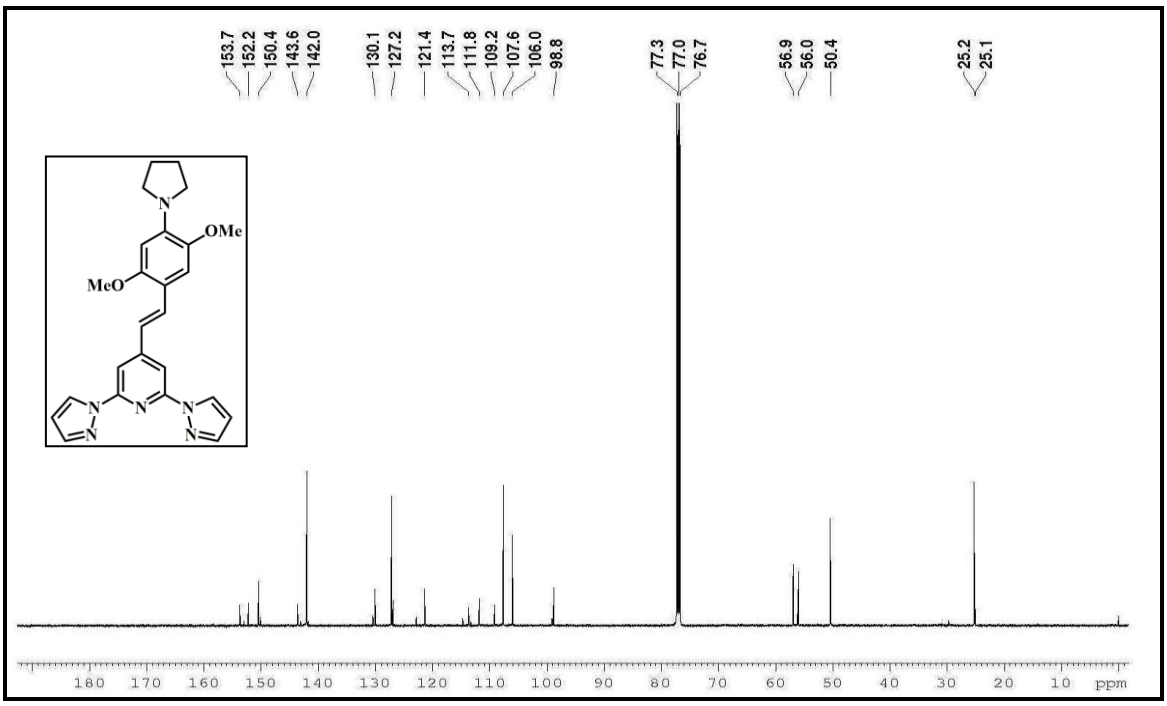

## Spectrum 3.5. $^{1}H$, $^{13}C$ NMR of compound 6

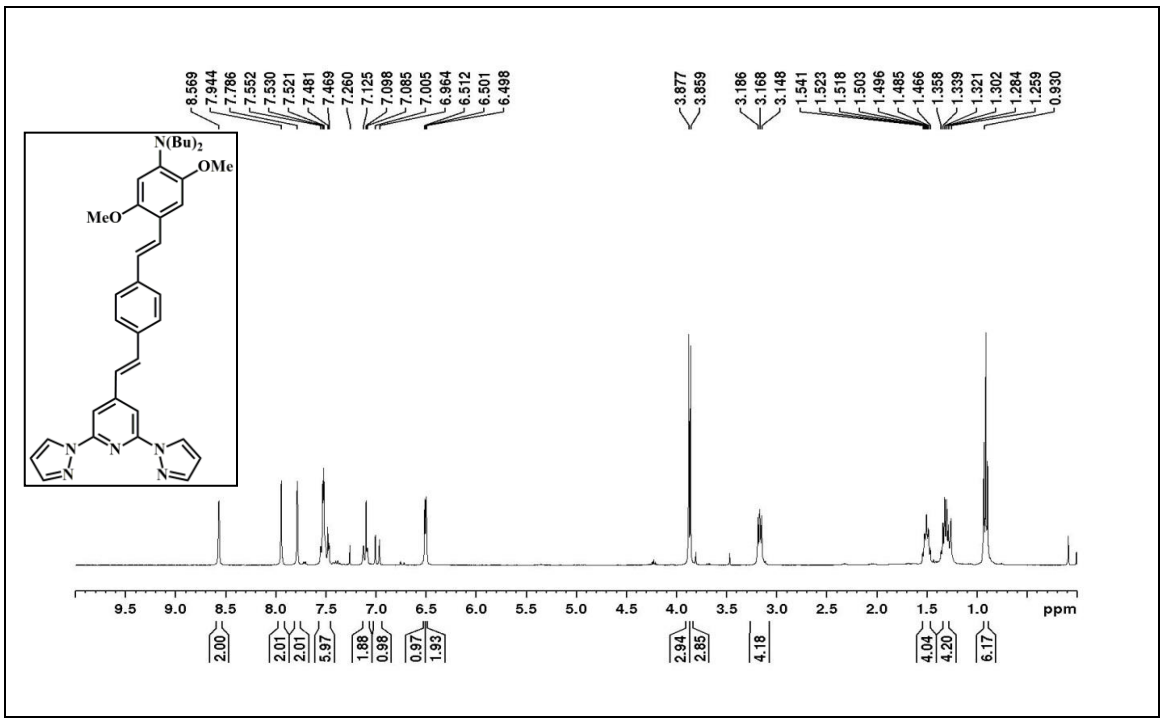


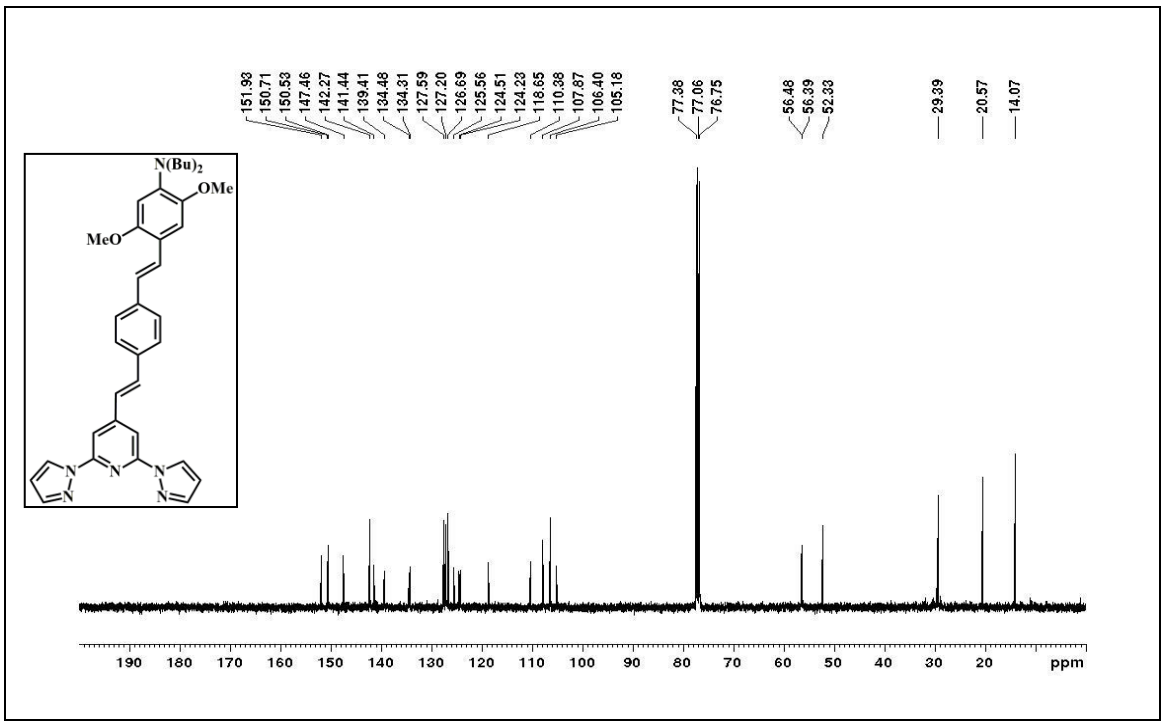


## Spectrum 3.6. $^{1}H$, $^{13}C$ NMR of compound 7

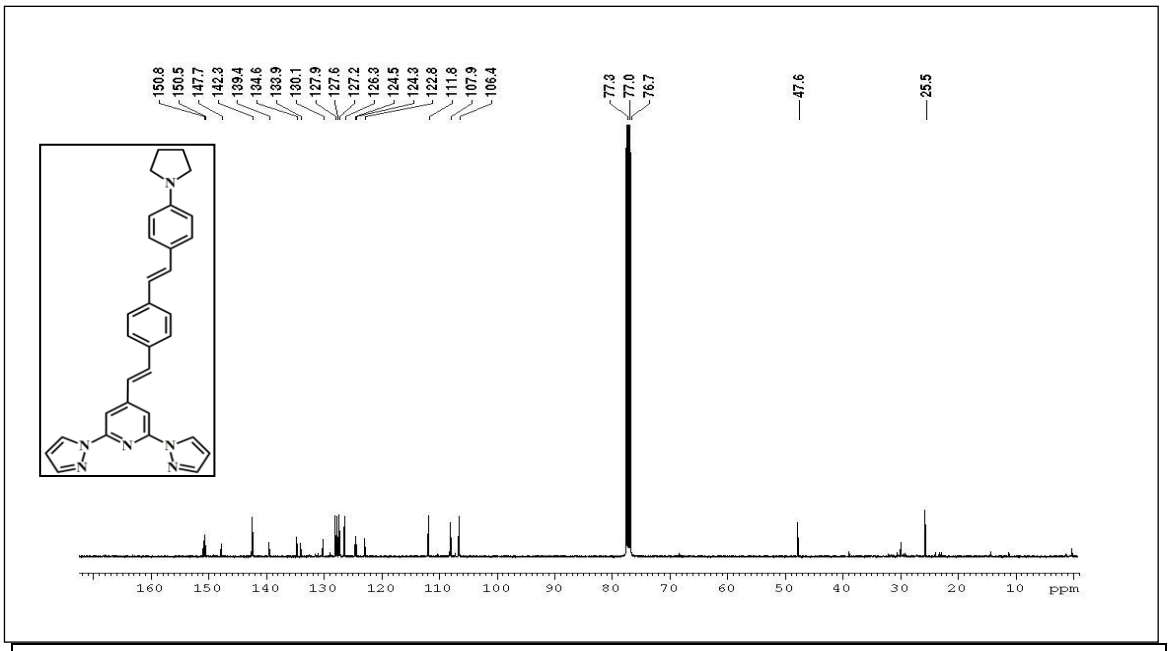
150.8
150.5
147.7
142.3
139.4
134.6
133.9
130.1
127.9
127.6
127.2
126.3
124.5
124.3
122.8
111.8
107.9
106.4
77.3
77.0
76.7
47.6
25.5
160 150 140 130 120 110 100 90 80 70 60 50 40 30 20 10 ppm

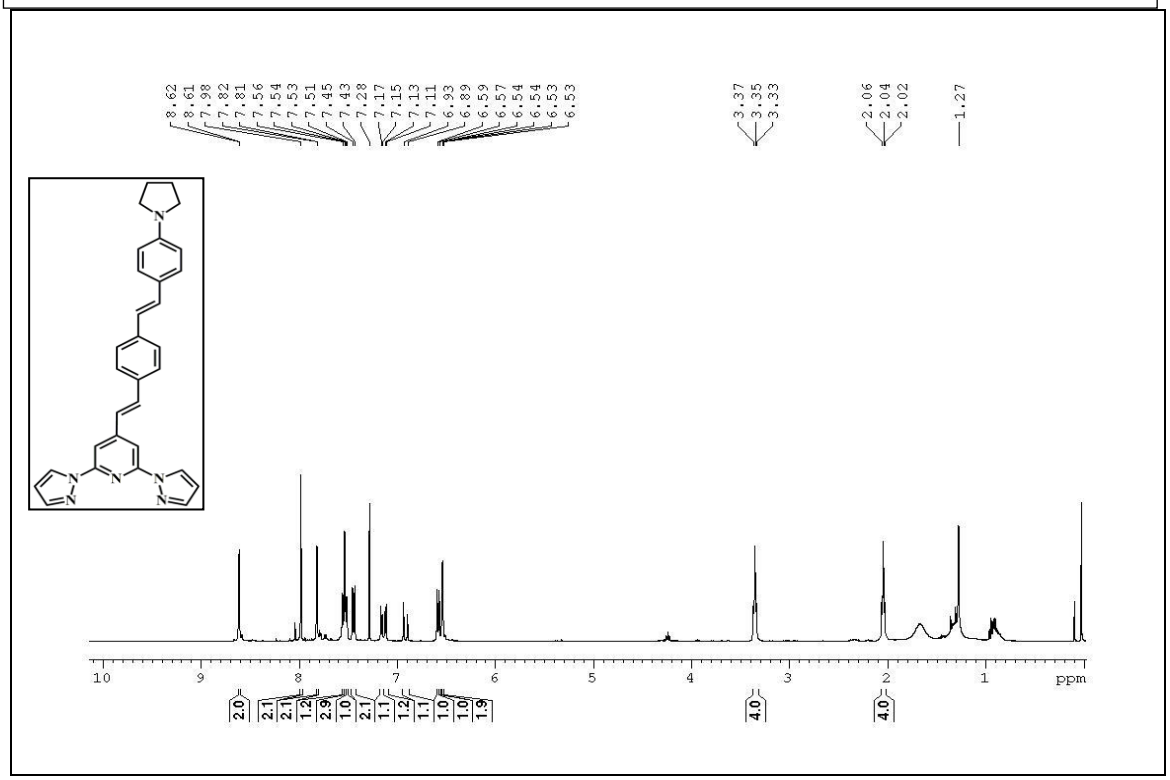
8.62
8.61
7.98
7.82
7.81
7.56
7.54
7.53
7.51
7.45
7.43
7.28
7.17
7.15
7.13
7.11
6.93
6.89
6.59
6.57
6.54
6.54
6.53
6.53
3.37
3.35
3.33
2.06
2.04
2.02
1.27
10 9 8 7 6 5 4 3 2 1 ppm
2.0
2.1
2.1
1.2
2.9
1.0
2.1
1.1
1.2
1.1
1.0
1.0
1.9
4.0
4.0

## Spectrum 3.7. $^{1}H$, $^{13}C$ NMR of compound 8

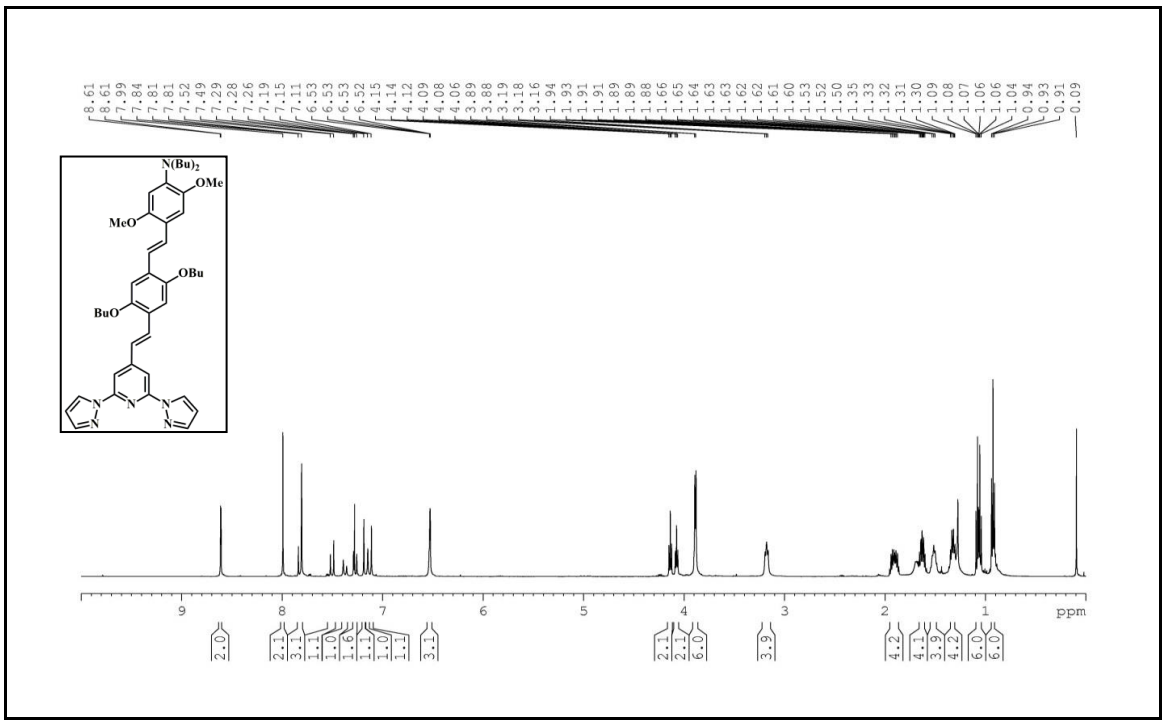


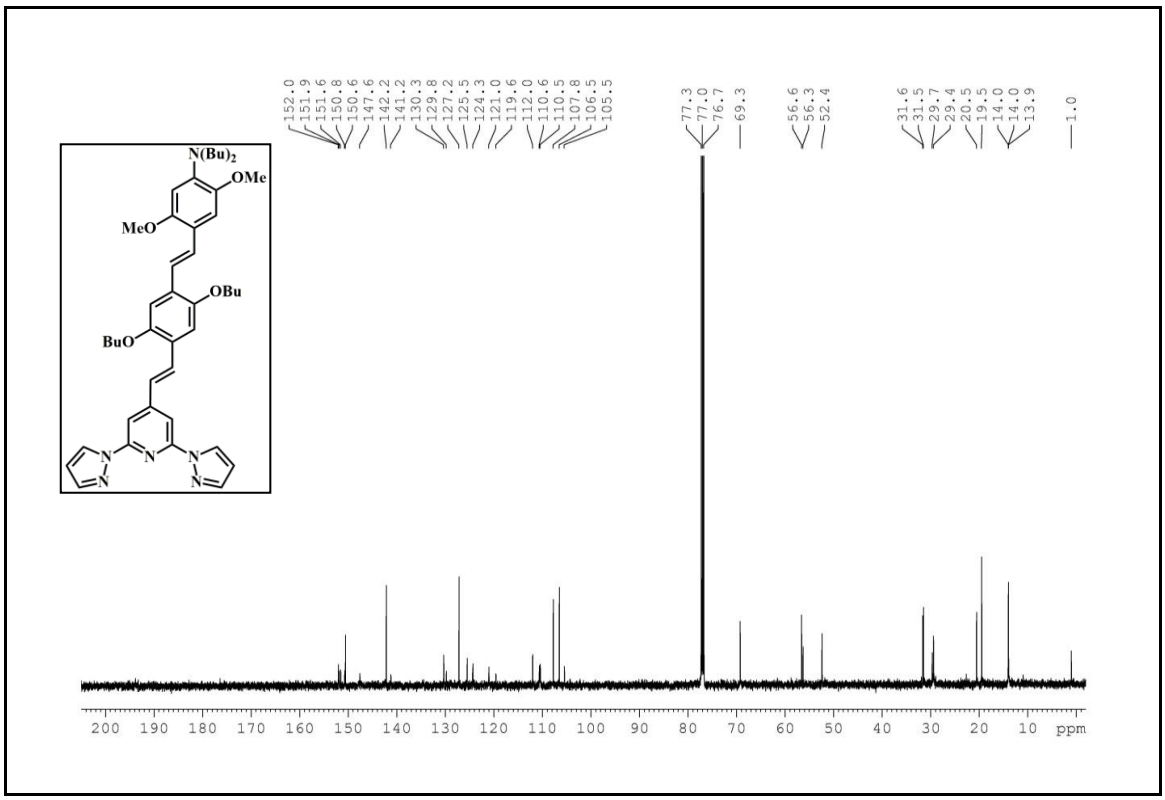

## Spectrum 4.8. $^{1}H$, $^{13}C$ NMR of compound 9

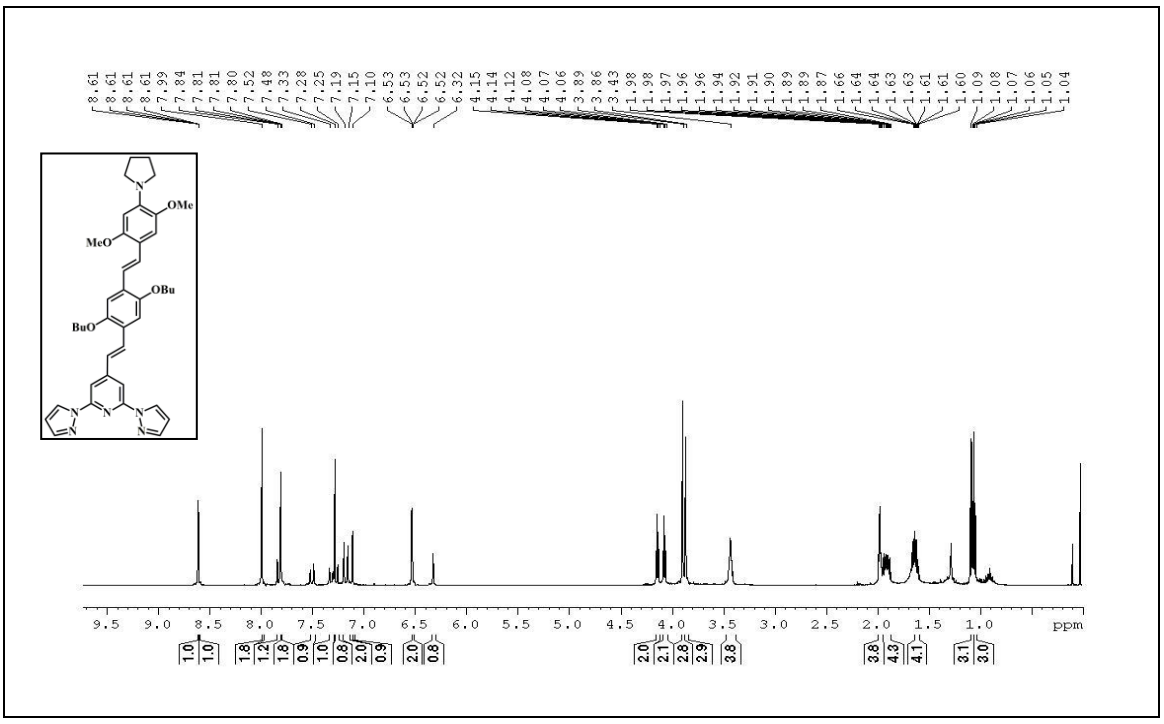


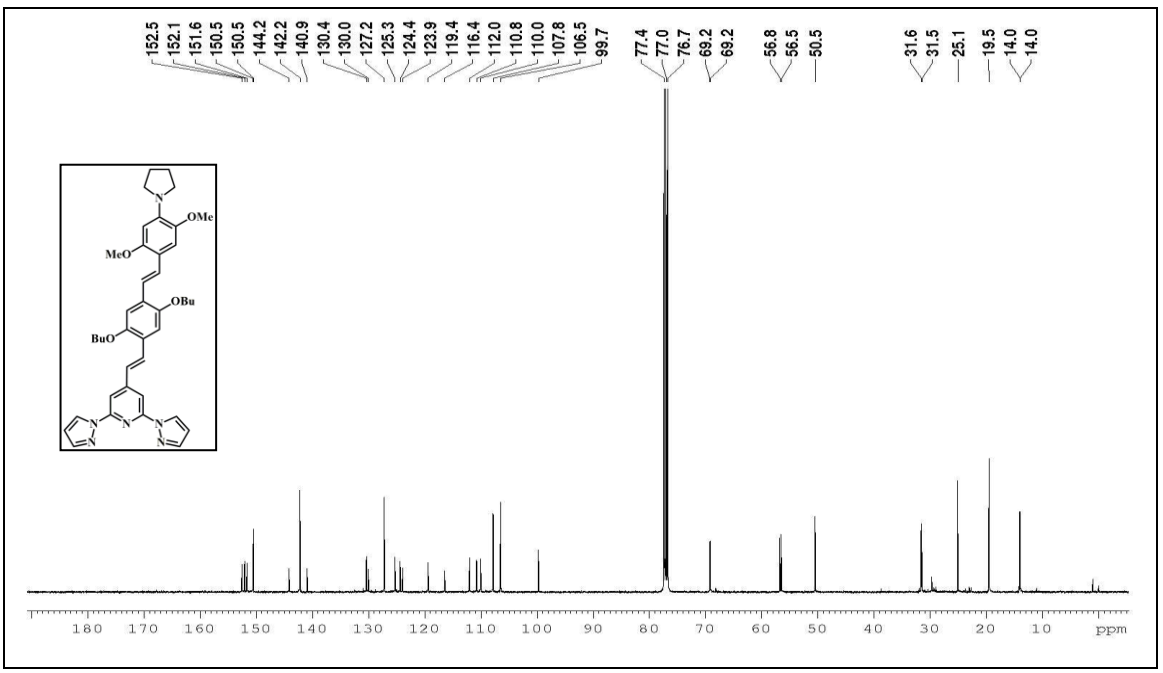

### 3.5. References

(1) Herschel, J. F. W. On a Case of Superficial Colour Presented by a Homogeneous Liquid Internally Colourless. *Phil. Trans. R. Soc. Lond.* **1845**, *135*, 143-145.

(2) Meier, H. Conjugated Oligomers with Terminal Donor-Acceptor Substitution. *Angew. Chem. Int Ed. Engl.* **2005**, *44*, 2482-2506.

(3). Grabowski, Z. R.; Rotkiewicz, K.; Rettig, W. Structural Changes Accompanying Intramolecular Electron Transfer: Focus on Twisted Intramolecular Charge-Transfer States and Structures. *Chem. Rev.* **2003,** *103* , 3899-4032.

(4). Glasbeek, M.; Zhang, H. Femtosecond Studies of Solvation and Intramolecular Configurational Dynamics of Fluorophores in Liquid Solution. *Chem. Rev.* **2004,** *104*, 1929-1954.

(5). Soujanya, T.; Philippon, A.; Leroy, S.; Vallier, M.; Fages, F. Tunable Photophysical Properties of Two 2,2‘-Bipyridine-Substituted Pyrene Derivatives. *J. Phys. Chem. A* **2000,** *104*, 9408-9414.

(6). Slama-Schwok, A.; Blanchard-Desce, M.; Lehn, J. M. Intramolecular Charge Transfer in Donor-Acceptor Molecules. *J. Phys. Chem.* **1990,** *94*, 3894-3902.

(7). Takaya, T.; Saha, S.; Hamaguchi, H.-o.; Sarkar, M.; Samanta, A.; Iwata, K. Charge Resonance Character in the Charge Transfer State of Bianthryls: Effect of Symmetry Breaking on Time-Resolved Near-IR Absorption Spectra. *J. Phys. Chem. A* **2006**, *110*, 4291-4295.

(8). Mondal, J. A.; Sarkar, M.; Samanta, A.; Ghosh, H. N.; Palit, D. K. Charge-Transfer-Induced Twisting of the Nitro Group. *J. Phys. Chem. A* **2007**, *111*, 6122-6126.

(9). Felouat, A.; D’Aléo, A.; Charaf-Eddin, A.; Jacquemin, D.; Le Guennic, B.; Kim, E.; Lee, K. J.; Woo, J. H.; Ribierre, J.-C.; Wu, J. W.; Fages, F. Tuning the Direction of Intramolecular Charge Transfer and the Nature of the Fluorescent State in a T-Shaped Molecular Dyad. *J. Phys. Chem. A* **2015,** *119*, 6283-6295.

(10). Horng, M. L.; Gardecki, J. A.; Papazyan, A.; Maroncelli, M. Subpicosecond Measurements of Polar Solvation Dynamics: Coumarin 153 Revisited. *J. Phys. Chem.* **1995**, *99*, 17311-17337.

(11). Bagchi, B.; Fleming, G. R.; Oxtoby, D. W. Theory of Electronic Relaxation in Solution in the Absence of an Activation Barrier. *J. Chem. Phys.* **1983,** *78*, 7375-7385.

(12). Videlot-Ackermann, C.; Brisset, H.; Zhang, J.; Ackermann, J.; Nénon, S.; Fages, F.; Marsal, P.; Tanisawa, T.; Yoshimoto, N. Influence of Phenyl Perfluorination on Charge

Transport Properties of Distyryl-Oligothiophenes in Organic Field-Effect Transistors. *J. Phys. Chem. C* **2009,** *113*, 1567-1574.

(13). Curtis, M. D.; Cao, J.; Kampf, J. W. Solid-State Packing of Conjugated Oligomers: From π-Stacks to the Herringbone Structure. *J. Am. Chem. Soc.* **2004,** *126*, 4318-4328.

(14) Chen, S. Y.; Xu, X. J.; Liu, Y. Q.; Yu, G.; Sun, X. B.; Qiu, W. F.; Ma, Y. Q.; Zhu, D. B. Synthesis and Characterization of n-Type Materials for Non-Doped Organic Red-Light-Emitting Diodes. *Adv. Funct. Mater.* **2005**, *15*, 1541-1546.

(15) Lai, R. Y.; Fabrizio, E. F.; Lu, L.; Jenekhe, S. A.; Bard, A. J. Synthesis, Cyclic Voltammetric Studies, and Electrogenerated Chemiluminescence of a New DonorAcceptor Molecule: 3,7-[Bis[4-phenyl-2-quinolyl]]-10-methylphenothiazine. *J. Am. Chem. Soc.* **2001**, *123*, 9112-9118.

(16) Wong, M. S.; Li, Z. H.; Tao, Y.; D'Iorio, M. Synthesis and Functional Properties of Donor−Acceptor π-Conjugated Oligomers. *Chem. Mater.* **2003**, *15*, 1198-1203.

(17) Jiao, G. -S.; Thoresen, L. H.; Burgess, K. Fluorescent, Through-Bond Energy Transfer Cassettes for Labeling Multiple Biological Molecules in One Experiment. *J. Am. Chem. Soc.* **2003**, *125*, 14668-14669.

(18) Sarma, M.; Chatterjee, T.; Ghanta, S.; Das, S. K. D-π-A-A-π-D Prototype 2,2′-Bipyridine Dyads Exhibiting Large Structure and Environment-Sensitive Fluorescence: Synthesis, Photophysics, and Computation. *J. Org. Chem.* **2012**, *77*, 432-444.

(19) Bodapati, R.; Sarma, M.; Kanakati, A.; Das, S. K. Asymmetrically Substituted and π-Conjugated 2,2′-Bipyridine Derivatives: Synthesis, Spectroscopy, Computation, and Crystallography. *J. Org. Chem.* **2015**, *80*, 12482-12491.

(20) Umehara, K.; Kuwata, S.; Ikariya, T. N–N Bond Cleavage of Hydrazines with a Multiproton-Responsive Pincer-Type Iron Complex. *J. Am. Chem. Soc.* **2013**, *135*, 6754-6757.

(21) Mola, J.; Mas-Marza, E.; Sala, X.; Romero, I.; Rodríguez, M.; Viñas, C.; Parella, T.; Llobet, A. Ru-Hbpp-Based Water-Oxidation Catalysts Anchored on Conducting Solid Supports. *Angew. Chem.* **2008**, *120*, 5914-5916.

(22) Zhu, X. J.; Holliday, B. J. Electropolymerization of a Ruthenium(II) Bis(pyrazolyl)pyridine Complex to Form a Novel Ru-Containing Conducting Metallopolymer. *Macromol. Rapid Commun.* **2010**, *31*, 904-909.

(23) Hu, J.; Zhang, D.; Harris, F. W. Ruthenium(III) Chloride Catalyzed Oxidation of Pyrene and 2,7-Disubstitued Pyrenes: An Efficient, One-Step Synthesis of Pyrene-4,5-diones and Pyrene-4,5,9,10-tetraones. *J. Org. Chem.* **2005**, *70* , 707-708.

(24) Li, F.; Hor, T. S. A. Facile Synthesis of Nitrogen Tetradentate Ligands and Their Applications in CuI-Catalyzed N-Arylation and Azide–Alkyne Cycloaddition. *Chem. Eur. J.* **2009**, *15*, 10585-10592.

(25) Schäfer, B.; Greisch, J.-F.; Faus, I.; Bodenstein, T.; Šalitroš, I.; Fuhr, O.; Fink, K.; Schünemann, V.; Kappes, M. M.; Ruben, M. Divergent Coordination Chemistry: Parallel Synthesis of [2×2] Iron(II) Grid-Complex Tauto-Conformers. *Angew. Chem. Int. Ed.* **2016**, *55*, 10881-10885.

(26) Sheldrick. G.M.; SHELX-97, Program for Crystal Structure Solution and Analysis, University of Gottingen, Gottingen, Germany, **1997**.

(27) Nihei, M.; Takahashi, N.; Nishikawa, H.; Oshio, H. Spin-crossover Behavior and Electrical Conduction Property in Iron(ii) Complexes with Tetrathiafulvalene Moieties. *Dalton Trans.* **2011,** *40*, 2154-2156.

(28) Frisch, M. J.; Trucks, G. W.; Schlegel, H. B.; Scuseria, G. E.; Robb, M. A.; Cheeseman, J. R.; Scalmani, G.; Barone, V.; Mennucci, B.; Petersson. G. A. *et al.* Gaussian 09, revision B.01; Gaussian, Inc.: Wallingford, CT, **2010**.

(29) Tomasi, J.; Mennucci, B.; Cammi, R. Quantum Mechanical Continuum Solvation Models. *Chem. Rev.* **2005**, *105*, 2999-3094.

(30) Furche, F.; Ahlrichs, R. Adiabatic Time-dependent Density Functional Methods for Excited State Properties. *J. Chem. Phys.* **2002**, *117*, 7433-7447.

(31) Scalmani, G.; Frisch, M. J.; Mennucci, B.; Tomasi, J.; Cammi, R.; Barone, V. Geometries and Properties of Excited States in the Gas Phase and in Solution: Theory and Application of a Time-dependent Density Functional Theory Polarizable Continuum Model. *J. Chem. Phys.* **2006**, *124*, 094-107.

(32) Cossi, M.; Barone, V. Time-dependent Density Functional Theory for Molecules in Liquid Solutions. *J. Chem. Phys.* **2001**, *115*, 4708-4717.

(33) Improta, R.; Barone, V.; Santoro, F. Ab Initio Calculations of Absorption Spectra of Large Molecules in Solution: Coumarin C153. *Angew. Chem. Int. Ed.* **2007**, *46*, 405-408.

(34) Adamo. C.; Jacquemin. D. The Calculations of Excited-state Properties with Time-Dependent Density Functional Theory: *Chem. Soc. Rev*. **2013**, *42*, 845-856.

(35) Krawczyk, P. Time-Dependent Density Functional Theory Caclculations of the Solvatochromism of some Sulfonamide Fluorochromes. *J. Mol. Model*. **2015**, *21*, 1-18.

(36) Chibani, S.; Guennic, B, L.; Charaf-Eddin, A.; Maury, O.; Andraud, C.; Jacquemin, D. On the Computation of Adiabatic Energies in Aza-Boron-Dipyrromethene Dyes. *J. Chem. Theory. Comput*. **2012**, *8*, 3303-3313.

# Chromophore 4, a Unique $Cu^{2+}$ Sensor: Emergence of a New Fe(II) Complex with Conjugated Bis(pyrazolyl)pyridine Derivative

# 4

**ABSTRACT**: The preceding chapter demonstrated syntheses and photo-physical properties of a series of conjugated bis(pyrazolyl)pyridine derivatives (**3-9**, Chart 3.1). This chapter deals with one of this chromophore, namely chromophore **4**, which has been explored further as a selective $Cu^{2+}$ ion sensor. An extensive screening study of chromophore **4** with diverse metal acetates prompted us to explore the syntheses of diverse metal coordination complexes with chromophore **3** as a ligand. However, we could succeed to synthesize only Fe(II) coordination complex with a particular chromophore **3** as a ligand $\mathbf{L_1}$ (see Scheme 2). Figure 4.1 shows fluorescence quenching with various metal acetates and it has been found that copper acetate quenches the fluorescence completely with chromophore **4** in MeOH solution. The resulting synthesized Fe(II) coordination complex (complex **1**, Scheme 4.1) has unambiguously been characterized by single crystal X-ray crystallographyA new iron-2,6-bis(pyrazolyl)pyridine complex $[Fe(L_1)_2](BF_4)_2$ (**1**) ($L_1$ = π-conjugated 2,6-bis(pyrazolyl)pyridine derivative, see scheme 4.1) has been prepared by the treatment of $\mathbf{L_1}$ with iron(II) tetrafluoroborate hexahydrate in acetone solution. Complex **1** was characterized by IR spectral studies and elemental analyses including single crystal X-ray crystallography. Complex **1** crystallizes in monoclinic system with space group $P2_1/n$ and exhibits supramolecular interaction through C−H···F hydrogen bonding interactions leading to 2-D layers in the relevant crystal structure. Both the ligand $\mathbf{L_1}$ and complex **1** exhibit absorption in the visible region in their acetone solutions. In complex **1**, the electronic absorption band is observed at longer wavelength (~ 480 nm) compared to that (~ 400 nm) observed for the ligand $\mathbf{L_1}$. The absorption spectral results of ligand $\mathbf{L_1}$ and complex **1** are also in good agreement with the results obtained from DFT and TD-DFT calculations.

## 4.1. Introduction

Last several years, in our laboratory, we have been exploring diverse inorganic and organic systems that can be described as functional materials.[1-3] As a part of our research on exploring functional materials, we have recently developed interests in fluorescent chemosensors and reported our first success in selective sensing of $Fe^{3+}$ ion and $IO_4^-$ ion by a metallocycle host.[4] Fluorescent sensing has received great attention due to its simple

operation, high selectivity, and sensitivity. The metal-selective fluorescent chemosensors are widely exploited to detect biologically or environmentally relevant metal ions. $Cu^{2+}$ ion is a biologically as well as a magnetically active metal ion, which is potentially important to be detected by a fluorescent sensor.[5-7] The strong fluorescence quenching for the most of the luminescent sensors for Cu(II) ion is due to the fast electron and energy transfer involving paramagnetic copper center.[8-12] Exploring the chemistry of coordination complexes with 2,6-bis(pyrazolyl)pyridine ligand system is of great interest in modern inorganic chemistry because of their potential applications in the field of magnetic materials.[13] The $[Fe(bpp)_2]^{2+}$ (bpp = 2,6-bis(pyrazolyl)pyridine derivatives) family of complexes is extensively used in the field of spin-crossover research.[14] This class of complexes can easily undergo spin-crossover even at the temperatures close to room temperature and the synthetic methods are available to functionalize every position of the 2,6-bis(pyrazolyl)pyridine ligand frame work of the relevant coordination complexes.[15] This prompted synthetic chemists to synthesize multifunctional Fe complexes of 2,6-bis(pyrazolyl)pyridine ligand to introduce photo-isomersable,[16] redox active,[17] and fluorescence enhancive[18] substituents to the possible positions of pertinent 2,6-bis(pyrazolyl)pyridine ligands. Ruben and coworkers[19] reported several metal complexes of 2,6-bis(pyrazolyl)pyridine derivatives and explored their structure-function relationship. Multiple bistability and tristability with dual spin state conversion in ion-pair complex $\{[Fe(bpp)_2]$-$[Ni(mnt)_2]_2\}$ was widely studied by Oshio and co-workers.[20] The present chapter deals with an iron complex with π-conjugated 2,6-bis(pyrazolyl)pyridine ligand system. We have synthesized $[Fe(L_1)_2](BF_4)_2$ (**1**) ($L_1$ = π-conjugated 2,6-bis(pyrazolyl)pyridine derivative, see scheme 1) and characterized **1** unambiguously by single crystal X-ray structure determination. We have also performed density functional theory calculations to understand the UV-visible spectral results of the ligand as well as its metal complex.

## 4.2. Experimental Section

### 4.2.1. Materials and Methods

All reagents and solvents were commercially available and used without purification. All reactions were carried out under inert atmosphere unless otherwise stated. Column chromatography was performed on silica gel (100-200 mesh). Thin-layer chromatography (TLC) plates were visualized with UV light in an iodine chamber. Unless stated otherwise, all reagents were purchased from commercial sources and used without additional purification. THF was freshly distilled over Na-benzophenone ketyl. $^{1}H$ NMR and $^{13}C$ NMR spectra were recorded on a Bruker 400 MHz machine in $CDCl_3$ as a solvent with TMS as a reference unless otherwise indicated. Micro-analytical (C, H, N) data were obtained with a FLASH EA 1112 Series CHNS analyzer. Infrared (IR) spectra were recorded as KBr pellets on a JASCO- 5300 FT-IR spectrophotometer at 298 K. High-resolution mass spectroscopy (HRMS) (ESI-TOF) equipment was used to record mass spectra for isolated compounds where appropriate. Absorbance spectra were recorded on a Shimadzu model UV-3600 spectrophotometer and fluorescence emission spectra have been recorded on a Jobin Yvon Horiba model Fluoromax-4 spectrofluorometer.

### 4.2.2. Synthesis

**Synthesis.** Ligand $L_1$ and chromophore **4** (chapter 3, chart 3.1) has been synthesized using an efficient Horner-Wadsworth-Emmons (HWE) reaction path as discussed in the preceding chapter 3. After purification by column chromatography was done, the molecular structure of ligand $\mathbf{L_1}$ was determined by IR-, NMR ($^{1}H$ and $^{13}C$)-, and mass-spectral studies including CHNS analyses.

### 4.2.3. X-ray Crystallography

Single crystals, suitable for facile structural determination for the Compounds **2** and **3** were measured on a Bruker D8 quest PHOTON 100 CMOS system under Mo-Kα (λ = 0.71073 Å) graphite monochromatic X-Ray beam. Data processing was accomplished by using SAINT PLUS and structures were solved by using SHELXS-97 and refined using SHELXL-14/7 program.[21] All non-hydrogen atoms were refined anisotropically by full matrix least square cycles on $F^2$. Hydrogen atoms were introduced on calculated positions and included in the refinement riding on their respective parent atoms. Crystal data, structure refinement parameters for complex **1** are summarized in Table 4.1 and selected bond lengths in Table 4.2.

## 4.3. Results and Discussion

### 4.3.1 Highly selective turn-off phenomenon of 2,6-bis(pyrazolyl)pyridine based fluorescent sensor for recognition of $Cu^{2+}$

The titration experiments for the synthesized compound **4** were studied with several metal acetates ($Na^+$, $K^+$, $Mn^{2+}$, $Fe^{2+}$, $Co^{2+}$, $Ni^{2+}$, $Cu^{2+}$, $Zn^{2+}$, $Cd^{2+}$, $Hg^{2+}$, $Pb^{2+}$, $Cs^+$, $U^{3+}$), commonly found in chemical media. Concentration was maintained as identical for all metal ions in methanol solvent, which was titrated at an excitation wavelength of 408 nm. The emission data were recorded two minutes after a metal acetate solution was added. Indeed, as shown in Figure 4.1a, drastically quenching in the emission of fluorophore **4** demonstrated that $Cu^{2+}$ alone shows a distinct mark in its fluorescence spectrum (almost labeled with X-axis, tiny emission intensity!), which can be observed even by naked eye. The chelation-enhanced fluorescence quenching (CHEQ) effect may be the reason for this particular quenching response to $Cu^{2+}$ ions. The paramagnetic (hypothetical) copper (II) coordination complex (a $d^9$ system) with molecule **4** (as a ligand) seems to be responsible for this quenching.[22]Apart from that, some of other metal ions $M^{2+}$ (Ni, Co, Hg, Zn) and $Na^+$ acetate solution also quench the emission to a small extent compared to the $Cu^{2+}$ as shown in Figure 4.1(a). Interestingly, when we added cadmium acetate solution to the solution of fluorophore **4**, we found that, there was a redshift of about 45 nm (*i.e.*, 559 nm to 604 nm).The fluorescence titration of compound **4** was performed by varying concentrations of $Cu^{2+}$ ions. Initial titration started with 10 μL of 1 mM $Cu^{2+}$ to the stock solution and it was sequentially increased up to 220 μL in the step size of 10 μL. The fluorescence intensity values of fluorophore **4** were inversely proportional to the concentration of $Cu^{2+}$ (Figure 4.1b). The titration of $10^{-5}$ mM methanol solution of fluorophore **4** with $3\times10^{-6}$ mM methanol solution of $Cu^{2+}$ ion showed a regular decrease of the fluorescence intensities in 559 nm as we increase the concentration of the $Cu^{2+}$ ions as shown in Figure 6b. The relevant Stern-Volmer constant, calculated from the equation $I_0/I = 1 + K_{sv}[Q]$, is found to be $K_{sv} = 21.2$ from the plot as shown in Figure 4.1c.

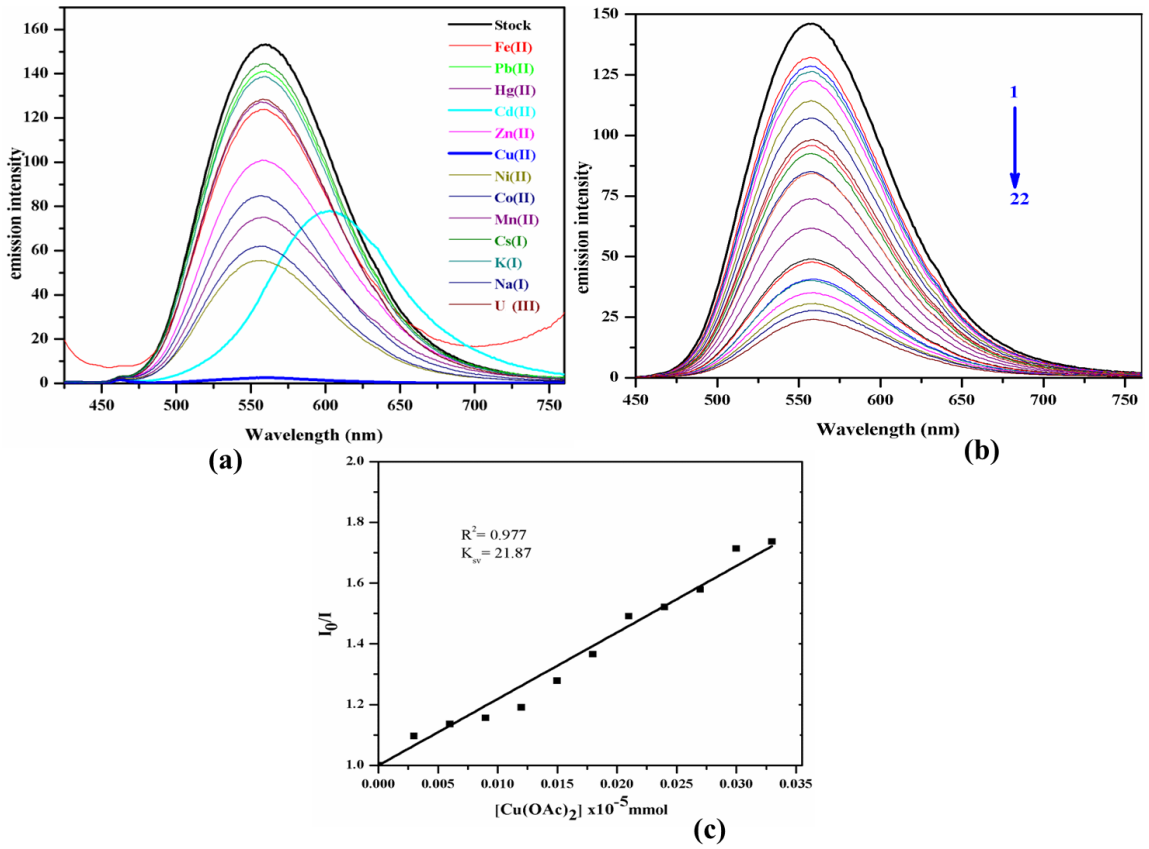


**Figure 4.1**. (a) Fluorescence spectra of chromophore **4** upon addition of different cations ($M^{n+}$) in their acetate salts in methanol ($\lambda_{ex}$ = 408 nm). (b) Fluorescence titration of chromophore 4 in methanol with increasing $Cu^{2+}$ concentration (addition 1mM solution of 10 µL $Cu^{2+}$ ions per time; $\lambda_{ex}$ = 408 nm). (c) Stern–Volmer plot for the chromophore **4** with $Cu^{2+}$.

### 4.3.2. Synthesis of the complex (1).

Under nitrogen atmosphere, A solution of ligand $\mathbf{L_1}$ (0.028 g, 0.27 mmol) and $Fe(BF_4)_2.6H_2O$ (0.045 g, 0.13 mmol) in acetone (20 mL) was stirred at room temperature for 1h. The solution was filtered and concentrated to about 8 mL, and diethyl ether layered on the top of conical (15 mL) flask. After one week, red color needle-shaped crystals of complex **1** deposited in the bottom of the conical flask, red crystals and it crystallized in P$2_1$/n space group belonging to the monoclinic space group. (See; Figure 4.2 and Table 4.1) Yield: 0.030 g ; Anal. Calcd. for ($C_{46}H_{44}B_2F_8FeN_{12}$): C, 55.56; H, 4.46; N, 16.90. Found: C,55.26; H, 4.52; N, 16.85; IR (KBr pellet) ($\upsilon$/$cm^{-1}$) for complex **1**: 2957s, 1598w, 1386m, 1200s, 1030w, 921s

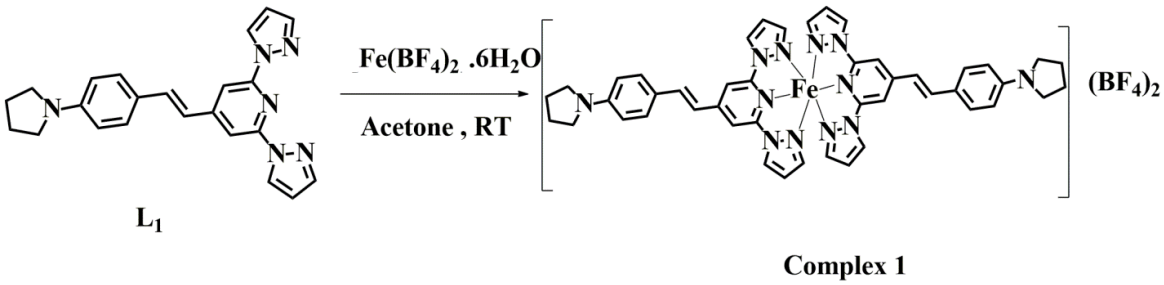


**Scheme 4.1.** Synthesis of complex **1** presented in the study.

### 4.3.3. Description of the Crystal Structures

Complex **1** has been synthesized by direct reaction of $Fe(BF_4)_2.6H_2O$ with ligand $\mathbf{L_1}$, under inert condition. The resulting synthesized Fe(II) coordination compound (complex **1**, scheme 1) has been characterized by single-crystal X-ray crystallography. Complex **1** was crystallized in monoclinic system and space group $P2_1/n$. The relevant thermal ellipsoidal plot is shown in Figure 4.2(a). In the crystal lattice, each molecular complex **1** is surrounded by two distorted (is it disordered) tetrafluoroborate counter anions. The relevant crystal data and structure refinement parameters have been given in Table 1. Interestingly in the crystal structure, the molecules undergo C–H···F intermolecular hydrogen bonding interactions leading to a supramolecular layered structure as shown in Figure 4.2(b). The bond length and bond angles of complex **1** are represented in Tables 2 and 3. Fe−N bond distances and concerned bite angles around the coordination sphere are good indicators of the spin state of a Fe(II) complex. Relevant literature[18] shows that , when 2,6-bis(pyrazolyl)pyridine ligand associated complexes yield Fe−N bond distances in the range of 1.93−1.97 Å, the relevant complexes are low spin Fe(II) complexes. On the other hand, when the Fe−N bond distances are in the range of 2.14−2.20 Å , the pertinent complexes are high spin Fe(II) complexes. Also, the Σ parameter (deg), which is the summation of the deviation from 90° of the twelve bite angles around the central $Fe^{II}$ ion, can range from 85° to 96° in low-spin complexes and from 145° to 197° in high-spin complexes. In the present study, the average Fe−N bond distance and Σ parameter were found 2.03 Å and 116.81° respectively. This indicates that, the complex **1** is associated with low spin state of Fe(II). We performed DFT and TDDFT calculations in solution state to corroborate the low spin state Fe(II).

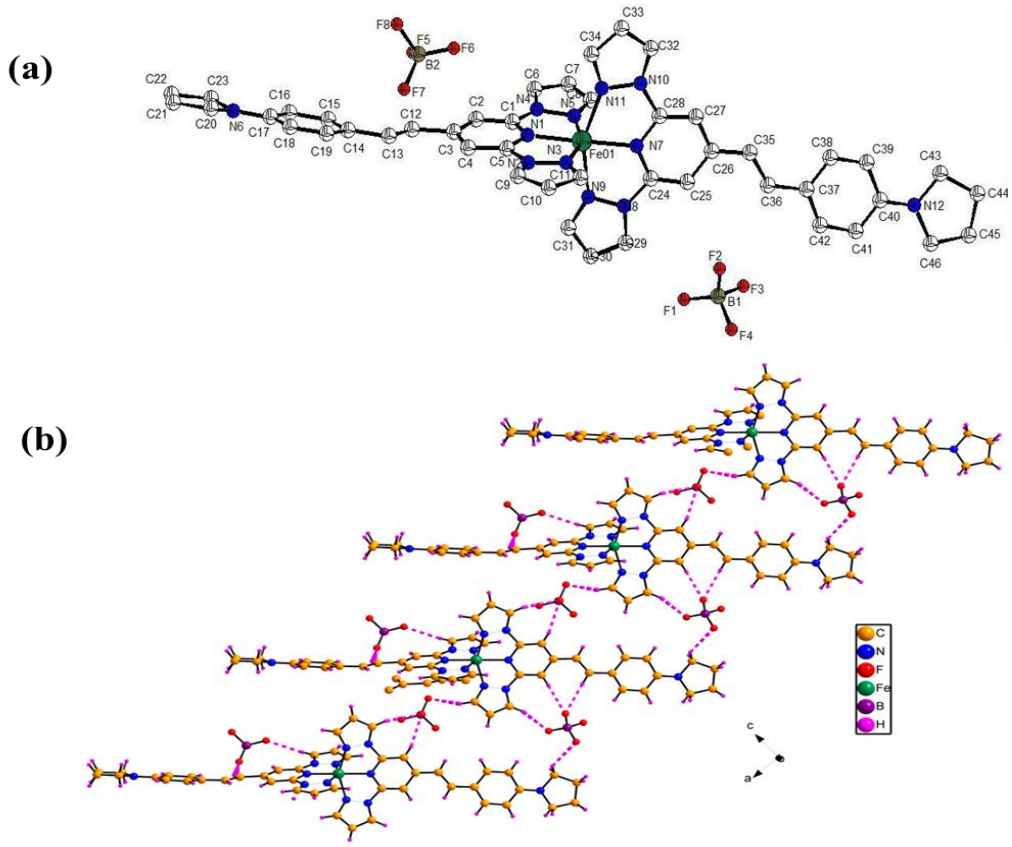


**Figure 4.2.** Thermal ellipsoidal plot of (a) Complex **1** (50% probability), hydrogen's are omitted for clarity (top) (b) The molecular packing diagram of Complex **1** characterized by C–H···F weak interactions (bottom).

### 4.3.4. UV-vis spectra of the ligand ($L_1$) and Complex 1:

The absorption spectra of the complex **1** and corresponding ligand $\mathbf{L_1}$ were recorded in acetone solvent at room temperature (298±2 K) as shown in Figure 4.3a. The absorption spectra of ligand $\mathbf{L_1}$ and complex **1** exhibit a broadband at 408 nm and 477 nm respectively. Ligand absorption bands are clearly indicated to the intra-ligand charge transfer (ILCT) bands which are originated due to charge delocalization from donor (pyrrolidine) group to acceptor(2,6-bis(pyrazolyl)pyridine acceptor through the π-transmitter in the 'push-pull' molecule. The absorption band at 408 nm observed for ligand $\mathbf{L_1}$ gets red-shifted to 477 nm on forming coordination complex **1**. The absorption band at 477 nm, observed in the electronic spectrum of complex **1**, corresponds to the energy of the combination of ligand-to-metal charge transfer (LMCT) and ligand to ligand charge transfer (LLCT) in the iron (II) complex, which can be explained by density functional theory (DFT) calculations (*vide infra*).

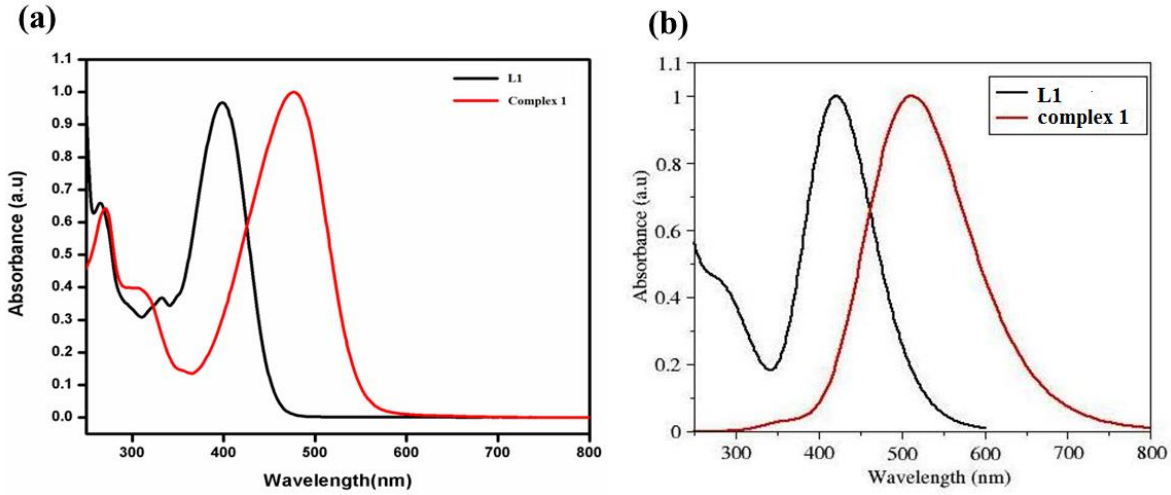


**Figure 4.3.** (a) Experimental UV–visible absorption spectra (left) and (b) theoretical absorption spectra (right) of complex **1** and concerned ligand $\mathbf{L_1}$ in acetone solutions.

### 4.3.5. Theoritical studies

Computational simulations of the ground-state electronic structures of the complex **1** and ligand $\mathbf{L_1}$ were performed by using density functional theory (DFT). The time-dependent density functional theory (TDDFT)[22, 23] was employed for the excitation of the complex **1** and ligand $\mathbf{L_1}$ both in the gas phase and solvent phase (acetone) calculations. The solvent phase calculations were performed using the self-consistent reaction field (SCRF) method, where solute (complex **1** or ligand $\mathbf{L_1}$) was placed in the solvent cavity (acetone). The polarizable continun model approach was implemented to create the solvent cavity.[24] Theoretical calculations throughout the study were done with the hybrid functional B3LYP, which includes Hartree–Fock (HF) exchange as well as DFT exchange correlations. Non-local correlations were accounted for by the Lee, Yang, and Parr (LYP) functional. The 6-31G(d, p) basis set of Pople was used in these calculations. All the computational calculations were performed with a Gaussian-09 suite of programs.[25] The energy minimized structures of the complex **1** and ligand $\mathbf{L_1}$ were confirmed by subsequent frequency calculations of the optimized structures. It is noted that all frequencies obtained from these calculations are positive. The vertical excitations of the complex **1** and ligand $\mathbf{L_1}$ were calculated by considering ground state energy minimized structures of complex **1** and ligand $\mathbf{L_1}$ as a reference, both in gas phase and solvent medium.

The energy minimized structures of ligand **$L_1$** and complex **1** are shown in Figure 4.4. It is found that three nitrogen sites, 1N, 3N and 12N, are present in the ligand (**$L_1$**), which make coordination with metal (Fe) by donating their lone pair electrons. Two such ligands attaches with the iron's six coordination sites resulting in the formation of complex **1**, as shown in Figure 4.4b. The energy minimization calculations of ligand **$L_1$** and complex **1** were performed in both gas phase and solvent (acetone) phase. It is found that bare ligand **$L_1$** is stabilized in the solvent phase by ~8 kcal/mol compared to the gas phase, whereas, the complex **1** is stabilized in solvent phase by ~95 kcal/mol compared to its gas phase structure. Hence, it can be concluded that metal-ligand interaction is more favorable in presence of solvent (acetone).

To study the excitations of the complex **1**, we first examine the nature of excitation of the ligand **$L_1$** in both gas and solvent phase. It is found that the first optically bright excitation of ligand **$L_1$** is observed at ~385 nm with oscillator strength of (*f*) = 1.1862 in the gas phase. This transition corresponds to $S_0 \rightarrow S_1$ and full contribution (~99%) of this excitation comes from its highest occupied molecular orbital (HOMO) and lowest unoccupied molecular orbital (LUMO). The pictorial diagram of HOMO and LUMO of the ligand is presented in Figure 4.5a. The same excitation of the ligand is found at ~ 421 nm with *f* =1.2902 in presence of acetone solvent. It is seen from these calculations that a red shift of ligand excitation ($S_0 \rightarrow S_1$) and an increment of optical brightness are observed in presence of solvent (solvatochromic effect). The reason behind this redshift is that the LUMO of the ligand **$L_1$** gets more stabilized (~0.2378 eV) compared to the HOMO (~0.0365 eV) in presence of solvent. That is why, the HOMO-LUMO energy gap is decreased in presence of solvent (3.2237 eV) compared to gas phase (3.4250 eV). A further inspection of the HOMO-LUMO diagram, presented in Figure 4.5a, indicates that charge density (electron density) is transferred from the pyrrolidine (donor) moiety to the bis(pyrazolyl)pyridine moiety (acceptor) through the conjugation situated at the ligand **$L_1$**.

The excitation of the complex **1** is also calculated in the gas phase and in solvent medium. An optically bright transition of the complex **1** is found at ~552 nm with *f* =2.6753 value in gas phase. This transition is dominated by electron transfer from HOMO-1 → LUMO (43%) and HOMO → LUMO+1 (44%). The same transition in solvent medium is observed at ~512 nm with *f* = 1.4126 and the transition is dominated by electron transfer from HOMO-4 → LUMO+9 (22%), HOMO-3 → LUMO+6 (19%), HOMO-1 → LUMO (17%) and HOMO → LUMO+1 (19%). The diagrams of the participated MOs on this

transition are presented in panels b, c, d and e of Figure 4.5. The blue shift (solvatochromic effect) of the present transition might be attributed due to the involvement of electron transfer from core occupied MOs (HOMO-4, HOMO-3) to the energetically higher unoccupied MOs (LUMO+9, LUMO+6). It can be seen from Figures 4.4b and 4.4c respectively, that a dispersed electron density is situated at the ligand in HOMO-4 and HOMO-3, whereas in LUMO+9 and LUMO+6, the electron density is concentrated near the surroundings ligands and its metal (Fe) atom. Hence this transition can be assigned as 'Ligand-to-Metal' charge transfer (LMCT). On the other hand, a careful inspection of Figures 4.5d and 4.5e show that electron density of the HOMO-1 and HOMO is dominantly situated in one of the ligands, whereas, near the metal (Fe), electron density is very less. The LUMO diagram of the same figures (Figures 4.5d and 4.5e) indicates a sharing of electron density between two ligands and a slight increment of electron density at the metal. Hence, this transition also be assigned as 'Ligand-to-Ligand' charge transfer (LLCT).[26-28] Therefore, this electronic transition can be attributed to mixed ligand-metal-ligand-ligand charge transfer (LMLLCT), as the contributions from LMCT (41%) and LLCT (36%) processes are nearly same. The normalized theoretical absorption spectra of the ligand $\mathbf{L_1}$ and complex **1** are presented in Figure 4.3b.

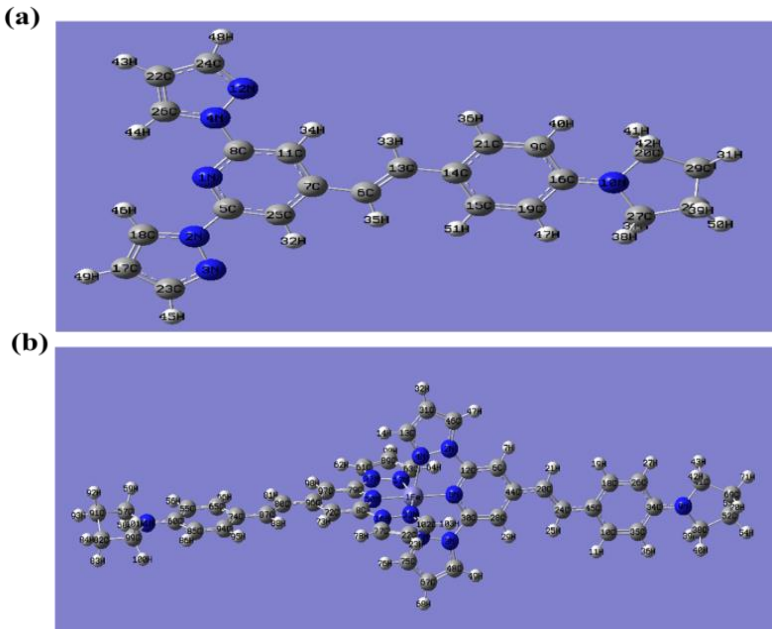


**Figure 4.4.** (a) Optimized structures of ligand ($\mathbf{L_1}$) and (b) complex **1** in acetone. Optimization is performed with B3LYP hybrid functional using 6-31G(d,p) basis set in CPCM solvation model.

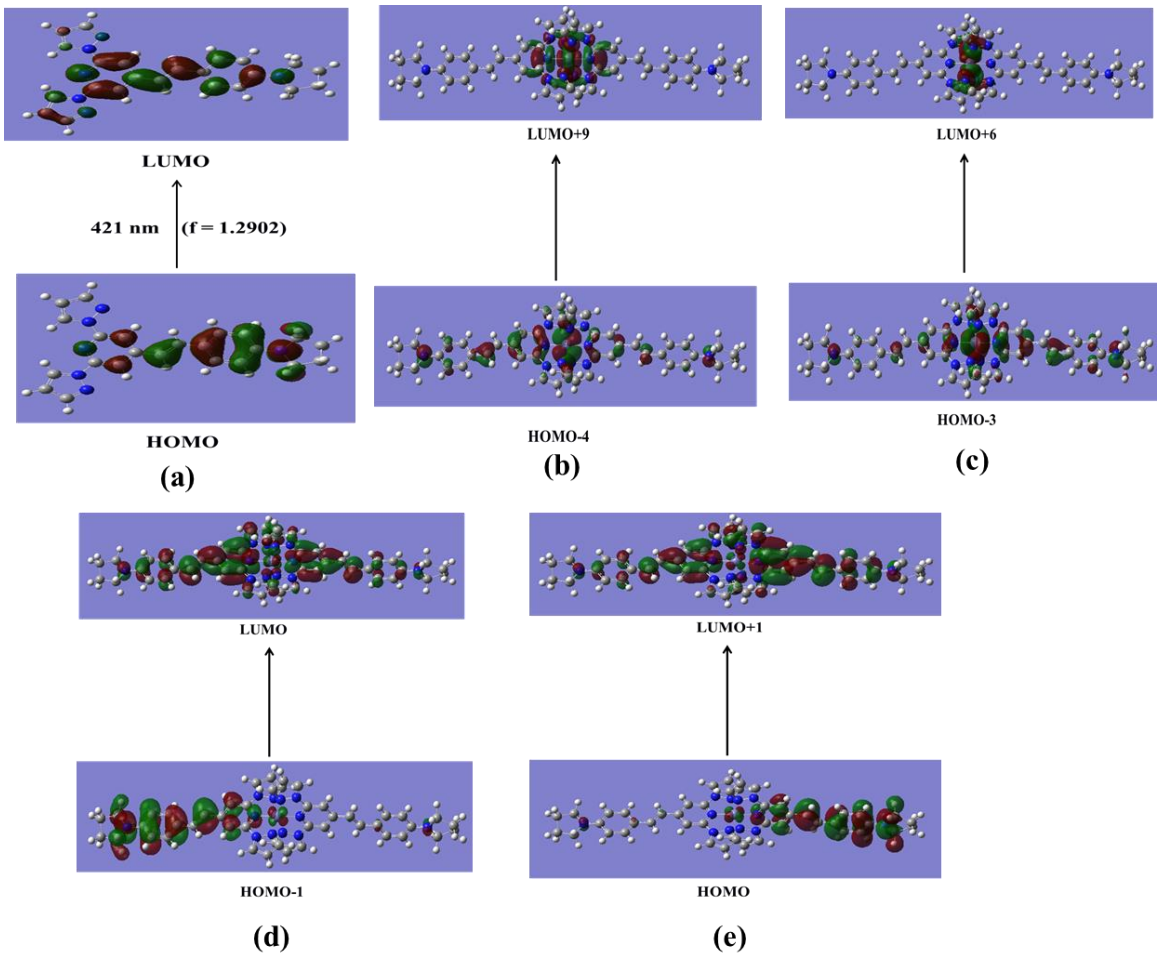


**Figure 4.5.** Photo-excitations: (a) ligand $\mathbf{L_1}$ and (b-e) complex **1**. Relevant contributions of complex **1** MOs are: (b) 22% (acetone solvent), (c) 19% (acetone solvent), (d) 43% (gas phase) and (e) 44% (gas phase). Calculations are performed with time-dependent density functional theory (TDDFT) using B3LYP hybrid functional and 6-31G(d,p) basis set in CPCM solvation model.

### 4.4. Summary.

This chapter deals with a mono-nuclear Fe(II) coordination complex $[Fe(L_1)_2](BF_4)_2$ (**1**) ($\mathbf{L_1}$ = π-conjugated 2,6-bis(pyrazolyl)pyridine derivative), which has been unambiguously characterized by single crystal X-ray crystallography. From the crystallographic data of this complex and the relevant literature, this compound has tentatively been assigned as a

low spin Fe(II) complex. DFT calculations are performed on the ligand $\mathbf{L_1}$ and complex **1** in gas phase as well as in solution phase (acetone) considering the complex as a low spin Fe(II) complex to corroborate the experimental electronic absorption spectra of both ligand and the resulting complex **1**. Since the experimental electronic absorption spectra and calculated absorption spectra agree very well, we believe that the complex **1** is a low spin complex. Magnetic studies of complex **1** are under progress in our laboratory. We have shown that molecule **4** can be described as a selective molecular sensor for the recognition of $Cu^{2+}$ ion; we have demonstrated this by fluorescence experiments of compound **4** with a series of metal ions (as acetates). Among all metal acetates, we took, only copper acetate quenches the fluorescence extensively.

**Table 4.1.** Crystallographic data and structure refinement for complex **1**

| | |
|---|---|
| Empirical formula | $C_{46}H_{44}B_2F_8FeN_{12}$ |
| Formula weight | 994.4 |
| Temperature (K) | 293(2) K |
| Crystal size (mm) | 0.10x 0.11 x 0.12 |
| Crystal system | Monoclinic |
| Space group | $P2_1/n$ |
| Z | 4 |
| Wavelength ( Å) | 0.71073 |
| Unit cell dimensions | |
| a [Å] | 11.9798(10) |
| b [Å] | 18.1432(15) |
| c [Å] | 24.4189(19) |
| α [º] | 90 |
| β [º] | 93.425(3) |
| γ [º] | 90 |
| Volume [$Å^3$] | 5298.0(7) |
| Calculated density ($Mg/m^{-3}$) | 1.247 |
| Reflections collected/ unique | 41957/11611 |
| R(int) | 0.1094 |
| F(000) | 2048 |
| Max. and min. transmission | 0.978 and 0.982 |
| Theta range for data collection (deg.) | 2.24 to 27.54 |
| Refinement method | Full-matrix least- squares on $F^2$ |
| Data/restrains/parameters | 11611/0/623 |
| Goodness-of-fit on $F^2$ | 0.984 |
| $R_1/wR_2$ [I>2sigma(I)] | 0.1101/ 0.3139 |
| R1/WR2 (all data) | 0.2012 / 0.3539 |
| Largest diff. peak and hole e.Å-3 | 0.890 and -0.366 |

**Table 4.2.** Bond lengths in the crystal structure of complex **1**

| | | | |
|---|---|---|---|
| Fe(01)-N(1) | 1.988(6) | C(27)-C(28) | 1.367(7) |
| Fe(01)-N(7) | 1.997(4) | C(27)-C(26) | 1.400(7) |
| Fe(01)-N(3) | 2.037(7) | C(5)-N(1) | 1.324(10) |
| Fe(01)-N(11) | 2.061(5) | C(5)-N(2) | 1.405(9) |
| Fe(01)-N(9) | 2.065(6) | C(5)-C(4) | 1.420(11) |
| Fe(01)-N(5) | 2.066(5) | N(12)-C(40) | 1.338(7) |
| N(10)-C(32) | 1.328(7) | N(12)-C(46) | 1.460(7) |
| N(10)-N(11) | 1.406(6) | N(12)-C(43) | 1.463(7) |
| N(10)-C(28) | 1.417(6) | C(42)-C(37) | 1.368(7) |
| N(8)-N(9) | 1.369(6) | C(42)-C(41) | 1.390(7) |
| N(8)-C(24) | 1.390(6) | C(34)-C(33) | 1.404(9) |
| N(11)-C(34) | 1.328(6) | N(9)-C(31) | 1.331(8) |
| N(7)-C(28) | 1.342(7) | N(2)-C(9) | 1.328(10) |
| N(7)-C(24) | 1.344(6) | N(2)-N(3) | 1.410(9) |
| B(2)-F(6) | 1.326(9) | B(2)-F(7) | 1.362(9) |
| B(2)-F(5) | 1.400(12) | B(1)-F(3) | 1.383(13) |

**Table 4. 3.** Bond Angles in the crystal structure of complex **1**

| | | | |
|---|---|---|---|
| N(1)-Fe(01)-N(3) | 78.1(3) | C(5)-N(1)-Fe(01) | 120.5(5) |
| N(7)-Fe(01)-N(3) | 111.3(2) | C(17)-N(6)-C(23) | 126.1(6) |
| N(1)-Fe(01)-N(11) | 106.23(19) | N(6)-C(23)-C(22) | 106.7(6) |
| N(7)-Fe(01)-N(11) | 76.96(17) | N(2)-C(9)-C(10) | 107.5(9) |
| N(3)-Fe(01)-N(11) | 96.9(2) | C(13)-C(12)-C(3) | 124.2(9) |
| N(1)-Fe(01)-N(9) | 100.5(2) | N(6)-C(20)-C(21) | 105.9(7) |
| N(7)-Fe(01)-N(9) | 76.17(18) | F(6)-B(2)-F(8) | 111.4(9) |
| N(3)-Fe(01)-N(9) | 91.4(2) | F(6)-B(2)-F(7) | 116.5(7) |
| N(3)-Fe(01)-N(5) | 155.1(3) | N(3)-C(11)-C(10) | 107.5(9) |
| C(32)-N(10)-N(11) | 111.0(4) | F(2)-B(1)-F(3) | 107.9(11) |
| C(32)-N(10)-C(28) | 132.6(5) | F(1)-B(1)-F(3) | 110.5(9) |
| C(34)-N(11)-Fe(01) | 142.4(4) | F(2)-B(1)-F(4) | 107.3(8) |
| C(31)-N(9)-Fe(01) | 140.7(6) | N(2)-N(3)-Fe(01) | 112.7(4) |
| C(9)-N(2)-N(3) | 112.7(7) | C(1)-N(4)-N(5) | 115.2(6) |
| C(37)-C(38)-C(39) | 121.9(5) | N(10)-C(32)-C(33) | 108.3(6) |
| C(35)-C(36)-C(37) | 129.5(5) | N(2)-N(3)-Fe(01) | 112.7(4) |

## 4.5. References

(1) Supriya, S.; Das, S. K. Reversible Single Crystal to Single Crystal Transformation through Fe−O(H)Me/Fe−$OH_2$ Bond Formation/Bond Breaking in a Gas−Solid Reaction at an Ambient Condition. *J. Am. Chem. Soc.* **2007,** *129*, 3464-3465.

(2) Supriya, S.; Das, S. K. Solid-to-solid Formation at the Solid-liquid Interface Leading to a Chiral Coordination Polymer from an Achiral Monomer. *Chem. Comm.* **2011,** *47*, 2062-2064.

(3) Madhu, V.; Sabbani, S.; Kishore, R.; Naik, I. K.; Das, S. K. Mechanical Motion in the Solid State and Molecular Recognition: Reversible Cis-trans Transformation of an Organic Receptor in a Solid-liquid Crystalline State Reaction Triggered by Anion Exchange. *CrystEngComm* **2015,** *17*, 3219-3223.

(4) Kumar, G.; Guda, R.; Husain, A.; Bodapati, R.; Das, S. K. A Functional Zn(II) Metallacycle Formed from an N-Heterocyclic Carbene Precursor: A Molecular Sensor for Selective Recognition of $Fe^{3+}$ and $IO^{4-}$ Ions. *Inorg. Chem. 2017, 56 , 5017–5025*.

(5) Boal, A. K.; Rosenzweig, A. C. Structural Biology of Copper Trafficking. *Chem. Rev.* **2009**, *109*, 4760-4779.

(6) Davis, A. V.; O'Halloran, T. V. A Place for Thioether Chemistry in Cellular Copper Ion Recognition and Trafficking. *Nat. Chem. Biol.* **2008**, *4*, 148-151.

(7) Kim, B.-E.; Nevitt, T.; Thiele, D. J. Mechanisms for Copper Acquisition, Distribution and Regulation. *Nat. Chem. Biol.* **2008**, *4*, 176-185.

(8) Bergonzi, R.; Fabbrizzi, L.; Licchelli, M.; Mangano, C. Molecular Switches of Fluorescence Operating Through Metal Centred Redox Couples. *Coord. Chem. Rev.* **1998**, *170*, 31-46.

(9) Gonzáles, A. P. S.; Firmino, M. A.; Nomura, C. S.; Rocha, F. R. P.; Oliveira, P. V.; Gaubeur, I. Peat as a Natural Solid-Phase for Copper Preconcentration and Determination in a Multicommuted Flow System Coupled to Flame Atomic Absorption Spectrometry. *Anal. Chim. Acta.* **2009**, *636*, 198-204.

(10) Becker, J. S.; Zoriy, M. V.; Pickhardt, C.; Palomero-Gallagher, N.; Zilles, K. Imaging of Copper, Zinc, and Other Elements in Thin Section of Human Brain Samples (Hippocampus) by Laser Ablation Inductively Coupled Plasma Mass Spectrometry. *Anal. Chem.* **2005**, *77*, 3208-3216.

(11) Liu, Y.; Liang, P.; Guo, L. Nanometer Titanium Dioxide Immobilized on Silica Gel as Sorbent for Preconcentration of Metal Ions Prior to Their Determination by Inductively Coupled Plasma Atomic Emission Spectrometry. *Talanta.* **2005**, *68*, 25-30.

(12) Pathirathna, P.; Yang, Y.; Forzley, K.; McElmurry, S. P.; Hashemi, P. Fast-Scan Deposition-Stripping Voltammetry at Carbon-Fiber Microelectrodes: Real-Time, Subsecond, Mercury Free Measurements of Copper. *Anal. Chem.* **2012**, *84*, 6298-6302.

(13).Halcrow, M. A. The synthesis and coordination chemistry of 2,6-bis(pyrazolyl)pyridines and related ligands — Versatile terpyridine analogues. *Coord. Chem. Rev.* **2005,** *249*, 2880-2908.

(14). Halcrow, M. A. Iron(II) complexes of 2,6-di(pyrazol-1-yl)pyridines—A versatile system for spin-crossover research. *Coord. Chem. Rev.* **2009**, *253*, 2493-2514.

(15). Halcrow, M. A. Recent advances in the synthesis and applications of 2,6-dipyrazolylpyridine derivatives and their complexes. *New J. Chem.* **2014,** *38*, 1868-1882.

(16). Hasegawa, Y.; Sakamoto, R.; Takahashi, K.; Nishihara, H. Bis[(E)-2,6-bis(1H-pyrazol-1-yl)-4-styrylpyridine]iron(II) Complex: Relationship between Thermal Spin Crossover and Crystal Solvent. *Inorg. Chem.* **2013,** *5*, 1658-1665.

(17). Nihei, M.; Han, L.; Oshio, H. Magnetic Bistability and Single-Crystal-to-Single-Crystal Transformation Induced by Guest Desorption. *J. Am. Chem. Soc.* **2007,** *129*, 5312-5313.

(18). Gonzalez-Prieto, R.; Fleury, B.; Schramm, F.; Zoppellaro, G.; Chandrasekar, R.; Fuhr, O.; Lebedkin, S.; Kappes, M.; Ruben, M. Tuning the spin-transition properties of pyrene-decorated 2,6-bispyrazolylpyridine based Fe(ii) complexes. *Dalton Trans.* **2011,** *40*, 7564-7570.

(19). Rajadurai, C.; Schramm, F.; Brink, S.; Fuhr, O.; Ghafari, M.; Kruk, R.; Ruben, M. Spin Transition in a Chainlike Supramolecular Iron(II) Complex. *Inorg. Chem.* **2006,** *45*, 10019-10021.

(20). Nihei, M.; Tahira, H.; Takahashi, N.; Otake, Y.; Yamamura, Y.; Saito, K.; Oshio, H. Multiple Bistability and Tristability with Dual Spin-State Conversions in $[Fe(dpp)_2][Ni(mnt)_2]_2 \cdot MeNO_2$. *J. Am. Chem. Soc.* **2010,** *132*, 3553-3560.

(21) Bruker. *SADABS*, *SMART*, *SAINT* and *SHELXTL*, **2000** (Bruker AXS Inc., Madison, Wisconsin,USA

(22) Varnes, A. W.; Dodson, R. B.; Wehry, E. L. Interactions of transition-metal ions with photoexcited states of flavines. Fluorescence quenching studies. *J. Am. Chem. Soc.***1972**, *94*, 946–950

(23) Scalmani, G.; Frisch, M. J.; Mennucci, B.; Tomasi, J.; Cammi, R.; Barone, V. Geometries and properties of excited states in the gas phase and in solution: Theory and application of a time-dependent density functional theory polarizable continuum model. *J. Chem. Phys.* **2006,** *124*, 094107.

(24) Tomasi, J.; Mennucci, B.; Cammi, R. Quantum Mechanical Continuum Solvation Models. *Chem. Rev.* **2005,** *105*, 2999-3094.

(25) Frisch, M. J.; Trucks, G. W.; Schlegel, H. B.; Scuseria, G. E.; Robb, M. A.; Cheeseman, J. R.; Scalmani, G.; Barone, V.; Mennucci, B.; Petersson. G. A. et al. Gaussian 09, revision B.01; Gaussian, Inc.: Wallingford, CT, 2010.

(26) Acosta, A.; Zink, J. I.; Cheon, J. Ligand to Ligand Charge Transfer in (Hydrotris(pyrazolyl)borato)(triphenylarsine)copper(I). *Inorg. Chem.* **2000,** *39*, 427-432.

(27) Takahashi, K.; Hasegawa, Y.; Sakamoto, R.; Nishikawa, M.; Kume, S.; Nishibori, E.; Nishihara, H. Solid-State Ligand-Driven Light-Induced Spin Change at Ambient Temperatures in Bis(dipyrazolylstyrylpyridine)iron(II) Complexes. *Inorg. Chem.* **2012,** *51*, 5188-5198.

(28) Huo, P.; Chen, T.; Hou, J.-L.; Yu, L.; Zhu, Q.-Y.; Dai, J. Ligand-to-Ligand Charge Transfer within Metal–Organic Frameworks Based on Manganese Coordination Polymers with Tetrathiafulvalene-Bicarboxylate and Bipyridine Ligands. *Inorg. Chem.* **2016,** *55*, 6496-6503.

# A Flexible Molecular Receptor Isolated in an Unusual Intermediate Conformation: Computation, Crystallography, Hirshfeld Surface Analysis and Synthesis of $\{Cu(mnt)_2\}_2$ Ion pair Complex

5

**Abstract:** 1,1''-1,4-phenylene-bis(methylene)bis-4,4'-bipyridinium cation $[C_{28}H_{24}N_4]^{2+}$ (**c**), an organic receptor that generally crystallizes in its *trans*-conformation, has recently been shown to be isolated in its *cis*-conformation in an ion paired compound $[C_{28}H_{24}N_4][Zn(dmit)_2] \cdot 2DMF$ ($dmit^{2-}$ = 1,3-dithiole-2-thione-4,5-dithiolate). In this article, we have demonstrated that the same receptor $[C_{28}H_{24}N_4]^{2+}$ (**c**) can also be stabilized in an unusual intermediate conformation (neither *cis* nor *trans*) with $PF_6^-$ anion in compound $[C_{28}H_{24}N_4](PF_6)_2 \cdot$(1,4-dioxane) (**1**). The energetically favored *trans* conformation has been described in its nitrate salt $[C_{28}H_{24}N_4](NO_3)_2 \cdot 2H_2O$ (**2**). Compounds **1** and **2**, crystallizing in triclinic and monoclinic systems with space groups *P-1* and $P2_1/n$ respectively, have additionally been characterized by Hirshfeld surface analysis. The density functional theory calculations are performed to understand the internal mechanism of the stability of various conformers of cationic receptor **c**, compound **1** and compound **2**. In conjunction with the electronic stability of the conformers, the natural bond orbital analysis and conformational equilibrium constants at different temperatures are also calculated to find out the sources of the different stability of the various conformers of experimentally synthesized compounds. The ion pair complex **1** of the same cation receptor was synthesized under acidic condition.

## 5.1. Introduction

Intermolecular interactions in the solid state continue to be a topic of great interest in the field of supramolecular as well as materials chemistry because of its fundamental importance for the formation of higher organized chemical systems that result from the association of two or more chemical species.[1-2] Depending upon the function and need of selectivity in the molecular assembly processes, several types of weak but specific (mostly noncovalent) intermolecular interactions are involved that include ion pairing,[3] hydrogen bonding,[4] arene-arene ($\pi$-$\pi$) stacking interactions[5-7] etc. The biological processes,[8-10] that encounter such non-covalent interactions, are substrate-enzyme complex formation, the protein folding, the formation of membranes, antiportation of neutral and ionic species through membranes etc. In these intermolecular interactions, particularly between substrate and receptor (e.g., the active site of the enzyme), the receptor is generally flexible to undergo conformational changes to accommodate the substrate in an optimal geometry, comparable to 'lock-and-key fit' situation.[11]

Mimicking such conformational change using a specific substance is a great challenge to modern chemistry researchers. Many captivating, structurally diverse receptors (hosts) have been designed and synthesized for the purpose of studying the interactions between the receptor (host) and substrate (guest). Besides well-characterized macrocycles (hosts), e.g., cyclophanes,[12] cyclodextrins,[13] cryptophanes,[14] cucurbiturils,[15] carcerands,[16] supramolecular capsules[17] etc., acyclic compounds with cavities of flexible size, that are generally termed as molecular tweezers and clefts, proved to be effective synthetic receptors.[18] A molecular tweezer is defined as a synthetic receptor that contains two aromatic (complexing) chromophores connected by a single spacer. A cleft is nothing but a molecular tweezer having converged functional groups (receptors) that are separated by 10-12 Å (with the help of the spacer) to create a cavity for guest/substrate binding.[19] We report here an organic acyclic receptor cation having two aromatic side-arms (4,4'-bipyridines) connected by a single spacer (1,4-phenylene-bis(methylene)), namely, 1,1''-1,4-phenylene-bis(methylene)bis-4,4'-bipyridinium cation $[C_{28}H_{24}N_4]^{2+}$ (**c**), which can interconvert between its *syn*- / (cleft-like) and *anti*- conformations as shown in Scheme 1 (left and right respectively). The receptor cation **c** can also be isolated in an unusual intermediate conformation (Scheme 5.1, middle). In this contribution, we have described synthesis and crystal structures of $[C_{28}H_{24}N_4](PF_6)_2\cdot$(1,4-dioxane) (**1.(1,4dioxane)**) and

$[C_{28}H_{24}N_4](NO_3)_2 \cdot 2H_2O$ (**2·2H2O**) having an *intermediate* and *anti*-conformation respectively. We have also performed Hirshfeld surface analysis on compounds **1·(1,4-dioxane))** and **2·2H2O** to rationalize molecular conformations of their cationic receptors.

In order to understand this unusual isolation of compound **1** with an intermediate conformation, we performed quantum mechanical calculations using density functional theory and we tried to understand internal mechanism of the stability of different conformers of the cationic receptor **c**, compound **1** and compound **2.** The electronic stability of the conformers were analysed by considering isodesmic reaction between the cationic receptor **c** and donor anions, $PF_6^-$ and $NO_3^-$, following the principles of thermodynamics. The different conformational analyses of the compound **1** have been performed by fixing the 1N-24C-52C-29N dihedral angle at different values (see in the text for details). On the other hand, stability of these compounds on excitation is also measured by evaluating the energy gap between highest occupied molecular orbital (HOMO) and lowest unoccupied molecular orbital (LUMO) at the electronic ground state of the respective compounds. The possible interactions between the occupied donor orbitals and unoccupied acceptor orbitals in these compounds are also calculated by using second-order perturbation theory as implemented in natural bond orbital analysis (NBO). As a result of these analyses, the sources of the different stabilities of the various conformers of the respective compounds can be accounted and results are discussed in details in the text. At last, we calculated the equilibrium constants of various conformational equilibria among the different conformers of the respective compounds to confirm the results of the above analyses by taking the experimental conformational equilibrium constant values between the cis-2-butene and trans-2-butene at different temperature as a reference.

**Scheme 5.1**

**Syn- / Cleft-like**

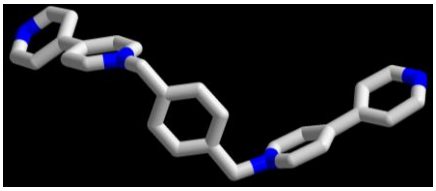

**Intermediate**

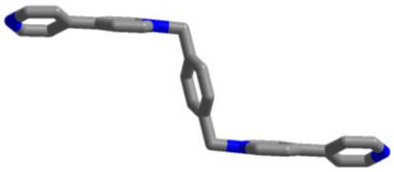

**Anti- / Trans-**

## 5.2. Experimental Section

### 5.2.1. Materials and Methods

All reagents and solvents were commercially available and used without further purification. Elemental analysis (C, H and N) were obtained with a FLASH EA 1112 Series CHNS analyser. FT-IR spectra were recorded in the range 400-4000 $cm^{-1}$ with a JASCO FT/IR-5300 spectrometer using KBr pellet. $^1H$ NMR spectra were recorded on Bruker DRX- 400 spectrometer using $Si(CH_3)_4$ as an internal standard.

### 5.2.2. Synthesis

**Synthesis of compound $[C_{28}H_{24}N_4](PF_6)_2 \cdot$(1,4-dioxane) (1)**

150 mg (0.568 mmol) of 1,4-bis(bromomethyl)benzene, dissolved in 10 mL of dry acetonitrile, were added dropwise to a refluxing solution of 4,4'−bipyridine (500 mg, 3.2 mmol) in 10 mL of acetonitrile. The reaction mixture was then refluxed for an additional 2 h. The $[C_{28}H_{24}N_4]Br_2$ salt was and comes out as insoluble white solid. The precipitate was washed with acetonitrile and dried in vacuum. This product was then dissolved in warm water and subsequently, it was treated with $NH_4PF_6$. This results in the precipitation of $[C_{28}H_{24}N_4](PF_6)_2$(1,1'–1,4-phenylene-bis(methylene)bis–4,4'-bipyridinium–bis(hexafluorophosphate). Yield: 0.276 g (~70%). This can be described as crude $PF_6$ salt of **c**, $[C_{28}H_{24}N_4](PF_6)_2$. This crude product was recrystallized by the vapor diffusion of diethylether into a solution of $[C_{28}H_{24}N_4](PF_6)_2$ in a mixed solvents of DMF:1,4-dioxane (1:3) into the single crystals of $[C_{28}H_{24}N_4](PF_6)_2 \cdot$(1,4-dioxane) (**1·(1,4-dioxane)).** Anal. Calcd. for ($C_{32}H_{32}F_{12}N_4O_2P_2$): C, 48.37; H, 4.06; N, 7.05. Found: C, 48.26; H, 4.11; N, 7.12. IR (KBr pellet) ($\upsilon$/$cm^{-1}$) :3134s, 3074w, 2150w, 1699m, 1639s, 1502m, 1460s, 1421m, 1215s, 1184m, 1010m, 835s, 557s, 515w. $^1H$ NMR (DMSO-$d_6$): δ 9.28(d, J=6.647, 4H); 8.81(d, J=6.51, 4H); 8.62(d, J=6.48, 4H); 7.97(d, J=6.491, 4H); 7.66(S, 4H); 5.89(S, 4H).

**Synthesis of compound $[C_{28}H_{24}N_4](NO_3)_2 \cdot 2H_2O$ (2·2$H_2O$).**

Compound **2·2$H_2O$** was synthesized by an ion exchange method as follows: 0.07 g (0.1 mmol) of $[C_{28}H_{24}N_4](PF_6)_2$ was taken in a 10mL round bottom flask and 0.034 g (0.2 mmol) of $AgNO_3$ was taken in an another 10mL round bottom flask.Then the two round bottom flasks were fitted into two terminals of a λ-shaped glass tube. Then the whole λ

tube was filled by $CH_3CN$ solution keeping the whole system closed. After two weeks, colorless needle-shaped crystals of $[C_{28}H_{24}N_4](NO_3)_2 \cdot 2H_2O$ (**2·2H$_2$O**) deposited on the top of the λ tube. Yield: 0.048 g (84%). Anal. Calcd. for ($C_{28}H_{28}N_6O_8$): C, 58.33; H, 4.89; N, 14.58. Found: C, 58.26; H, 4.95; N, 14.49. IR (KBr pellet) ($\upsilon$/cm$^{-1}$) for **2·2H$_2$O**: 3323m, 3107w, 3020w, 1633s, 1593w, 1545m, 1523m, 1493m, 1350 ($NO_3^-$)s, 1211w, 1161m, 1070w, 895w, 823s, 771s, 727m, 513m, 478w.

**Synthesis of [4-(4-pyridiniumyl)-1-{4-[4-pyridiniumyl)-1-pyridin-iumylmeth-yl] benzyl}-pyridinium]- tetra(hexafluorophosphate)**

Before the synthesis of the ion-pair complex **1**, we isolated the corresponding cation receptor with $PF_6$ anion by following ion exchange method under acidic condition**:** The bromide salt of the cation (see below, scheme 4) was dissolved in water and this solution was acidified by dil. HCl until its pH reached to 2. Then the $PF_6$ salt was obtained by adding the aq. solution of $NH_4PF_6$.

**Synthesis of [4-(4-pyridiniumyl)-1-{4-[4-pyridiniumyl)-1-pyridin-iumylmeth -yl] benzyl}-pyridinium][Cu(mnt)$_2$]$_2$, [C$_{28}$H$_{26}$N$_4$][Cu(mnt)$_2$]$_2$ ·4DMF ( Complex 1)**

Complex **1** was synthesied by ion exchange method as follows: 0.1 g (0.1 mmol) of $[C_{28}H_{26}N_4](PF_6)_4$ was disolved in 10mL of $CH_3CN$ in a 15mL-round bottom flask and 0.165 g (0.2 mmol) of $[Bu_4N]_2[Cu(mnt)_2]$ was dissolved in a 10mL $CH_3CN$ in an another round bottom flask. Both flasks were fitted with two terminals of a λ shaped- glass tube and then the glass tube was completely filled by $CH_3CN$ solvent keeping the whole system closed. After 25 days, the dark-brown crystals of $C_{28}H_{26}N_4][Cu(mnt)_2]_2 \cdot 4DMF$ (**1**) got separated. Yield: 0.1 g (72%). (KBr pellet) ($\upsilon$/cm$^{-1}$) for **2**: 3441m, 2195s, 1633s, 1543w, 1460s, 1149s, 812s, 771m, 505m.

**5.2.3. Single crystal X-ray structure determination of the compounds 1-2**

$[C_{28}H_{24}N_4](PF_6)_2 \cdot$(1,4-dioxane) (**1·(1,4-dioxane))** was measured at 100 K and $[C_{28}H_{24}N_4](NO_3)_2 \cdot 2H_2O$ (**2·2H2O**) was measured at 298 K on a Bruker SMART APEX CCD area detector system [λ(Mo-Kα) = 0.71073 Å] with a graphite monochromator. 2400 frames were recorded with an ω scan width of 0.3$^o$, each for 8 s. Crystal-detector distance was 60 mm with a collimator of 0.5 mm. The SMART software[20] was used for intensity data acquisition and the SAINTPLUS software[20] was used for data extraction. Absorption

correction was performed with the help of SADABS program.[20] Programs of SHELX-97[21] were used for structure solution by direct methods and least-square refinement on $F^2$. All non-hydrogen atoms were refined anisotropically. Hydrogen atoms on aromatic ring were introduced on calculated positions and included in the refinement riding on their respective parent atoms. Detailed information about crystal data and structure determination are summarized in Table 5.1.

## 5.3. Results and discussion

### 5.3.1. Synthesis

The crude $[C_{28}H_{24}N_4](PF_6)_2$ is synthesized from 1,4-bis(bromomethyl)benzene and 4,4'−bipyridine (Scheme 5.2). This crude solid is then crystallized from DMF-1,4-dioxane to obtain the single crystals of compound $[C_{28}H_{24}N_4](PF_6)_2$·(1,4-dioxane) (**1·(1,4-dioxane))**). The nitrate salt (compound **2·2H2O**) could not be synthesized from a direct method, but this can be prepared from the crude PF6-salt of compound 1·(1,4-dioxane)) by an ion exchange method with silver nitrate (Scheme 5.3.). Schematic representation for the preparation of the tetrapositive salt of the organic cation $[C_{28}H_{26}N_4](PF_6)_4$ (Scheme 5.4.) and

Schematic representation for the preparation of $[C_{28}H_{26}N_4][Cu(mnt)_2]_2$ ·4DMF (complex **1**) (Scheme 5.5)

**Scheme 5.2**

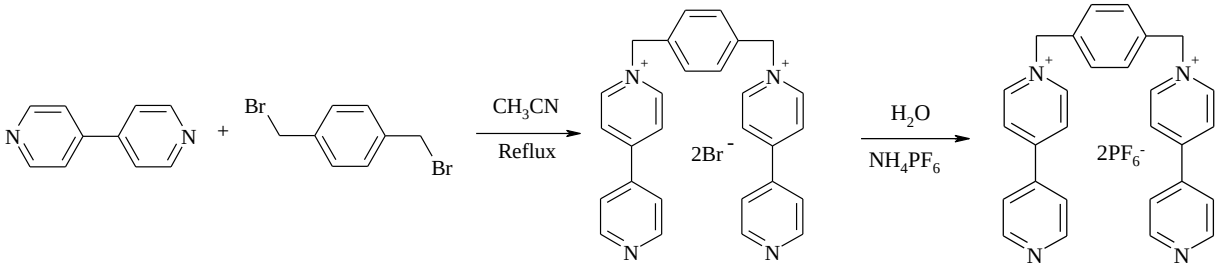


**Scheme 5.3**

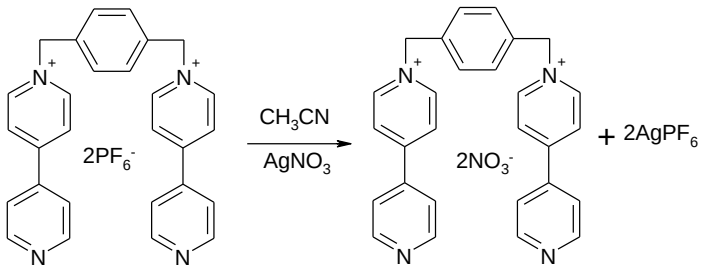

**Scheme 5.4**

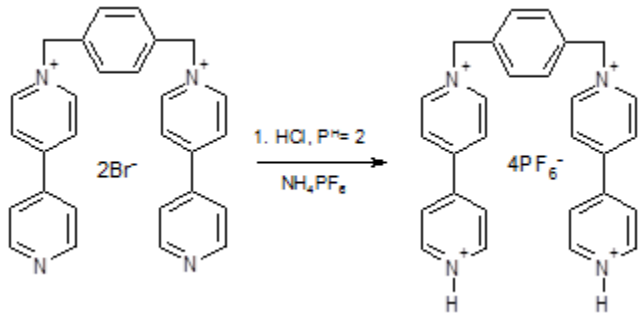


**Scheme 5.5**

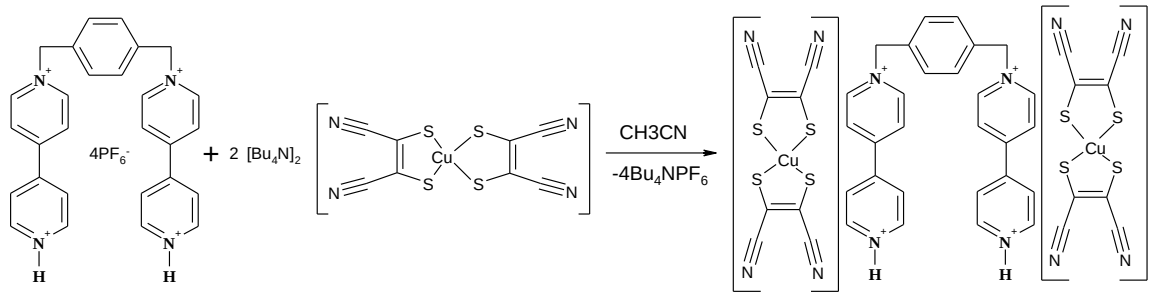


Compounds **1, 2** and complex **1** have been characterized by IR spectral studies, $^{1}$H NMR studies including elemental analyses and finally unambiguously by single crystal X-ray crystallography.

### 5.3.2. Description of crystal structures

The bromide salt of the title cationic receptor $[C_{28}H_{24}N_4]^{2+}$ (**c**), $[C_{28}H_{24}N_4]Br_2$ was structurally characterized and the usual *anti*-conformation of the cation **c** (Scheme 1, right) is found in the crystal structure of $[C_{28}H_{24}N_4]Br_2$.[22] When these off-white crystals of $[C_{28}H_{24}N_4]Br_2$ are suspended in MeCN solvent with few drops of DMF ([**c**]$Br_2$ crystals are not soluble in this medium) dissolving an excess amount of $[Bu_4N]_2[Zn(dmit)_2]$ and stirred for about an week, the off-white solid of $[C_{28}H_{24}N_4]Br_2$ becomes dark brown with the conversion of $[C_{28}H_{24}N_4][Zn(dmit)_2]$·in a solid-liquid interface crystalline state reaction. In the red-brown solid of compound $[C_{28}H_{24}N_4][Zn(dmit)_2]$, the cationic receptor $[C_{28}H_{24}N_4]^{2+}$ (**c**) has *syn*-conformation (Scheme 5.1, left), as observed in the crystal

structure of $[C_{28}H_{24}N_4][Zn(dmit)_2]\cdot 2DMF$**.**[23] By exploiting the flexible nature of this acyclic cationic receptor $[C_{28}H_{24}N_4]^{2+}$ (**c**), we could demonstrate the reversible *syn-anti* conformational change of **c** in solid to solid transformations (equation 1). We wanted to exploit further the flexible nature of $[C_{28}H_{24}N_4]^{2+}$

$[C_{28}H_{24}N_4][Zn(dmit)_2]\cdot 2DMF$ (2) (solid phase) + $[Bu_4N]Br$ (soln. Phase)
$\rightleftharpoons [C_{28}H_{24}N_4]Br_2$ (1) (solid phase) + $[Bu_4N]_2[Zn(dmit)_2]$ (soln. Phase) (equation 1)

(**c**) by crystallizing this cation with diverse anions and we synthesized compound *[*$C_{28}H_{24}N_4](PF_6)_2\cdot$(1,4-dioxane) (**1·(1,4-dioxane))**) (with $PF_6^-$ anion) and compound $[C_{28}H_{24}N_4](NO_3)_2\cdot 2H_2O$ (**2·2H2O**) (with $NO_3^-$ anion).

Compound $C_{28}H_{24}N_4](PF_6)_2\cdot$(1,4-dioxane) (**1.(1,4-doxane)**) crystallizes in the triclinic system with space group *P-1* and concerned single crystal X-ray data parameters, obtained at 100 K, are described in Table 5.1. The thermal ellipsoidal plot of the compound **1·(1,4-dioxane))** is displayed in Figure 5.1 and the relevant selected bond lengths and angles are described in Table 5.2. Interestingly, the cation **c**, observed in the crystal structure of $C_{28}H_{24}N_4](PF_6)_2\cdot$(1,4-dioxane) (**1·(1,4-dioxane))**) adopts an

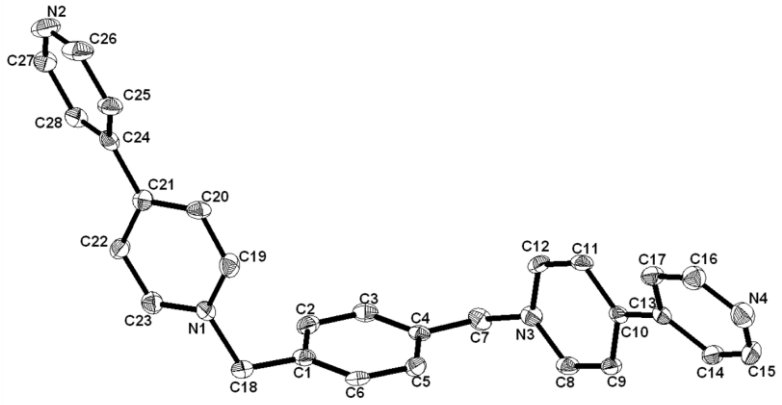


**Figure 5.1** Thermal ellipsoidal plot (30 % probability) of organic receptor $[C_{28}H_{24}N_4]^{2+}$ in compound $[C_{28}H_{24}N_4](PF_6)_2\cdot$(1,4-dioxane) (**1·(1,4-dioxane))**); anions, solvent molecules and hydrogens are omitted for clarity.

intermediate conformation which is in-between *syn*- and *anti*- conformations (Scheme 5.1, middle and Figure 5.1). We believe that inter-cation-anion hydrogen bonding interactions (mostly C–H···F hydrogen bonds) between the cation receptor **c** and anion $PF_6^-$ are responsible for this unusual intermediate conformation of **c** in the crystal struture

of compound **1·(1,4-dioxane)).** The C–H···F hydrogen bonding environment around the $PF_6^-$ anion is given in Figure 5.2. The relevant hydrogen bonding parameters are presented in Table 3. In other words, in the crystal structure,

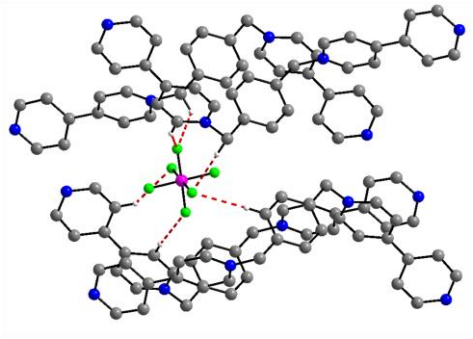

**Figure 5.2.** C-H···F hydrogen bonding environment around a $PF_6$ anion in $[C_{28}H_{24}N_4](PF_6)_2$·(1,4-dioxane) (**1·1,4-dioxane)**).

the stability of intermediate conformation (between *syn* and *anti*) of the organic receptor $[C_{28}H_{24}N_4]^{2+}$ (**c**) in compound $[C_{28}H_{24}N_4](PF_6)_2$·(1,4-dioxane) (**1·(1,4-dioxane))**) can be rationalized by its strong hydrogen bonding interactions with surrounding $PF_6^-$ anions resulting in a three-dimensional supramolecular network that have well-defined void spaces, occupied by the lattice 1,4-dioxane molecules as shown in Figure 5.3. We have also performed density functional theory (DFT) calculations to understand this intermediate conformation of **c** in compound 1·(1,4-dioxane)) (*vide infra*).

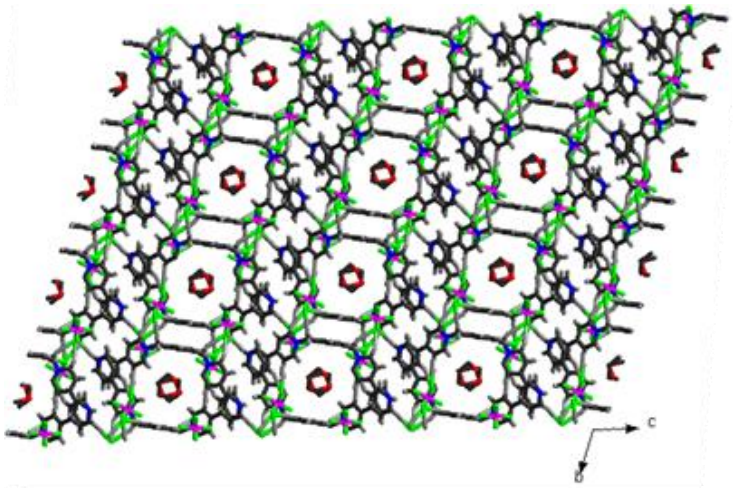

**Figure 5.3.** View (wire-frame representation) of the molecular packing of $[C_{28}H_{24}N_4](PF_6)_2$·(1,4-dioxane) (**1·(1,4-dioxane)**) (4×4) cells; color code: F, green; P, purple; C, gray; N, blue; O, red; H, medium gray.

Compound $[C_{28}H_{24}N_4](NO_3)_2 \cdot 2H_2O$ (**2·2H$_2$O**) crystallizes in monoclinic system with space group *P2$_1$/n*. The X-ray analysis of a single crystal of compound **2·2H$_2$O** reveals that the dication $[C_{28}H_{24}N_4]^{2+}$ (**c**) adopts an usual *anti*-conformation with respect to the two bipyridine units of the para-xylene ring as shown in Figure 5.4. In the asymmetric unit of the concerned crystal structure, one lattice water molecule (O4, located in a general position) exists with half of the cationic receptor (**c**) and one nitrate anion. Thus the molecular formula of compound **2·2H$_2$O** consists of a full molecule of cationic receptor, two nitrate anions and two lattice water molecules.

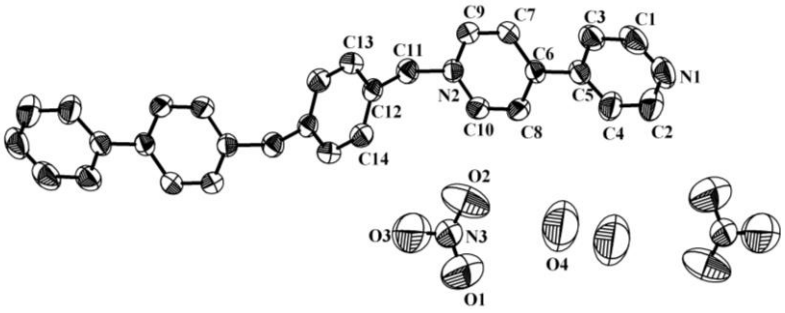


**Figure 5.4.** Thermal ellipsoidal plot of the asymmetric unit of compound $[C_{28}H_{24}N_4](NO_3)_2$·2H$_2$O (**2·2H$_2$O**), hydrogen atoms are not shown for clarity (50% probability).

Interestingly, the lattice water molecule (O4) forms a water dimer with same water molecule (these are related by a symmetry operation) using a very strong hydrogen bond (2.395 Å) as shown in Figure 5.5(a), left. The inter-water-dimer hydrogen bonding interactions (2.678 Å) lead to the formation of an one-dimensional zig-zag water chain (Figure 5(a), right). Each water molecule of this water chain is further hydrogen bonded (2.912 Å) to an oxygen atom ($O_2$) of the surrounding nitrate anion (Figure 5.5(b)). In the crystal structure of compound $[C_{28}H_{24}N_4](NO_3)_2 \cdot 2H_2O$ (**2·2H$_2$O**), the stair-case-like (*anti*-conformation) dications $[C_{28}H_{24}N_4]^{2+}$ (**c**) pack to form zig- zag arrays with two

nitrate anions and two crystal water molecules, inserted in between the dications as shown in Figure 5.6(a). The corresponding space filling plot (without nitrate anions and lattice water molecules) is shown in Figure 5.6(b).

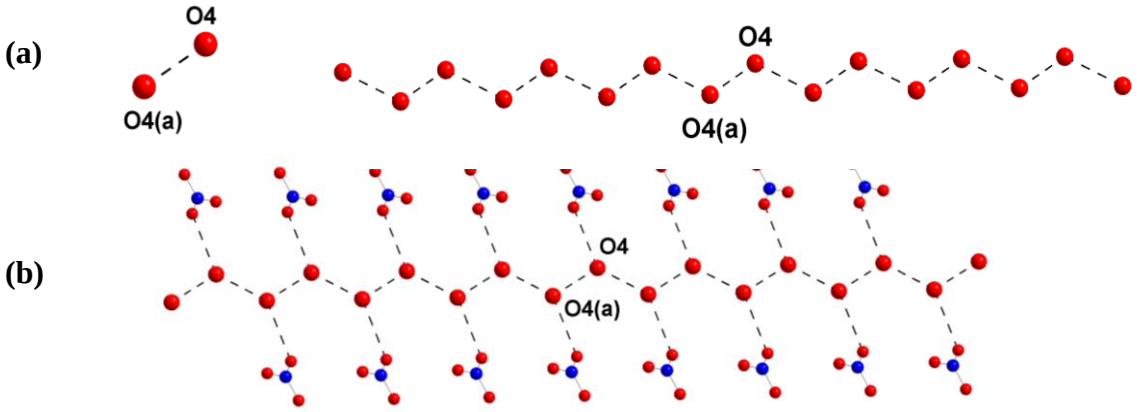


**Figure 5.5. (a)** left**:** Supramolecular water dimer and right: its one-dimensional chain-like arrangement formed from hydrogen bonding interactions of O4 and O4(a), that are related by a symmetry operation: a, 2-x, 1-y, -z.(b) Extended water structure formed from the solvent water molecule (O4), showing its hydrogen bonding interactions with its surrounding nitrate anions.

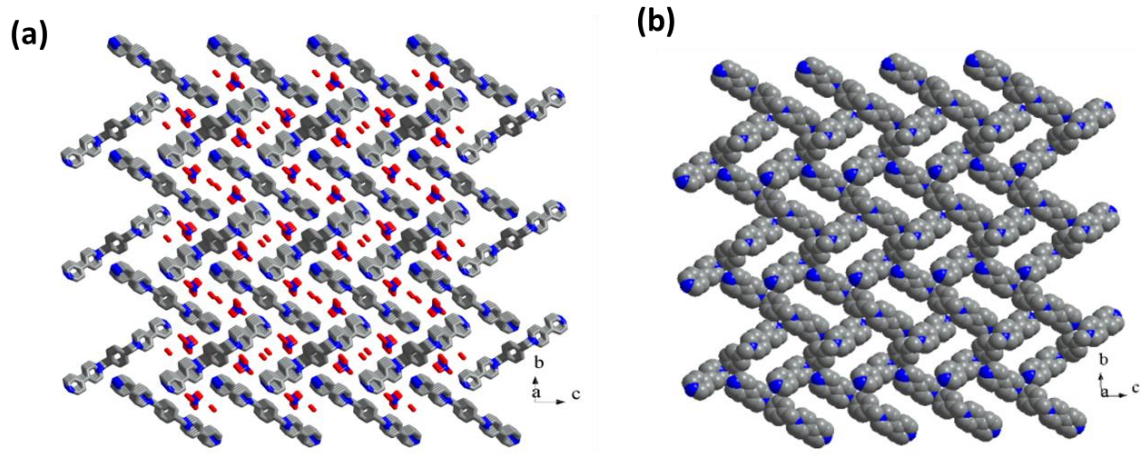


**Figure 5.6. (a)** Packing diagram consisting of the dication $[C_{28}H_{24}N_4]^{2+}$, $NO_3^-$ anion and crystal water molecules in **2·2H$_2$O**. Hydrogen atoms are not shown for clarity. **(b)** View

(face filling representation) of the molecular packing of $[C_{28}H_{24}N_4]^{2+}$ cations in the $[C_{28}H_{24}N_4][NO_3]_2 \cdot 2H_2O$ (**2·2H$_2$O**) (3×3) cells. Color code: N, blue; C, gray; O, red. The hydrogen atoms, nitrate anions and water molecules are not shown for clarity

**Organic receptor $[C_{28}H_{24}N_4]^{2+}$ (c) take up its usual anti-conformation in compound 2·2H$_2$O (nitrate salt) and is stabilized in an unusual intermediate-conformation in compound 1·(1,4-dioxane)) ($PF_6$ salt)! Why is it so? A supramolecular analysis from respective crystal structures.**

The usual energetically favored conformation of the cationic receptor $[C_{28}H_{24}N_4]^{2+}$ (**c**) is *anti*, observed in the crystal structure of compound $[C_{28}H_{24}N_4](NO_3)_2 \cdot 2H_2O$ (**2·2H$_2$O**). The deviation from this usual *anti*-conformation of **c** can be explained by considering supramolecular hydrogen bonding interactions of this dication (**c**) with its surrounding anions ($PF_6^-$ anion in case of compound **1·(1,4-dioxane))** and $NO_3^-$ anion in the case of compound **2·2H$_2$O).** The supramolecular hydrogen bonding interactions around the cationic receptor (**c**) can be 'balanced' as well as 'unbalanced'. The receptor **c** is flexible and it can undergo conformational change from *anti* (Scheme 5.1, right) to an *intermediate* (Scheme 1, middle) through syn (Scheme 5.1, left). However, this movement (conformational change) can be restricted by the number of supramolecular interactions with its surrounding anions. As shown in Figure 5.7(a), there are un-balanced supramolecular H-bonding interactions around the di-cation **c**; the unbalanced supramolecular interactions mean un-equivalent interactions with respect to the central part of the molecule. This di-cation has two bipyridine side arms with respect to the central phenylene ring: one side arm is involved with three C–H···F hydrogen bonds, in which the bipyridine ring of the side arm has only one C–H···F contact. On the other hand, in the other side arm, both bipyridine rings are involved in four C–H···F hydrogen bonds (Figure 5.7(a)). These un-equivalent supramolecular hydrogen bonding interactions (one side bipyridine ring with one H-bond and the other side bipyridine ring with four H-bonds), called unbalanced supramolecular interactions, around **c** enable this system to adopt an unusual intermediate conformation (Scheme 5.1, middle). The supramolecular hydrogen bonding interactions around **c** in compound $[C_{28}H_{24}N_4](NO_3)_2 \cdot 2H_2O$ (**2·2H$_2$O**) is shown in Figure 5.7(b). In the crystal structure of compound **2·2H$_2$O**, there are

balanced/equivalent C–H···O hydrogen bonding interactions around **c** with respect to the central phenylene ring (Figure 7(b)). Both side arms of **c** are hydrogen bonded with its surrounding $NO_3^-$ anions in such a way that hydrogen bonding force of one arm would cancel that of other arm. Thus there is an equivalent force along all the sides of cationic receptor $[C_{28}H_{24}N_4]^{2+}$ (**c**), which implies that there is no more distortion from its usual *anti*-conformation. This justifies the *anti*-conformation of **c** in compound **2·2H$_2$O**. The *anti*-conformation of **c** in compound **2·2H$_2$O** and an *intermediate* conformation of **c** in compound **1·(1,4-dioxane))** can also be corroborated by DFT calculations, Hirshfeld surface analysis and 2D finger plots, described in the succeeding sections.

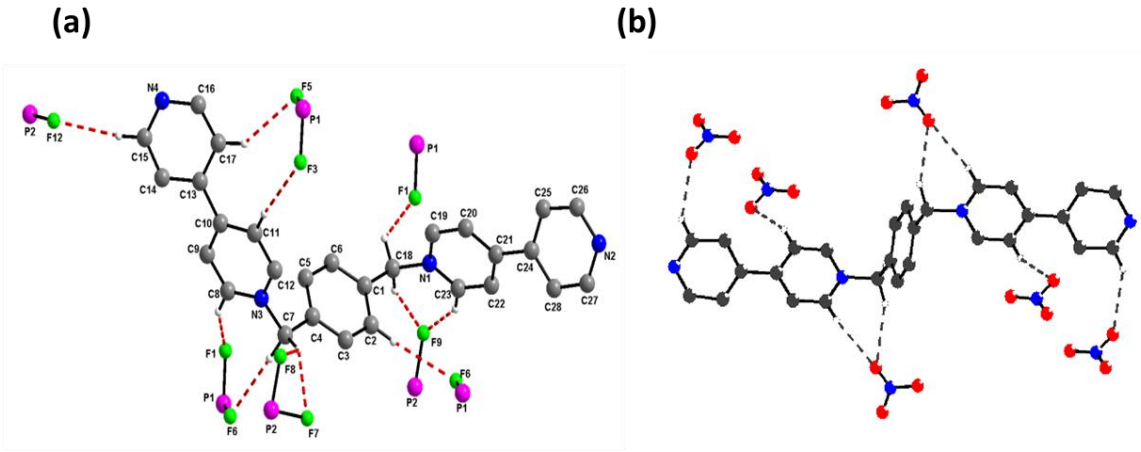


**Figure 5.7**. (a) Unbalanced/unsymmetrical C–H···F hydrogen bonding interactions around the cationic receptor $[C_{28}H_{24}N_4]^{2+}$, observed in the crystal structure of compound $[C_{28}H_{24}N_4](PF_6)_2$·(1,4-dioxane) (**1·(1,4-dioxane)**. (b) Balanced/symmetrical C–H···O hydrogen bonding interactions around $C_{28}H_{24}N_4]^{2+}$, found in the crystal of compound $[C_{28}H_{24}N_4](NO_3)_2$·2H$_2$O (**2·2H$_2$O**)

## Crystal structure description of complex 1

The single crystals are crystallized in the monoclinic system with space group *P2$_1$/c*. A thermal ellipsoidal plot of complex **1** with non-hydrogen atom labeling is presented in Figure 5.7(c).

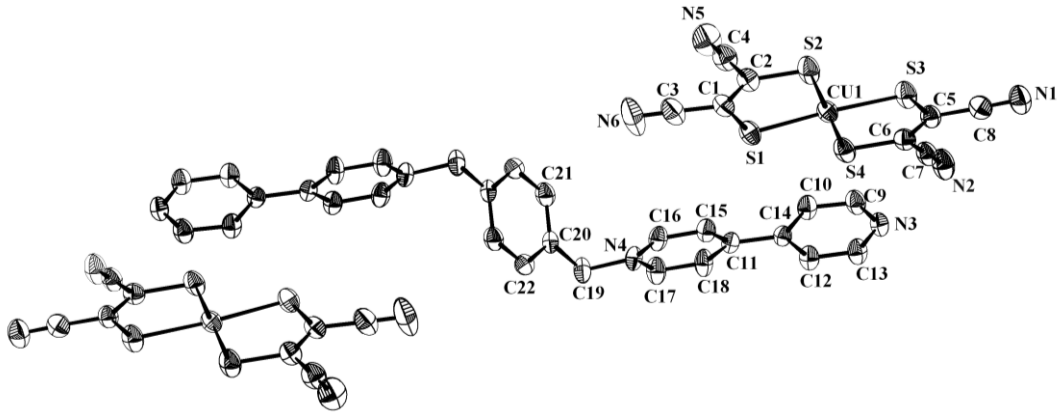


**Figure 5.7.** (c) Thermal ellipsoidal plot of $[C_{28}H_{26}N_4][Cu(mnt)_2]_2$ in $[C_{28}H_{26}N_4][Cu(mnt)_2]_2 \cdot 4DMF$ (**1**). Hydrogen atoms and solvent molecules are not shown for clarity.

### 5.3.4. Hirshfeld surface analysis

The hydrogen-bonding supramolecular interactions around the cationic receptor $[C_{28}H_{24}N_4]^{2+}$ (**c**) with surrounding associated anions are further analyzed with the Hirshfeld Surfaces (HSs) and 2D fingerprint plots (FPs), which are generated by using the software Crystal explorer 3.1.[24-25] based on the pertinent CIF files. Hirshfeld surfaces mapped with different properties e.g., $d_e$, $d_{norm}$, shape index, curvedness, have been proven to be an useful visualization tool for the analysis of supramolecular intermolecular interactions and crystal packing behavior of molecules.[26-27] The 3D Hirshfeld surfaces offer more insight into long- and short-range interactions, experienced by the relevant molecules, and 2D finger plots, derived from the HSs provide the nature, type and relative contribution of the intermolecular interactions. The HSs of the present cationic receptor $[C_{28}H_{24}N_4]^{2+}$ (**c**) experiences unbalanced

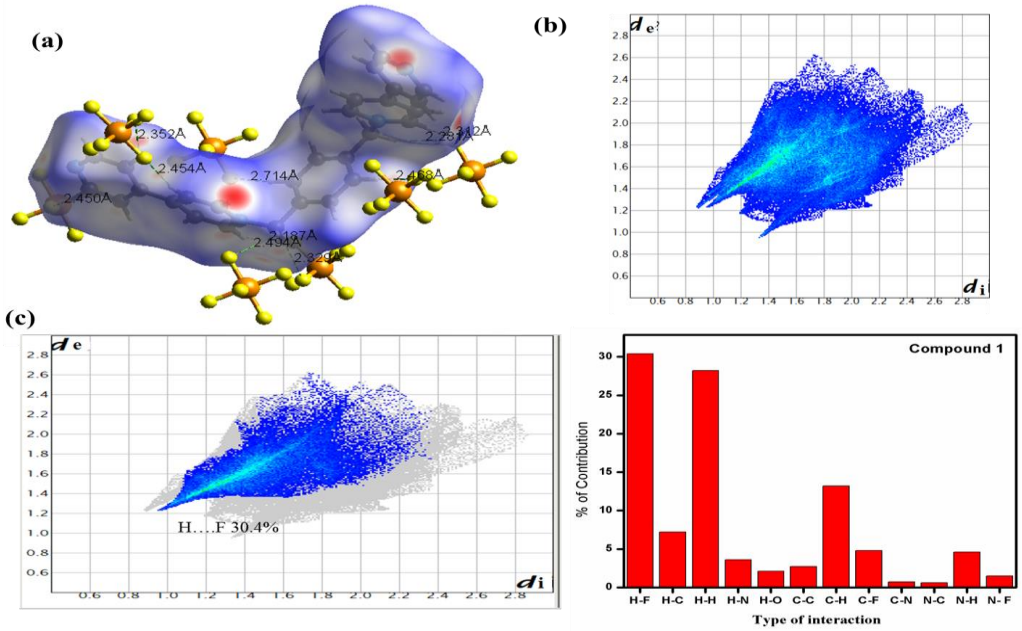


**Figure 5.8** Hirshfeld surfaces mapped with **(a)** $d_{norm}$ ranging from –0.376 (red) to 1.441 (blue), (b) 2D finger print plots with $d_i$ and $d_e$ ranging from 1.0 to 2.8 Å, (c) H···F interactions (left) and percentage contribution of all other interactions around the cation (right) in compound **1**.

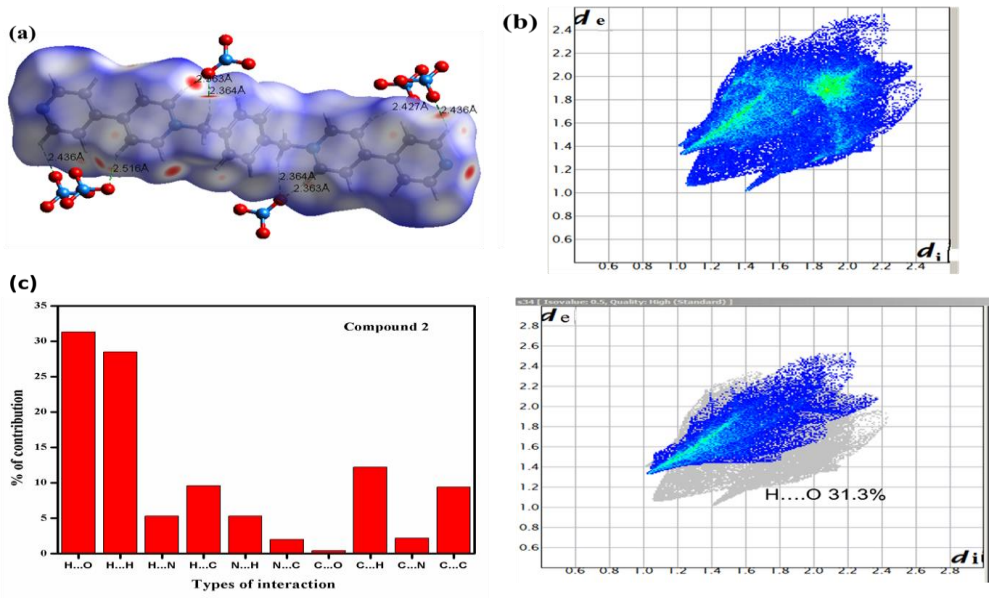


**Figure 5.9** Hirshfeld surfaces mapped with (a) $d_{norm}$ ranging from -0.179 (red) to 1.360 (blue), (b) 2D finger print plots with $d_i$ and $d_e$ ranging from 1.0 to 2.8 A°, (c) percentage of contributions from all other interactions around the cation (left ) and H···O interactions (right) in compound 2**.**

and balanced hydrogen bonding interactions with $PF_6^-$ and $NO_3^-$ anions in compound **1** and compound **2** respectively, that have been mapped over $d_{norm}$ (–0.3 to 1.45 Å in compound **1** and –0.1 to 1.4 Å in compound **2** as shown in Figures 5.8 and 5. 9 respectively. All are the deep red spots, seen in the $d_{norm}$ surface, represent the interactions, whereas the blue spots indicate the areas without close contacts. The intensity of the red spots on the Hirshfeld Surfaces of the cationic receptor **c** in compounds **1** and **2** clearly indicate that it has been experiencing unbalanced and balanced hydrogen bonding inteactions with $PF_6^-$ and $NO_3^-$ anions respectively (compare Figures 5.8a and 5.9a respectively). Among noncovalent interactions, experienced by the cationic receptor **c** in compound $[C_{28}H_{24}N_4](PF_6)_2$·(1,4-dioxane) (**1**), contribution from H···F interactions, which is nearly 30.4% (Figure 5.8c). The relative contributions from other different interactions are calculated and given in Figure 5.8c (right). In the case of $[C_{28}H_{24}N_4](NO_3)_2·2H_2O$ (**2**), and dominating H···O (basically C–H···O hydrogen bonds) and H···H interactions are nearly 25.2% and 28.5% respectively among all other interactions as shown in Figure 5.9c (left).

### 5.3.4. Theoretical Calculations

Computational simulations of the different conformers of cationic receptor **c**, compound **1** and compound 2 were performed with density functional theory (DFT) as implemented in Gaussian 09[28] suite programming package. Computational data evaluation through out the present study were performed with B3LYP hybrid functional,[29-33] which includes Hartree-Fock (HF) exchange as well as DFT exchange correlations. The non-local correlations part is taken care by Lee, Yang and Parr (LYP) functional. All calculations were performed using Pople's 6-31+G(d,p) basis set. The calculations of minimum energy conformers of the cationic receptor **c**, compound **1** and compound **2** were confirmed by subsequent frequency calculations of the optimized geometry at the ground state of the respective conformers. We note that no imaginary frequency was found at the optimized geometry of the conformers.

Natural bond orbital (NBO) analysis was performed to find out the different intra molecular interactions in cationic receptor **c**, compound 1·(1,4-dioxane)) and compound 2·2H2O. The possible interaction between the filled donor orbital (i) and vaccent acceptor

orbital (j) was accounted in the NBO analysis. The stabilization energy of the donor-acceptor interaction [$E^{(2)}(i,j)$] was calculated by second-order perturbation theory. The stabilization energy [$E^{(2)}(i,j)$] associated with the electron delocalization between the donor (i) and acceptor (j) orbitals can be expressed as:

$$E^{(2)}(i,j) = q_i \frac{[F(i,j)]^2}{E_j - E_i} \quad \textbf{(1)}$$

Where, $q_i$ is the orbital occupancy, $E_i$, $E_j$ are diagonal elements and $F_{i,j}$ are the off-diagonal elements of the NBO Fock matrix.

Equilibrium constant (K) between the different conformers of cationic receptor **c** and compound 1 were calculated by considering the ratio of number of reactant (r, more stable conformer) and product (p, less stable conformer) molecules at equilibrium.[29-33] The ratio of r and p can be expressed as:

$$\frac{N_p}{N_r} = \left(\frac{q_p}{q_r}\right) e^{-\frac{\Delta E}{RT}} \quad \textbf{(2)}$$

Where, $N_p$, $N_r$ are the number of product and reactant molecules at equilibrium. The partition functions of the product and reactant are designated as $q_p$, $q_r$, respectively. $\Delta E$ is the total energy difference between the reactant and product and R is the universal gas constant. T represents the temperature in Kelvin. So the equilibrium constant of these conformers can be expressed as:

$$K = \left(\frac{q_p}{q_r}\right) e^{-\frac{\Delta E}{RT}} \quad \textbf{(3)}$$

or,

$$K = \left(\frac{q_p^{vib} q_p^{rot}}{q_r^{vib} q_r^{rot}}\right) e^{-\frac{\Delta E}{RT}} \quad \textbf{(4)}$$

Where $q_p^{vib}$, $q_p^{rot}$, $q_r^{vib}$ and $q_r^{rot}$ are the vibrational and rotational partition functions of the product and reactant, respectively. The translational partition functions of reactant and product are equal and hence cancel out. The electronic ground states of product and reactant are non-degenerate; hence electronic partition function is unity. To validate the above Eq. (4), we calculated the equilibrium constants (K) between cis-2-butene and trans-2-butene, conformers of 2-butene at different temperatures and compared with the available experimental values.[34]

**Computational studies on different conformers of cationic receptor $[C_{28}H_{24}N_4]^{2+}$ (c), compound $[C_{28}H_{24}N_4](PF_6)_2$ (1), and compound $[C_{28}H_{24}N_4](NO_3)_2$ (2).**

In continuation of experimental work on cationic receptor **c**, we also performed the theoretical calculations to find out its conformational structures as such **c** and in compounds **1** and **2** including the stability of those conformers in gas phase. It is found that its *anti*-conformer ($E_{elec}$ = –1299.97188 a.u.) is more stable by ~1.65 kcal/mol than its *syn* conformer ($E_{elec}$ = –1299.96926 a.u.). The atom numbering is shown to the respective figures to facilitate the discussion. The conformers of the compounds and the atom numbering are made by GaussView5 software.[35] The structures of the other conformers of **c** around the 1N-24C-52C-29N dihedral angle are shown in Figure 5.10. The energy profile diagram corresponding to these different dihedral angles is shown in Figure 11. The structures of different conformers are optimized at the interval of 20° dihedral angle. It is found that *anti*-conformer with 1N-24C-52C-29N dihedral angle of –180° is the most stable conformer than the other conformers, whereas *syn* conformer is the least stable conformer. Energy of the intermediate conformers rises very steeply between the –240° to –120° 1N-24C-52C-29N dihedral angle, whereas the steepness of the curve decreases after that (cf. Figure 11). Analysis of the energy profile diagram (cf. Figure 5.11) provides the energy difference between the most stable and least stable structure, which is ~3 kcal/mol. Thus, this cationic receptor $[C_{28}H_{24}N_4]^{2+}$ (**c**) is flexible to form ion pair complexes with diverse anions in a wide range of 1N-24C-52C-29N dihedral angles. We have chosen two different anions $PF_6^-$ and $NO_3^-$ in this study to obtain the ion pair compounds $[C_{28}H_{24}N_4](PF_6)_2]$ (**1**) and $[C_{28}H_{24}N_4](NO_3)_2]$ (**2**) respectively; the preferable conformations of **c** (cationic receptor) in presence $PF_6^-$ anion (compound **1**) and $NO_3^-$ anion (compound **2**) are discussed here. It is found that the compound **2** always prefers to form an *anti*-conformation of **c** with 1N-24C-52C-29N dihedral angle of ~167°. But in the case of compound **1** both *anti* (with1N-24C-52C-29N dihedral angle of ~180°) and *syn* (1N-24C-52C-29N

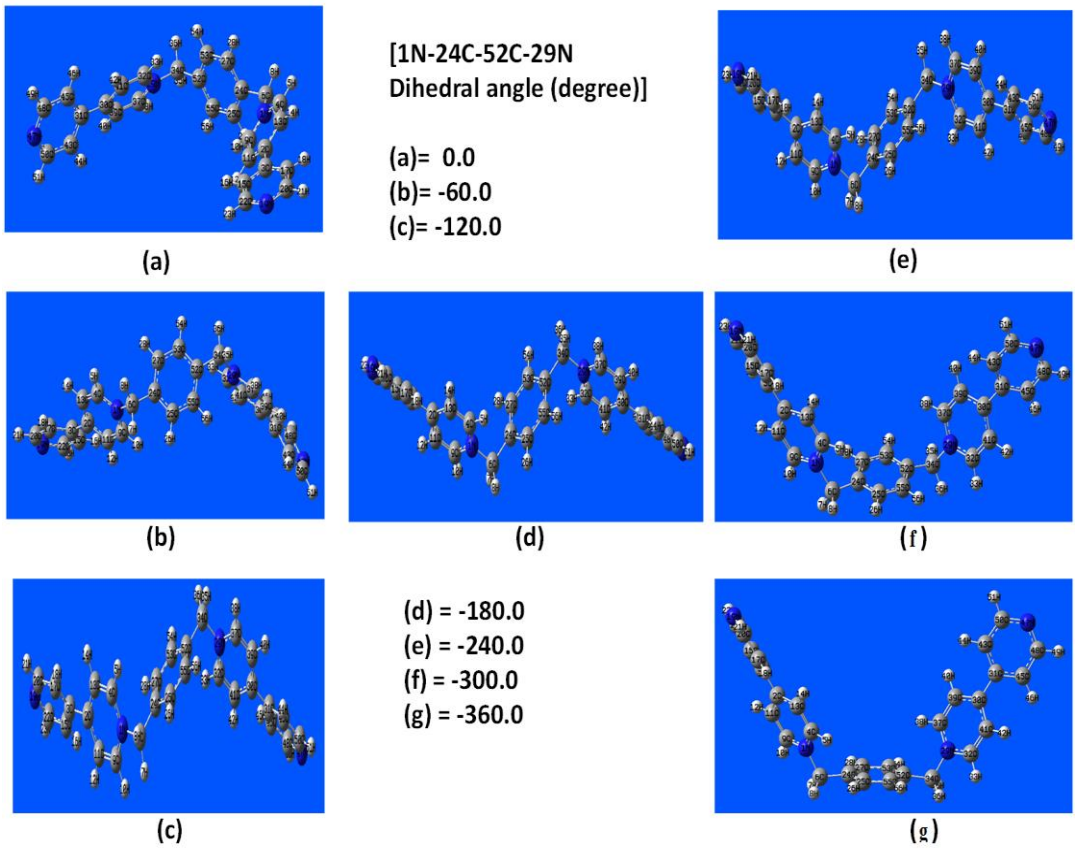


**Figure 5.10** Energy minimized structures of different conformers of cationic receptor **c**.

dihedral angle of ~8$^{o}$) conformers of **c** are formed with different stabilization energy. The optimized structures of these preferred conformers in compound **2** and in compound **1** with the H-bond indication are shown in panels (a) – (f) of Figure 12. Panel (a) is the *anti* conformer of **c** in compound **2** and panels (b) – (f) are different intermediate conformers of **c** in compound 1. The stabilization energy of the *anti*-conformer of compound 2 is ~229 kcal/mol, whereas the same for the *anti*- and *syn*-conformers of compound **1** are ~215 kcal/mol and ~230 kcal/mol, respectively.

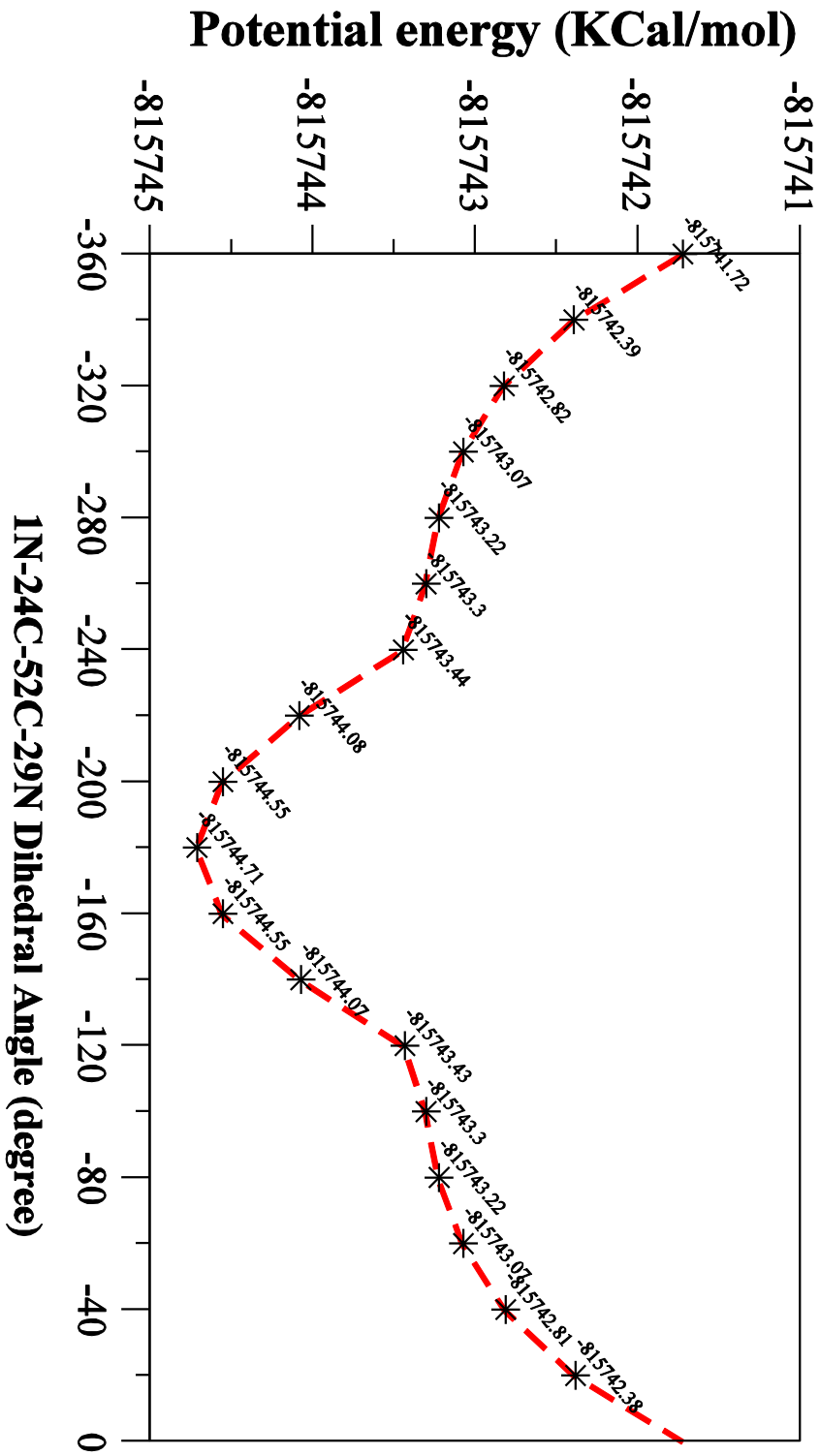


**Figure 5.11.** Potential energy analysis at different 1N-24C-52C-29N dihedral angles of cationic receptor **c**.

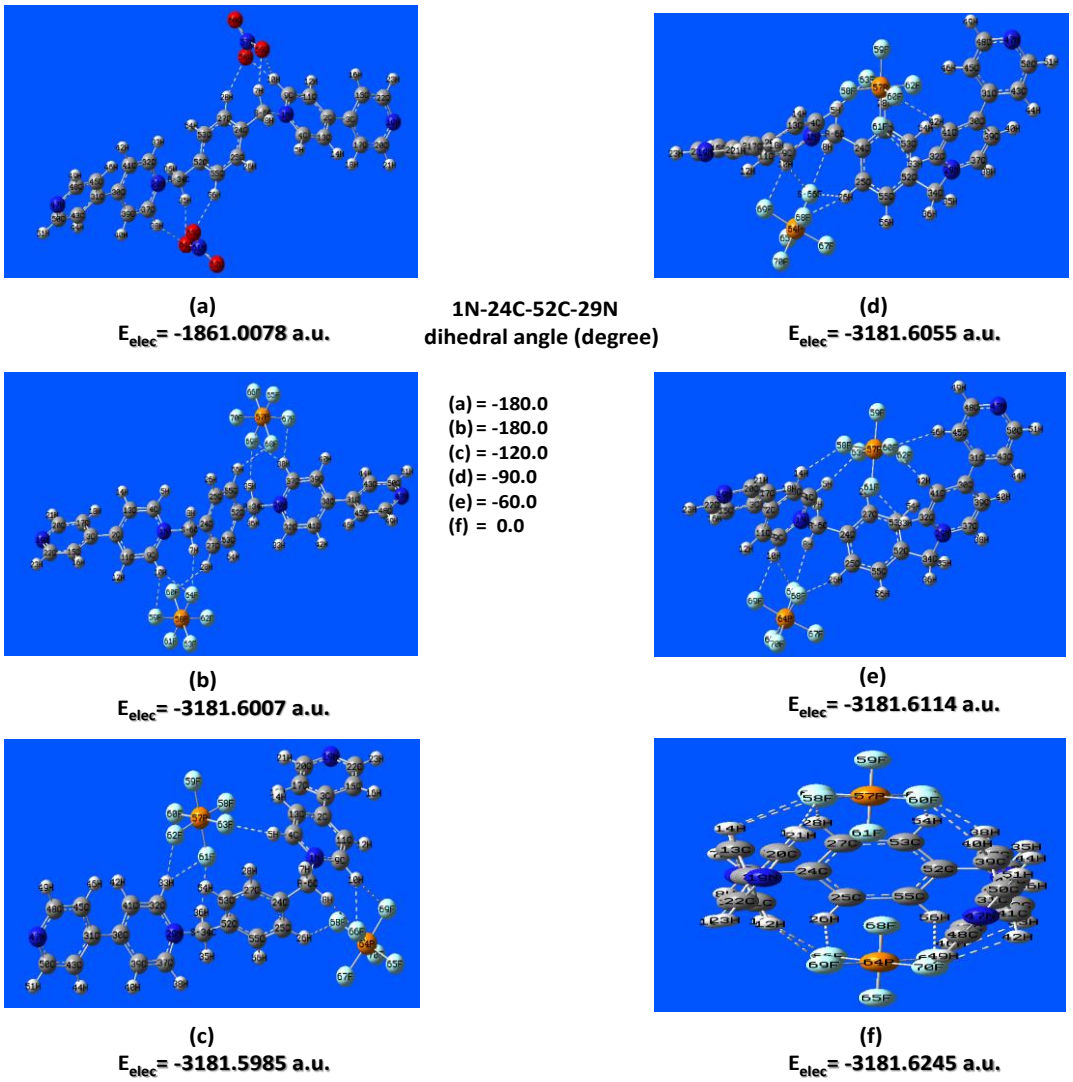


**Figure 5.12.** Energy minimized structures of *anti*-conformer in compound **2** (panel (a)) and various conformers in compound **1**. (panels (b) – (f)).

Thus, the calculations of stabilization energy indicate that the *syn* conformer of compound 1. is more preferable than its *anti*-conformer. The stabilization energies of the intermediate conformers of **c** in compound 1 are also calculated to obtain more detailed conformational analysis of compound 1.

The calculated stabilization energies of the intermediates with 1N-24C-52C-29N dihedral angles of –120°, –90° and –60° are ~214 kcal/mol, ~215 kcal/mol, ~222 kcal/mol respectively. The optimized structures of these intermediates with H-bond indication are shown in panels (c), (d) and (e) of Figure 5.12, respectively. A graphical representation of

the stabilization energies of various conformers of **c** in compound 1 with different 1N-24C-52C-29N dihedral angles is shown in Figure 5.13. It is seen from Figure 5.13 that the stabilization energy of the conformers is decreased in comparison to *anti*-conformer ($-180^o$) to $-120^o$ ($-240^o$) 1N-24C-52C-29N dihedral angle. Whereas an increment of stabilization energy is observed in different intermediate conformers in compound 1 in the range of $-100^o$ to $0^o$ 1N-24C-52C-29N dihedral angle. It is noted that the stabilization energies of the conformers of Figure 13 should be differed from the actual stabilization energies calculated for -180˚, -120˚, -90˚, -60˚ and 0˚ 1N-24C-52C-29N dihedral angles, as the parameter 1N-24C-52C-29N dihedral angle of these conformers (cf. Figure 5.13) is not optimized. The above discussion on stabilization energies of different conformers of **c** in compound **1** indicates that the energy difference between the different conformers in the $-100^o$ to $0^o$ 1N-24C-52C-29N dihedral angle range is a small amount. Thus according to this calculation, the anion $PF_6^-$ prefers to form the ion pair complex either with *syn* conformer of **c** or with an intermediate conformer of **c** (cationic receptor).

The HOMO and LUMO diagrams of the conformers of cationic receptor **c**, compound **1** and compound **2** are shown in Figure 5.14 [ panels (a) and (b) for cationic receptor **c**; panel (c) for compound **2**; panels (d) and (e) for compound **1**). Figure 5.14 shows that the HOMOs of *syn*-cationic receptor as such (Figure 14a), *anti*-cationic receptor as such (Figure 5.14b), compound **2** (Figure 5.14c), *anti*-conformer of compound **1** (Figure 5.14d) and *syn*-conformer of compound **1** (Figure 5.14e) are stabilized by ~75, ~73, ~47, ~95 and ~97 kcal/mol, respectively compared to their respective LUMOs. These data indicate that the HOMO-LUMO stabilization is increased during the ion pair complex formation of cationic receptor (**c**) with $PF_6^-$ anion, whereas the same is decreased during the ion pair complex formation of cationic receptor (**c**) with $NO_3^-$ anion.

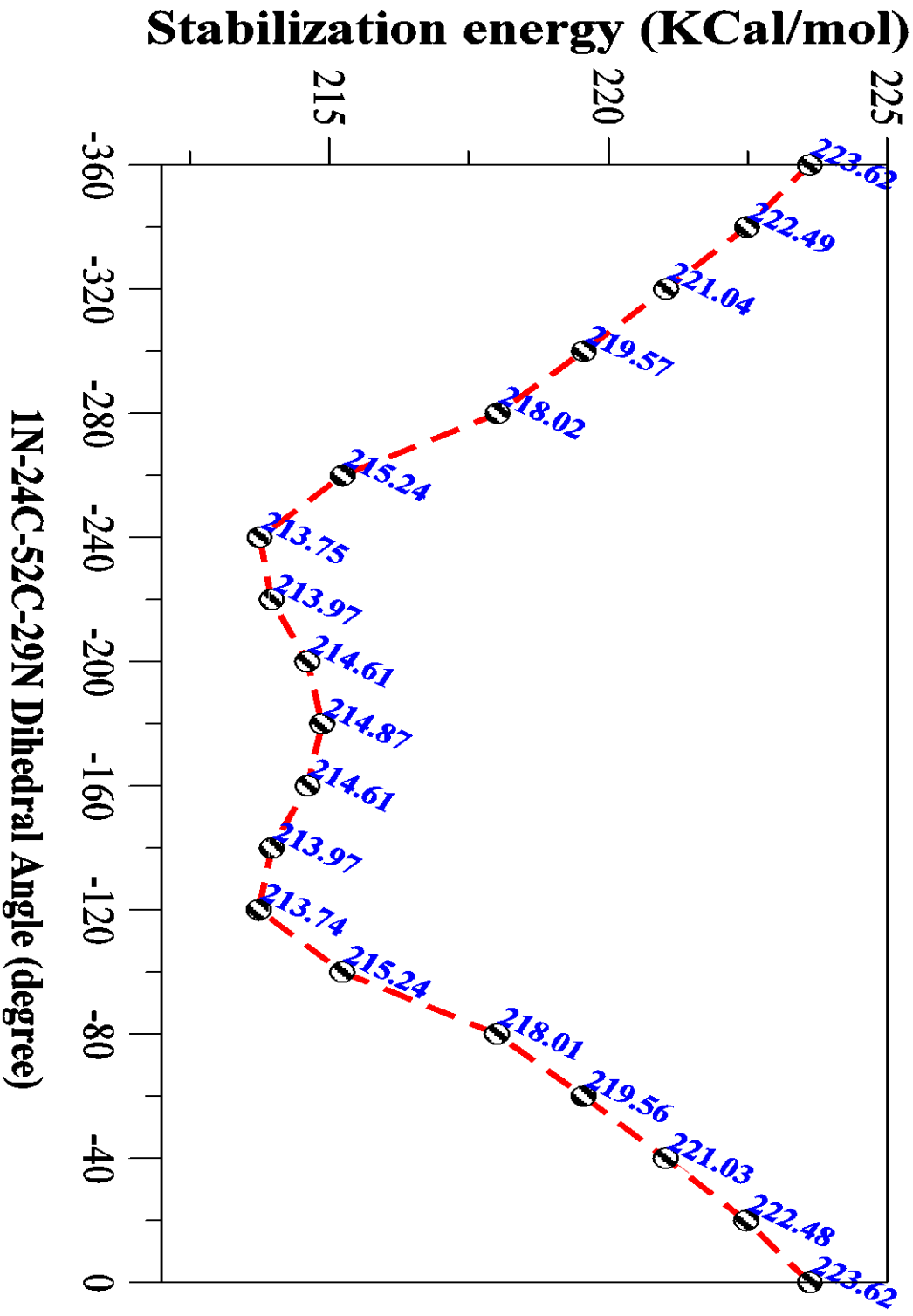


**Figure 5.13.** A diagram of stabilization energies at various 1N-24C-52C-29N dihedral angles **c** in compound **1.**

**Natural bond orbital (NBO) analysis.** In order to have more insight into the stabilization of compounds **1** and **2** with respect to the conformations of receptor cation **c**, we

performed the NBO analysis of the different conformers of these compounds. The results of the donor-acceptor interactions of different conformers of compound **1** and compound **2** are given in Table 6. The donor orbital (*i*), acceptor orbital (*j*), calculated second-order interaction energies between the donor-acceptor orbitals [$E^2$ (*i*,*j*)] and H-bond distances in compound **2** and that in different conformers of compound **1** are given in this table. NBO analysis of compound **2** indicates that ~ 60 kcal/mol stabilization energy is acquired due to the H-bond formation between the oxygen (O) lone pairs (LP) and σ* C–H bonds. It is found that both the $NO_3^-$ anions interact symmetrically through H-bonds with the two bipyridine sides of the cationic receptor **c** (Figure 5.12a; see also Figure 5.7b, the experimental crystallographic evidence). That is why, **c** in compound **2** prefers *anti* conformation. A minute inspection of the Figure 5.12a and its NBO analysis indicate that the H-bond interaction between LP of 64 O and σ* of 37C–38H on the one bipyridine side of the cationic receptor (**c**) stabilizes the compound **2** by ~14 kcal/mol with 1.943 Å H-bond distance. On the other hand, H-bond between LP of 58 O and σ* of 9C–10H on the other bipyridine side of the cationic receptor (**c**) gives the compound **2** more stability by ~ 21 kcal/mol with 1.833 Å H-bond distance. These two marginally different symmetric H-bonding interactions of the two opposite bipyridine sides of the cationic receptor (**c**) makes the compound **2** somewhat different orientation from the actual *anti*-conformation. Thus, the compound **2** prefers a predominantly *anti*-orientation with 1N-24C-52C-29N dihedral angle of ~167$^o$ (not exactly 180$^o$) as shown in Figure 5.12a. On the other hand, the different conformational orientations with 1N-24C-52C-29N dihedral angles of -180$^o$, -120$^o$, -90$^o$, -60$^o$ and -8$^o$ of compound **1** show ~22, ~26, ~32, ~36 and ~32 kcal/mol stability, respectively, on H-bonding interactions between the LPs of different F atoms and different σ* C–H bonds in compound **1**. Therefore, this result (consistent with energy minimized calculations, *vide supra*) also suggests that $PF_6^-$ anion prefers to form an ion pair complex either with intermediate (-90$^o$, -60$^o$) or *syn* orientation (-8$^o$) of the cationic receptor **c**. A symmetric H-bond formation around **c** with respect to its two bipyridine sides is observed (Figure 5.12b). This can be also encountered from the data given in Table 6. The H-bonding interaction between the LP of 64F and σ* 9C–10H bond on the one bipyridine side and the H-bond between LP of 69F σ* 37C–38H bond on the other bipyridine side provide similar ~6 kcal/mol of stabilization. Similarly, the LP of 59F and σ* 9C–10H bond on the one bipyridine side and the LP of 67F σ* 37C–38H bond on the other bipyridine side provide similar ~3 kcal/mol of stabilization. These symmetric H-

bonding interactions give the proper *anti*-orientation conformer of compound **1** as shown in Figure 5.12b. This type of symmetric H-bonding interactions are absent in other conformers of compound **1** as shown in Figures 5.12c, 5.12d and 5.12e. In the case of *syn* conformer of compound **1** (Figure 5.12f), an unbalanced symmetric H-bonding interaction is observed between the LP of 62 F and σ* of 37C–38H bond and LP of 66 F and σ* of 9C–10H bond. Both the H-bonding interaction stabilize the molecule by ~5 kcal/mol and has the bond distance of 2.18 A˚ . The same is observed in the H-bond, initiated by LPs of 58F, 70F, 60F and 69F atoms. These are the forces behind the stability and *syn* orientation of the conformer of compound **1** (Figure 5.12f). The NBO analysis shows that the overall H-bonding stability is highest in the conformer of compound **1** with the 1N-24C-52C-29N dihedral of -60$^{o}$, an intermediate one (not -8$^{o}$, *syn* conformer). Thus, this study also indicates that $PF_6^-$ anion prefers to form an unusual intermediate conformation of **c** or its syn conformation, whereas $NO_3^-$ anion prefers to form normal *anti* conformation of **c**, cationic receptor.

In order to validate the above discussion, we performed the equilibrium constant (K) calculations between different conformers of cationic receptor **c** and the compound **1** The calculated values of K at different temperature (T, Kelvin) are given in Table 5.7. It is found that *anti* conformer of cationic receptor **c** is dominant than *syn* conformer of it at the equilibrium in the temperature range of 100-800 K. The percentage of *syn* conformer is increased with the temperature. The *syn* conformer of cationic receptor **c** occupies only 1.16% at the room temperature (300K). Similar analysis of the conformers of compound **1** shows that *syn* conformer is dominant than *anti* conformer at their equilibrium at different temperatures (Table 5.7). Even at room temperature (300K), the conversion of *syn* to *anti* is not expected to be achievable. An increment of this conversion is observed from 650 K temperature. So it is expected that the barrier of *syn-anti* conversion of compound **1** can be overcome at higher temperature. Similar analysis of two intermediate conformers with 1N-24C-52C-29N dihedral angle of -90$^{o}$ and -60$^{o}$ indicates that these two conformers are dominant than *anti*-conformer of compound **1** in the respective equilibrium. The increment of this conversion with temperature is higher than the *syn-anti* conversion of compound **1**. An opposite scenario is observed considering the intermediate conformer with 1N-24C-52C-29N dihedral angle of -120˚ and *anti*-conformer equilibrium of compound **1**. In this case, *anti*-conformer is found as a dominant in the equilibrium. So the calculations of K between different conformers of compound **1** also suggest that the $PF_6^-$ anion prefers to

form complex with cationic receptor **c** at its syn or intermediate (-90˚ and -60˚) orientations.

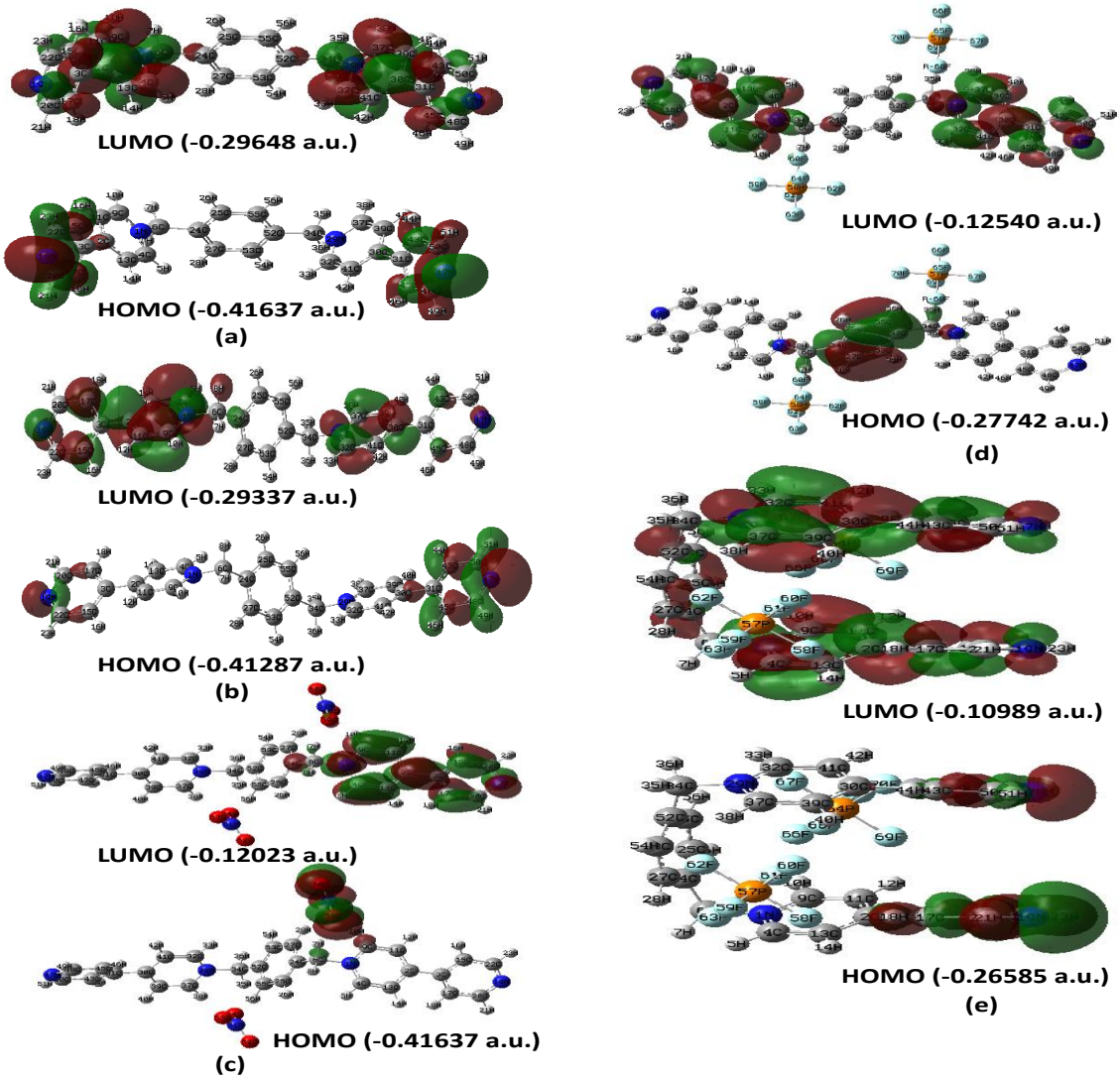


**Figure 5.14.** HOMO-LUMO diagrams of (a) syn- conformer of cationic receptor, (b) anti- conformer of cationic receptor, (c) anti- conformer of compound **2,** (d) anti- conformer of compound **1** and (e) syn- conformer of compound **1.**.

## 5.4. Summary

An organic receptor, 1,1''-1,4-phenylene-bis(methylene)bis-4,4'-bipyridinium cation $[C_{28}H_{24}N_4]^{2+}$ (**c**) was known to be isolated as its *anti*- as well as its *syn*-conformations. In the present work, we have isolated this cationic receptor as an unusual intermediate conformation (neither *syn* nor *anti*) with $PF_6^-$ anion in compound $[C_{28}H_{24}N_4](PF_6)_2 \cdot$(1,4-dioxane) (**1·(1,4-dioxane)**). The energetically favored *anti* conformation of this organic cation has been described in its nitrate salt $[C_{28}H_{24}N_4](NO_3)_2 \cdot 2H_2O$ (**2·2H$_2$O**). Both compounds are characterized by single crystal X-ray crystallography. We have a given rationale of why an atypical intermediate conformer of the title receptor is stabilized with $PF_6^-$ anion and a typical *anti*-form of this receptor is isolated with nitrate anion, with the help of supramolecular hydrogen bonding interactions and Hirshfeld surface analysis.

A detailed theoretical account of the stability of the various conformers of the cationic receptor $[C_{28}H_{24}N_4]^{2+}$ (**c**), compound $[C_{28}H_{24}N_4](PF_6)_2$ (**1**) and compound $[C_{28}H_{24}N_4](NO_3)_2$ (**2**) has been discussed in this study by calculating their electronic stability, HOMO–LUMO stabilization and NBO analysis. Final conclusion of their stability is obtained by calculation of conformational equilibrium constants at different temperatures between the conformers of the cationic receptor **c** and compound **1**. It is found that *anti* form of the cationic receptor **c** is more stable than its syn orientation, whereas, in presence of $PF_6^-$ anion, it prefers *syn* or an intermediate (with 1N-24C-52C-29N dihedral angles of -60$^o$ and -90$^o$) conformers. An opposite scenario of usual *anti* orientation of the cationic recepector **c** with little deviation is observed, when the cationic receptor **c** binds with $NO_3^-$ anion. A symmetric interaction through H-bonds between the two bipyridine sides of the cationic receptor **c** and two $NO_3^-$ anions is the main cause behind the *anti*-orientation of the compound **2**, whereas, an unbalanced symmetric H-bonding interactions between the LP of F atoms ($PF_6^-$ anion) and σ* of C-H bonds (cationic receptor **c**) give the compound **2** unusual *syn* or intermediate orientation. Complex **1** isolated and structurally characterized by single crystal X-ray studies and this ion pair complex obtained in 1:1 ration of $[4,4'–H_2bpy]^{2+}$ as a cation and $[Cu(mnt)_2]^{2-}$ as an anion.

**Table 5.1.** Crystal data and structural refinement parameters for compounds **1·(1,4-dioxane)** and **2·2H$_2$O**

| | **1·(1,4-dioxane)** | **2·2$H_2O$** | **Complex 1** |
|---|---|---|---|
| Empirical formula | $C_{32}H_{32}F_{12}N_4O_2P_2$ | $C_{28}H_{28}N_6O_8$ | $C_{56}H_{54}N_{16}O_4S_8Cu_2$ |
| Formula weight | 794.56 | 576.56 | 1398.71 |
| Temperature (K) | 100(2) K | 298 K | 298(2) |
| Crystal system | triclinic | monoclinic | monoclinic |
| space group | P-1 | P21/n | $P2_1/c$ |
| Z | 2 | 2 | 2 |
| Wavelength(A) | 0.71073 | 0.71073 | 0.71073 |
| a [Å] | 9.2462(7) | 4.5103(9) | 8.8715(4) |
| b [Å] | 11.7988(9) | 19.774(4) | 13.0448(6) |
| c [Å] | 16.7537(13) | 15.054(3) | 28.3836(13) |
| α [º] | 106.49(10) | 90 | 98.1630(10) |
| β [º] | 103.76(10) | 97.786(4) | 90 |
| γ [º] | 98.33(10) | 90 | 90 |
| Volume [$Å^3$] | 1657.3(2) | 1331.2(5) | 3251.5(3) |
| Calculated density ($Mg/m^{-3}$) | 1.592 | 1.428 | 1.429 |
| Reflections collected/ unique | 15442/4749 | 15147/3145 | 37472 / 7862 |
| R(int) | 0.0408 | 0.0604 | 0.0915 |
| F(000) | 812 | 604 | 1440 |
| Max. and min. transmission | 0.985 and 0.954 | 0.956 and 0.989 | 0.935 and 0.976 |
| Theta range for data collection (deg.) | 1.33 to 25.07 | 0.956 to 28.23 | 1.72 to 28.30 |
| Refinement method | Full-matrix least-square on $F^2$ | Full-matrix least-square on $F^2$ | Full-matrix least-square on $F^2$ |
| Data/restrains/parameters | 5829/0/469 | 3145/0/190 | 7862 / 0 / 396 |
| Goodness-of-fit on $F^2$ | 1.198 | 1.003 | 0.875 |
| $R_1/wR_2$ [I>2sigma(I)] | 0.0713/0.1378 | 0.0915/0/0.264 | 0.0431/0.1015 |
| $R_1/WR_2$ (all data) | 0.0900/0.1452 | 0.142/0.304 | 0.0892/0.1119 |
| Largest diff. peak and hole $e.Å^{-3}$ | 0.501 and -0.270 | 0.487 and -0.284 | 0.561/-0.210 |

**Table 5. 2.** Complete list of bond lengths [Å] and angles [deg] for $C_{28}H_{24}N_4](PF_6)_2$·(1,4-dioxane) (**1**)

| | | | |
|---|---|---|---|
| C(7)-N(3) | 1.474(5) | O(1)-C(29)-C(30)#1 | 109.8(3) |
| C(8)-N(3) | 1.343(5) | O(2)-C(31)-C(32)#2 | 111.3(3) |
| C(9)-C(10) | 1.393(5) | C(23)-N(1)-C(19) | 120.6(3) |
| C(11)-C(12) | 1.361(5) | C(19)-N(1)-C(18) | 118.2(3) |
| C(13)-C(17) | 1.193(5) | C(30)-O(1)-C(29) | 108.7(3) |
| C(18)-N(1) | 1.347(4) | F(4)-P(1)-F(2) | 179.85(18) |
| C(26)-N(2) | 1.333(5) | F(7)-P(2)-F(9) | 89.71(13) |
| C(29)-C(30)#1 | 1.492(6) | N(2)-C(26)-C(25) | 123.8(4) |
| C(32)-C(31)#2 | 1.485(6) | N(4)-C(16)-C(17) | 125.0(4) |
| F(1)-P(1) | 1.594(2) | N(1)-C(23)-C(22) | 121.6(3) |

Symmetry transformations used to generate equivalent atoms#1-x+2,-y+1,-z #2 -x+1,-y+1,-z+2.

**Table 5.3.** Geometrical parameters of the C–H···F, C–H···N and C–H···F hydrogen bonds (Å, $^{o}$) involved in supramolecular networks of compounds **1· (1,4-dioxane)** and **2·2H$_2$O**.[a] D=donor; A=acceptor.

| D-H···A | d(D-H) | d(H···A) | d(D···A) | <(DHA) |
|---|---|---|---|---|
| C(22)-H(22)...N(4)#3 | 0.95 | 2.42 | 3.308(5) | 155.9 |
| C(28)-H(28)...N(4)#3 | 0.95 | 2.65 | 3.482(5) | 146.3 |
| C(9)-H(9)...N(2)#4 | 0.95 | 2.42 | 3.302(5) | 154 |
| C(8)-H(8)...F(1)#5 | 0.95 | 2.3 | 3.156(4) | 149.4 |
| C(7)-H(7A)...F(6)#5 | 0.99 | 2.42 | 3.411(4) | 178.2 |
| C(7)-H(7B)...F(7)#6 | 0.99 | 2.54 | 3.422(4) | 149.1 |
| C(2)-H(2)...F(6)#7 | 0.95 | 2.59 | 3.509(4) | 161.7 |
| C(23)-H(23)...F(9)#8 | 0.95 | 2.43 | 3.286(4) | 150.5 |
| C(18)-H(18A)...F(9)#8 | 0.99 | 2.37 | 3.304(4) | 157.8 |
| C(11)-H(11)...F(3) | 0.95 | 2.58 | 3.524(4) | 170.3 |
| C(17)-H(17)...F(5) | 0.95 | 2.46 | 3.266(4) | 143 |
| C(15)-H(15)...F(12)#9 | 0.95 | 2.58 | 3.501(4) | 164 |

Symmetry transformations used to generate equivalent atoms: #3 x-1,y,z-1 #4 x+1,y+1,z+1 #5 x,y+1,z #6 -x,-y+1,-z+1 #7 -x,-y+1,-z #8 x,y+1,z-1 #9 x+1,y+1,z

**Table 5.4.** Complete list of bond lengths [Å] and angles [deg] for $[C_{28}H_{24}N_4](NO_3)_2 \cdot 2H_2O$ (**2**)

| | | | |
|---|---|---|---|
| N(2)-C(10) | 1.329(4) | C(10)-N(2)-C(9) | 119.9(2) |
| N(2)-C(9) | 1.351(4) | N(2)-C(10)-C(8) | 121.4(3) |
| N(2)-C(11) | 1.497(3) | N(2)-C(9)-C(7) | 121.1(3) |
| C(6)-C(8) | 1.390(4) | C(1)-N(1)-C(2) | 115.1(3) |
| C(5)-C(4) | 1.138(5) | N(1)-C(2)-C(4) | 125.1(4) |
| N(1)-C(1) | 1.315(5) | O(3)-N(3)-O(2) | 120.6(5) |
| N(3)-O(3) | 1.152(5) | N(1)-C(1)-C(3) | 124.9(4) |
| N(3)-O(1) | 1.181(5) | C(12)-C(13)-C(14)#1 | 121.4(3) |
| C(14)-C(13)#1 | 1.397(4) | N(1)-C(1)-C(3) | 124.9(4) |
| C(12)-C(14) | 1.384(4) | C(12)-C(14)-C(13)#1 | 119.6(3) |

Symmetry transformations used to generate equivalent atoms:#1-x+1,-y+1,-z+1

**Table 5.5**. Hydrogen bonds for compound 2 [ Å and °].

| D–H···A | d(D···H) | d(H···A) | d(D···A) | <(DHA) |
|---|---|---|---|---|
| O(4)-H(30)...O(1) | 0.98 | 2.41 | 3.199 | 136 |
| O(4)-H(30)...O(2) | 0.98 | 1.97 | 2.924 | 162 |
| C(1)-H(1)...O(3)#1 | 1.08 | 2.44 | 3.202 | 127 |
| C(7)-H(7)...O(3) | 1.08 | 2.44 | 3.412 | 149 |
| C(9)-H(9)...N(1)#2 | 1.08 | 2.41 | 3.443 | 158 |
| C(10)-H(10)...O(2)#3 | 1.08 | 2.37 | 3.218 | 135 |
| C(11)-H(11B)...O(2)#3 | 1.08 | 2.37 | 3.338 | 147 |

Symmetry transformations used to generate equivalent atoms:

#1 -1+x, y, z #2 3/2+x, 1/2-y, 1/2+z #3 3/2-x, 1/2+y, 1/2-z

**Table 5.6**. NBO analysis of some selected bonds of compound **2**, *trans*, intermediates.

(1N-24C-52C-29N= -120˚, -90˚, -60˚) and cis conformers of compound **1**.

| Donor NBO (i) | Acceptor NBO (j) Compound 2 | Stabilization Energy $E^2$ (i,j) (Kcal/mol) | H-bond diatance (Å) |
|---|---|---|---|
| 63 O [LP] | 55C-56H [BD*] | 6.55 | 2.142 |
| 64 O [LP] | 37C-38H [BD*] | 14.41 | 1.943 |
| 64 O [LP] | 34C-35H [BD*] | 7.46 | 2.136 |
| 58 O [LP] | 9C-10H [BD*] | 21.46 | 1.833 |
| 58 O [LP] | 27C-28H [BD*] | 2.99 | 2.184 |
| 59 O [LP] | 6C-7H [BD*] | 5.74 | 1.992 |
| 59 O [LP] | 9C-10H [BD*] | 1.00 | 2.376 |
| **Trans conformer of compound 1** | | | |
| 62 F [LP] | 27C-28H [BD*] | 1.61 | 2.225 |
| 63 F [LP] | 27C-28H [BD*] | 0.06 | 2.582 |
| 64 F [LP] | 9C-10H [BD*] | 6.07 | 2.183 |
| 67 F [LP] | 37C-38H [BD*] | 2.94 | 2.183 |
| 67 F [LP] | 39C-40H [BD*] | 0.12 | 2.804 |
| 68 F [LP] | 55C-56H [BD*] | 3.30 | 2.224 |
| 69 F [LP] | 37C-38H [BD*] | 6.07 | 2.057 |
| 69 F [LP] | 34C-35H [BD*] | 4.88 | 2.143 |
| 69 F [LP] | 55C-56H [BD*] | 0.51 | 2.583 |
| 70 F [LP] | 55C-56H [BD*] | 1.60 | 2.443 |

| | | | |
|---|---|---|---|
| **Intermediate conformer of compound 1** **1N-24C-52C-29N=-120˚** | | | |
| 61 F [LP] | 32C-33H [BD*] | 4.31 | 2.181 |
| 61 F [LP] | 34C-36H [BD*] | 1.99 | 2.255 |
| 62 F [LP] | 32C-33H [BD*] | 3.37 | 2.148 |
| 63 F [LP] | 4C-5H [BD*] | 2.99 | 2.222 |
| 66 F [LP] | 6C-8H [BD*] | 1.94 | 2.148 |
| 66 F [LP] | 9C-10H [BD*] | 5.03 | 2.103 |
| 68 F [LP] | 25C-26H [BD*] | 2.37 | 2.250 |
| 69 F [LP] | 9C-10H [BD*] | 3.62 | 2.164 |
| **Intermediate conformer of compound 1** 1N-24C-52C-29N=-90˚ | | | |
| 60 F [LP] | 41C-42H [BD*] | 3.80 | 2.217 |
| 61 F [LP] | 32C-33H [BD*] | 1.99 | 2.261 |
| 63 F [LP] | 4C-5H [BD*] | 8.13 | 2.060 |
| 66 F [LP] | 6C-8H [BD*] | 3.83 | 2.190 |
| 66 F [LP] | 9C-10H [BD*] | 5.38 | 2.080 |
| 66 F [LP] | 25C-26H [BD*] | 0.97 | 2.486 |
| 68 F [LP] | 25C-26H [BD*] | 4.70 | 2.167 |
| 69 F [LP] | 9C-10H [BD*] | 3.33 | 2.170 |
| **Intermediate conformer of compound 1** **1N-24C-52C-29N=-60˚** | | | |

| | | | |
|---|---|---|---|
| 58 F [LP] | 13C-14H [BD*] | 1.66 | 2.396 |
| 60 F [LP] | 41C-42H [BD*] | 4.50 | 2.162 |
| 60 F [LP] | 45C-46H [BD*] | 2.29 | 2.405 |
| 61 F [LP] | 32C-33H [BD*] | 2.46 | 2.238 |
| 63 F [LP] | 4C-5H [BD*] | 8.06 | 2.059 |
| 66 F [LP] | 9C-10H [BD*] | 5.50 | 2.078 |
| 66 F [LP] | 6C-8H [BD*] | 2.98 | 2.200 |
| 68 F [LP] | 25C-26H [BD*] | 4.56 | 2.174 |
| 69 F [LP] | 9C-10H [BD*] | 3.37 | 2.174 |
| **Cis conformer of compound 1** | | | |

| | | | |
|---|---|---|---|
| 58 F [LP] | 17C-18H [BD*] | 3.75 | 2.273 |
| 58 F [LP] | 13C-14H [BD*] | 1.17 | 2.367 |
| 60 F [LP] | 39C-40H [BD*] | 2.84 | 2.280 |
| 62 F [LP] | 37C-38H [BD*] | 4.96 | 2.176 |
| 62 F [LP] | 53C-54H [BD*] | 1.73 | 2.319 |
| 63 F [LP] | 4C-5H [BD*] | 0.55 | 2.532 |
| 63 F [LP] | 27C-28H [BD*] | 1.23 | 2.461 |
| 66 F [LP] | 9C-10H [BD*] | 4.92 | 2.179 |
| 66 F [LP] | 25C-26H [BD*] | 1.73 | 2.319 |
| 67 F [LP] | 32C-33H [BD*] | 0.53 | 2.545 |
| 67 F [LP] | 55C-56H [BD*] | 1.25 | 2.454 |
| 69 F [LP] | 11C-12H [BD*] | 2.87 | 2.278 |
| 70 F [LP] | 41C-42H [BD*] | 1.17 | 2.366 |
| 70 F [LP] | 45C-46H [BD*] | 3.67 | 2.277 |

**Table 5.7.** Calculated values of equilibrium constants (K) at different temperature (in Kelvin) of different equilibrium exist between the different conformers of cationic receptor **c** and compound **1**.

| Temp (K) | Trans **c**⇌cis **c** | Cis1⇌Trans1 | Intermediate (-60˚)⇌ Trans 1 | Intermediate (-90˚)⇌Trans 1 | Intermediate (-120˚) ⇌Trans1 |
|---|---|---|---|---|---|
| 100 | 0.00004 | 0.00000 | 0.00000 | 0.00000 | - |
| 150 | 0.00071 | 0.00000 | 0.00000 | 0.00031 | 928 |
| 200 | 0.00286 | 0.00000 | 0.00000 | 0.00362 | 269 |
| 250 | 0.00663 | 0.00000 | 0.00003 | 0.01586 | 128 |
| 300 | 0.01160 | 0.00000 | 0.00027 | 0.04232 | 78 |
| 350 | 0.01730 | 000000 | 0.00134 | 0.08510 | 55 |
| 400 | 0.02334 | 0.00001 | 0.00441 | 0.14345 | 42 |
| 450 | 0.02946 | 0.00010 | 0.01113 | 0.21506 | 34 |
| 500 | 0.03548 | 0.00054 | 0.02331 | 0.29707 | 29 |
| 550 | 0.04131 | 0.00214 | 0.04266 | 0.38670 | 26 |
| 600 | 0.04689 | 0.00676 | 0.07057 | 0.48149 | 23 |
| 650 | 0.05219 | 0.01791 | 0.10798 | 0.57941 | 21 |
| 700 | 0.05720 | 0.04127 | 0.15545 | 0.67885 | 19 |
| 750 | 0.06193 | 0.08505 | 0.21313 | 0.77853 | 18 |
| 800 | 0.06638 | 0.16010 | 0.28085 | 0.87752 | 17 |

## 5.5. References

(1) Klärner, F.-G.; Kahlert, B. Molecular Tweezers and Clips as synthetic Receptors. Molecular Recognition and Dynamics in Receptor−Substrate Complexes. *Acc. Chem. Res.* **2003**, *36*, 919-932.

(2) Lehn. J. – M. *Supramolecular Chemistry. Concepts and Perspectives*, VCH, Weinheim, **1995**.

(3) Gallivan, J. P.; Dougherty, D. A. A Computational Study of Cation−π Interactions vs Salt Bridges in Aqueous Media: Implications for Protein Engineering. *J. Am. Chem. Soc.* **2000**, *122*, 870-874.

(4) Prins, L. J.; Reinhoudt, D. N.; Timmerman, P. Noncovalent Synthesis using Hydrogen Bonding. *Angew. Chem. Int. Ed.* **2001**, *40*, 2382-2426.

(5) Sinnokrot, M. O.; Valeev, E. F.; Sherrill, C. D. Estimates of the Ab Initio Limit for π−π Interactions: the Benzene Dimer. *J. Am. Chem. Soc.* **2002**, *124*, 10887-10893.

(6) Sokolov, A. N.; Friščić, T.; MacGillivray, L. R. Enforced Face-to-Face Stacking of Organic Semiconductor Building Blocks within Hydrogen-Bonded Molecular Cocrystals. *J. Am. Chem. Soc.* **2006**, *128*, 2806-2807.

(7) Nohra, B.; Graule, S.; Lescop, C.; Réau, R. Mimicking [2,2]-Paracyclophane Topology: molecular Clips for the Coordination-Driven Cofacial Assembly of π-Conjugated systems. *J. Am. Chem. Soc.* **2006**, *128*, 3520-3521.

(8) Meyer, E. A.; Castellano, R. K.; Diederich, F. Interactions with Aromatic Rings in Chemical and Biological Recognition. *Angew. Chem. Int. Ed.* **2003**, *42*, 1210-1250.

(9) Neelakandan, P. P.; Hariharan, M.; Ramaiah, D. Synthesis of a Novel Cyclic Donor−Acceptor Conjugate for Selective Recognition of ATP. *Org. Lett.* **2005**, *7*, 5765-5768.

(10) Kim, E.-i.; Paliwal, S.; Wilcox, C. S. Measurements of Molecular Electrostatic Field Effects in Edge-to-Face Aromatic Interactions and CH-π Interactions with Implications for Protein Folding and Molecular Recognition. *J. Am. Chem. Soc.* **1998,** *120*, 11192-11193.

(11) Fráusto da Silva. J. J. R.; Williams. R. J. P. *The Biological Chemistry of the Elements, the Inorganic Chemistry of Life,* Oxford University Press, Oxford, **1991**, Chapter 10.

(12) Philp, D.; Stoddart, J. F. Self-Assembly in Natural and Unnatural Systems. *Angew. Chem. Int. Ed. Engl.* **1996**, *35*, 1154-1196.

(13) Rekharsky, M. V.; Inoue, Y. Complexation Thermodynamics of Cyclodextrins. *Chem. Rev.* **1998,** *98*, 1875-1918.

(14) Collet. A.; Dutasta. J. P.; Lozach. B.; Canceill. J. Cyclotriveratrylenes and Cryptophanes :Their Synthesis and Applications to Host-Guest Chemistry and to the Design of New Materials. *Top. Curr. Chem.* **1993**, *165*, 103-129.

(15) Lee, J. W.; Samal, S.; Selvapalam, N.; Kim, H. J.; Kim, K. Cucurbituril homologues and derivatives: new opportunities in supramolecular chemistry. *Acc. Chem. Res.* **2003**, *36*, 621-630.

(16) Warmuth, R.; Yoon, J. Recent Highlights in Hemicarcerand Chemistry. *Acc. Chem. Res.* **2001**, *34*, 95-105.

(17) Corbellini, F.; Mulder, A.; Sartori, A.; Ludden, M. J. W.; Casnati, A.; Ungaro, R.; Huskens, J.; Crego-Calama, M.; Reinhoudt, D. N. Assembly of a Supramolecular Capsule on a Molecular Printboard. *J. Am. Chem. Soc.* **2004**, *126*, 17050-17058.

(18) Harmata. M. In Encyclopedia of Supramolecular Chemistry, Molecular Clefts and Tweezers, Atwood. J. L.; Steed. J. W. Marcel Dekker. Eds. NewYork, **1997**, Vol. 2, pp 887-900.

(19) Klärner, F.-G.; Panitzky, J.; Bläser, D.; Boese, R. Synthesis and supramolecular structures of molecular clips. *Tetrahedron.* **2001**, *57*, 3673-3687.

(20) Bruker. SADABS, SMART, SAINT and SHELXTL, Bruker AXS Inc., Madison, Wisconsin, USA, **2000**.

(21) Sheldrick. G.M.; SHELX-97, Program for Crystal Structure Solution and Analysis, University of Gottingen, Gottingen, Germany, **1997**.

(22) Liu, S.-A.; Kuo, T.-S.; Lee, G.-H.; Shiu, K.-B. Sensitivity in Supramolecular Architectures of Polyaromatic Salts Containing Two Singly-Pimerized Bipyridines. J. Chin. Chem. Soc. **2007**, 54, 607-611.

(23) Madhu, V.; Sabbani, S.; Kishore, R.; Naik, I. K.; Das, S. K. Mechanical motion in the solid state and molecular recognition: reversible cis–trans transformation of an organic receptor in a solid–liquid crystalline state reaction triggered by anion exchange. *CrystEngComm.* **2015,** *17*, 3219-3223.

(24) Brouwer, E. B.; Udachin, K. A.; Enright, G. D.; Ripmeester, J. A. Amine guest size and hydrogen-bonding influence the structures of -butylcalix[4]arene inclusions. *Chem. Commun.* **2000**, 1905-1906.

(25) Wolff. S. K.; Grimwood. D. J.; McKinnon. J. J.; Turner. M. J.; Jayatilaka. D.; and Spackman. M. A. Crystal Explorer 3.1 (**2013**), University of Western Australia, Crawley, Western, Australia, **2005–2013**, http://hirshfeldsurface.net/ CrystalExplorer.

(26) Soman. R.; Sujatha. S.; and Arunkumar. C. Quantitative crystal structure analysis of fluorinated porphyrins. J. Fluorine Chem. **2014**, *163*, 16.

(27) Titi. H. M.; Patra. R.; and Goldberg. I. Exploring Supramolecular Self-Assembly of Tetraarylporphyrins by Halogen Bonding: Crystal Engineering with Diversely Functionalized Six-Coordinate Tin(L)2–Porphyrin Tectons. *Chem. – Eur. J.* **2013**, *19*, 14941.

(28) Frisch, M. J.; Trucks, G. W.; Schlegel, H. B.; Scuseria, G. E.; Robb, M. A.; Cheeseman, J. R.; Scalmani, G.; Barone, V.; Mennucci, B.; Petersson. G. A. *et al.* Gaussian 09, revision B.01; Gaussian, Inc.: Wallingford, CT, **2010**.

(29) Li, P.; Bu, Y.; Ai, H. Density Functional Studies on Conformational Behaviors of Glycinamide in Solution. *J. Phys. Chem. B.* **2004**, *108*, 1405-1413.

(30) Li, H.-Y.; Pu, M.; Liu, K.-H.; Zhang, B.-F.; Chen, B.-H. A density-functional theory study on double-bond isomerization of 1-butene to cis-2-butene catalyzed by zeolites. *Chem. Phys. Lett.* **2005,** *404*, 384-388.

(31) Justino, L. L. G.; Ramos, M. L.; Abreu, P. E.; Carvalho, R. A.; Sobral, A. J. F. N.; Scherf, U.; Burrows, H. D. Conformational Studies of Poly(9,9-dialkylfluorene)s in Solution Using NMR Spectroscopy and Density Functional Theory Calculations. *J. Phys. Chem. B.* **2009**, *113*, 11808-11821.

(32) Haghdadi, M.; Farokhi, N. Density functional theory(DFT) calculations of conformational energies and interconversion pathways in 1, 2, 7-thiadiazepane. J. *Serb. Chem. Soc.* **2011**, *76*, 395-406.

(33) Szczepaniak, M.; Moc, J. Conformational studies of gas-phase ribose and 2-deoxyribose by density functional, second order PT and multi-level method calculations: the pyranoses, furanoses, and open-chain structures. *Carbohydrate Research.* **2014**, *384*, 20-36.

(34) Happel, J.; Hnatow, M. A.; Mezaki, R. Isomerization equilibrium constants of n-butanes. *J. Chem. Eng. Data.* **1971**, *16*, 206-209.

(35) GaussView, Version 5, Dennington, Roy; Keith, Todd; Millam, John. Semichem Inc., Shawnee Mission, KS, **2009**.

# Concluding Remarks and Future Scope of the Present Work

In the second chapter of this thesis, we have described the new square-planar nickel (III)-bis(quinoxaline-6,7-dithiolate) complexes demonstrating their electronic spectral properties. Ion-pair compounds of cationic organic molecule with anionic metal dithiolene complexes will be taken up further to demonstrate their device properties such as magnetic, conducting, NLO, liquid crystals, *etc*. properties. This work is under progress in our laboratory. Work demonstrated in the chapters 3 and 4, includes spectroscopy as the main characterization tool. A series of donor-acceptor π-conjugated 2,6-bis(pyrazolyl)pyridine derivatives has been synthesized following standard and well-known organic synthetic methodologies and characterized through spectroscopy. 2,6-bis(pyrazolyl)pyridine derivatives are excellent tridentate chelating ligands for metal ion coordination. Metal complexes of 2,6-bis(pyrazolyl)pyridines are more useful as photosensitizers and they act as electron reservoirs due to their π-conjugated aromatic systems and they have the ability to photo stabilize the complexes. So we wish to extend this interesting system and a large amount of work has already been obtained in this direction. In the chapter 5 of this thesis, we have discussed about unusual intermediate conformation of 1,1''-1,4-phenylene-bis(methylene)bis-4,4'-bipyridinium cation $[C_{28}H_{24}N_4]^{2+}$ (**c**) receptor, which can interconvert between its *syn*- and *anti*-conformations, which were explaind by theoritical calculation.This work has opened a new area, that explores the possibility of interactions between $[M(dithiolene)_2]^{2-}$ anions and variety of mechanically interlocked cationic systems such as cyclophane, rotaxane and catenane. It would be very interesting to assemble interlocked components (such as cyclophane, rotaxane, and catenane as cations) and the classical metal dithiolene complex anion in a single supramolecular system. The syntheses of such systems are in progress in our laboratory.

# List of Publications

1. **Indavath K. Naik**, Sarkar. R and Samar K. Das *Eur. J. Inorg. Chem.* **2015,** *33*, 5523-5533. (**Chapter 2**)
2. **Indavath K. Naik**, Ramakrishna.B, Sarkar. R, Mondal. N and Samar K. Das (*Manuscript to be submitted*). (**Chapter 3)**
3. **Indravath K. Naik**, Sarkar. R and Samar K. Das (*Manuscript under preparation*).(**Chapter 4)**
4. **Indravath K. Naik**, Sarkar. R, Madhu. V, Bolligarla. R, Kishore. R and Samar K. Das J. Phys. Chem A **2017**, 121, 3274-3286. (**Chapter 5)**
5. Madhu. V, Bolligarla. R, **Indravath K. Naik**, Raju. M and Samar K. Das *Eur. J. Inorg. Chem.* **2016**, *26*, 4257-4264.
6. Madhu. V, Supriya. S, Kishore. R , **Indravath K. Naik** and Samar K. Das *CrystEngComm* **2015**, *17*, 3219-3223.

# Posters and Presentations

**1)** Chemfest-2015, 12th Annual In-House Symposium, Feb-2015, UoH.

**2)** Modern Trends in Inorganic Chemistry (MTIC-XVI), Dec-2015, Jadavpur University, India (International).

सत्यमेव जयते

THE JOURNAL OF PHYSICAL CHEMISTRY A

Article

pubs.acs.org/JPCA

# An Organic Receptor Isolated in an Unusual Intermediate Conformation: Computation, Crystallography, and Hirshfeld Surface Analysis

Indravath Krishna Naik, Rudraditya Sarkar, Vedichi Madhu, Ramababu Bolligarla, Ravada Kishore, and Samar K. Das*

School of Chemistry, University of Hyderabad, Hyderabad 500 046, India

Supporting Information

**ABSTRACT:** 1,1″-1,4-Phenylene-bis(methylene)bis-4,4′-bipyridinium cation $[C_{28}H_{24}N_4]^{2+}$ (**c**), an organic receptor that generally crystallizes in its anti conformation, has recently been shown to be isolated in its syn conformation in an ion-paired compound $[C_{28}H_{24}N_4][Zn(dmit)_2]\cdot 2DMF$ ($dmit^{2-}$ = 1,3-dithiole-2-thione-4,5-dithiolate; DMF = dimethylformamide). In this article, we demonstrated that the same receptor $[C_{28}H_{24}N_4]^{2+}$ (**c**) can also be stabilized in an unusual intermediate conformation (neither syn nor anti) with $PF_6^-$ anion in compound $[C_{28}H_{24}N_4](PF_6)_2\cdot$(1,4-dioxane) (**1**·(1,4-dioxane)). The energetically favored anti conformation has been described in its nitrate salt $[C_{28}H_{24}N_4](NO_3)_2\cdot 2H_2O$ (**2**·$2H_2O$). Compounds **1**·(1,4-dioxane) and **2**·$2H_2O$, crystallizing in triclinic and monoclinic systems with space groups $P\bar{1}$ and $P2_1/n$, respectively, were additionally characterized by Hirshfeld surface analysis. The density functional theory calculations are performed to understand the internal mechanism of the stability of various conformers of cationic receptor **c**, compound **1**, and compound **2**. In conjunction with the electronic stability of the conformers, the natural bond orbital analysis and conformational equilibrium constants at different temperatures are also calculated to find out the sources of the different stability of the various conformers of experimentally synthesized compounds.

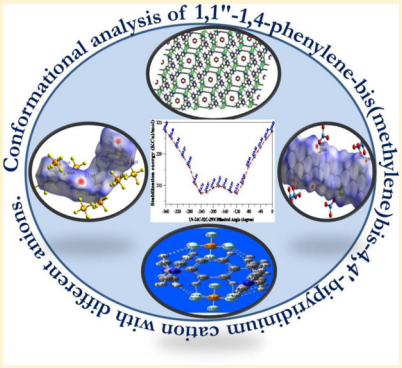


## INTRODUCTION

Intermolecular interactions in the solid state continue to be a topic of great interest in the field of supramolecular as well as materials chemistry because of its fundamental importance for the formation of higher organized chemical systems that result from the association of two or more chemical species.[1,2] Depending upon the function and need of selectivity in the molecular assembly processes, several types of weak but specific (mostly noncovalent) intermolecular interactions are involved that include ion pairing,[3] hydrogen bonding,[4] arene−arene ($\pi-\pi$) stacking interactions,[5−7] etc. The biological processes[8−10] that encounter such noncovalent interactions are substrate−enzyme complex formation, the protein folding, the formation of membranes, antiportation of neutral and ionic species through membranes, etc. In these intermolecular interactions, particularly between substrate and receptor (e.g., the active site of the enzyme), the receptor is generally flexible to undergo conformational changes to accommodate the substrate in an optimal geometry, comparable to "lock-and-key fit" situation.[11]

Mimicking such conformational change using a specific substance is a great challenge to modern chemistry researchers. Many captivating, structurally diverse receptors (hosts) have been designed and synthesized for the purpose of studying the interactions between the receptor (host) and substrate (guest). Besides well-characterized macrocycles (hosts), for example, cyclophanes,[12] cyclodextrins,[13] cryptophanes,[14] cucurbiturils,[15] carcerands,[16] supramolecular capsules,[17] etc., acyclic compounds with cavities of flexible size, that are generally termed as molecular tweezers and clefts, proved to be effective synthetic receptors.[18] A molecular tweezer is defined as a synthetic receptor that contains two aromatic (complexing) chromophores connected by a single spacer. A cleft is nothing but a molecular tweezer having converged functional groups (receptors) that are separated by 10−12 Å (with the help of the spacer) to create a cavity for guest/substrate binding.[19] We report here an organic acyclic receptor cation having two aromatic side-arms (4,4′-bipyridines) connected by a single spacer (1,4-phenylene-bis(methylene)), namely, 1,1″-1,4-phenylene-bis(methylene)bis-4,4′-bipyridinium cation $[C_{28}H_{24}N_4]^{2+}$ (**c**), which can interconvert between its syn (cleftlike) and anti conformations as shown in Scheme 1 (left and right, respectively). The receptor cation **c** can also be isolated in an unusual intermediate conformation (Scheme 1, middle). In this contribution, we described synthesis and crystal structures of $[C_{28}H_{24}N_4](PF_6)_2\cdot$(1,4-dioxane) (**1**·(1,4-dioxane)) and $[C_{28}H_{24}N_4](NO_3)_2\cdot 2H_2O$ (**2**·$2H_2O$) having an *intermediate* and anti conformation, respectively. The hexafluorophosphate

**Received:** January 4, 2017
**Revised:** April 6, 2017
**Published:** April 6, 2017





DOI: 10.1021/acs.jpca.7b00091
J. Phys. Chem. A 2017, 121, 3274−3286

**Scheme 1**

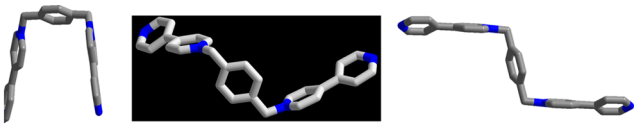


($PF_6^-$) salts of the same cation **c** have been reported earlier: in one of these, **c** is in anti form,[20] and in the other salt,[21] **c** has a similar conformation, found in **1**·(1,4-dioxane). However, both reports focused only on their respective crystal structures of the concerned hexafluorophosphate ($PF_6^-$) salts including their supramolecular sturctures. We undertook this work to compare the syn and anti conformations of **c** in **1**·(1,4-dioxane) and **2**·2$H_2O$, respectively, emphasizing the role of hydrogen bonding of surrounding anions. We also performed Hirshfeld surface analyses on the crystal structures of **1**·(1,4-dioxane) and **2**·2$H_2O$ to rationalize the molecular conformations of **c** in their respective salts.

To understand the unusual conformation of the cation **c** in compound **1**·(1,4-dioxane), we performed quantum mechanical calculations using density functional theory, and we tried to understand internal mechanism of the stability of different conformers of the cationic receptor **c**, compound **1**, and compound **2**. The electronic stability of the conformers were analyzed by considering isodesmic reaction between the cationic receptor **c** and donor anions, $PF_6^-$ and $NO_3^-$, following the principles of thermodynamics. On the one hand, the different conformational analyses of compound **1** were performed by fixing the 1N-24C-52C-29N dihedral angle at different values (see in the text for details). On the other hand, stability of these compounds on excitation is also measured by evaluating the energy gap between highest occupied molecular orbital (HOMO) and lowest unoccupied molecular orbital (LUMO) at the electronic ground state of the respective compounds. The possible interactions between the occupied donor orbitals and unoccupied acceptor orbitals in these compounds are also calculated by using second-order perturbation theory as implemented in natural bond orbital analysis (NBO). As a result of these analyses, the sources of the different stabilities of the various conformers of the respective compounds can be accounted, and results are discussed in details in the text. At last, we calculated the equilibrium constants of various conformational equilibria among the different conformers of the respective compounds to confirm the results of the above analyses by taking the experimental conformational equilibrium constant values between the *cis*-2-butene and *trans*-2-butene at different temperature as a reference.

## EXPERIMENTAL, PHYSICAL, AND THEORETICAL METHODS

**Physical Measurements.** All reagents and solvents were commercially available and used without further purification. Elemental analyses (C, H, and N) were obtained with a FLASH EA 1112 Series CHNS analyzer. Fourier transform infrared (FT-IR) spectra were recorded in the range of 400−4000 $cm^{-1}$ with a JASCO FT/IR-5300 spectrometer using KBr pellet. $^1$H NMR spectra were recorded on Bruker DRX-400 spectrometer using $Si(CH_3)_4$ as an internal standard.

**Synthesis of Compound $[C_{28}H_{24}N_4](PF_6)_2$·(1,4-dioxane) (1·(1,4-dioxane)).** 1,4-Bis(bromomethyl)benzene (150 mg, 0.568 mmol), dissolved in 10 mL of dry acetonitrile, was added dropwise to a refluxing solution of 4,4′-bipyridine (500 mg, 3.2 mmol) in 10 mL of acetonitrile. The reaction mixture was then refluxed for additional 2 h. The $[C_{28}H_{24}N_4]Br_2$ salt came out as insoluble white solid. The precipitate was washed with acetonitrile and dried in vacuum. This product was then dissolved in warm water, and subsequently, it was treated with $NH_4PF_6$. This results in the precipitation of $[C_{28}H_{24}N_4](PF_6)_2$ (1,1′-1,4-phenylene-bis(methylene)bis-4,4′-bipyridinium-bis-(hexafluorophosphate). Yield: 0.276 g (∼70%). This can be described as crude $PF_6$ salt of **c**, $[C_{28}H_{24}N_4](PF_6)_2$. This crude product was recrystallized by the vapor diffusion of diethyl ether into a solution of $[C_{28}H_{24}N_4](PF_6)_2$ in a mixed solvent of dimethylformamide (DMF)/1,4-dioxane (1:3) into the single crystals of $[C_{28}H_{24}N_4](PF_6)_2$·(1,4-dioxane) (**1**·(1,4-dioxane)). Anal. Calcd for ($C_{32}H_{32}F_{12}N_4O_2P_2$): C, 48.37; H, 4.06; N, 7.05. Found: C, 48.26; H, 4.11; N, 7.12%. IR (KBr pellet) ($\upsilon$/$cm^{-1}$): 3134s, 3074w, 2150w, 1699m, 1639s, 1502m, 1460s, 1421m, 1215s, 1184m, 1010m, 835s, 557s, 515w. $^1$H NMR (deuterated dimethyl sulfoxide (DMSO-$d_6$)): $\delta$ 9.28(d, $J$ = 6.647, 4H); 8.81(d, $J$ = 6.51, 4H); 8.62(d, $J$ = 6.48, 4H); 7.97(d, $J$ = 6.491, 4H); 7.66(S, 4H); 5.89(S, 4H).

**Synthesis of Compound $[C_{28}H_{24}N_4](NO_3)_2$·2$H_2O$ (2·2$H_2O$).** Compound 2·2$H_2O$ was synthesized by an ion exchange method as follows: 0.07 g (0.1 mmol) of $[C_{28}H_{24}N_4](PF_6)_2$ was taken in a 10 mL round-bottom flask, and 0.034 g (0.2 mmol) of $AgNO_3$ was taken in an another 10 mL round-bottom flask. Then the two round-bottom flasks were fitted into two terminals of a $\lambda$-shaped glass tube. Then the whole $\lambda$ tube was filled by $CH_3CN$ solution keeping the whole system closed. After two weeks, colorless needle-shaped crystals of $[C_{28}H_{24}N_4](NO_3)_2$·2$H_2O$ (2·2$H_2O$) were deposited on the top of the $\lambda$ tube. Yield: 0.048 g (84%). Anal. Calcd for ($C_{28}H_{28}N_6O_8$): C, 58.33; H, 4.89; N, 14.58. Found: C, 58.26; H, 4.95; N, 14.49%. IR (KBr pellet) ($\upsilon$/$cm^{-1}$) for 2·2$H_2O$: 3323m, 3107w, 3020w, 1633s, 1593w, 1545m, 1523m, 1493m, 1350 ($NO_3^-$)s, 1211w, 1161m, 1070w, 895w, 823s, 771s, 727m, 513m, 478w.

**X-ray Crystallography.** $[C_{28}H_{24}N_4](PF_6)_2$·(1,4-dioxane) (**1**·(1,4-dioxane)) was measured at 100 K, and $[C_{28}H_{24}N_4](NO_3)_2$·2$H_2O$ (2·2$H_2O$) was measured at 298 K on a Bruker SMART APEX CCD area detector system [$\lambda$(Mo K$\alpha$) = 0.710 73 Å] with a graphite monochromator. 2400 frames were recorded with an $\omega$ scan width of 0.3°, each for 8 s. Crystal-detector distance was 60 mm with a collimator of 0.5 mm. The SMART software[22] was used for intensity data acquisition, and the SAINTPLUS software[22] was used for data extraction. Absorption correction was performed with the help of SADABS program.[22] Programs of SHELX-97[23] were used for structure solution by direct methods and least-squares refinement on $F^2$. All non-hydrogen atoms were refined anisotropically. Hydrogen atoms on aromatic ring were introduced on calculated positions and included in the refinement riding on their respective parent atoms. We tried to locate the hydrogen atoms of solvent water molecules in the crystal structure of compound 2·2$H_2O$ through differential Fourier maps but could not succeed. Therefore, the O−H···O hydrogen-bonding distances in the supramolecular structure of water in compound 2·2$H_2O$ were described as O···O separations (taking O···O distance in the range from 2.395 to 2.950 Å). Detailed information about crystal data and structure determination are summarized in Table 1.

**Computational Methods.** Computational simulations of the different conformers of cationic receptor **c**, compound **1**,


DOI: 10.1021/acs.jpca.7b00091
J. Phys. Chem. A 2017, 121, 3274−3286

**Table 1. Crystallographic Data and Structure Refinement for Compound 1·(1,4-dioxane) and 2·2H$_2$O**

| | 1·(1,4-dioxane) | 2·2H$_2$O |
|---|---|---|
| empirical formula | $C_{32}H_{32}F_{12}N_4O_2P_2$ | $C_{28}H_{28}N_6O_8$ |
| formula weight | 794.56 | 576.56 |
| temperature (K) | 100(2) K | 273 (2) K |
| crystal size (mm) | 0.20 × 0.16 × 0.06 | 0.21 × 0.17 × 0.14 |
| crystal system | triclinic | monoclinic |
| space group | $P\bar{1}$ | $p21/n$ |
| $Z$ | 2 | 2 |
| wavelength (Å) | 0.710 73 | 0.710 73 |
| unit cell dimensions | | |
| $a$ [Å] | 9.2462(7) | 4.5103(9) |
| $b$ [Å] | 11.7988(9) | 19.774(4) |
| $c$ [Å] | 16.7537(13) | 15.054(3) |
| $\alpha$ [deg] | 106.49(10) | 90 |
| $\beta$ [deg] | 103.76(10) | 97.786(4) |
| $\gamma$ [deg] | 98.33(10) | 90 |
| volume [Å$^3$] | 1657.3(2) | 1331.2(5) |
| calculated density (mg/m$^{-3}$) | 1.592 | 1.428 |
| reflections collected/unique | 15 442/5829 | 15 147/3145 |
| $R$(int) | 0.0408 | 0.0604 |
| $F$(000) | 812 | 604 |
| max and min transmission | 0.985 and 0.954 | 0.956 and 0.989 |
| $\theta$ range for data collection (deg) | 1.33 to 25.07 | 0.956 to 28.23 |
| refinement method | full-matrix least-squares on $F^2$ | full-matrix least-squares on $F^2$ |
| data/restraints/parameters | 5829/0/469 | 3145/0/190 |
| goodness-of-fit on $F^2$ | 1.198 | 1.003 |
| $R_1/wR_2$ [$I > 2\sigma(I)$] | 0.0713/0.1378 | 0.0915/0/0.264 |
| $R_1/wR_2$ (all data) | 0.0900/0.1452 | 0.142/0.304 |
| largest diff peak and hole | 0.501 and −0.270 e·Å$^{-3}$ | 0.487 and −0.284 e·Å$^{-3}$ |

and compound **2** were performed with density functional theory (DFT) as implemented in Gaussian 09[24] suite programming package. Computational data evaluation throughout the present study was performed with B3LYP hybrid functional,[25−29] which includes Hartree−Fock (HF) exchange as well as DFT exchange correlations. The nonlocal correlations part is taken care of by Lee, Yang, and Parr (LYP) functional. All calculations were performed using Pople's 6-31G(d,p) basis set. The calculations of minimum-energy conformers of the cationic receptor **c**, compound **1**, and compound **2** were confirmed by subsequent frequency calculations of the optimized geometry at the ground state of the respective conformers. We note that no imaginary frequency was found at the optimized geometry of the conformers. The first thirty-four lowest frequencies of each conformer are given in Table S1 in the Supporting Information.

Natural bond orbital (NBO) analysis was performed to find out the different intramolecular interactions in cationic receptor **c**, compound **1**, and compound **2**. The possible interaction between the filled donor orbital (i) and vacant acceptor orbital (j) was accounted for in the NBO analysis. The stabilization energy of the donor−acceptor interaction $[E^{(2)}(i,j)]$ was calculated by second-order perturbation theory. The stabilization energy $[E^{(2)}(i,j)]$ associated with the electron delocalization between the donor (i) and acceptor (j) orbitals can be expressed as

$$E^{(2)}(i,j) = q_i \frac{[F(i,j)]^2}{E_j - E_i} \quad (1)$$

where $q_i$ is the orbital occupancy, $E_i$ and $E_j$ are diagonal elements, and $F_{i,j}$ are the off-diagonal elements of the NBO Fock matrix.

Equilibrium constant ($K$) between the different conformers of cationic receptor **c** and compound **1** were calculated by considering the ratio of number of reactant ($r$, more stable conformer) and product ($p$, less stable conformer) molecules at equilibrium.[25−29] The ratio of $r$ and $p$ can be expressed as

$$\frac{N_p}{N_r} = \left(\frac{q_p}{q_r}\right) e^{-\Delta E/RT} \quad (2)$$

where $N_p$ and $N_r$ are the number of product and reactant molecules at equilibrium. The partition functions of the product and reactant are designated as $q_p$ and $q_r$, respectively. $\Delta E$ is the total energy difference between the reactant and product, and $R$ is the universal gas constant. $T$ represents the temperature in Kelvin. So the equilibrium constant of these conformers can be expressed as

$$K = \left(\frac{q_p}{q_r}\right) e^{-\Delta E/RT} \quad (3)$$

or,

$$K = \left(\frac{q_p^{vib} q_p^{rot}}{q_r^{vib} q_r^{rot}}\right) e^{-\Delta E/RT} \quad (4)$$

where $q_p^{vib}$, $q_p^{rot}$, $q_r^{vib}$, and $q_r^{rot}$ are the vibrational and rotational partition functions of the product and reactant, respectively. The translational partition functions of reactant and product are equal and hence cancel out. The electronic ground states of product and reactant are nondegenerate; hence, electronic partition function is unity. To validate the above eq 4, we calculated the equilibrium constants ($K$) between *cis*-2-butene and *trans*-2-butene, conformers of 2-butene at different temperatures, and compared them with the available experimental values.[30] The calculated rotational constants, symmetry numbers of these conformers are given in Table S2 in the Supporting Information. The rotational and vibrational partition functions of these conformers at different temperatures are given in Table S3 in the Supporting Information. This comparison between the experimental and theoretical $K$ values of *cis*-2-butene ⇌ *trans*-2-butene equilibrium at different temperatures is given in Table S4 in the Supporting Information. It is found that theoretically evaluated $K$ values between *cis*-2-butene and *trans*-2-butene equilibrium are in good accord with the experimental values.[30] The values of rotational constants, symmetry number, $q^{rot}$ and $q^{vib}$ of the conformers of cationic receptor and compound **1** are also given in the Tables S2 and S3 in the Supporting Information to make the theoretical analysis easier in latter sections.



DOI: 10.1021/acs.jpca.7b00091
J. Phys. Chem. A 2017, 121, 3274−3286

Scheme 2

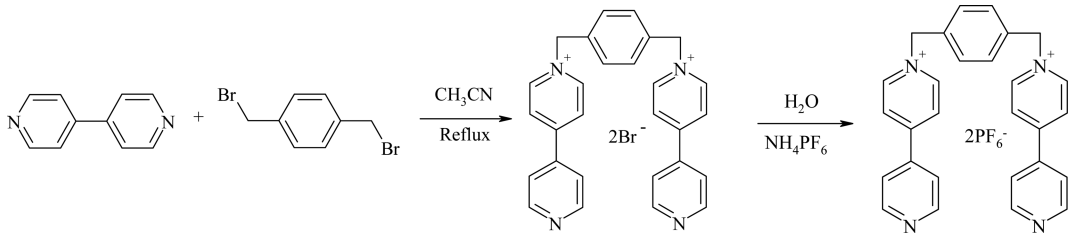


## RESULTS AND DISCUSSION

**Synthesis.** The crude $[C_{28}H_{24}N_4](PF_6)_2$ is synthesized from 1,4-bis(bromomethyl)benzene and 4,4′-bipyridine (Scheme 2). This crude solid is then crystallized from DMF−1,4-dioxane to obtain the single crystals of compound $[C_{28}H_{24}N_4](PF_6)_2$·(1,4-dioxane) (**1**·(1,4-dioxane)). The nitrate salt (compound **2**·2H2O) could not be synthesized from a direct method, but this can be prepared from the crude $PF_6$ salt of compound **1**·(1,4-dioxane) by an ion exchange method with silver nitrate (Scheme 3). Compounds **1** and **2** were

Scheme 3

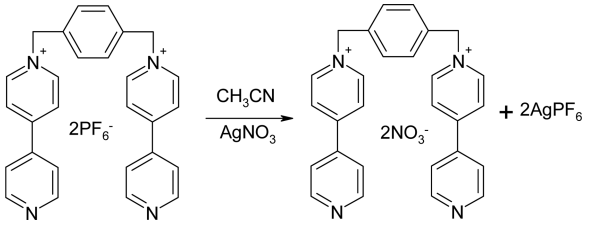


characterized by IR spectral studies, $^1$H NMR studies including elemental analyses, and finally unambiguously by single-crystal X-ray crystallography.

**Crystal Structure Description and Discussion.** The bromide salt of the title cationic receptor $[C_{28}H_{24}N_4]^{2+}$ (**c**), $[C_{28}H_{24}N_4]Br_2$ was structurally characterized, and the usual anti conformation of the cation **c** (Scheme 1, right) is found in the crystal structure of $[C_{28}H_{24}N_4]Br_2$.[21] When these off-white crystals of $[C_{28}H_{24}N_4]Br_2$ are suspended in MeCN solvent with few drops of DMF ($[\mathbf{c}]Br_2$ crystals are not soluble in this medium) dissolving an excess amount of $[Bu_4N]_2[Zn(dmit)_2]$ and stirred for about a week, the off-white solid of $[C_{28}H_{24}N_4]Br_2$ becomes dark brown with the conversion of $[C_{28}H_{24}N_4][Zn(dmit)_2]$·in a solid−liquid interface crystalline state reaction. In the red-brown solid of compound $[C_{28}H_{24}N_4][Zn(dmit)_2]$, the cationic receptor $[C_{28}H_{24}N_4]^{2+}$ (**c**) has syn conformation (Scheme 1, left), as observed in the crystal structure of $[C_{28}H_{24}N_4][Zn(dmit)_2]$·2DMF.[31] By exploiting the flexible nature of this acyclic cationic receptor $[C_{28}H_{24}N_4]^{2+}$ (**c**), we could demonstrate the reversible syn−anti conformational change of **c** in solid-to-solid antiformations (eq 5). We wanted to exploit further the flexible nature of $[C_{28}H_{24}N_4]^{2+}$

$$[C_{28}H_{24}N_4][Zn(dmit)_2]\cdot 2DMF(\text{solid phase}) + [Bu_4N]Br(\text{soln. phase}) \rightleftharpoons [C_{28}H_{24}N_4]Br_2(\text{solid phase}) + [Bu_4N]_2[Zn(dmit)_2](\text{soln. phase}) \quad (5)$$

(**c**) by crystallizing this cation with diverse anions, and we synthesized compound $[C_{28}H_{24}N_4](PF_6)_2$·(1,4-dioxane) (**1**·(1,4-dioxane)) (with $PF_6^-$ anion) and compound $[C_{28}H_{24}N_4](NO_3)_2$·2$H_2O$ (**2**·2$H_2O$) (with $NO_3^-$ anion).

Compound $C_{28}H_{24}N_4](PF_6)_2$·(1,4-dioxane) (**1**·(1,4-dioxane)) crystallizes in the triclinic system with space group $P\bar{1}$, and concerned single-crystal X-ray data parameters, obtained at 100 K, are described in Table 1. The thermal ellipsoidal plot of the compound **1**·(1,4-dioxane) is displayed in Figure 1, and the relevant selected bond lengths and angles are described in Table 2. Interestingly, the cation **c**, observed in the crystal structure of $C_{28}H_{24}N_4](PF_6)_2$·(1,4-dioxane) (**1**·(1,4-dioxane)), adopts an intermediate conformation that is between syn and anti conformations (Scheme 1, middle and Figure 1). We believe that intercation−anion hydrogen-bonding interactions (mostly C−H···F hydrogen bonds) between the cation receptor **c** and anion $PF_6^-$ are responsible for this unusual intermediate conformation of **c** in the crystal struture of compound **1**·(1,4-dioxane).

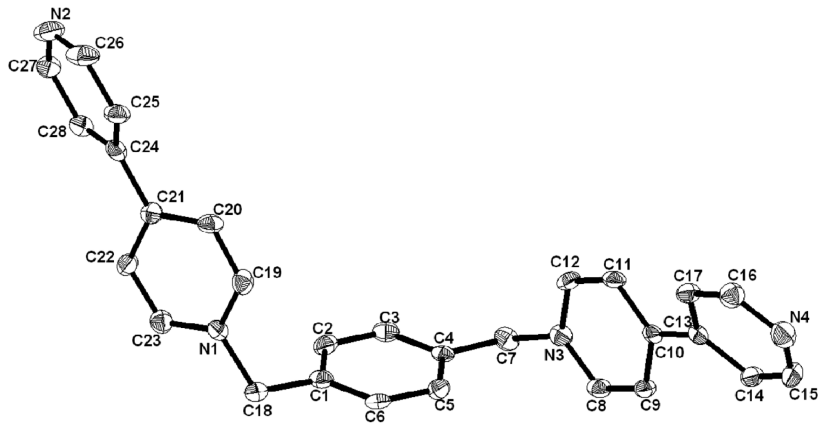


**Figure 1.** Thermal ellipsoidal plot (30% probability) of organic receptor $[C_{28}H_{24}N_4]^{2+}$ in compound $[C_{28}H_{24}N_4](PF_6)_2$·(1,4-dioxane) (**1**·(1,4-dioxane)); anions, solvent molecules, and hydrogens are omitted for clarity.



DOI: 10.1021/acs.jpca.7b00091
J. Phys. Chem. A 2017, 121, 3274−3286

Table 2. Complete List of Bond Lengths [Å] and Angles [deg] for $C_{28}H_{24}N_4](PF_6)_2$·(1,4-dioxane) (1·(1,4-dioxane))

| | | | |
|---|---|---|---|
| C(7)−N(3) | 1.474(5) | C(18)−N(1) | 1.347(4) |
| C(8)−N(3) | 1.343(5) | C(26)−N(2) | 1.333(5) |
| C(9)−C(10) | 1.393(5) | C(29)−C(30)#1[a] | 1.492(6) |
| C(11)−C(12) | 1.361(5) | C(32)−C(31)#2 | 1.485(6) |
| C(13)−C(17) | 1.193(5) | F(1)−P(1) | 1.594(2) |
| O(1)−C(29)−C(30)#1[a] | 109.8(3) | F(4)−P(1)−F(2) | 179.85(18) |
| O(2)−C(31)−C(32)#2 | 111.3(3) | F(7)−P(2)−F(9) | 89.71(13) |
| C(23)−N(1)−C(19) | 120.6(3) | N(2)−C(26)−C(25) | 123.8(4) |
| C(19)−N(1)−C(18) | 118.2(3) | N(4)−C(16)−C(17) | 125.0(4) |
| C(30)−O(1)−C(29) | 108.7(3) | N(1)−C(23)−C(22) | 121.6(3) |

[a]Symmetry antiformations used to generate equivalent atoms: #1 $-x + 2, -y + 1, -z$; #2 $-x + 1, -y + 1, -z + 2$.

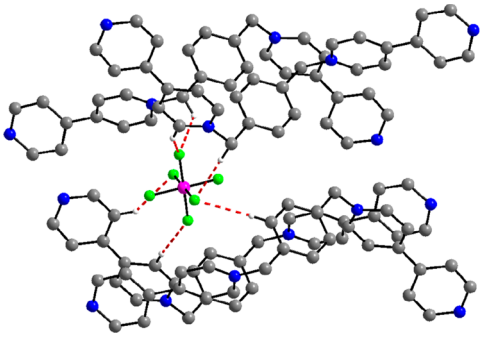

Figure 2. C−H···F hydrogen-bonding environment around a $PF_6$ anion in $[C_{28}H_{24}N_4](PF_6)_2$·(1,4-dioxane) (1·(1,4-dioxane)).

The C−H···F hydrogen-bonding environment around the $PF_6^-$ anion is given in Figure 2. The relevant hydrogen-bonding parameters are presented in Table 3. In other words,

Table 3. Hydrogen Bonds for Compound 1·(1,4-dioxane) [Å and deg]

| D−H···A[a] | d(D−H) | d(H···A) | d(D···A) | ∠(DHA) |
|---|---|---|---|---|
| C(22)−H(22)···N(4)#3 | 0.95 | 2.42 | 3.308(5) | 155.9 |
| C(28)−H(28)···N(4)#3 | 0.95 | 2.65 | 3.482(5) | 146.3 |
| C(9)−H(9)···N(2)#4 | 0.95 | 2.42 | 3.302(5) | 154.0 |
| C(8)−H(8)···F(1)#5 | 0.95 | 2.30 | 3.156(4) | 149.4 |
| C(7)−H(7A)···F(6)#5 | 0.99 | 2.42 | 3.411(4) | 178.2 |
| C(7)−H(7B)···F(7)#6 | 0.99 | 2.54 | 3.422(4) | 149.1 |
| C(2)−H(2)···F(6)#7 | 0.95 | 2.59 | 3.509(4) | 161.7 |
| C(23)−H(23)···F(9)#8 | 0.95 | 2.43 | 3.286(4) | 150.5 |
| C(18)−H(18A)···F(9)#8 | 0.99 | 2.37 | 3.304(4) | 157.8 |
| C(11)−H(11)···F(3) | 0.95 | 2.58 | 3.524(4) | 170.3 |
| C(17)−H(17)···F(5) | 0.95 | 2.46 | 3.266(4) | 143.0 |
| C(15)−H(15)···F(12)#9 | 0.95 | 2.58 | 3.501(4) | 164.0 |

[a]Symmetry transformations used to generate equivalent atoms. #3 $x - 1, y, z - 1$; #4 $x + 1, y + 1, z + 1$; #5 $x, y + 1, z$; #6 $-x, -y + 1, -z + 1$; #7 $-x, -y + 1, -z$; #8 $x, y + 1, z - 1$; #9 $x + 1, y + 1, z$.

in the crystal structure, the stability of intermediate conformation (between syn and anti) of the organic receptor $[C_{28}H_{24}N_4]^{2+}$ (**c**) in compound $[C_{28}H_{24}N_4](PF_6)_2$·(1,4-dioxane) (1·(1,4-dioxane)) can be rationalized by its strong hydrogen-bonding interactions with surrounding $PF_6^-$ anions resulting in a three-dimensional supramolecular network that have well-defined void spaces, occupied by the solvent 1,4-dioxane molecules as shown in Figure 3. We also performed DFT calculations to understand this intermediate conformation of **c** in compound 1·(1,4-dioxane) (vide infra).

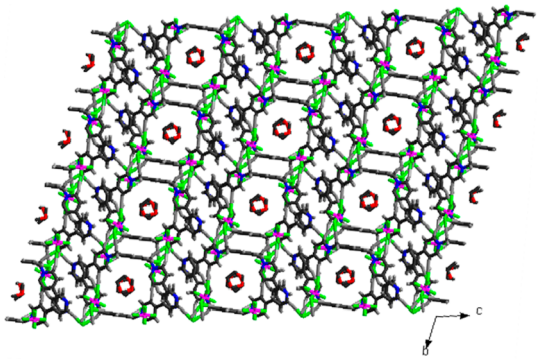

Figure 3. View (wire-frame representation) of the molecular packing of $[C_{28}H_{24}N_4](PF_6)_2$·(1,4-dioxane) (1·(1,4-dioxane)) (4 × 4) cells; color code: F, green; P, purple; C, gray; N, blue; O, red; H, medium gray.

Compound $[C_{28}H_{24}N_4](NO_3)_2·2H_2O$ (2·2H$_2$O) crystallizes in monoclinic system with space group $P2_1/n$. The X-ray analysis of a single crystal of compound 2·2H$_2$O reveals that the dication $[C_{28}H_{24}N_4]^{2+}$ (**c**) adopts an usual anti conformation with respect to the two bipyridine units of the *para*-xylene ring as shown in Figure 4. In the asymmetric unit of the concerned crystal structure, one lattice water molecule (O4, located in a general position) exists with half of the cationic receptor (**c**) and one nitrate anion. Thus, the molecular formula of compound 2·2H$_2$O consists of a full molecule of cationic receptor, two nitrate anions, and two lattice water molecules.

Interestingly, the solvent water molecule (O4) arranges in the form of a water chain (a centrosymmetric array) with two different hydrogen-bonding distances (2.395 and 2.678 Å). A small fragment of the chain is formed by the hydrogen-bonding interaction (2.395 Å) between O4 and O4(a) (Figure 5a, left). These fragments are connected further by a relatively larger H-bond distance (2.678 Å) to form the water chain (Figure 5a, right).

Each water molecule of this water chain is further hydrogen-bonded (2.912 Å) to an oxygen atom (O2) of the surrounding nitrate anion (Figure 5b). In the crystal structure of compound $[C_{28}H_{24}N_4](NO_3)_2·2H_2O$ (2·2H$_2$O), the staircaselike (anti conformation) dications $[C_{28}H_{24}N_4]^{2+}$ (**c**) pack to form zigzag arrays with two nitrate anions and two crystal water molecules, inserted between the dications as shown in Figure 6a. The corresponding space-filling plot (without nitrate anions and lattice water molecules) is shown in Figure 6b.

Organic receptor $[C_{28}H_{24}N_4]^{2+}$ (**c**) takes its usual anticonformation in compound 2·2H$_2$O (nitrate salt) and is stabilized in an unusual intermediate conformation in compound 1·(1,4-dioxane) ($PF_6$ salt)! Why is it so? A supramolecular analysis from respective crystal structures.



DOI: 10.1021/acs.jpca.7b00091
J. Phys. Chem. A 2017, 121, 3274−3286

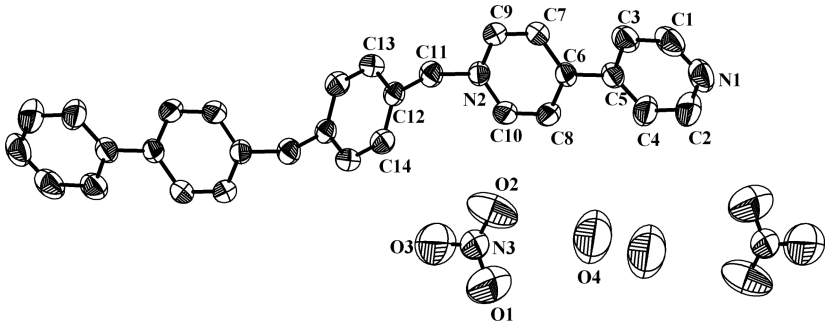


**Figure 4.** Thermal ellipsoidal plot of the asymmetric unit of compound $[C_{28}H_{24}N_4](NO_3)_2{\cdot}2H_2O$ (**2**·$2H_2O$); hydrogen atoms are not shown for clarity (50% probability).

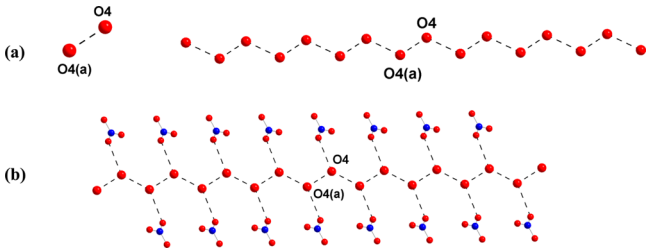


**Figure 5.** (a, left) Supramolecular water dimer and (a, right) its one-dimensional chainlike arrangement formed from hydrogen-bonding interactions of O4 and O4(a), which are related by a symmetry operation: $2 - x$, $1 - y$, $-z$. (b) Extended water structure formed from the solvent water molecule (O4), showing its hydrogen-bonding interactions with its surrounding nitrate anions.

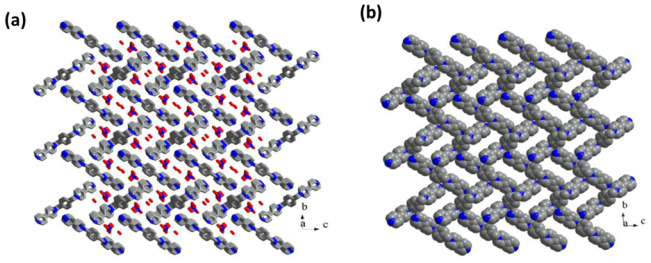


**Figure 6.** (a) Packing diagram consisting of the dication $[C_{28}H_{24}N_4]^{2+}$, $NO_3^-$ anion, and crystal water molecules in **2**·$2H_2O$. Hydrogen atoms are not shown for clarity. (b) View (face-filling representation) of the molecular packing of $[C_{28}H_{24}N_4]^{2+}$ cations in the $[C_{28}H_{24}N_4][NO_3]_2{\cdot}2H_2O$ (**2**·$2H_2O$) (3 × 3) cells. Color code: N, blue; C, gray; O, red. The hydrogen atoms, nitrate anions, and water molecules are not shown for clarity.

The usual energetically favored conformation of the cationic receptor $[C_{28}H_{24}N_4]^{2+}$ (**c**) is anti, observed in the crystal structure of compound $[C_{28}H_{24}N_4](NO_3)_2{\cdot}2H_2O$ (**2**·$2H_2O$); see Table 4 for bond lengths and angles of this compound. The deviation from this usual anti conformation of **c** can be explained by considering supramolecular hydrogen-bonding interactions of this dication (**c**) with its surrounding anions ($PF_6^-$ anion in case of compound **1**·(1,4-dioxane) and $NO_3^-$ anion in the case of compound **2**·$2H_2O$). The supramolecular hydrogen-bonding interactions around the cationic receptor (**c**) can be "balanced" as well as "unbalanced". The receptor **c** is flexible, and it can undergo conformational change from anti (Scheme 1, right) to an *intermediate* (Scheme 1, middle) through syn (Scheme 1, left). However, this movement (conformational change) can be restricted by the number of supramolecular interactions with its surrounding anions. As shown in Figure 7a,

**Table 4. Complete List of Bond Lengths [Å] and Angles [deg] for $[C_{28}H_{24}N_4](NO_3)_2{\cdot}2H_2O$ (2·$2H_2O$)**

| | | | |
|---|---|---|---|
| N(2)−C(10) | 1.329(4) | N(1)−C(1) | 1.315(5) |
| N(2)−C(9) | 1.351(4) | N(3)−O(3) | 1.152(5) |
| N(2)−C(11) | 1.497(3) | N(3)−O(1) | 1.181(5) |
| C(6)−C(8) | 1.390(4) | C(14)−C(13)#1[a] | 1.397(4) |
| C(5)−C(4) | 1.138(5) | C(12)−C(14) | 1.384(4) |
| C(10)−N(2)−C(9) | 119.9(2) | O(3)−N(3)−O(2) | 120.6(5) |
| N(2)−C(10)−C(8) | 121.4(3) | N(1)−C(1)−C(3 | 124.9(4) |
| N(2)−C(9)−C(7) | 121.1(3) | C(12)−C(13)−C(14)#1 | 121.4(3) |
| C(1)−N(1)−C(2) | 115.1(3) | N(1)−C(1)−C(3) | 124.9(4) |
| N(1)−C(2)−C(4) | 125.1(4) | C(12)−C(14)−C(13)#1 | 119.6(3) |

[a]Symmetry transformations used to generate equivalent atoms: #1 $-x + 1$, $-y + 1$, $-z + 1$.

there are unbalanced supramolecular H-bonding interactions around the dication **c**; the unbalanced supramolecular interactions mean unequivalent interactions with respect to the central part of the molecule. This dication has two bipyridine side arms with respect to the central phenylene ring. In the case of compound **1**·(1,4-dioxane), one side arm is involved with five C−H···F hydrogen bonds, and the other side arm is involved in six C−H···F hydrogen bonds as shown in Figure 7a. These unequivalent supramolecular hydrogen-bonding interactions, called unbalanced supramolecular interactions, around **c** enable this system to adopt an unusual intermediate conformation (Scheme 1, middle). The supramolecular hydrogen-bonding interactions around **c** in compound $[C_{28}H_{24}N_4](NO_3)_2{\cdot}2H_2O$ (**2**·$2H_2O$) is shown in Figure 7b, and the hydrogen-bond data for this compound are given in Table 5. In the crystal structure of compound **2**·$2H_2O$, there are balanced/equivalent C−H···O hydrogen-bonding interactions around **c** with respect to the central phenylene ring (Figure 7b). Both side arms of **c** are hydrogen-bonded with its surrounding $NO_3^-$ anions in such a way that hydrogen-bonding force of one arm would cancel that of other arm. Thus, there is an equivalent force along all the sides of cationic receptor $[C_{28}H_{24}N_4]^{2+}$ (**c**), which implies that there is no more distortion from its usual anti-conformation. This justifies the anti-conformation of **c** in compound **2**·$2H_2O$. The anti conformation of **c** in compound **2**·$2H_2O$ and an *intermediate* conformation of **c** in compound **1** can also be corroborated by DFT calculations, Hirshfeld surface analysis, and two-dimensional (2D) finger plots, described in the succeeding sections.

**Hirshfeld Surface Analysis.** The hydrogen-bonding supramolecular interactions around the cationic receptor $[C_{28}H_{24}N_4]^{2+}$ (**c**) with surrounding associated anions are further analyzed with the Hirshfeld Surfaces (HSs) and 2D fingerprint plots (FPs),


DOI: 10.1021/acs.jpca.7b00091
J. Phys. Chem. A 2017, 121, 3274−3286

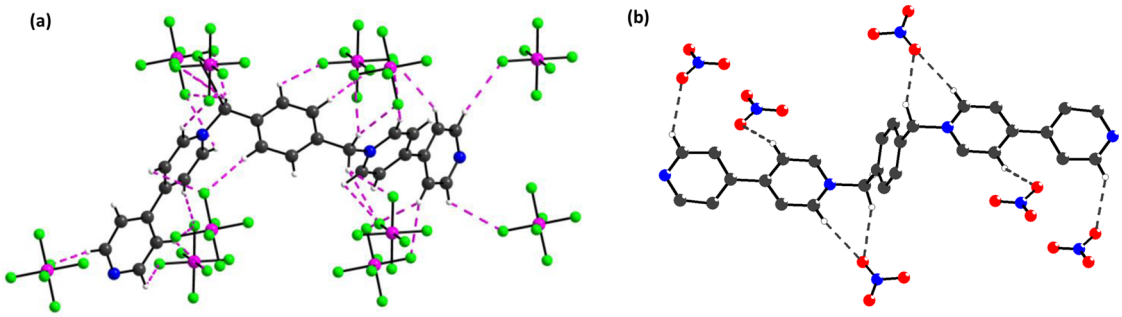


**Figure 7.** (a) Unbalanced/unsymmetrical C−H···F hydrogen-bonding interactions around the cationic receptor $[C_{28}H_{24}N_4]^{2+}$, observed in the crystal structure of compound $[C_{28}H_{24}N_4](PF_6)_2\cdot$(1,4-dioxane) (**1**·(1,4-dioxane)). (b) Balanced/symmetrical C−H···O hydrogen-bonding interactions around $C_{28}H_{24}N_4]^{2+}$, found in the crystal of compound $[C_{28}H_{24}N_4](NO_3)_2\cdot 2H_2O$ (**2**·2$H_2O$).

**Table 5. Hydrogen Bonds for Compound 2·2$H_2O$ [Å and deg]**

| D−H···A | d(D···H) | d(H···A) | d(D···A) | ∠(DHA) |
|---|---|---|---|---|
| O(4)−H(30)···O(1) | 0.98 | 2.41 | 3.199 | 136 |
| O(4)−H(30)···O(2) | 0.98 | 1.97 | 2.924 | 162 |
| C(1)−H(1)···O(3)#1[a] | 1.08 | 2.44 | 3.202 | 127 |
| C(7)−H(7)···O(3) | 1.08 | 2.44 | 3.412 | 149 |
| C(9)−H(9)···N(1)#2 | 1.08 | 2.41 | 3.443 | 158 |
| C(10)−H(10)···O(2)#3 | 1.08 | 2.37 | 3.218 | 135 |
| C(11)-H(11B)···O(2)#3 | 1.08 | 2.37 | | 147 |

[a]Symmetry transformations used to generate equivalent atoms: #1 1 + *x*, *y*, *z*; #2 3/2 + *x*, 1/2 − *y*, 1/2 + *z*; #3 3/2 − *x*, 1/2 + *y*, 1/2 − *z*.

which are generated by using the software Crystal Explorer 3.1,[32,33] based on the pertinent CIF files. Hirshfeld surfaces mapped with different properties, for example, $d_e$, $d_{norm}$, shape index, curvedness, have been proven to be an useful visualization tool for the analysis of supramolecular intermolecular interactions and crystal-packing behavior of molecules.[34,35] The three-dimensional (3D) Hirshfeld surfaces offer more insight into long- and short-range interactions, experienced by the relevant molecules, and 2D finger plots, derived from the HSs provide the nature, type, and relative contribution of the intermolecular interactions. The HSs of the present cationic receptor $[C_{28}H_{24}N_4]^{2+}$ (**c**) experience unbalanced and balanced hydrogen-bonding interactions with $PF_6^-$ and $NO_3^-$ anions in compound **1**·(1,4-dioxane) and compound **2**·2$H_2O$, respectively, that were mapped over $d_{norm}$ (−0.3 to 1.45 Å in compound **1**·(1,4-dioxane) and −0.1 to 1.4 Å in compound **2**·2$H_2O$ as shown in Figures 8 and 9, respectively; see also Figures S2 and S3 of Supporting Information for HSs mapped with the shape index and curvedness). All are the deep red spots, seen in the $d_{norm}$ surface, represent the interactions, whereas the blue spots indicate the areas without close contacts. The intensity of the red spots on the Hirshfeld Surfaces of the cationic receptor **c** in compounds **1**·(1,4-dioxane) and **2**·2$H_2O$ clearly indicate that it has been experiencing unbalanced and balanced hydrogen-bonding inteactions with $PF_6^-$ and $NO_3^-$ anions, respectively (compare Figures 8a and 9a, respectively). Among noncovalent contacts, experienced by the cationic receptor **c** in compound $[C_{28}H_{24}N_4](PF_6)_2\cdot$(1,4-dioxane) (**1**·(1,4-dioxane)), the major interactions are H···F (30.4%) and H···H (28.2%) as shown in Figure 8c (right). The relative contributions from other different interactions are calculated and given in Figure 8c (left). In the case of $[C_{28}H_{24}N_4](NO_3)_2\cdot 2H_2O$ (**2**·2$H_2O$), the dominating H···O (basically C−H···O hydrogen bonds) and H···H interactions are nearly 31.3% and 28.5%, respectively, among all other interactions as shown in Figure 9c (left).

**Computational Studies on Different Conformers of Cationic Receptor $[C_{28}H_{24}N_4]^{2+}$ (c), Compound $[C_{28}H_{24}N_4](PF_6)_2$ (1), and Compound $[C_{28}H_{24}N_4](NO_3)_2$ (2).** In continuation of experimental work on cationic receptor **c**, we also performed the theoretical calculations to find out its conformational structures such as **c** and in compounds **1** and **2** including the stability of those conformers in gas phase. It is found that its anti conformer ($E_{elec}$ = −1299.971 88 au) is more stable by ∼1.65 kcal/mol than its syn conformer ($E_{elec}$ = −1299.969 26 au). The atom numbering is shown to the respective figures to facilitate the discussion. The conformers of the compounds and the atom numbering are made by GaussView5 software.[36] The *x*,*y*,*z* coordinates of the anti and syn conformers of the cationic receptor **c** at its ground-state energy-minimized structure are given in Tables S5 and S6 in the section of Supporting Information. The structures of the other conformers of **c** around the 1N-24C-52C-29N dihedral angle are shown in Figure 10. The energy-profile diagram corresponding to these different dihedral angles is shown in Figure 11. The structures of different conformers are optimized at the interval of 20° dihedral angle. It is found that anti-conformer with 1N-24C-52C-29N dihedral angle of −180° is the most stable conformer than the other conformers, whereas syn conformer is the least-stable conformer. Energy of the intermediate conformers rises very steeply from −180° to −240° and from −180° to −120°, 1N-24C-52C-29N dihedral angle, whereas the steepness of the curve decreases in both sides, after the above-mentioned range of dihedral angles (cf. Figure 11). Analysis of the energy-profile diagram (cf. Figure 11) provides the energy difference between the most-stable and least-stable structures, which is ∼3 kcal/mol. Thus, this cationic receptor $[C_{28}H_{24}N_4]^{2+}$ (**c**) is flexible to form ion pair complexes with diverse anions in a wide range of 1N-24C-52C-29N dihedral angles. We chose two different anions $PF_6^-$ and $NO_3^-$ in this study to obtain the ion-pair compounds $[C_{28}H_{24}N_4](PF_6)_2]$ (**1**) and $[C_{28}H_{24}N_4](NO_3)_2]$ (**2**), respectively; the preferable conformations of **c** (cationic receptor) in presence $PF_6^-$ anion (compound **1**) and $NO_3^-$ anion (compound **2**) are discussed here. It is found that the compound **2** always prefers to form an anti-conformation of **c** with 1N-24C-52C-29N dihedral angle of ∼167°. But in the case of compound **1**, both anti (with1N-24C-52C-29N dihedral angle of ∼180°) and syn (1N-24C-52C-29N dihedral angle of ∼8°) conformers of **c** are formed with different stabilization energy. The optimized structures of these preferred conformers


DOI: 10.1021/acs.jpca.7b00091
J. Phys. Chem. A 2017, 121, 3274−3286

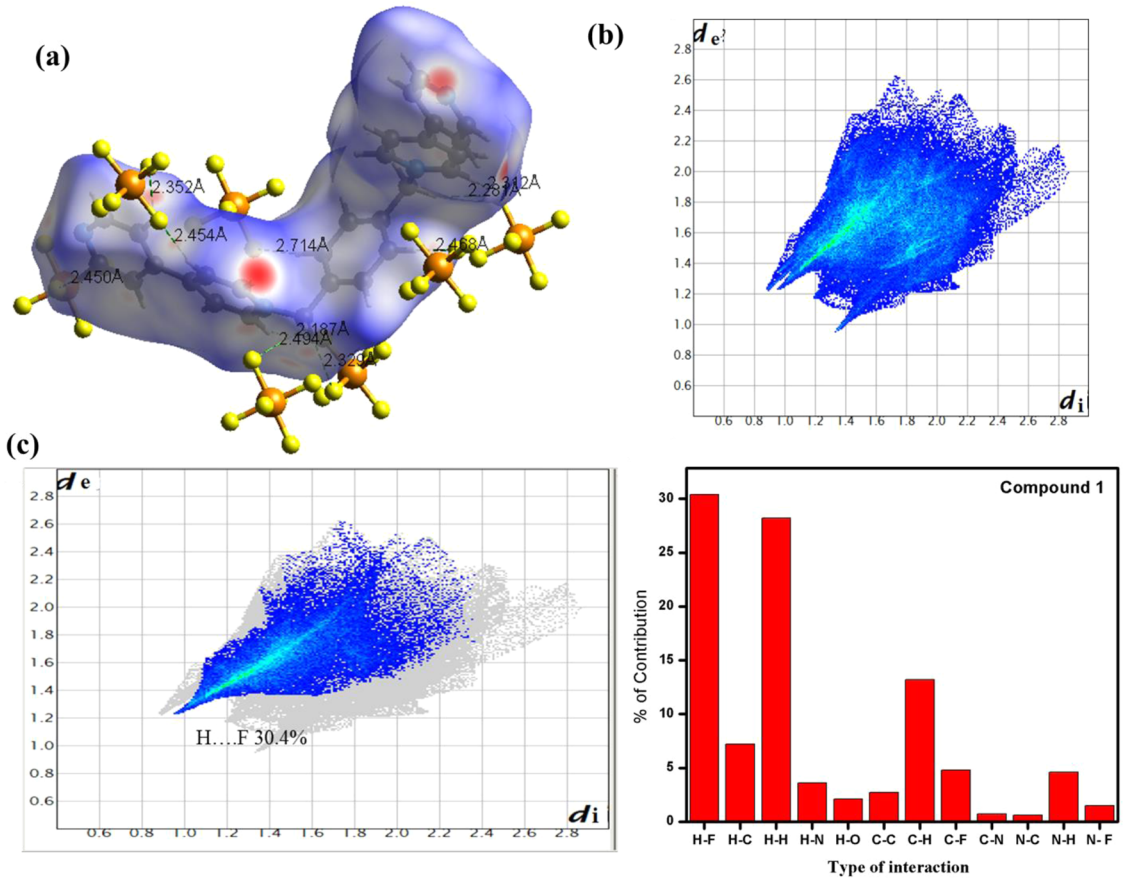


**Figure 8.** Hirshfeld surfaces mapped with (a) $d_{norm}$ ranging from −0.376 (red) to 1.441 (blue), (b) 2D fingerprint plots with $d_i$ and $d_e$ ranging from 1.0 to 2.8 Å, (c) H···F interactions (left) and percentage contribution of all other interactions around the cation (right) in compound **1**·(1,4-dioxane).

in compound **2** and in compound **1** with the H-bond indication are shown in panels (a–f) of Figure 12. Panel (a) is the anti conformer of **c** in compound **2**, and panels (b–f) are different conformers of **c** in compound **1**. The stabilization energy of the anti conformer of compound **2** is ∼229 kcal/mol, whereas the same for the anti and syn conformers of compound **1** are ∼215 and ∼230 kcal/mol, respectively. Thus, the calculations of stabilization energy indicate that the syn conformer of compound **1** is more preferable than its anti-conformer. The stabilization energies of the intermediate conformers of **c** in compound **1** are also calculated to obtain more detailed conformational analysis of compound **1**.

The calculated stabilization energies of the intermediates with 1N-24C-52C-29N dihedral angles of −120°, −90°, and −60° are ∼214, ∼215, ∼222 kcal/mol, respectively. The optimized structures of these intermediates with H-bond indication are shown in panels (c–e) of Figure 12, respectively. A graphical representation of the stabilization energies of various conformers of **c** in compound **1** with different 1N-24C-52C-29N dihedral angles is shown in Figure 13. It is seen from Figure 13 that the stabilization energy of the conformers is decreased in comparison to anti conformer (−180°) to −120° (−240°) 1N-24C-52C-29N dihedral angle, whereas an increment of stabilization energy is observed in different intermediate conformers in compound **1** in the range from −100° to 0° 1N-24C-52C-29N dihedral angle. It is noted that the stabilization energies of the conformers of Figure 13 should be differed from the actual stabilization energies calculated for −180°, −120°, −90°, −60°, and 0° 1N-24C-52C-29N dihedral angles, as the parameter 1N-24C-52C-29N dihedral angle of these conformers (cf. Figure 13) is not optimized. The above discussion on stabilization energies of different conformers of **c** in compound **1** indicates that the energy difference between the different conformers in the −100° to 0° 1N-24C-52C-29N dihedral angle range is a small amount. Thus, according to this calculation, the anion $PF_6^-$ prefers to form the ion-pair complex either with syn conformer of **c** or with an intermediate conformer of **c** (cationic receptor). A similar conformation of **c**, found in the crystal structure of **1**·(1,4-dioxane), has also been observed in the crystal structure of **c**·2$PF_6$ by K.-B. Shiu and co-workers[21] as far as relevant N···C···C···N torsion angles are concerned [98.08° for **1**·(1,4-dioxane) and 97.28° for **c**·2$PF_6$].

The HOMO and LUMO diagrams of the conformers of cationic receptor **c**, compound **1**, and compound **2** are shown in Figure 14 [panels (a, b) for cationic receptor **c**; panel (c) for compound **2**; panels (d, e) for compound **1**]. Figure 14 shows that the HOMOs of syn cationic receptor as such (Figure 14a), anti-cationic receptor as such (Figure 14b), compound **2** (Figure 14c), anti-conformer of compound **1** (Figure 14d), and syn conformer of compound **1** (Figure 14e) are stabilized by ∼75, ∼73, ∼47, ∼95, and ∼97 kcal/mol, respectively, compared to their respective LUMOs. These data indicate that the HOMO–LUMO stabilization is increased during the ion-pair complex formation of cationic receptor (**c**) with $PF_6^-$ anion, whereas the same is decreased during the ion-pair complex formation of cationic receptor (**c**) with $NO_3^-$ anion.



DOI: 10.1021/acs.jpca.7b00091
J. Phys. Chem. A 2017, 121, 3274–3286

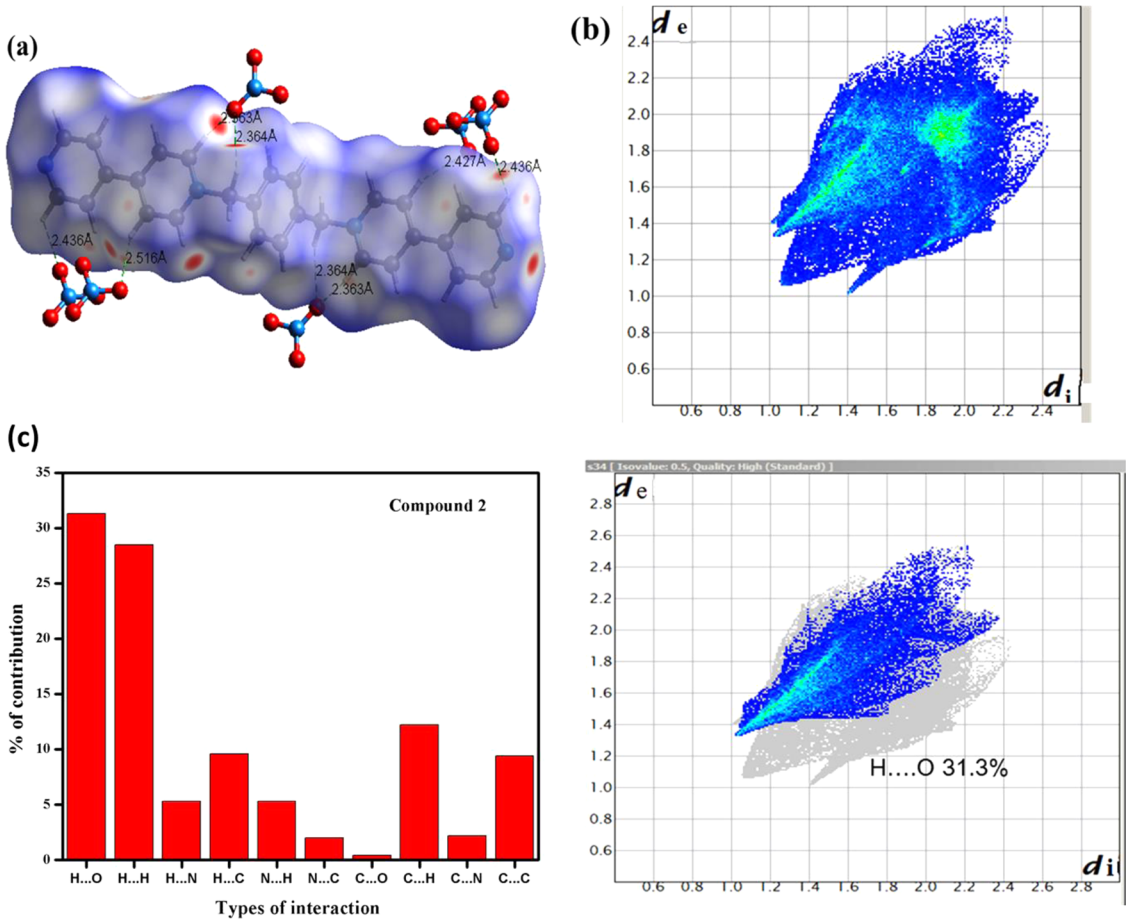


**Figure 9.** Hirshfeld surfaces mapped with (a) $d_{norm}$ ranging from −0.179 (red) to 1.360 (blue), (b) 2D fingerprint plots with $d_i$ and $d_e$ ranging from 1.0 to 2.8 Å, (c) percentage of contributions from all other interactions around the cation (left) and H···O interactions (right) in compound **2**·2$H_2O$.

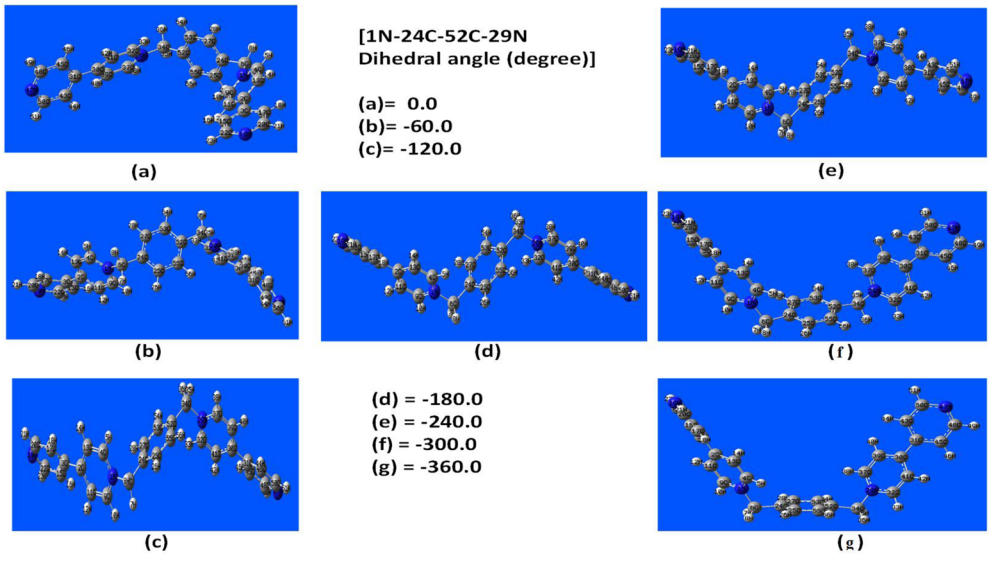


**Figure 10.** Energy-minimized structures of different conformers of cationic receptor **c**.

**Natural Bond Orbital (NBO) Analysis.** To have more insight into the stabilization of compounds **1** and **2** with respect to the conformations of receptor cation **c**, we performed the NBO analysis of the different conformers of these compounds. The results of the donor−acceptor interactions of different conformers of compound **1** and compound **2** are given in Table 6. The donor orbital ($i$), acceptor orbital ($j$), calculated second-order interaction energies between the donor−acceptor orbitals [$E^2$ ($i$,$j$)] and H-bond distances in compound **2**, and that energy in different conformers of compound **1** is given in this table. NBO analysis of compound **2** indicates that ∼60 kcal/mol stabilization energy is acquired due to the H-bond formation between the oxygen (O) lone pairs (LP) and $\sigma^*$ C−H bonds. It is found that both the $NO_3^-$ anions


DOI: 10.1021/acs.jpca.7b00091
J. Phys. Chem. A 2017, 121, 3274−3286

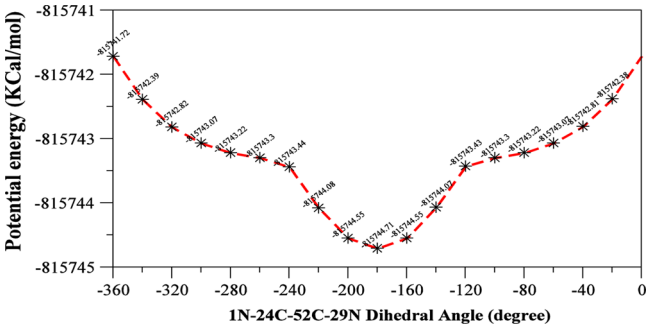


**Figure 11.** Potential-energy analysis at different 1N-24C-52C-29N dihedral angles of cationic receptor **c**.

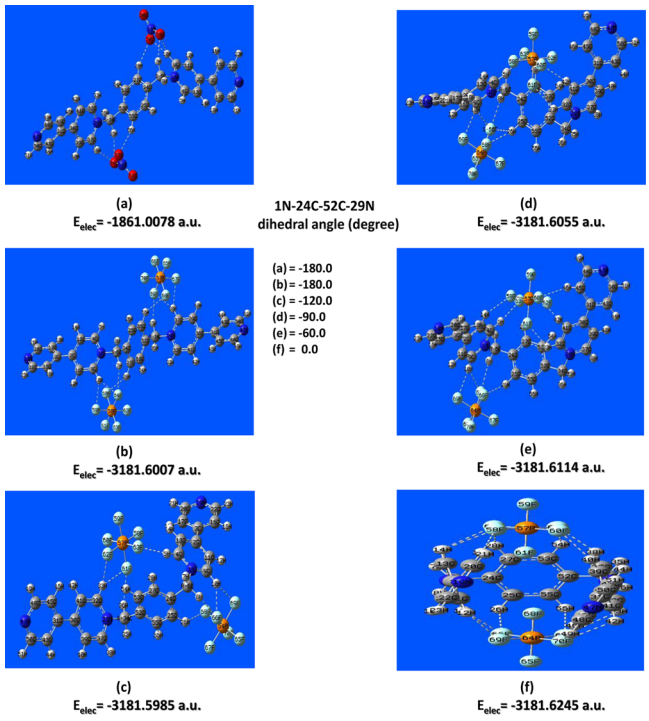


**Figure 12.** Energy-minimized structures of anti-conformer in compound **2** (a) and various conformers in compound **1** (b–f).

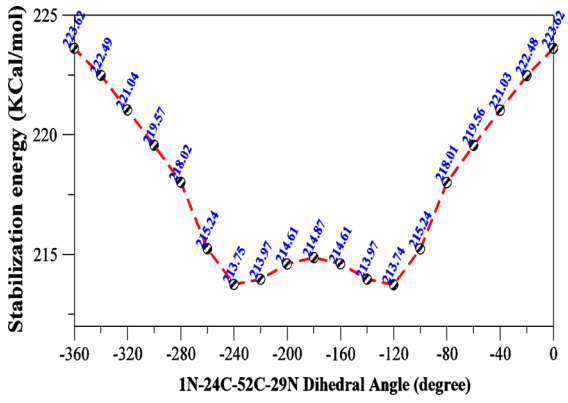


**Figure 13.** A diagram of stabilization energies at various 1N-24C-52C-29N dihedral angles in **c** in compound **1**.

interact symmetrically through H-bonds with the two bipyridine sides of the cationic receptor **c** (Figure 12a; see also Figure 7b, the experimental crystallographic evidence). That is why **c** in

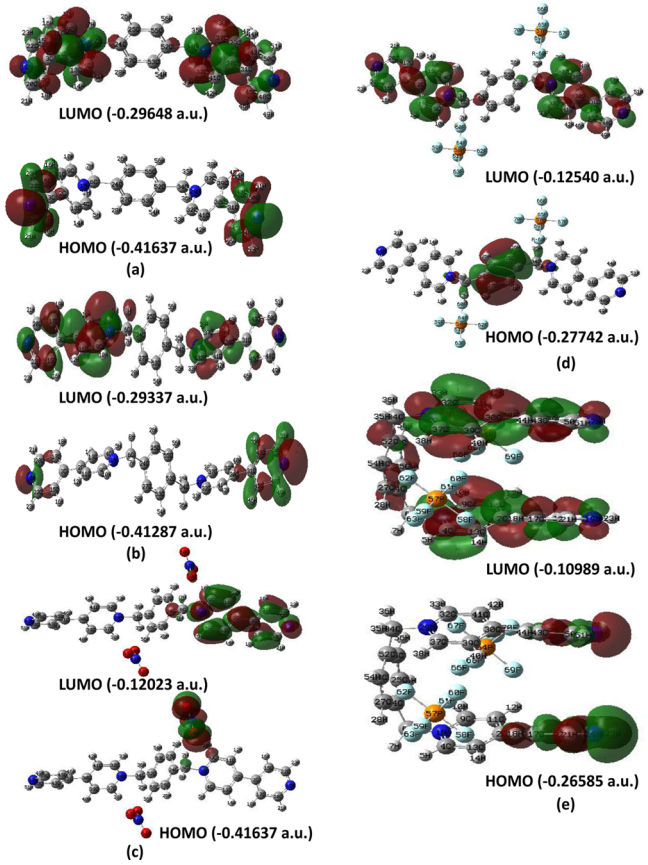


**Figure 14.** HOMO–LUMO diagrams of (a) syn conformer of cationic receptor, (b) anti conformer of cationic receptor, (c) anti conformer of compound **2**, (d) anti conformer of compound **1**, and (e) syn conformer of compound **1**.

compound **2** prefers anti conformation. On the one hand, a minute inspection of the Figure 12a and its NBO analysis indicate that the H-bond interaction between LP of 64 O and $\sigma^*$ of 37C–38H on the one bipyridine side of the cationic receptor (**c**) stabilizes the compound **2** by ∼14 kcal/mol with 1.943 Å H-bond distance. On the other hand, H-bond between LP of 58 O and $\sigma^*$ of 9C–10H on the other bipyridine side of the cationic receptor (**c**) gives the compound **2** more stability by ∼21 kcal/mol with 1.833 Å H-bond distance. These two marginally different symmetric H-bonding interactions of the two opposite bipyridine sides of the cationic receptor (**c**) make the compound **2** somewhat different orientation from the actual anti-conformation. Thus, on the one hand, the compound **2** prefers a predominantly anti-orientation with 1N-24C-52C-29N dihedral angle of ∼167° (not exactly 180°) as shown in Figure 12a. On the other hand, the different conformational orientations with 1N-24C-52C-29N dihedral angles of −180°, −120°, −90°, −60°, and −8° of compound **1** show ∼22, ∼26, ∼32, ∼36, and ∼32 kcal/mol stability, respectively, on H-bonding interactions between the LPs of different F atoms and different $\sigma^*$ C–H bonds in compound **1**. Therefore, this result (consistent with energy-minimized calculations, vide supra) also suggests that $PF_6^-$ anion prefers to form an ion-pair complex either with intermediate (−90°, −60°) or syn (−8°) orientation of the cationic receptor **c**. A symmetric H-bond formation around **c** with respect to its two bipyridine sides is observed (Figure 12b). This can be also encountered from the data given in Table 6. The H-bonding interaction between the


DOI: 10.1021/acs.jpca.7b00091
J. Phys. Chem. A 2017, 121, 3274–3286

Table 6. NBO Analysis of Some Selected Bonds of Compound 2; anti, Intermediates[a]

| donor NBO (i) | acceptor NBO (j) | stabilization energy $E^2$ (i,j) (kcal/mol) | H-bond distance (Å) |
|---|---|---|---|
| compound **2** | | | |
| 63 O [LP] | 55C-56H [BD*] | 6.55 | 2.142 |
| 64 O [LP] | 37C-38H [BD*] | 14.41 | 1.943 |
| 64 O [LP] | 34C-35H [BD*] | 7.46 | 2.136 |
| 58 O [LP] | 9C-10H [BD*] | 21.46 | 1.833 |
| 58 O [LP] | 27C-28H [BD*] | 2.99 | 2.184 |
| 59 O [LP] | 6C-7H [BD*] | 5.74 | 1.992 |
| 59 O [LP] | 9C-10H [BD*] | 1.00 | 2.376 |
| anti conformer of compound **1** | | | |
| 62 F [LP] | 27C-28H [BD*] | 1.61 | 2.225 |
| 63 F [LP] | 27C-28H [BD*] | 0.06 | 2.582 |
| 64 F [LP] | 9C-10H [BD*] | 6.07 | 2.183 |
| 67 F [LP] | 37C-38H [BD*] | 2.94 | 2.183 |
| 67 F [LP] | 39C-40H [BD*] | 0.12 | 2.804 |
| 68 F [LP] | 55C-56H [BD*] | 3.30 | 2.224 |
| 69 F [LP] | 37C-38H [BD*] | 6.07 | 2.057 |
| 69 F [LP] | 34C-35H [BD*] | 4.88 | 2.143 |
| 69 F [LP] | 55C-56H [BD*] | 0.51 | 2.583 |
| 70 F [LP] | 55C-56H [BD*] | 1.60 | 2.443 |
| intermediate conformer of compound **1** 1N-24C-52C-29*N* = −120° | | | |
| 61 F [LP] | 32C-33H [BD*] | 4.31 | 2.181 |
| 61 F [LP] | 34C-36H [BD*] | 1.99 | 2.255 |
| 62 F [LP] | 32C-33H [BD*] | 3.37 | 2.148 |
| 63 F [LP] | 4C-5H [BD*] | 2.99 | 2.222 |
| 66 F [LP] | 6C-8H [BD*] | 1.94 | 2.148 |
| 66 F [LP] | 9C-10H [BD*] | 5.03 | 2.103 |
| 68 F [LP] | 25C-26H [BD*] | 2.37 | 2.250 |
| 69 F [LP] | 9C-10H [BD*] | 3.62 | 2.164 |
| intermediate conformer of compound **1** 1N-24C-52C-29*N* = −90° | | | |
| 60 F [LP] | 4c-42H [BD*] | 3.80 | 2.217 |
| 61 F [LP] | 32C-33H [BD*] | 1.99 | 2.261 |
| 63 F [LP] | 4C-5H [BD*] | 8.13 | 2.060 |
| 66 F [LP] | 6C-8H [BD*] | 3.83 | 2.190 |
| 66 F [LP] | 9C-10H [BD*] | 5.38 | 2.080 |
| 66 F [LP] | 25C-26H [BD*] | 0.97 | 2.486 |
| 68 F [LP] | 25C-26H [BD*] | 4.70 | 2.167 |
| 69 F [LP] | 9C-10H [BD*] | 3.33 | 2.170 |
| intermediate conformer of compound **1** 1N-24C-52C-29*N* = −60° | | | |
| 58 F [LP] | 13C-14H [BD*] | 1.66 | 2.396 |
| 60 F [LP] | 4c-42H [BD*] | 4.50 | 2.162 |
| 60 F [LP] | 45C-46H [BD*] | 2.29 | 2.405 |
| 61 F [LP] | 32C-33H [BD*] | 2.46 | 2.238 |
| 63 F [LP] | 4C-5H [BD*] | 8.06 | 2.059 |
| 66 F [LP] | 9C-10H [BD*] | 5.50 | 2.078 |
| 66 F [LP] | 6C-8H [BD*] | 2.98 | 2.200 |
| 68 F [LP] | 25C-26H [BD*] | 4.56 | 2.174 |
| 69 F [LP] | 9C-10H [BD*] | 3.37 | 2.174 |
| syn conformer of compound **1** | | | |
| 58 F [LP] | 17C-18H [BD*] | 3.75 | 2.273 |
| 58 F [LP] | 13C-14H [BD*] | 1.17 | 2.367 |
| 60 F [LP] | 39C-40H [BD*] | 2.84 | 2.280 |
| 62 F [LP] | 37C-38H [BD*] | 4.96 | 2.176 |
| 62 F [LP] | 53C-54H [BD*] | 1.73 | 2.319 |
| 63 F [LP] | 4C-5H [BD*] | 0.55 | 2.532 |
| 63 F [LP] | 27C-28H [BD*] | 1.23 | 2.461 |
| 66 F [LP] | 9C-10H [BD*] | 4.92 | 2.179 |
| 66 F [LP] | 25C-26H [BD*] | 1.73 | 2.319 |
| 67 F [LP] | 32C-33H [BD*] | 0.53 | 2.545 |
| 67 F [LP] | 55C-56H [BD*] | 1.25 | 2.454 |
| 69 F [LP] | 1c-12H [BD*] | 2.87 | 2.278 |
| 70 F [LP] | 4c-42H [BD*] | 1.17 | 2.366 |
| 70 F [LP] | 45C-46H [BD*] | 3.67 | 2.277 |

[a](1N-24C-52C-29*N* = −120°, −90°, −60°) and syn conformers of compound **1**.

LP of 64F and $\sigma^*$ 9C−10H bond on the one bipyridine side and the H-bond between LP of 69F $\sigma^*$ 37C−38H bond on the other bipyridine side provide similar ∼6 kcal/mol of stabilization. Similarly, the LP of 59F and $\sigma^*$ 9C−10H bond on the one bipyridine side and the LP of 67F $\sigma^*$ 37C−38H bond on the other bipyridine side provide similar ∼3 kcal/mol of stabilization. These symmetric H-bonding interactions give the proper anti-orientation conformer of compound **1** as shown in Figure 12b. This type of symmetric H-bonding interactions is absent in other conformers of compound **1** as shown in Figures 12c−e. In the case of syn conformer of compound **1** (Figure 12f), an unbalanced symmetric H-bonding interaction is observed between the LP of 62F and $\sigma^*$ of 37C−38H bond and LP of 66F and $\sigma^*$ of 9C−10H bond. Both the H-bonding interactions stabilize the molecule by ∼5 kcal/mol and have the bond distance of 2.18 Å. The same is observed in the H-bond, initiated by LPs of 58F, 70F, 60F, and 69F atoms. These are the forces behind the stability and syn orientation of the conformer of compound **1** (Figure 12f). The NBO analysis shows that the overall H-bonding stability is highest in the conformer of compound **1** with the 1N-24C-52C-29N dihedral of −60°, an intermediate one (not −8°, syn conformer). Thus, this study also indicates that $PF_6^-$ anion prefers to form an unusual intermediate conformation of **c** or its syn conformation, whereas $NO_3^-$ anion prefers to form normal anti conformation of **c**, cationic receptor.

To validate the above discussion, we performed the equilibrium constant calculations between different conformers of cationic receptor **c** and the compound **1**. The calculated values of equilibrium constant at different temperature ($T$, kelvin) are given in Table 7. It is found that anti conformer of cationic receptor **c** is dominant than syn conformer of it at the equilibrium in the temperature range of 100−800 K. The percentage of syn conformer is increased with the temperature. The syn conformer of cationic receptor **c** occupies only 1.16% at the room temperature (300 K). Similar analysis of the conformers of compound **1** shows that syn conformer is dominant than anti conformer at their equilibrium at different temperatures (Table 7). Even at room temperature (300 K), the conversion of syn to anti is not expected to be achievable. An increment of this conversion is observed from 650 K temperature. So it is expected that the barrier of syn−anti conversion of compound **1** can be overcome at higher temperature. Similar analysis of two intermediate conformers with 1N-24C-52C-29N dihedral angle of −90° and −60° indicates that these two conformers are dominant than anti conformer of compound **1** in the respective equilibrium. The increment of this conversion with temperature is higher than the syn−anti conversion of compound **1**. An opposite scenario is observed considering the intermediate conformer with 1N-24C-52C-29N dihedral angle of −120° and anti-conformer equilibrium of compound **1**. In this case, anti-



DOI: 10.1021/acs.jpca.7b00091
J. Phys. Chem. A 2017, 121, 3274−3286

Table 7. Calculated Values of Equilibrium Constants ($K$) at Different Temperature (in Kelvin) of Different Equilibrium Existing between the Different Conformers of Cationic Receptor c and Compound 1

| temp (K) | anti c ⇌ syn c | syn1 ⇌ anti 1 | intermediate (−60°) ⇌ anti 1 | intermediate (−90°) ⇌ anti 1 | intermediate (−120°) ⇌ anti 1 |
|---|---|---|---|---|---|
| 100 | 0.000 04 | 0.000 00 | 0.000 00 | 0.000 00 | |
| 150 | 0.000 71 | 0.000 00 | 0.000 00 | 0.000 31 | 928 |
| 200 | 0.002 86 | 0.000 00 | 0.000 00 | 0.003 62 | 269 |
| 250 | 0.006 63 | 0.000 00 | 0.000 03 | 0.015 86 | 128 |
| 300 | 0.011 60 | 0.000 00 | 0.000 27 | 0.042 32 | 78 |
| 350 | 0.017 30 | 000 000 | 0.001 34 | 0.085 10 | 55 |
| 400 | 0.023 34 | 0.000 01 | 0.004 41 | 0.143 45 | 42 |
| 450 | 0.029 46 | 0.000 10 | 0.011 13 | 0.215 06 | 34 |
| 500 | 0.035 48 | 0.000 54 | 0.023 31 | 0.297 07 | 29 |
| 550 | 0.041 31 | 0.002 14 | 0.042 66 | 0.386 70 | 26 |
| 600 | 0.046 89 | 0.006 76 | 0.070 57 | 0.481 49 | 23 |
| 650 | 0.052 19 | 0.017 91 | 0.107 98 | 0.579 41 | 21 |
| 700 | 0.057 20 | 0.041 27 | 0.155 45 | 0.678 85 | 19 |
| 750 | 0.061 93 | 0.085 05 | 0.213 13 | 0.778 53 | 18 |
| 800 | 0.066 38 | 0.160 10 | 0.280 85 | 0.877 52 | 17 |

conformer is found as a dominant in the equilibrium. So the calculations of equilibrium constant between different conformers of compound **1** also suggest that the $PF_6^-$ anion prefers to form complex with cationic receptor **c** at its syn or intermediate (−90° and −60°) orientations.

## SUMMARY

An organic receptor, 1,1″-1,4-phenylene-bis(methylene)bis-4,4′-bipyridinium cation $[C_{28}H_{24}N_4]^{2+}$ (**c**), was known to be isolated as its anti as well as its syn conformations. In the present work, we have isolated this cationic receptor as an unusual intermediate conformation (neither syn nor anti) with $PF_6^-$ anion in compound $[C_{28}H_{24}N_4](PF_6)_2$·(1,4-dioxane) (**1**·(1,4-dioxane)). The energetically favored anti conformation of this organic cation has been described in its nitrate salt $[C_{28}H_{24}N_4](NO_3)_2·2H_2O$ (**2**·$2H_2O$). Both compounds are characterized by single-crystal X-ray crystallography. We have a given rationale of why an atypical intermediate conformer of the title receptor is stabilized with $PF_6^-$ anion and a typical anti form of this receptor is isolated with nitrate anion, with the help of supramolecular hydrogen-bonding interactions and Hirshfeld surface analysis.

A detailed theoretical account of the stability of the various conformers of the cationic receptor $[C_{28}H_{24}N_4]^{2+}$ (**c**), compound $[C_{28}H_{24}N_4](PF_6)_2$ (**1**), and compound $[C_{28}H_{24}N_4](NO_3)_2$ (**2**) has been discussed in this study by calculating their electronic stability, HOMO−LUMO stabilization, and NBO analysis. Final conclusion of their stability is obtained by calculation of conformational equilibrium constants at different temperatures between the conformers of the cationic receptor **c** and compound **1**. It is found that anti form of the cationic receptor **c** is more stable than its syn orientation, whereas, in the presence of $PF_6^-$ anion, it prefers syn or an intermediate (with 1N-24C-52C-29N dihedral angles of −60° and −90°) conformers. An opposite scenario of usual anti orientation of the cationic receptor **c** with little deviation is observed, when the cationic receptor **c** binds with $NO_3^-$ anion. A symmetric interaction through H bonds between the two bipyridine sides of the cationic receptor **c** and two $NO_3^-$ anions is the main cause behind the anti orientation of the compound **2**, whereas an unbalanced symmetric H-bonding interaction between the LP of F atoms ($PF_6^-$ anion) and $\sigma^*$ of C−H bonds (cationic receptor **c**) give the compound **2** unusual syn or intermediate orientation.

## ASSOCIATED CONTENT

### Supporting Information

The Supporting Information is available free of charge on the ACS Publications website at DOI: 10.1021/acs.jpca.7b00091.

Elemental analyses plots; Hirshfeld surface analysis plots; first lowest 30 four vibrational frequencies (in $cm^{-1}$) of the optimized structures of anti and syn cationic receptor **c** conformers and different conformers of compound **2** (in a tabular form); rotational constant values ($A$, $B$, $C$ in GHz) and symmetry numbers for different conformers of 2-butene, cationic receptor **c** and compound **1** (in a tabular form); rotational ($q^{rot}$) and vibrational ($q^{vib}$) partition functions values of different conformers of 2-butene, cationic receptor **c**, and compound **1** at different temperatures (in a tabular form); calculated and experimental equilibrium constants ($K$) at different temperatures (in kelvin) between *cis*-2-butene and *trans*-2-butene (in a tabular form). The $x$, $y$, $z$ coordinates of the ground-state energy-minimized structure of the different conformers of the cationic receptor **c**, compound **1**, and compound **2**, the conformational analysis of the cationic receptor **c** and compound **1** with respect to benzene torsional angle (PDF)

## AUTHOR INFORMATION


### Corresponding Author

*Phone: +91-40-2313-4853. E-mail: skdas@uohyd.ac.in. (S.K.D.)

### ORCID

Rudraditya Sarkar: 0000-0001-7915-8625

Samar K. Das: 0000-0002-9536-6579


### Notes

The authors declare no competing financial interest.

CCDC 1525549 and CCDC 1023590 contain the supplementary crystallographic data for compounds **1**·(1,4-dioxane) and **2**·$2H_2O$, respectively. Relevant crystal data can be obtained free of charge via https://www.ccdc.cam.ac.uk/conts/retrieving.html or from the Cambridge Crystallographic Data Centre, 12



DOI: 10.1021/acs.jpca.7b00091
J. Phys. Chem. A 2017, 121, 3274−3286

Union Road, Cambridge CB2 1EZ, U.K.; fax: (+44) 1223−336−033; or e-mail: deposit@ccdc.cam.ac.uk.

## ■ ACKNOWLEDGMENTS

We thank SERB, DST, Government of India, for financial support (Project No. SB/S1/IC-34/2013). We are grateful to UGC, New Delhi, for UPE-II grant. R.S. acknowledges UGC, New Delhi, India, for his doctoral fellowship. Our special thanks to Prof. S. Mahapatra, School of Chemistry, Univ. of Hyderabad, for his help in theoretical calculations and CMSD for computational facility.

## ■ REFERENCES

(1) Klärner, F.-G.; Kahlert, B. Molecular Tweezers and Clips as Synthetic Receptors. Molecular Recognition and Dynamics in Receptor−Substrate Complexes. *Acc. Chem. Res.* **2003**, *36*, 919−932.
(2) Lehn, J.-M. *Supramolecular Chemistry. Concepts and Perspectives;* VCH: Weinheim, Germany, 1995.
(3) Gallivan, J. P.; Dougherty, D. A. A Computational Study of Cation−$\pi$ Interactions vs Salt Bridges in Aqueous Media: Implications for Protein Engineering. *J. Am. Chem. Soc.* **2000**, *122*, 870−874.
(4) Prins, L. J.; Reinhoudt, D. N.; Timmerman, P. Noncovalent Synthesis Using Hydrogen Bonding. *Angew. Chem., Int. Ed.* **2001**, *40*, 2382−2426.
(5) Sinnokrot, M. O.; Valeev, E. F.; Sherrill, C. D. Estimates of the Ab Initio Limit for $\pi$−$\pi$ Interactions: the Benzene Dimer. *J. Am. Chem. Soc.* **2002**, *124*, 10887−10893.
(6) Sokolov, A. N.; Friščić, T.; MacGillivray, L. R. Enforced Face-to-Face Stacking of Organic Semiconductor Building Blocks within Hydrogen-Bonded Molecular Cocrystals. *J. Am. Chem. Soc.* **2006**, *128*, 2806−2807.
(7) Nohra, B.; Graule, S.; Lescop, C.; Réau, R. Mimicking [2,2]-Paracyclophane Topology: Molecular Clips for the Coordination-Driven Cofacial Assembly of $\pi$-Conjugated systems. *J. Am. Chem. Soc.* **2006**, *128*, 3520−3521.
(8) Meyer, E. A.; Castellano, R. K.; Diederich, F. Interactions with Aromatic Rings in Chemical and Biological Recognition. *Angew. Chem., Int. Ed.* **2003**, *42*, 1210−1250.
(9) Neelakandan, P. P.; Hariharan, M.; Ramaiah, D. Synthesis of a Novel Cyclic Donor−Acceptor Conjugate for Selective Recognition of ATP. *Org. Lett.* **2005**, *7*, 5765−5768.
(10) Kim, E.-i.; Paliwal, S.; Wilcox, C. S. Measurements of Molecular Electrostatic Field Effects in Edge-to-Face Aromatic Interactions and CH-$\pi$ Interactions with Implications for Protein Folding and Molecular Recognition. *J. Am. Chem. Soc.* **1998**, *120*, 11192−11193.
(11) Fráusto da Silva, J. J. R.; Williams, R. J. P. *The Biological Chemistry of the Elements, the Inorganic Chemistry of Life;* Oxford University Press: Oxford, England, 1991; Chapter 10.
(12) Philp, D.; Stoddart, J. F. Self-Assembly in Natural and Unnatural Systems. *Angew. Chem., Int. Ed. Engl.* **1996**, *35*, 1154−1196.
(13) Rekharsky, M. V.; Inoue, Y. Complexation Thermodynamics of Cyclodextrins. *Chem. Rev.* **1998**, *98*, 1875−1918.
(14) Collet, A.; Dutasta, J. P.; Lozach, B.; Canceill, J. Cyclotriveratrylenes and Cryptophanes:Their Synthesis and Applications to Host-Guest Chemistry and to the Design of New Materials. *Top. Curr. Chem.* **1993**, *165*, 103−129.
(15) Lee, J. W.; Samal, S.; Selvapalam, N.; Kim, H. J.; Kim, K. Cucurbituril Homologues and Derivatives: New Opportunities in Supramolecular Chemistry. *Acc. Chem. Res.* **2003**, *36*, 621−630.
(16) Warmuth, R.; Yoon, J. Recent Highlights in Hemicarcerand Chemistry. *Acc. Chem. Res.* **2001**, *34*, 95−105.
(17) Corbellini, F.; Mulder, A.; Sartori, A.; Ludden, M. J. W.; Casnati, A.; Ungaro, R.; Huskens, J.; Crego-Calama, M.; Reinhoudt, D. N. Assembly of a Supramolecular Capsule on a Molecular Printboard. *J. Am. Chem. Soc.* **2004**, *126*, 17050−17058.
(18) Harmata, M. In *Encyclopedia of Supramolecular Chemistry, Molecular Clefts and Tweezers;* Atwood, J. L., Steed, J. W., Eds.; Marcel Dekker: New York, 1997; Vol. 2, pp 887−900.
(19) Klärner, F.-G.; Panitzky, J.; Bläser, D.; Boese, R. Synthesis and Supramolecular Structures of Molecular Clips. *Tetrahedron* **2001**, *57*, 3673−3687.
(20) Fyfe, M. C. T.; Stoddart, J. F.; White, A. J. P.; Williams, D. J. Novel Clay-Like and Helical Superstructures Generated using Arene-Arene Interactions. *New J. Chem.* **1998**, *22*, 155−157.
(21) Liu, S.-A.; Kuo, T.-S.; Lee, G.-H.; Shiu, K.-B. Sensitivity in Supramolecular Architectures of Polyaromatic Salts Containing Two Singly-Pimerized Bipyridines. *J. Chin. Chem. Soc. (Weinheim, Ger.)* **2007**, *54*, 607−611.
(22) Bruker. *SADABS, SMART, SAINT, and SHELXTL;* Bruker AXS Inc.: Madison, WI, 2000.
(23) Sheldrick, G. M. *SHELX-97,* Program for Crystal Structure Solution and Analysis; University of Gottingen: Gottingen, Germany, 1997.
(24) Frisch, M. J.; Trucks, G. W.; Schlegel, H. B.; Scuseria, G. E.; Robb, M. A.; Cheeseman, J. R.; Scalmani, G.; Barone, V.; Mennucci, B.; Petersson, G. A. et al. *Gaussian 09,* Revision B.01; Gaussian, Inc.: Wallingford, CT, 2010.
(25) Li, P.; Bu, Y.; Ai, H. Density Functional Studies on Conformational Behaviors of Glycinamide in Solution. *J. Phys. Chem. B* **2004**, *108*, 1405−1413.
(26) Li, H.-Y.; Pu, M.; Liu, K.-H.; Zhang, B.-F.; Chen, B.-H. A Density-Functional Theory Study on Double-Bond Isomerization of 1-Butene to Cis-2-Butene Catalyzed by Zeolites. *Chem. Phys. Lett.* **2005**, *404*, 384−388.
(27) Justino, L. L. G.; Ramos, M. L.; Abreu, P. E.; Carvalho, R. A.; Sobral, A. J. F. N.; Scherf, U.; Burrows, H. D. Conformational Studies of Poly(9,9-dialkylfluorene)s in Solution Using NMR Spectroscopy and Density Functional Theory Calculations. *J. Phys. Chem. B* **2009**, *113*, 11808−11821.
(28) Haghdadi, M.; Farokhi, N. Density Functional Theory(DFT) Calculations of Conformational Energies and Interconversion Pathways in 1, 2, 7-Thiadiazepane. *J. Serb. Chem. Soc.* **2011**, *76*, 395−406.
(29) Szczepaniak, M.; Moc, J. Conformational Studies of Gas-Phase Ribose and 2-Deoxyribose by Density Functional, Second Order PT and Multi-Level Method Calculations: the Pyranoses, Furanoses, and Open-Chain Structures. *Carbohydr. Res.* **2014**, *384*, 20−36.
(30) Happel, J.; Hnatow, M. A.; Mezaki, R. Isomerization Equilibrium Constants of n-Butanes. *J. Chem. Eng. Data* **1971**, *16*, 206−209.
(31) Madhu, V.; Sabbani, S.; Kishore, R.; Naik, I. K.; Das, S. K. Mechanical Motion in the Solid State and Molecular Recognition: Reversible Cis−Trans Transformation of an Organic Receptor in a Solid−Liquid Crystalline State Reaction Triggered by Anion Exchange. *CrystEngComm* **2015**, *17*, 3219−3223.
(32) Brouwer, E. B.; Udachin, K. A.; Enright, G. D.; Ripmeester, J. A. Amine Guest Size and Hydrogen-Bonding Influence the Structures of -Butylcalix[4]arene Inclusions. *Chem. Commun.* **2000**, 1905−1906.
(33) Wolff, S. K.; Grimwood, D. J.; McKinnon, J. J.; Turner, M. J.; Jayatilaka, D.; Spackman, M. A. *Crystal Explorer* 3.1, 2013; University of Western Australia: Crawley, Australia; http://hirshfeldsurface.net/; CrystalExplorer.
(34) Soman, R.; Sujatha, S.; Arunkumar, C. Quantitative Crystal Structure Analysis of Fluorinated Porphyrins. *J. Fluorine Chem.* **2014**, *163*, 16−22.
(35) Titi, H. M.; Patra, R.; Goldberg, I. Exploring Supramolecular Self-Assembly of Tetraarylporphyrins by Halogen Bonding: Crystal Engineering with Diversely Functionalized Six-Coordinate Tin(L)2−Porphyrin Tectons. *Chem. - Eur. J.* **2013**, *19*, 14941−14949.
(36) Dennington, R.; Keith, T.; Millam, J. *GaussView,* Version 5; Semichem Inc.: Shawnee Mission, KS, 2009.


DOI: 10.1021/acs.jpca.7b00091
J. Phys. Chem. A 2017, 121, 3274−3286

EurJIC European Journal of Inorganic Chemistry

ChemPubSoc Europe

FULL PAPER

DOI:10.1002/ejic.201500739

# Bis(quinoxaline-dithiolato)nickel(III) Complexes $[Bu_4N][Ni^{III}(6,7\text{-qdt})_2]$ and $[Ph_4P][Ni^{III}(Ph_2 6,7\text{-qdt})_2]\cdot CHCl_3$ (6,7-qdt = Quinoxaline-6,7-dithiolate; $Ph_2$6,7-qdt = Diphenylquinoxaline-6,7-dithiolate): Synthesis, Spectroscopy, Electrochemistry, DFT Calculations, Crystal Structures and Hirshfeld Surface Analysis

**Indravath Krishna Naik,[a] Rudraditya Sarkar,[a] and Samar K. Das*[a]**

**Keywords:** Nickel / UV/Vis spectroscopy / Electrochemistry / Crystal structures / Supramolecular chemistry / ESR spectroscopy / Density functional calculations

Two bis(quinoxaline-dithiolato)nickel(III) complexes $[Bu_4N][Ni^{III}(6,7\text{-qdt})_2]$ (**1**; 6,7-qdt = quinoxaline-6,7-dithiolate) and $[Ph_4P][Ni^{III}(Ph_2 6,7\text{-qdt})_2]\cdot CHCl_3$ (**2**; $Ph_2$6,7-qdt = diphenylquinoxaline-6,7-dithiolate) have been synthesized from their $Ni^{II}$ analogues by iodine oxidation. Compounds **1** and **2** have been characterized by routine spectral analysis and single-crystal X-ray structure determination. Nickel(III) complexes **1** and **2** exhibit redshifted absorption bands compared with their $Ni^{II}$ analogues; the electronic absorption spectral studies have been corroborated by DFT calculations. Electrochemical studies on **1** and **2** are consistent with those of their $Ni^{II}$ analogues. Electron spin resonance (ESR) studies confirm that nickel is present in both **1** and **2** in its +3 oxidation state. This is also consistent with the fact that only one cation ($Bu_4N^+$ for **1** and $Ph_4P^+$ for **2**) is present in the respective crystal structures. The crystal structures of both compounds are characterized by C–H···S and C–H···N hydrogen-bonding interactions. Hirshfeld surface analyses have been studied to gain deep insight into the hydrogen-bonding interactions around/among the coordination complex anions.

## Introduction

Metal–dithiolene complexes have been of considerable interest to synthetic inorganic chemists for more than four decades. In recent years, the design and synthesis of metal–bis(dithiolene) complexes have drawn great attention because of their potential applications as conducting and magnetic,[1] nonlinear optical materials[2] and near-infrared (NIR) dyes.[3] Square-planar bis(dithiolene) metal coordination complexes are generally characterized by a high degree of delocalization within the chelate ring involving the metal ion, which contributes considerably to the low-energy electronic transition between the HOMO and the LUMO.[4] This large delocalization is responsible for metal–dithiolene complexes showing absorption bands in the near-infrared (NIR) region. In the last few years, we and others have been working on transition-metal–dithiolene coordination complexes from the perspective of supramolecular chemistry[5] as well as bioinorganic chemistry.[6] Recently, we reported on the influence of substituents of the coordinated dithiolato ligands on the electronic and electrochemical properties of a new square-planar nickel(II)–bis(quinoxaline-6,7-dithiolate) system.[7] These ligands, because of their non-innocent behaviour, can stabilize coordination complexes in several oxidation states of the pertinent metal.[4] Generally, the dianionic state ($M^{II}$ oxidation state) is the most stable state for bis(dithiolene) complexes, but in some cases they can be isolated as monoanionic ($M^{III}$ oxidation state) or even as neutral complexes ($M^{IV}$ oxidation state). $Ni^{III}$–dithiolene complexes are of special interests because of their importance in the context of bioinorganic chemistry[8] and catalysis.[9] The bioinorganic aspect of nickel(III)–dithiolene complexes is related to the modelling of the active sites of [NiFe]$H_2$ase, for which extended X-ray absorption fine structure (EXAFS)/electron paramagnetic resonance (EPR) studies indicate that the formal oxidation state of the Ni centre in the resting state of the active site is paramagnetic $Ni^{III}$.[8] The catalytic importance of $Ni^{III}$ coordination complexes can be recognized by the fact that recently nickel(III) complexes have been employed as catalysts in C–C and C–heteroatom bond-formation reactions.[9] This prompted us to explore $Ni^{III}$ coordination complexes. The present

[a] School of Chemistry, University of Hyderabad, P. O. Central University, Hyderabad 500046, India
E-mail: skdas@uohyd.ac.in
samar439@gmail.com
http://chemistry.uohyd.ac.in/~skd/

Supporting information for this article is available on the WWW under http://dx.doi.org/10.1002/ejic.201500739.

work deals with two nickel(III)–dithiolene complexes $[Bu_4N][Ni(6,7\text{-qdt})_2]$ (**1**; 6,7-qdt = quinoxaline-6,7-dithiolate) and $[Ph_4P][Ni(Ph_26,7\text{-qdt})_2]\cdot CHCl_3$ (**2**; $Ph_26,7$-qdt = diphenylquinoxaline-6,7-dithiolate). We have chosen a phenyl group as a substituent attached to the aromatic ring in compound **2** to investigate the influence of the phenyl substituent on the electronic and electrochemical properties of a bis(dithiolate)$Ni^{III}$ square-planar coordination complex (for example, compound **2**) with respect to an unsubstituted one (compound **1**). We describe here the synthesis, crystal structures, spectroscopy and electrochemistry of compounds **1** and **2**, including DFT calculations and Hirshfeld surface analyses of the complex anions.

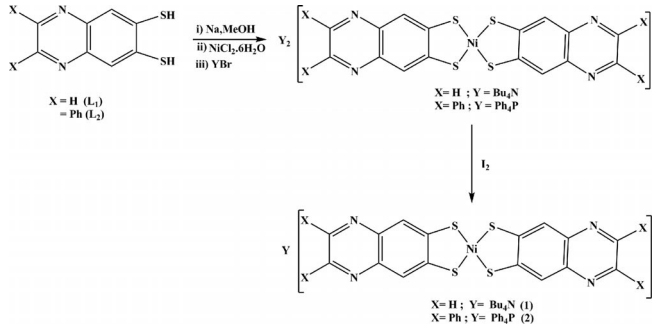


Scheme 2. Synthesis of $Ni^{III}$-bis(6,7-quinoxaline-dithiolate) compounds **1** and **2**.

## Results and Discussion

### Synthesis and General Characterization

The synthetic route for the synthesis of the two dithiolate ligands used in this study ($\mathbf{L_1}$ and $\mathbf{L_2}$) is shown in Scheme 1. The synthesis of the corresponding $Ni^{II}$–(bis)dithiolato complexes $[Bu_4N]_2[Ni^{II}(6,7\text{-qdt})_2]$ and $[Ph_4P]_2[Ni^{II}(Ph_26,7\text{-qdt})_2]$ was performed by a procedure reported earlier and shown in Scheme 2.[7] The electrochemical studies of these two $Ni^{II}$ compounds demonstrate that they can be oxidized at a low potential to the corresponding one-electron oxidized compounds $[Bu_4N][Ni^{III}(6,7\text{-qdt})_2]$ (**1**) and $[Ph_4P][Ni^{III}(Ph_26,7\text{-qdt})_2]\cdot CHCl_3$ (**2**). Accordingly, we synthesized compounds **1** and **2** by chemical oxidation of $[Bu_4N]_2[Ni^{II}(6,7\text{-qdt})_2]$ and $[Ph_4P]_2[Ni^{II}(Ph_26,7\text{-qdt})_2]$, respectively, by using iodine as shown in Scheme 2.

### UV/Vis/NIR Spectra

The UV/Vis/NIR spectra of compound **1** and its parent compound $[Bu_4N]_2[Ni^{II}(6,7\text{-qdt})_2]$ are shown in part a of Figure 1. The electronic spectra of compound **2** and its corresponding parent compound $[Ph_4P]_2[Ni^{II}(Ph_26,7\text{-qdt})_2]$ in DMF solutions are shown in part b of Figure 1. In our earlier report, we assigned the absorption bands at 619 and 662 nm for the parent $Ni^{II}$ compounds $[Bu_4N]_2[Ni^{II}(6,7\text{-qdt})_2]$ and $[Ph_4P]_2[Ni^{II}(Ph_26,7\text{-qdt})_2]$, respectively, in DMF solutions to mixed-metal-ligand-to-ligand charge-transfer transitions based on DFT calculations because relevant the HOMOs include mixed metal-ligand-based orbitals and the LUMOs were defined as ligand-based π-MOs.[7] Careful analysis of these spectra reveals the appearance of weak features beyond 800 nm, which were explained by the presence of oxidized impurities (corresponding to $Ni^{III}$ complexes), formed by oxidation with air of $[Bu_4N]_2[Ni^{II}(6,7\text{-qdt})_2]$ and $[Ph_4P]_2[Ni^{II}(Ph_26,7\text{-qdt})_2]$, which have very low oxidation potentials. Thus, when we oxidize these two $Ni^{II}$ complexes $[Bu_4N]_2[Ni^{II}(6,7\text{-qdt})_2]$ and $[Ph_4P]_2[Ni^{II}(Ph_26,7\text{-qdt})_2]$ chemically by iodine and isolated the compounds $[Bu_4N][Ni(6,7\text{-qdt})_2]$ (**1**) and $[Ph_4P][Ni(Ph_26,7\text{-qdt})_2]\cdot CHCl_3$ (**2**), we observe that the absorption bands at 619 and 662 nm for compounds $[Bu_4N]_2[Ni^{II}(6,7\text{-qdt})_2]$ and $[Ph_4P]_2[Ni^{II}(Ph_26,7\text{-qdt})_2]$, respectively, disappear. At the same time, broad bands at approximately 853 nm ($\varepsilon$ = 16320 $L\,mol^{-1}\,cm^{-1}$) and approximately 530 nm ($\varepsilon$ = 14280 $L\,mol^{-1}\,cm^{-1}$) appear for compound **1** as shown in Figure 1 (a). Similarly for compound **2**, absorption bands appear at approximately 880 nm ($\varepsilon$ = 8160 $L\,mol^{-1}\,cm^{-1}$) and approximately 554 nm ($\varepsilon$ = 12440 $L\,mol^{-1}\,cm^{-1}$) as shown in Figure 1 (b).

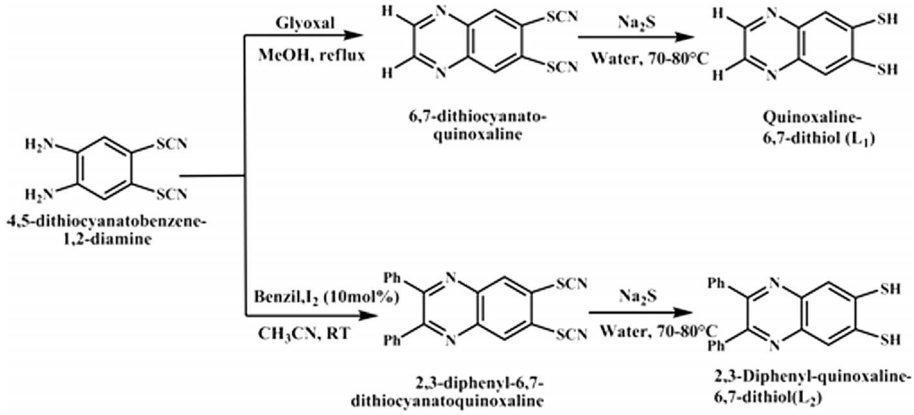


Scheme 1. Synthesis of quinoxaline dithiolate ligands $\mathbf{L_1}$ and $\mathbf{L_2}$.

 

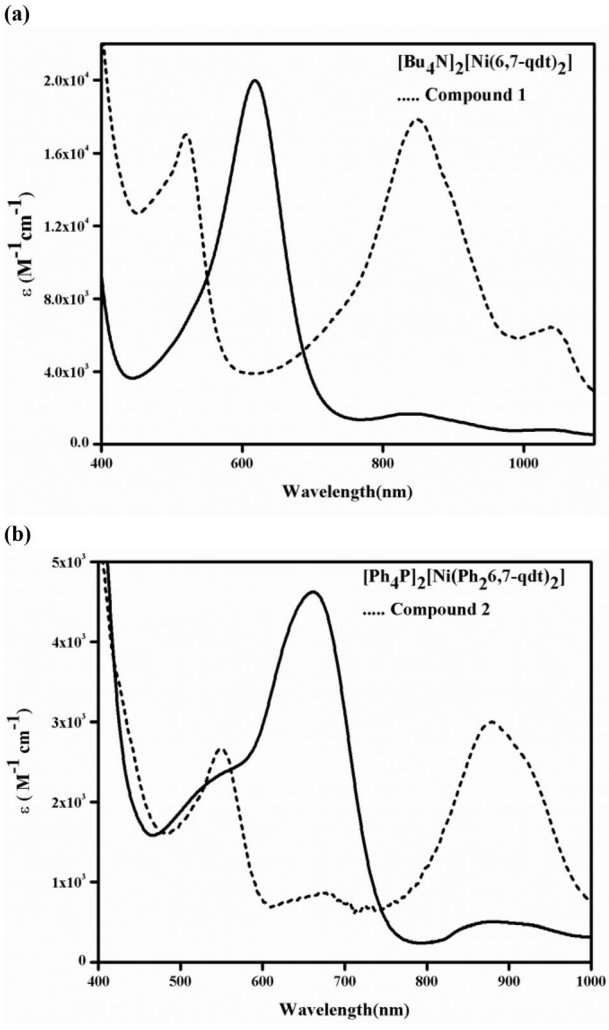


Figure 1. (a) UV/Vis/NIR spectra of compound **1** ($3.42\times 10^{-5}$ M) and corresponding parent compound $[Bu_4N]_2[Ni(6,7\text{-qdt})_2]$ ($4.64\times 10^{-5}$ M) in DMF solutions. (b) UV/Vis-NIR spectra of compound **2** ($5.4\times 10^{-5}$ M) and corresponding parent compound $[Ph_4P]_2[Ni(Ph_26,7\text{-qdt})_2]$ ($7.1\times 10^{-5}$ M) in DMF solutions.

## DFT Calculations

We performed ground-state electronic structure calculations for mono anions of compounds **1** and **2** by using density functional theory (DFT; see computational details in the Experimental Section), as implemented in the Gaussian 09 program.[10] Owing to the odd number of total electrons ($Ni^{III}$ ion, $d^7$ system), we found singly occupied α-spin HOMOs for both complex anions; at the same time, the comparable β-spin MO is vacant. The molecular orbital diagrams of the HOMOs and LUMOs of compounds **1** and **2** are given in the Supporting Information (Figures S8 and S9). Experimentally, we observed an absorption band for $[Bu_4N][Ni(6,7\text{-qdt})_2]$ (**1**) at 1060 nm. From the theoretical vertical excitation, determined by the time-dependent (TD) DFT method, this low-energy absorption band corresponds to the transition from β-spin HOMO to β-spin LUMO transition, (Figure 2, A); the theoretical value of this band is approximately 1272 nm as shown in Figure 2 (A). The low intensity of this band (Figure 1 (a), dotted line) is explained by its low oscillator strength (*f* value) of 0.0172. The second high-intensity absorption band observed for compound **1** appeared at 853 nm (Figure 1 (a), dotted line), which can theoretically be attributed to the β-spin HOMO–2 to β-spin LUMO transition as shown in Figure 2 (B). The theoretical value of this band is approximately 985 nm with a high oscillator strength of 0.2841. This transition at 853 nm (compound **1**) also contains a contribution from the transition from α-spin HOMO–6 to α-spin LUMO (Figure 1, C). The former transition (β-spin HOMO–2 to β-spin LUMO) has maximum 88% impact on the total absorption and the latter transition (α-spin HOMO–6 to α-spin LUMO, Figure 1, C) has a 12% contribution to the total absorption at 853 nm (theoretical value 985 nm). The third experimental absorption band of compound **1**, which appears at 530 nm (Figure 1 (a), dotted line), cannot be explained properly by DFT calculations, because the corresponding theoretical value (553 nm) is characterized by a poor oscillator strength (0.0001), even though the observed absorption (at 530 nm) is an intense band. The nickel ion does not have any significant role in the low-energy absorption at 1060 nm (Figure 1 (a), dotted line) of compound **1** (theoretical value 1272 nm) as shown in Figure 2 (A). Conversely, for the highly intense observed band at 853 nm (theoretical value 985 nm), the central metal (nickel) ion plays a crucial role (Figure 2, B and C). As shown in Figure 2 (B), β-spin HOMO–2 is of π-type character and β-spin LUMO is of π*-type character. We also find a contribution from the central metal (nickel) in the HOMOs (both HOMO–2 and HOMO–6) and high electron density in the π* orbitals of dithiolate ligands in the LUMOs. As both the HOMOs (Figure 2, B and C) include mixed-metal-ligand-based orbitals, we can say that the major transition (853 nm) is a "mixed-metal-ligand-to-ligand" (MMLL) charge-transfer transition.[7] Although the oxidation state of nickel in compound **1** is formally +3 (confirmed from ESR spectroscopy and electrochemical studies), electron density corresponds to the $3p_y$ atomic orbital (AO) of nickel is situated at the nickel centre in the β-spin HOMO–2 MO. All $3p_y$ AOs of the surrounding four sulfur donor atoms (all sulfur atoms have positive MO coefficients) and the central nickel $3p_y$ AO form a linear combination to create the π-bonding-type β-spin HOMO–2 (Figure 2, B). Owing to the participation of both ligand (sulfur donor) and metal (nickel) AOs, the present calculated HOMO is described as a mixed-metal-ligand-type of MO. In the case of the π*-type β-spin LUMO, the same AOs of sulfur (two sulfur atoms have positive MO coefficients and the other two sulfur atoms have negative MO coefficients) form the antibonding-type MO, where no contribution from the nickel atom is found. Thus, this LUMO is characterized only by ligand AOs. As a result, the overall transition, shown in Figure 2 (B), can be depicted as a "mixed-metal-ligand-to-ligand" transition.

Next, we concentrated our focus on $[Ph_4P][Ni(Ph_26,7\text{-qdt})_2]$ (**2**). A noticeable redshift of the most intense peak is observed in case of compound **2** compared with that of

 

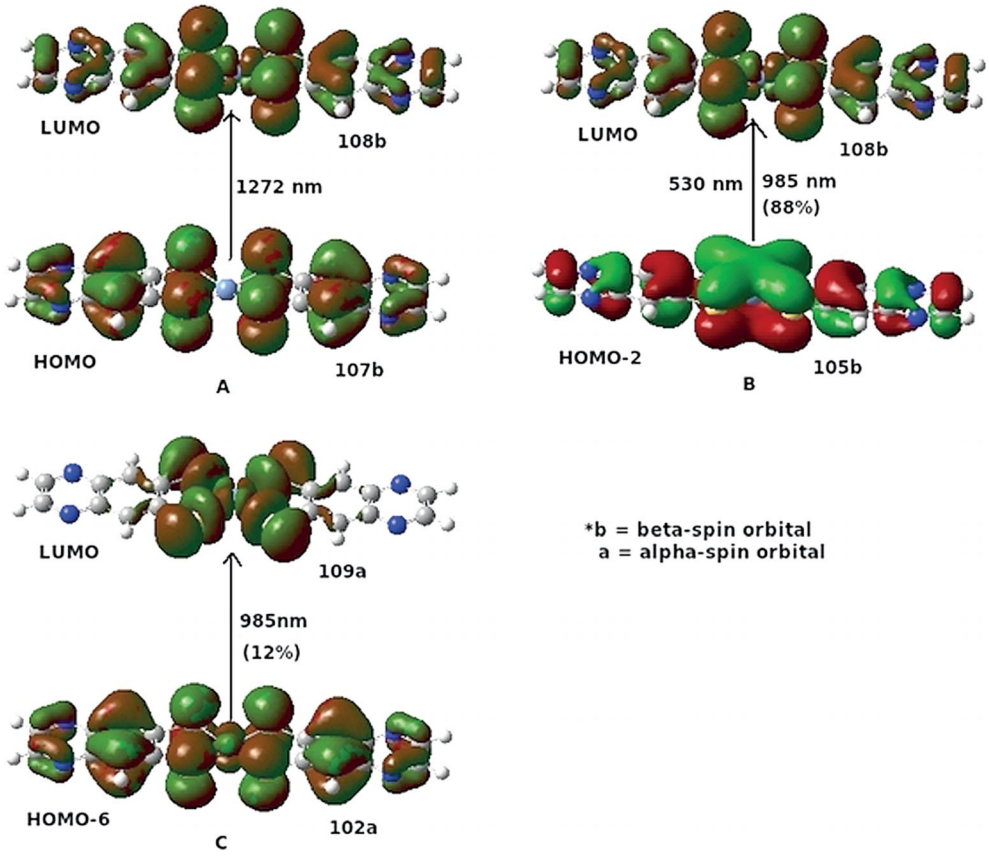


Figure 2. HOMO and LUMO diagrams originating from molecular orbital calculations for the mono anion of compound **1**.

$[Bu_4N][Ni(6,7\text{-qdt})_2]$ (**1**). Experimentally, the most intense absorption band is observed at 880 nm for compound **2**, which is 30 nm from the most intense peak of compound **1**. The theoretical value of this observed band at 880 nm is 1071 nm with an *f* value of 0.4736. This theoretical peak is attributed mainly to the transition from β-spin HOMO–3 to β-spin LUMO (Figure 3, A), which contributes 80% to the total observed absorption band at 880 nm. The rest of the contribution arises from β-spin HOMO–5 to β-spin LUMO (11%, Figure 3, B) and α-spin HOMO–7 to α-spin LUMO (9%, Figure 3, C) transitions. The other major absorption of compound **2**, for which the observed (554 nm) as well as theoretical (553 nm) values are almost identical, is attributed to the transition from β-spin HOMO–5 to β-spin LUMO, which contributes 54% to the total absorption at 554 nm (Figure 3, B), and also takes part in the absorption at 880 nm as mentioned earlier. As shown in Figure 3, A and C, it is clear that the maximum electron density cloud is situated around the central metal ion, nickel, which indicates that central metal ion has considerable contribution to the electronic absorption at 880 nm (compound **2**). Lateral overlap in HOMO–3 (Figure 3, A) indicates that it has a π-bonding nature (mixed-metal-ligand π orbitals), whereas the corresponding LUMO is ligand-based and π* in nature. Therefore, in the case of compound **2**, the major absorption at 880 nm can be assigned to "mixed-metal-ligand-to-ligand" (MMLL) charge-transfer transitions.[7] As observed in compound **1**, a similar scenario of linear combination of AOs is also observed in the case of compound **2**, where the $3p_z$ AOs of both nickel and sulfur are the participating orbitals.

It has already been mentioned that the most intense absorption band is observed at 880 nm for $[Ph_4P][Ni(Ph_26,7\text{-qdt})_2]\cdot CHCl_3$ (**2**), which is around 30 nm redshifted from the most intense peak (853 nm) of $[Bu_4N][Ni(6,7\text{-qdt})_2]$ (**1**). As we go from compound **1** to compound **2**, two phenyl groups per ligand are added as substituents, replacing two protons (Scheme 2). Particular substituents on an aromatic system can lead to mesomeric as well as inductive effects. The mesomeric effect arises from the delocalization of π-electrons between the substituent and aromatic core. On the other hand, the inductive effect is fully associated with the σ-electron system of the aromatic ring. In the case of $[Ph_4P][Ni(Ph_26,7\text{-qdt})_2]\cdot CHCl_3$ (**2**), both mesomeric and inductive effects are to be considered. This is because the substituted phenyl group (compound **2**) can be involved in both these effects. The inductive effect can be initiated by an electron-withdrawing substituent or by an electron-donating substituent. In the present study (compound **2**), the phenyl substituent acts as an electron-withdrawing group, which can be established from the following discussion. An electron-withdrawing group pulls the σ-electron density from the ligand by the inductive effect; thereby, reducing the repulsive Coulombic interactions between the electrons occupying the ligand-localized π-MOs and the electrons of the σ-system. Thus, an electron-withdrawing substituent in the

 

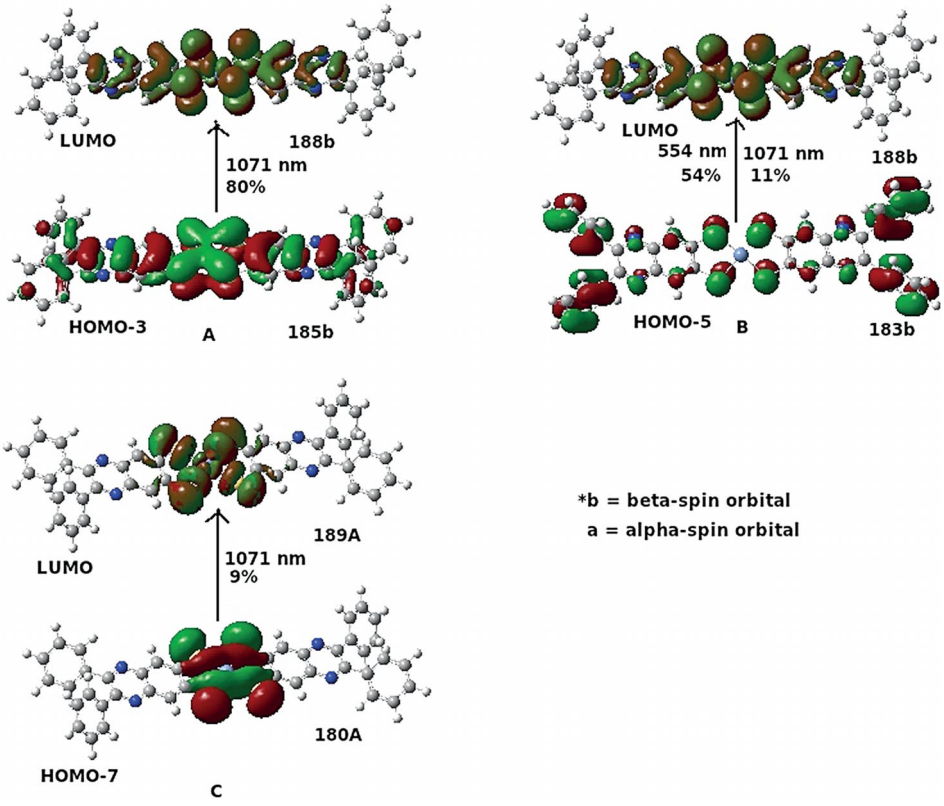


Figure 3. HOMO and LUMO diagrams originating from molecular orbital calculations for the mono anion of compound **2**.

present system causes a lowering of the energy of the LUMOs (because these are purely π-MO of the dithiolate ligand, Figures 1 and 2) without lowering the energy of the HOMOs significantly (because they are a mixture of nickel d-orbital character and dithiolate π-type orbitals). This should cause a redshift in the relevant electron absorption spectra (the energy gap between HOMO and LUMO would essentially be decreased). Conversely, an electron-releasing substituent in the present system would cause a blueshift in the electronic absorption spectra because the energy gap between the HOMO and LUMO would essentially be increased (an electron-donating group increases the electron density toward the dithiolate ligand and thereby increases the repulsive Columbic interactions between the ligand centred π-MOs and σ-electrons). Therefore, in the case of compound **2**, the substituent phenyl group acts as an electron-withdrawing group and causes the redshift of 30 nm in the pertinent electron absorption spectra when we go from compound **1** (no substituent) to compound **2** (phenyl group as a substituent).

In the case of the mesomeric effect, the substituent phenyl group (compound **2**) can share its π-electrons with the aromatic core associated with the dithiolato ligand by resonance. The prevalence of mesomeric effects in the present system is supported by DFT calculations. When we compare parts A and C in Figure 3 with parts B and C in Figure 2, we find relatively more electron density at the central metal ion in compound **2** (where the phenyl substituent exerts a mesomeric effect by resonance) in comparison to that at the central metal ion in compound **1** (where there is no substituent in place of hydrogen). The higher electron density at the central metal ion makes electronic transitions easier in the case of compound **2**, which probably causes the redshift of the more intense band compared with compound **1**. Thus, both inductive and mesmeric effects are responsible for this redshift, which is consistent with DFT calculations.

As shown in Figure 1 (a and b), the major electron absorption bands for $Ni^{III}$ complexes (compounds **1** and **2**) appear in redshifted regions compared with their parent $Ni^{II}$ analogues $[Bu_4N]_2[Ni^{II}(6,7\text{-qdt})_2]$ and $[Ph_4P]_2[Ni^{II}(Ph_2 6,7\text{-qdt})_2]$. Compounds **1** and **2** are one-electron oxidized products of their $Ni^{II}$ parent compounds $[Bu_4N]_2[Ni^{II}(6,7\text{-qdt})_2]$ and $[Ph_4P]_2[Ni^{II}(Ph_2 6,7\text{-qdt})_2]$. When compound $[Bu_4N]_2[Ni^{II}(6,7\text{-qdt})_2]$ is oxidized by iodine to its $Ni^{III}$ analogue (compound **1**), the electronic absorption band at 619 nm (parent $Ni^{II}$ compound) shifts to 853 nm (compound **1**). Similarly, when compound $[Ph_4P]_2[Ni^{II}(Ph_2 6,7\text{-qdt})_2]$ is oxidized by iodine to its $Ni^{III}$ form (compound **2**), the major electronic absorption band at 662 nm (parent $Ni^{II}$ compound) moves to 880 nm (compound **2**).

This large redshift (234 nm for compound **1** and 218 nm for compound **2**) of the major electronic absorption bands on going from $Ni^{II}$ to $Ni^{III}$ complexes can be attributed to the central metal ion, nickel, which, in its +3 oxidation state, pulls the σ-electron density from the coordinated dithiolate ligand and reduces the repulsion-type Coulombic interactions between the electrons in the σ-system and elec-

 

trons occupying the ligand-localized π-MOs. This causes the lowering of the energy of the LUMOs (purely π-MOs of the dithiolate ligand, see Figures 2 and 3) without lowering the energy of the HOMOs (mixed-metal-ligand π orbitals, Figures 2 and 3), resulting in the decrease in the energy gap between the HOMO and LUMO. This explains the large redshift in the electronic absorption maxima when the $Ni^{II}$ complex is oxidized to its $Ni^{III}$ analogue. Theoretically simulated absorption spectra for the $Ni^{III}$ complex anions of **1** and **2** are displayed in the Supporting Information (Figures S10 and S11).

### Electron Spin Resonance (ESR) Spectra

The ESR spectra of solid samples of $[Bu_4N][Ni^{III}(6,7\text{-qdt})_2]$ (**1**) and $[Ph_4P][Ni^{III}(Ph_2 6,7\text{-qdt})_2]\cdot CHCl_3$ (**2**) were recorded at room temperature and 123 K. The ESR spectra recorded at 123 K are presented in Figure 4. Compound **1** exhibits a rhombic-type signal: $g_x = 2.246$, $g_y = 2.156$ and $g_z = 2.065$. However, compound **2** shows an axial signal with $g_\perp > g_\parallel$: $g_\perp = 2.133$ and $g_\parallel = 2.049$. This is consistent with low-spin $Ni^{III}$ ($d^7$, $S = 1/2$) in a tetragonal geometry ($g_\perp > g_\parallel$) with one unpaired electron in the $d_{z^2}$ orbital.[11] The anisotropy in the ESR spectra implies some contribution from the d orbital of nickel to the total spin density, which is consistent with DFT calculations (see above). The ESR data suggest that the unpaired electrons in compounds **1** and **2** are not localized on the ligands because the ESR spectra do not show any sharp signal near $g = 2.003$ (an organic ligand radical usually shows a sharp signal at $g = 2.003$). The present ESR data and their comparison with those of already known mononuclear $Ni^{III}$ square-planar complexes[11] confirm that compounds **1** and **2** are formally $Ni^{III}$ complexes. The rhombic ESR feature (compound **1**) is not unusual for a square-planar $Ni^{III}$ complex because of distortion from the square-planar geometry. However, compound **2** exhibits an axial feature in its ESR spectrum, even though both complexes are square planar. It can be speculated that the presence of a solvent molecule ($CHCl_3$) in the crystal lattice of compound **2** might have made this difference. A square-planar bis(dithiolato)–$Ni^{III}$ complex showing an axial ESR feature is known.[12]

### Electrochemistry

We mentioned in our earlier report[7] that the parent compounds $[Bu_4N]_2[Ni^{II}(6,7\text{-qdt})_2]$ and $[Ph_4P]_2[Ni^{II}(Ph_2 6,7\text{-qdt})_2]$ of the present $Ni^{III}$ compounds $[Bu_4N][Ni^{III}(6,7\text{-qdt})_2]$ (**1**) and $[Ph_4P][Ni^{III}(Ph_2 6,7\text{-qdt})_2]\cdot CHCl_3$ (**2**) undergo reversible oxidation at very low oxidation potentials in MeOH solutions: $[Bu_4N]_2[Ni^{II}(6,7\text{-qdt})_2]$ undergoes oxidation at $E_{1/2} = +0.12$ V versus Ag/AgCl ($\Delta E = 74$ mV), corresponding to the $[Ni^{III}(6,7\text{-qdt})_2]^{1-}/[Ni^{II}(6,7\text{-qdt})_2]^{2-}$ redox couple, and $[Ph_4P]_2[Ni^{II}(Ph_2 6,7\text{-qdt})_2]$ undergoes oxidation at $E_{1/2} = +0.033$ V versus Ag/AgCl ($\Delta E = 65$ mV), corresponding to the $[Ni^{III}(Ph_2 6,7\text{-qdt})_2]^{1-}/[Ni^{II}(Ph_2 6,7\text{-qdt})_2]^{2-}$ couple. In the present study, we could not perform electrochemical studies in MeOH owing to low solubility. Compounds **1** and **2** are not freely soluble in MeOH. We, thus, performed the cyclic voltammetric studies of compounds **1** and **2** in DMF solutions, each containing 0.10 M $[Bu_4N]ClO_4$ as the supporting electrolyte. As shown in Figure 5, cyclic voltammograms of compounds **1** and **2** exhibit quasi-reversible reductive responses at $E_{1/2} = +0.225$ V versus Ag/AgCl ($\Delta E = 87$ mV) and $E_{1/2} = +0.044$ V versus Ag/AgCl ($\Delta E = 82$ mV), respectively. Based on the $E_{1/2}$ values of the oxidative responses of the $Ni^{II}$ analogues $[Bu_4N]_2[Ni^{II}(6,7\text{-qdt})_2]$ and $[Ph_4P]_2[Ni^{II}(Ph_2 6,7\text{-qdt})_2]$ in MeOH[7] as well as in DMF (see the Supporting Information), we can assign these reductive responses of compounds **1** and **2** to the $[Ni^{III}(6,7\text{-qdt})_2]^{1-}/[Ni^{II}(6,7\text{-qdt})_2]^{2-}$ and $[Ni^{III}(Ph_2 6,7\text{-qdt})_2]^{1-}/[Ni^{II}(Ph_2 6,7\text{-qdt})_2]^{2-}$ couples, respectively.

The lower reduction potential value (+0.044 V) for the $[Ni^{III}(Ph_2 6,7\text{-qdt})_2]^{1-}/[Ni^{II}(Ph_2 6,7\text{-qdt})_2]^{2-}$ couple (compound **2**) compared with that for the $[Ni^{III}(6,7\text{-qdt})_2]^{1-}/[Ni^{II}(6,7\text{-qdt})_2]^{2-}$ couple (compound **1**; +0.225 V) can be explained by the inductive effect of the phenyl substituents, which pull electrons from the metal–dithiolate chelate and,

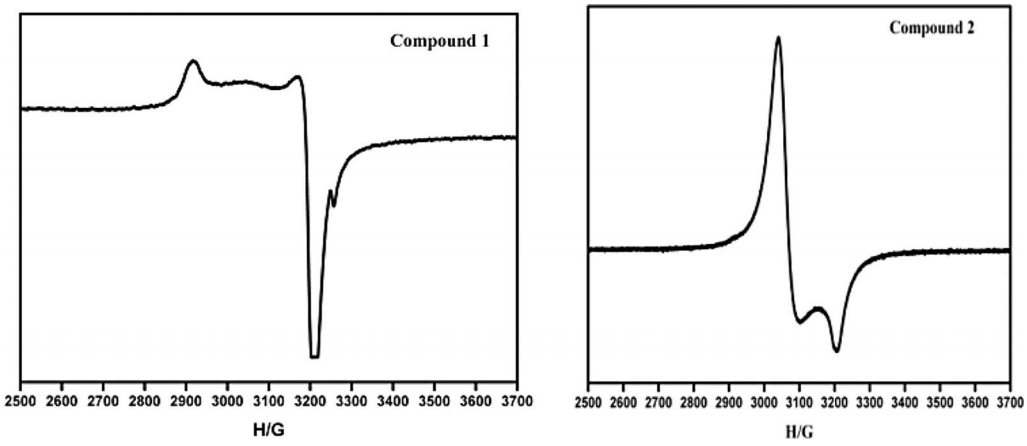


Figure 4. Electron spin resonance spectra of the compounds **1** (left) and **2** (right) in their powder form at 123 K.

 

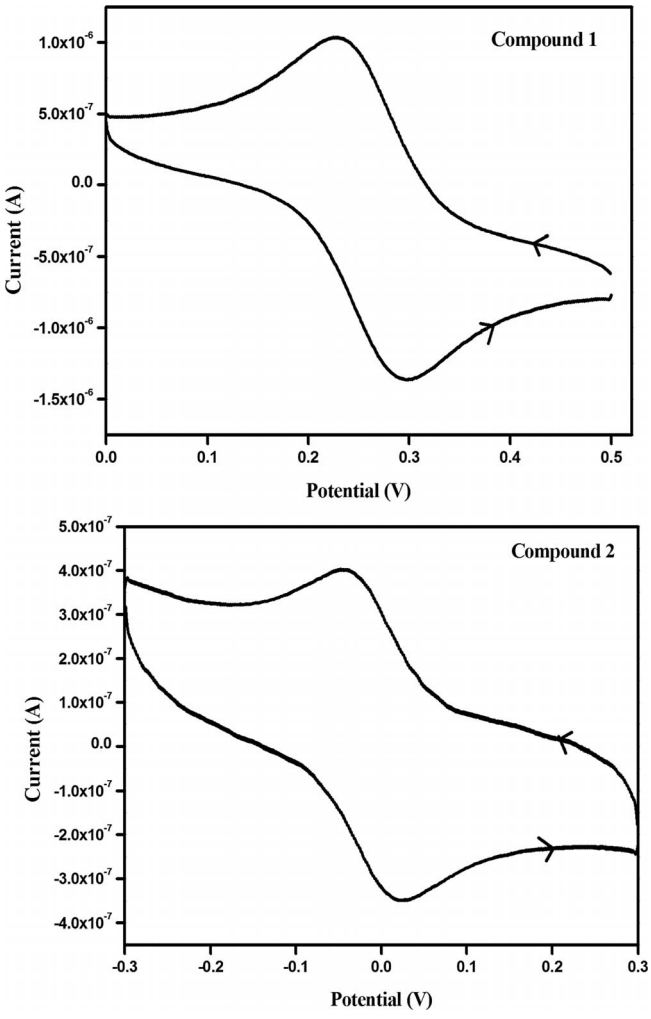


Figure 5. Cyclic voltammograms of compounds **1** (top) and **2** (bottom) in DMF solution. Scan rate=0.01 mV $s^{-1}$, V vs. Ag/AgCl.

thus, the relevant metal centre would be more easily reduced. The low reduction potential value of compound **2** compared with that of compound **1** can also be justified from the perspective of theoretical calculations, which show that the energy gap between the HOMO and LUMO is less in the case of compound **2** compared with that of compound **1**. In both cases (compounds **1** and **2**), the lowest unoccupied orbital is the β-spin LUMO (see above). If the system is reduced by one electron, the electron has to occupy the β-spin LUMO, which is more stabilized in the case of compound **2** (HOMO–LUMO gap is smaller). Thus, compound **2** would be reduced more easily (+0.044 V) than compound **1** (+0.225 V).

ESR spectroscopy (see above) and single-crystal X-ray crystallography (see below) indicate that the isolated compounds **1** and **2** have nickel in its +3 oxidation state. Keeping this in mind, during the cyclic voltammetric experiments, we took the first scans starting from the positive side (+0.5 V for compound **1** and +0.3 V for compound **2**) and we found first reduction followed by oxidation in the respective cyclic voltammograms (shown by arrows, Figure 5). Thus, the electrochemical experiments clearly point out that the oxidation state of nickel in the isolated compounds **1** and **2** is +3.

## Description of Crystal Structures

### $[Bu_4N][Ni\ (6,7\text{-}qdt)_2]$ (1)

The crystals of compound **1** suitable for single-crystal X-ray structure determination were obtained from acetonitrile solution by the vapour diffusion of diethyl ether. Crystallographic analysis revealed that compound **1** crystallizes in a monoclinic system with space group $P2_1/c$. The relevant asymmetric unit contains two crystallographically independent halves of the $[Ni(6,7\text{-}qdt)_2]^{1-}$ molecule and one tetrabutylammonium cation. The thermal ellipsoid diagram of the asymmetric unit in the crystal structure of compound **1** is shown in Figure 6 (a). The relevant molecular packing diagram is shown in Figure 6 (b). The basic crystallographic data for compound **1** are presented in Table 1 and selected bond angles and interatomic distances are described in Table 2. The geometry around nickel ion in both the crystallographically independent complexes is roughly square planar, consisting of four sulfur donor atoms from two 6,7-$qdt^{2-}$ dithiolato ligands. The relevant coordination angles are in the range 87.77(3)–92.23(3)° (Table 2). In the five-membered chelate rings involving the nickel ion, the Ni–S, C–S and C=C bond lengths are in the range 2.1431(7)–

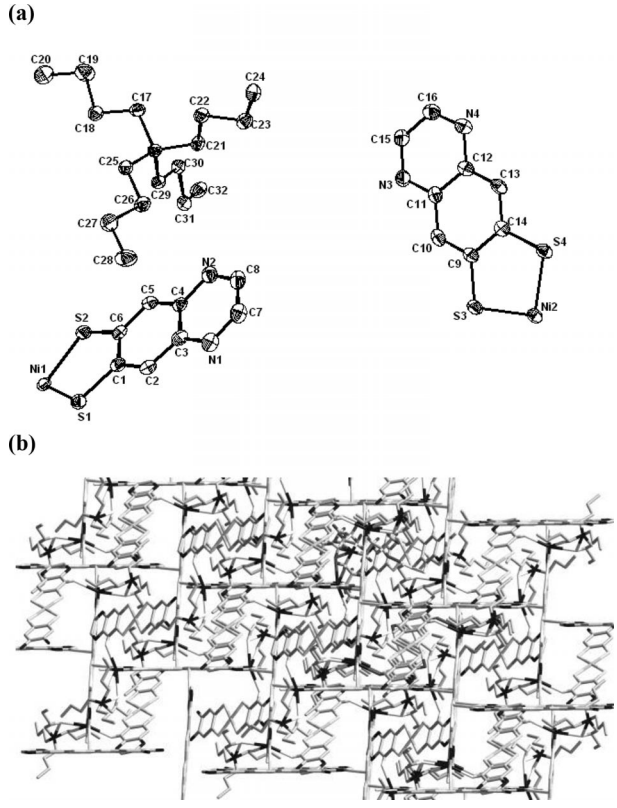


Figure 6. (a) Thermal ellipsoid plot (at the 50% probability level) of the asymmetric unit in the crystal structure of compound **1** (hydrogen atoms are omitted for clarity). (b) Molecular packing diagram for the crystal structure of compound **1**.

 

2.1555(7), 1.737(3)–1.746(3) and 1.423(4)–1.426(4) Å, respectively. The total charge of the $Ni^{III}$ complex anion $[Ni(6,7\text{-qdt})_2]^{1-}$ in compound $[Bu_4N][Ni(6,7\text{-qdt})_2]$ (**1**) is, unsurprisingly, –1, and this anionic charge is compensated by a $[Bu_4N]^+$ cation as observed in the crystal structure (Figure 6).

Table 1. Crystal data and structural refinement parameters for compounds **1** and **2**.

| | **1** | **2** |
|---|---|---|
| Empirical formula | $C_{32}H_{44}N_5NiS_4$ | $C_{65}H_{45}Cl_3N_4NiPS_4$ |
| Formula weight | 685.67 | 1206.32 |
| Temperature [K] | 100(2) | 100(2) |
| Crystal size [mm] | 0.20 × 0.12 × 0.08 | 0.21 × 0.18 × 0.12 |
| Crystal system | monoclinic | triclinic |
| Space group | $P2_1/c$ | $P\bar{1}$ |
| $Z$ | 4 | 2 |
| Wavelength [Å] | 0.71073 | 0.71073 |
| $a$ [Å] | 13.8384(9) | 13.294(10) |
| $b$ [Å] | 11.6926(8) | 15.018(12) |
| $c$ [Å] | 22.4558(12) | 15.677(12) |
| $\alpha$ [°] | 90 | 70.818(12) |
| $\beta$ [°] | 113.333 | 80.368(12) |
| $\gamma$ [°] | 90 | 84.916(13) |
| Volume [Å$^3$] | 3336.3(4) | 2913 |
| Calculated density [Mg m$^{-3}$] | 1.365 | 1.375 |
| Reflections collected/unique | 33936/6533 | 10208/6861 |
| $R$(int) | 0.0548 | 0.13 |
| $F$(000) | 1452 | 1242 |
| Max. and min. transmission | 0.9342 and 0.8465 | 0.922 and 0.8693 |
| $\Theta$ range for data collection [°] | 1.70–26.48 | 1.39–26.18 |
| Refinement method | full-matrix least-squares on $F^2$ | |
| Data/restraints/parameters | 6533/0/386 | 10208/0/706 |
| Goodness-of-fit on $F^2$ | 1.131 | 1.252 |
| $R_1/wR_2$ [$I > 2\sigma(I)$] | 0.0488/0.1029 | 0.1335/0.3135 |
| $R_1/wR_2$ (all data) | 0.0576/0.1069 | 0.1719/0.3319 |
| Largest diff. peak and hole [e Å$^{-3}$] | 0.548 and –0.281 | 1.275 and –0.944 |

Table 2. Selected bond lengths [Å] and angles [°] for compounds **1** and **2**.

| Compound 1[a] | | | |
|---|---|---|---|
| Ni(1)–S(1)#1 | 2.1431(7) | Ni(1)–S(2)#1 | 2.1442(7) |
| Ni(2)–S(3)#2 | 2.1555(7) | Ni(2)–S(4)#2 | 2.1473(7) |
| S(1)#1–Ni(1)–S(1) | 180.00(4) | S(1)–Ni(1)–S(2) | 92.23(3) |
| S(1)#1–Ni(1)–S(2) | 87.77(3) | S(4)–Ni(2)–S(3) | 92.16(3) |
| S(4)–Ni(2)–S(3)#2 | 87.85(3) | S(3)–Ni(2)–S(3)#2 | 180.00(4) |
| C(1)–S(1)–Ni(1) | 105.26(10) | C(6)–S(2)–Ni(1) | 105.33(10) |
| C(9)–S(3)–Ni(2) | 104.95(10) | C(14)–S(4)–Ni(2) | 104.92(10) |
| Compound **2**[b] | | | |
| Ni(1)–S(3) | 2.126(3) | Ni(1)–S(4) | 2.129(3) |
| Ni(2)–S(1) | 2.136(3) | Ni(2)–S(2) | 2.134(3) |
| S(3)–Ni(1)–S(4) | 92.03(12) | S(3)–Ni(1)–S(4)#1 | 87.97(12) |
| S(2)–Ni(2)–S(1) | 92.17(11) | S(2)#2–Ni(2)–S(1) | 87.83 (11) |
| S(2)–Ni(2)–S(2)#2 | 180 | S(1)#2–Ni(2)–S(1) | 180.00(16) |
| S(3)–Ni(1)–S(3)#1 | 179.9(1) | S(4)–Ni(1)–S(4)#1 | 180.00(12) |

[a] Symmetry transformations used to generate equivalent atoms: #1 $-x + 2, -y + 2, -z + 1$; #2 $-x + 1, -y + 1, -z + 2$. [b] #1 $-x + 1, -y, -z + 1$; #2 $-x + 2, -y + 1, -z + 1$.

To investigate the supramolecular structure, we looked at the C–H···S and C–H···N interactions in the crystal structure of compound **1**. We found that a supramolecular chain-like arrangement [Figure 7 (a)] is formed from anion–anion C–H···N interactions. On the other hand, inter-anion C–H···S hydrogen-bonding interactions are responsible for the formation of a two-dimensional layer-like supramolecular arrangement [Figure 7 (b)]. In addition to inter-anionic supramolecular interactions, inter-cation–anion interactions exist (see the Supporting Information, Figure S5). Hydrogen-bonding parameters for the crystal structure of compound **1** are shown in Table 3.

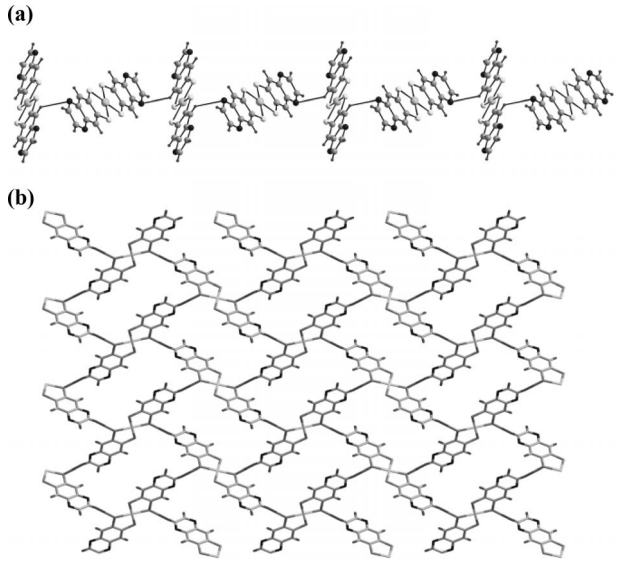


Figure 7. (a) Inter-molecular one dimensional supramolecular chain of $[Ni(6,7\text{-qdt})_2]^{1-}$ formed by C–H···N weak interactions. (b) Two-dimensional supramolecular layer-like structure formed by inter-anion C–H···S weak interactions (viewed along the crystallographic $a$-axis).

Table 3. Hydrogen-bond parameters for compound **1**.[a]

| D–H···A | $d$(D–H) [Å] | $d$(H···A) [Å] | $d$(D···A) [Å] | <(DHA)[b] [°] |
|---|---|---|---|---|
| C(29)–H(29A)···N(2) | 0.97 | 2.65 | 3.612(4) | 172.9 |
| C(26)–H(26B)···N(2) | 0.97 | 2.70 | 3.603(4) | 154.4 |
| C(13)–H(13)···N(2)#3 | 0.93 | 2.67 | 3.390(4) | 134.9 |
| C(23)–H(23B)···S(3)#3 | 0.97 | 2.90 | 3.797(3) | 154.7 |
| C(7)–H(7)···S(1)#4 | 0.93 | 2.81 | 3.733(3) | 169.6 |

[a] Symmetry transformations used to generate equivalent atoms: #3 $-x + 1, y - 1/2, -z + 3/2$; #4 $-x + 2, y - 1/2, -z + 3/2$. [b] <(DHA): dihedral angle.

### $[Ph_4P][Ni(Ph_26,7\text{-qdt})_2]\cdot CHCl_3$ (2)

Crystals of $[Ph_4P][Ni(Ph_26,7\text{-qdt})_2]\cdot CHCl_3$ (**2**) suitable for single-crystal X-ray structure determination were obtained from a $CHCl_3$ solution by vapour diffusion of diethyl ether. Compound **2** crystallizes in triclinic space group $P\bar{1}$. The asymmetric unit consists of two crystallographically independent halves of the $[Ni(Ph_26,7\text{-qdt})_2]^{1-}$ anion and one tetraphenylphosphonium cation along with a solvent molecule, as shown Figure 8 (a). The geometry around the $Ni^{3+}$ ion, which is coordinated by four sulfur atoms from two $Ph_26,7\text{-qdt}^{2-}$ ligands, is a square-planar geometry with S1–N2–S2 and S3–Ni1–S4 coordination angles of 92.17(11) and 92.03(12), respectively, from two different crystallographically independent molecules. In the five-membered

 

coordinated chelate rings of both the crystallographically independent molecules, the Ni–S, C–S and C=C bond lengths are in the range 2.1431(7)–2.1555(7), 1.711(3)–1.740(3) and 1.407(4)–1.419(4) Å, respectively.

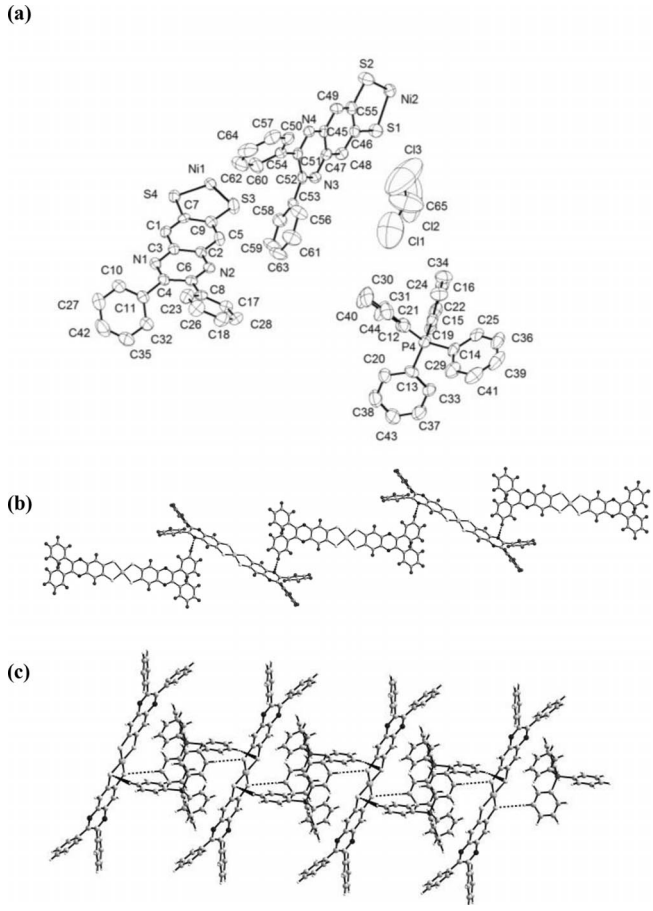


Figure 8. (a) Thermal ellipsoid diagram of compound **2** (at the 50% probability level), with hydrogen atoms omitted for clarity. (b) One-dimensional supramolecular chain-like arrangement formed by inter-anion interactions in the crystal structure of compound **2**. (c) Supramolecular chain-like structure formed by C–H···S weak interactions in compound **2**.

The crystal structure of compound **2** is also characterized by C–H···N and C–H···S supramolecular hydrogen-bonding interactions. The inter-anion C–H···N weak interactions lead to the formation of one-dimensional chain-like structure as shown in Figure 8 (b). On the other hand, the C–H···S hydrogen-bonding interactions between the complex anions and tetraphenylphosphonium cations lead to the construction of a sandwich-type extended arrangement as shown in Figure 8 (c).

## Hirshfeld Surface Analysis

The hydrogen-bonding supramolecular interactions around the complex anions $[Ni^{III}(6,7\text{-qdt})_2]^{1-}$ and $[Ni^{III}(Ph_2 6,7\text{-qdt})_2]^{1-}$ are further analysed with the Hirshfeld surfaces (HSs) and 2D fingerprint plots (FPs), which are generated by using the software Crystal explorer 3.1[13] based on the CIF file. The 3D Hirshfeld surfaces offer additional insight into the long- and short-range interactions experienced by the complex anions, and the 2D fingerprint plot, derived from the HSs, furnishes the nature, type and relative contribution of the intermolecular interactions. Generally, the directions and strengths of intermolecular interactions within the crystal are mapped onto the HSs by defining a descriptor "$d_{norm}$", which is a ratio of the distance of any surface point to the nearest interior ($d_i$) and exterior ($d_e$) atom to the van der Waals radii (vdW) of the concerned atoms.[14] Thus, when $d_{norm}$ is negative, the sum of $d_i$ and $d_e$, that is. the contact distance, is shorter than the sum of the relevant van der Waals radii, which is considered to be the closest contact and is visualized as red spots on the HSs as shown in Figure 9 (a). The white and blue colours indicate the contacts at vdW separation ($d_{norm}$ = 0). The intermolecular contacts contained in Tables 3 and 4 are effectively summarized as spots on the Hirshfeld surfaces; the large circular depressions (deep red), which are visible on the $d_{norm}$ surfaces, are indicators of hydrogen-bonding contacts. The small area and light colour on the surfaces indicate weaker and longer contacts, contacts other than hydrogen bonds.

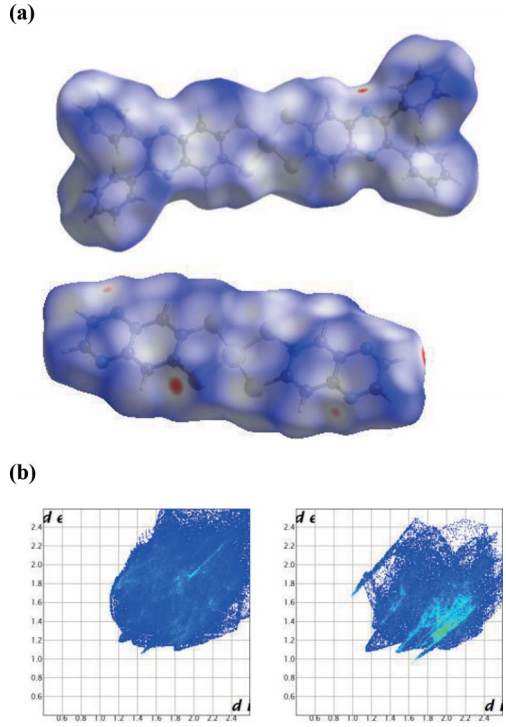


Figure 9. (a) Hirshfeld surfaces of the complex anions in compound **1** (top) and in compound **2** (bottom). (b) 2D fingerprint plots derived from HSs: compound **1** (left) and compound **2** (right).

Table 4. Hydrogen-bond parameters for compound **2**.[a]

| D–H···A | *d*(D–H) [Å] | *d*(H···A) [Å] | *d*(D···A) [Å] | <(DHA) [°] |
|---|---|---|---|---|
| C(24)–H(24)···S (4)#3 | 0.95 | 2.82 | 3.541(12) | 133 |
| C(28)–H(28)···N(3)#4 | 0.95 | 2.62 | 3.432(14) | 144 |

[a] Symmetry transformation used to generate equivalent atoms: #3 *x*, 1 + *y*, *z*; #4 1 – *x*, 1 – *y*, –*z*.

 

A plot of $d_i$ versus $d_e$ gives a 2D fingerprint plot [Figure 9 (b)], which identifies the occurrence of different kinds of intermolecular interactions. Complementary regions are visible in the fingerprint plots, where one molecule acts as a donor ($d_e > d_i$) and the other as an acceptor ($d_e < d_i$). The N···H close contacts vary from 13.9% in compound **1** to 5.5% in compound **2**. The C···H contacts vary from 20.5% in compound **1** to 15.6% in compound **2**. The S···H weak contacts vary from 21.8% in compound **1** to 8.4% in compound **2** (see Section 8 in the Supporting Information).

## Conclusion

We have described the synthesis and characterization of two $Ni^{III}$–bis(dithiolato) complexes, $[Bu_4N][Ni^{III}(6,7\text{-qdt})_2]$ (**1**) and $[Ph_4P][Ni^{III}(Ph_26,7\text{-qdt})_2]$ (**2**), that are based on unique dithiolene ligands. Compounds **1** and **2** are additionally characterized by electrochemical and ESR studies, in addition to their unambiguous characterization by single-crystal X-ray structure determination. The described compounds are unique in the sense that they get reduced reversibly at very low potentials. This demonstrates that their respective reduced analogues $[Bu_4N]_2[Ni^{II}(6,7\text{-qdt})_2]$ and $[Ph_4P]_2[Ni^{II}(Ph_26,7\text{-qdt})_2]$ can act as oxidation catalysts. The title compounds exhibit well-defined electronic absorption bands that have been corroborated with theoretical (DFT) calculations. This is a rare report in which theoretical calculations have been performed on a $Ni^{III}$–bis(dithiolato) system. The crystal structures of compounds **1** and **2** show interesting supramolecular hydrogen-bonding networks, formed by C–H···S and C–H···N weak contacts. Hirshfeld surfaces (HSs) and 2D fingerprint plots (FPs) corroborate these supramolecular interactions.

## Experimental Section

**General:** All the chemicals for the synthesis were commercially available and used as received. 1,2-Diaminobenzene-bis(thiocyanate) (**A**),[15] quinoxaline-6,7-dithiol ($H_26,7$-qdt; $\mathbf{L_1}$),[7] and $[Bu_4N]_2[Ni(6,7\text{-qdt})_2]$(**1a**),[7]diphenylquinoxaline-6,7-dithiol($\mathbf{L_2}$)[7]and $[Ph_4P]_2[Ni(Ph_26,7\text{-qdt})_2]$[7] were prepared according to literature procedures. Syntheses of metal complexes were performed under $N_2$ by using standard inert-atmosphere techniques. Solvents were dried by standard procedures. Microanalytical (C, H, N) data were obtained with a FLASH EA 1112 Series CHNS Analyzer. Infrared (IR) spectra were recorded from KBr pellets with a JASCO FT/IR-5300 spectrometer operating in the region 400–4000 $cm^{-1}$. $^1H$ NMR spectra of compounds were recorded with a Bruker DRX-400 spectrometer using $Si(CH_3)_4$ [TMS] as an internal standard. Electronic absorption spectra of solutions and diffuse reflectance spectra of solid compounds were recorded with a UV-3600 Shimadzu UV/Vis/NIR spectrophotometer. A Cypress model CS-1090/CS-1087 electroanalytical system was used for the cyclic voltammetric experiments. The electrochemical experiments were measured in DMF containing $[Bu_4N][ClO_4]$ as a supporting electrolyte, by using a conventional cell consisting of two platinum wires as the working and counter electrodes, and a Ag/AgCl electrode as a reference. The potentials reported here are uncorrected for junction contributions.

**$[Bu_4N][Ni(6,7\text{-qdt})_2]$ (1):** Mono anionic compound **1** was obtained as a brown powder by $I_2$ oxidation of the corresponding $[Bu_4N]_2[Ni^{II}(6,7\text{-qdt})_2]$ complex: a solution of $I_2$ (0.025 g, 0.1 mmol) in $CH_3CN$ (10 mL) was added dropwise to a filtered solution of $[Bu_4N]_2[Ni^{II}(6,7\text{-qdt})_2]$ (0.185 g, 0.2 mmol) in $CH_3CN$ (20 mL) and the mixture was allowed to stir for 2 h at room temperature. The resulting brown precipitate was filtered and washed with a small amount of methanol and hexane. Single crystals, suitable for X-ray diffraction, were grown by slow diffusion of diethyl ether into a $CH_3CN$ solution of the obtained solid, yield 0.115 g (84% based on $Ni^{II}$ complex used). $C_{32}H_{44}N_5NiS_4$ (685.67): calcd. C 56.05, H 6.47, N 10.21, S 18.71; found C 56.15, H 6.42, N 10.28, S 18.65. IR (KBr): $\tilde{\nu}$ = 3435 (br), 2959 (m), 1440 (w), 1413 (w), 1380 (w), 1172 (m), 1072 (w), 1019 (m), 876 (m), 783 (w), 597 (s), 515 (s) $cm^{-1}$.

**$[Ph_4P][Ni(Ph_26,7\text{-qdt})_2]$ (2):** Mono anionic compound **2** was obtained as a dark-brown powder by $I_2$ oxidation of the corresponding $[Ph_4P]_2[Ni^{II}(Ph_26,7\text{-qdt})_2]$ complex: a solution of $I_2$ (0.025 g, 0.1 mmol) in $CH_3CN$ (10 mL) was added dropwise to a filtered solution of $[Ph_4P]_2[Ni(Ph_26,7\text{-qdt})_2]$ (0.284 g, 0.2 mmol) in $CH_3CN$ (20 mL) and the mixture was allowed to stir for 2 h at room temperature. The resulting dark-brown powder precipitate was filtered and washed with a small amount of MeOH and hexane. Single crystals, suitable for X-ray diffraction, were grown by slow diffusion of diethyl ether into a $CHCl_3$ solution of the obtained dark-brown powder, yield 0.213 g (88% based on $Ni^{II}$ complex used). $C_{65}H_{45}Cl_3N_4NiPS_4$ (1206.32): calcd. C 64.71, H 3.76, N 4.64, S 10.63; found C 64.82, H 3.71, N 4.59, S 10.71. IR (KBr): $\tilde{\nu}$ = 3441 (br), 1424 (s), 1336 (w), 1190 (m), 1117 (w), 1080 (s), 1020 (w), 865 (w), 820 (w), 723 (m), 690 (m) $cm^{-1}$.

**X-ray Crystallography:** Single crystals, suitable for facile structural determination for the compounds **1** and **2**, were analysed with a three-circle Bruker SMART APEX CCD area detector system under a Mo-$K_\alpha$ ($\lambda$ = 0.71073 Å) graphite-monochromatic X-ray beam. The frames were recorded with an $\omega$ scan width of 0.3°, each for 10 s, with a crystal–detector distance of 60 mm, collimator 0.5 mm. Data reduction was performed by using SAINTPLUS.[15] Empirical absorption corrections were made by using equivalent reflections and were performed with the SADABS program.[16] The structures were solved by direct methods and least-squares refinement on $F^2$ for both compounds by using SHELXS-97.[16] All non-hydrogen atoms were refined anisotropically. The hydrogen atoms were included in the structure factor calculation by using a riding model. The crystallographic parameters, data collection and structure refinement of the compounds **1** and **2** are summarized in Table 1. Selected bond lengths and angles for the compounds **1** and **2** are listed in Table 2.

CCDC-1054536 (for **1**) and -1054537 (for **2**) contain the supplementary crystallographic data for this paper. These data can be obtained free of charge from the Cambridge Crystallographic Data Centre via www.ccdc.cam.ac.uk/data_request/cif.

**Computation:** Computational simulations for the ground-state as well as excited-state electronic structure calculations of the complex anions of compounds **1** and **2** were performed with the help of well-known density functional theory (DFT) by using the GAUSSIAN 09 suite programming package.[10] It is well known that the DFT can evaluate the ground-state electronic structure of a moiety exactly (especially for bigger molecules, e.g., a coordination complex anion), depending upon the functional used in the procedure. Theoretical calculations throughout the study were done with the hybrid functional B3LYP, which includes Hartree–Fock (HF) exchange as well as DFT exchange correlations. Non-local correlations were accounted for by the Lee, Yang and Parr (LYP) functional. The LanL2DZ basis set was used for Ni; whereas for

 

other atoms the 6-311G** basis set was used. Relativistic and other effects of the core electrons of the Ni atom have been accounted for by the inbuilt effective core potential (ECP) LanL2 of the LanL2DZ basis set. It should be mentioned that the polarization effect on C, S and N has been taken care of by incorporating five d-type Gaussian polarization functions into the basis set, whereas for H atoms three p-type polarization functions were included. The ground-state electronic structure calculation of the complex anions were performed by using the self-consistent reaction field (SCRF) procedure of the GAUSSIAN 09 programming package,[10] where solute complex ions are placed in the solvent cavity (DMF). The ground-state anionic complexes were obtained by full geometry optimization followed by frequency calculations. No imaginary frequencies (the lowest ten frequencies of each anionic complex are available in Section 7 of the Supporting Information) were obtained, which ensured that the optimized structure is not situated at any saddle point of the ground-state potential energy surface. Vertical excitations of the optimized structures were performed by employing the TD-B3LYP method[17] and using the same basis sets and same environment mentioned above. Other details of the computational output are described in the Supporting Information, Figure S7.

**Supporting Information** (see footnote on the first page of this article): HRMS spectra, computational outputs, 2D fingerprint plot derived from Hirshfeld surfaces, cyclic voltammograms, hydrogen-bonding interactions in the crystal structure of compound **1** and bond valence sum calculations for nickel in compounds **1** and **2**.

## Acknowledgments

The authors thank the Council of Scientific and Industrial Research (CSIR), Government of India [project number 01 (2556)/12/EMR-II] for financial support. The single-crystal X-ray diffraction facility at the University of Hyderabad by the Department of Science and technology (DST), New Delhi is highly acknowledged. The authors thank Mr. Suresh for helping us in the different stages of preparing the manuscript and Mr. Kumar for recording the ESR spectra. Our special thanks go to Professor S. Mahapatra, School of Chemistry and University of Hyderabad, for his help with the theoretical calculations and to the CMSD for computational facilities.

[1] a) R. Kato, *Chem. Rev.* **2004**, *104*, 5319–5346; b) X. M. Ren, S. Nishihara, T. Akutagawa, S. Noro, T. Nakamura, *Inorg. Chem.* **2006**, *45*, 2229–2234; c) M. L. Mercuri, P. Deplano, L. Pilia, A. Serpe, F. Artizzu, *Coord. Chem. Rev.* **2010**, *254*, 1419–1433; d) A. T. Coomber, D. Beljonne, R. H. Friend, J. L. Brédas, A. Charlton, N. Robertson, A. E. Underhill, M. Kurmoo, P. Day, *Nature* **1996**, *380*, 144–146; e) N. Robertson, L. Cronin, *Coord. Chem. Rev.* **2002**, *227*, 93–127.

[2] a) L. Serrano-Andrés, A. Avramopoulos, J. Li, P. Labéguerie, D. Bégué, V. Kellö, M. G. Papadopoulos, *J. Chem. Phys.* **2009**, *131*, 134312–134322; b) P. Deplano, L. Pilia, D. Espa, M. L. Mercuri, A. Serpe, *Coord. Chem. Rev.* **2010**, *254*, 1434–1447; c) C.-T. Chen, S.-Y. Liao, K.-J. Lin, L.-L. Lai, *Adv. Mater.* **1998**, *3*, 334–338.

[3] a) U. T. Mueller-Westerhoff, B. Vance, D. I. Yoon, *Tetrahedron* **1991**, *47*, 909–932; b) J.-F. Bai, J.-L. Zuo, W.-L. Tan, W. Ji, Z. Shen, H.-K. Fun, K. Chinnakali, I. A. Razak, X.-Z. You, C. M. Che, *J. Mater. Chem.* **1999**, *9*, 2419–2423; c) P. Deplano, M. L. Mercuri, G. Pintus, E. F. Trogu, *Comments Inorg. Chem.* **2001**, *22*, 353–374; d) M. C. Aragoni, M. Arca, T. Cassano, C. Denotti, F. A. Devillanova, R. Frau, F. Isaia, F. Lelj, V. Lippolis, L. Nitti, P. Romaniello, R. Tommasi, G. Verani, *Eur. J. Inorg. Chem.* **2003**, 1939–1947; e) S. I. G. Dias, S. Rabaca, I. C. Santos, L. C. J. Pereira, R. T. Henriques, M. Almeida, *Inorg. Chem. Commun.* **2012**, *15*, 102–105; f) P. Basu, A. Nigam, B. Mogesa, S. Denti, V. N. Nemykin, *Inorg. Chim. Acta* **2010**, *363*, 2857–2864.

[4] K. D. Karlin, E. I. Stiefel, *Progress in Inorganic Chemistry*, vol. 52: *Dithiolene Chemistry: Synthesis Properties, and Applications*, John Wiley, New York, **2004**.

[5] a) V. Madhu, S. K. Das, *Cryst. Growth Des.* **2014**, *14*, 2343–2356; b) V. Madhu, S. K. Das, *Dalton Trans.* **2011**, *40*, 12901–12908; c) V. Madhu, S. K. Das, *J. Chem. Sci.* **2006**, *118*, 611–617; d) V. Madhu, S. K. Das, *Polyhedron* **2004**, *23*, 1235–1242; e) R. Bolligarla, G. Durgaprasad, S. K. Das, *Inorg. Chem. Commun.* **2011**, *14*, 809–813; f) R. Bolligarla, S. K. Das, *CrystEngComm* **2010**, *12*, 3409–3412; g) X. Ribas, J. Dias, J. Morgado, K. Wurst, M. Almeida, J. Veciana, C. Rovira, *CrystEngComm* **2002**, *4*, 564–567.

[6] a) G. Durgaprasad, S. K. Das, *J. Chem. Sci.* **2015**, *127*, 295–305; b) G. Durgaprasad, R. Bolligarla, S. K. Das, *J. Organomet. Chem.* **2011**, *696*, 3097–3105; c) G. Durgaprasad, R. Bolligarla, S. K. Das, *J. Organomet. Chem.* **2012**, *706*, 37–45; d) G. Durgaprasad, S. K. Das, *J. Organomet. Chem.* **2012**, *717*, 29–40; e) N. M. F. S. A. Cerqueira, B. Pakhira, S. Sarkar, *J. Biol. Inorg. Chem.* **2015**, *20*, 323–335; f) B. K. Maiti, L. B. Maia, K. Pal, B. Pakhira, T. Aviles, I. Moura, S. R. Pauleta, J. L. Nunez, A. C. Rizzi, C. D. Brondino, S. Sarkar, J. J. G. Moura, *Inorg. Chem.* **2014**, *53*, 12799–12808.

[7] R. Bolligarla, S. N. Reddy, G. Durgaprasad, V. Sreenivasulu, S. K. Das, *Inorg. Chem.* **2013**, *52*, 66–76.

[8] C.-M. Lee, Y.-L. Chuang, C.-Y. Chiang, G.-H. Lee, W.-F. Liaw, *Inorg. Chem.* **2006**, *45*, 10895–10904.

[9] B. Zheng, F. Tang, J. Luo, J. W. Schultz, N. P. Rath, L. M. Mirica, *J. Am. Chem. Soc.* **2014**, *136*, 6499–6504.

[10] M. J. Frisch, G. W. Trucks, H. B. Schlegel, G. E. Scuseria, M. A. Robb, J. R. Cheeseman, G. Scalmani, V. Barone, B. Mennucci, G. A. Petersson, H. Nakatsuji, M. Caricato, X. Li, H. P. Hratchian, A. F. Izmaylov, J. Bloino, G. Zheng, J. L. Sonnenberg, M. Hada, M. Ehara, K. Toyota, R. Fukuda, J. Hasegawa, M. Ishida, T. Nakajima, Y. Honda, O. Kitao, H. Nakai, T. Vreven, J. A. Montgomery Jr., J. E. Peralta, F. Ogliaro, M. Bearpark, J. J. Heyd, E. Brothers, K. N. Kudin, V. N. Staroverov, R. Kobayashi, J. Normand, K. Raghavachari, A. Rendell, J. C. Burant, S. S. Iyengar, J. Tomasi, M. Cossi, N. Rega, J. M. Millam, M. Klene, J. E. Knox, J. B. Cross, V. Bakken, C. Adamo, J. Jaramillo, R. Gomperts, R. E. Stratmann, O. Yazyev, A. J. Austin, R. Cammi, C. Pomelli, J. W. Ochterski, R. L. Martin, K. Morokuma, V. G. Zakrzewski, G. A. Voth, P. Salvador, J. J. Dannenberg, S. Dapprich, A. D. Daniels, Ö. Farkas, J. B. Foresman, J. V. Ortiz, J. Cioslowski, D. J. Fox, *Gaussian 09*, revision C.01, Gaussian, Inc., Wallingford CT, **2010**.

[11] V. Madhu, S. K. Das, *Inorg. Chem.* **2008**, *47*, 5055–5070.

[12] D.-Y. Noh, M.-J. Kang, H.-J. Lee, J.-H. Kim, J.-H. Choy, *Bull. Korean Chem. Soc.* **1996**, *17*, 46–50.

[13] S. K. Wolff, D. J. Grimwood, J. J. McKinnon, M. J. Turner, D. Jayatilaka, M. A. Spackmann, *CrystalExplorer 3.1* (**2013**), University of Western Australia, Crawley, Western Australia, **2005–2013**, http://hirshfeldsurface.net.

[14] a) J. J. McKinnon, D. Jayatilka, M. A. Spackman, *Chem. Commun.* **2007**, 3814–3816; b) F. L. Hirshfeld, *Theor. Chim. Acta* **1977**, *44*, 129–138; c) M. A. Spackman, D. Jayatilaka, *CrystEngComm* **2009**, *11*, 19–32.

[15] J. L. Brusso, O. P. Clements, R. C. Haddon, M. E. Itkis, A. A. Leitch, R. T. Okely, R. W. Reed, J. F. Richardson, *J. Am. Chem. Soc.* **2004**, *126*, 8256–8265.

[16] Bruker AXS Inc., *SADABS*, *SMART*, *SAINT* and *SHELXTL*, Madison, Wisconsin, USA, **2000**.

[17] U. Salzner, *J. Chem. Theory Comput.* **2013**, *9*, 4064–4073.

Received: July 6, 2015
Published Online: November 4, 2015

 